The Dissertation Committee for Zhipeng Wang Certifies that this is the approved version of the following dissertation:

Total Synthese of (±)-Melicolones A and B, Design, Synthesis and Evaluation of Novel Carbazole Based Photocages

Committee:

Stephen F. Martin, Supervisor

Eric V. Anslyn

Kami L. Hull

Boris V. Zemelman

Total Syntheses of (±)-Melicolones A and B, Design, Synthesis and Evaluation of Novel Carbazole Based Photocages

by

Zhipeng Wang

Dissertation

Presented to the Faculty of the Graduate School of

The University of Texas at Austin

in Partial Fulfillment

of the Requirements

for the Degree of

Doctor of Philosophy

The University of Texas at Austin

August 2021

Dedication

To my mother and father for a lifetime support, and to Wang for all your love and support.

Acknowledgements

First and foremost, I would like to acknowledge Dr. Stephen F. Martin for taking me into his group and all the mentorship throughout the journey. I would also like to acknowledge all of the past and present members of the Martin group who have helped me along the way, in particular Grant Walby, Dr. Yan Lu, Dr. Hongfen Yang, Dr. Michael Wood, Dr. Daniel Klowsowski, Dr. Alan Meis, Dr. Lance Lepovitz, Chris Farley, Alex Goodnough, Zachary White, Dr. Rachel Wypych.

Abstract

Total Syntheses of (±)-Melicolones A and B, Design, Synthesis and Evaluation of Novel Carbazole Based Photocages

Zhipeng Wang, Ph.D.

The University of Texas at Austin, 2021

Supervisor: Stephen F. Martin

The first total syntheses of (±)-melicolone A and (±)-melicolone B was accomplished in a combined overall yield of 12.3% and a mere 9 steps from commercially available reagents. The synthesis features a novel rhodium(II) catalyzed 1,3-dipolar cycloaddition reactions of carbonyl ylide generated from an aliphatic aldehyde with rhodium carbene and an unsaturated vinylogous ester dipolarophile.

Two new carbazole photocages were designed, synthesized, and characterized. Both new carbazole photocages showed superior decaging properties compared with reported NDBF photocaged which are illustrated by the benzoic acid model system study at 390 nm and 400 nm. The decaging properties of modified photocage for phenol derivatives were evaluated by a modified tyrosine substrate, and efficient decaging was achieved at 360 nm. Lastly, a caged fluoroquinolone system was conducted to demonstrate the potency of modified photocage in anti-bacterial growth inhibition studies.

Table of Contents

List of Tables

List of Figures

List of Schemes

TOTAL SYNTHESES OF (±)-MELICOLONES A AND B

Chapter 1: Total Syntheses of (±)-Melicolones A and B

1.1 ISOLATION AND BIOLOGICAL ACTIVITIES

Melicope is a genus comprising around 230 shrubs and trees in the Rutaceae family, which is widely distributed in the tropical regions around the world, including the Hawaiian islands across the Pacific Ocean to tropical Asia, Australia and New Zealand.[1,2] Many of the *Melicope* species were utilized as folk medicines due to their pharmacological activities and previous studies revealed the presence of acetophenones, furoquinolines, coumarins, flavones, benzopyrans in these plants.[3-7] Prenylated acetophenones are regarded as the chemotaxonomic markers among all the constituents found in *Melicope* species.[8] Previous studies also showed the acetophenones isolated from *Melicope* species are usually substituted by prenyl or geranyl groups, and the aromatic structures have been mostly retained. Only limited number of examples having nonaromatic acetophenone compounds have been reported so far.[9]

(±)-Melicolone A (**1.1**) and (±)-melicolone B (**1.2**) were isolated from the leaves of *Melicope ptelefolia* by Luo and Kong groups in 2015 as a pair of prenylated acetophenone epimers with an unusual 9-oxatricyclo[3.2.1.1] nonane core (Figure 1.1).[10] Structurally, melicolones A and B represent the first examples of rearranged nonaromatic acetophenone derivatives with the 9-oxatricyclononane core structures, with a total of five stereogenic centers and a oxygen bridge. The highly dense functionality of these natural products makes their total synthesis challenging.

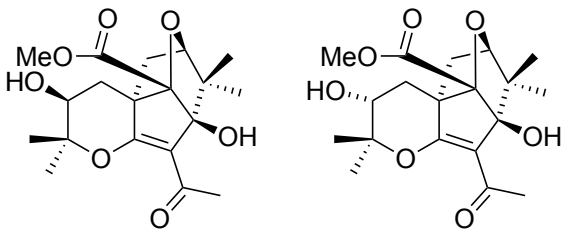

Melicolone A (**1.1**) Melicolone B (**1.2**)

Figure 1.1. Chemical structures of (±)-melicolone A (**1.1**) and (±)-melicolone B (**1.2**).

A plausible biosynthetic pathway for the melicolones has been proposed by Luo and Kong.[10] Starting from the acetophenone precursor **1.3** that has also been identified in the leaves of *Melicope ptelefolia*, a sequence of oxidation and prenylation of **1.3** afforded intermediate **1.4**, which then went through a nonface-selective epoxidation of the prenyl chain and a cyclization to afford intermediate **1.5** with four possible isomers. The intermediate **1.5** underwent an acyloin rearrangement followed by a methylation to generate stereoisomers **1.6** and **1.6'**. Then the C-12 on the prenyl chains of **1.6** and **1.6'** could cyclize with the C-1 below or above the plane respectively to form intermediates that would readily undergo dehydration to form the oxygen bridge moiety and form two enantiomeric pairs of epimers (+)-melicolones A/B and (-)-melicolones A/B.

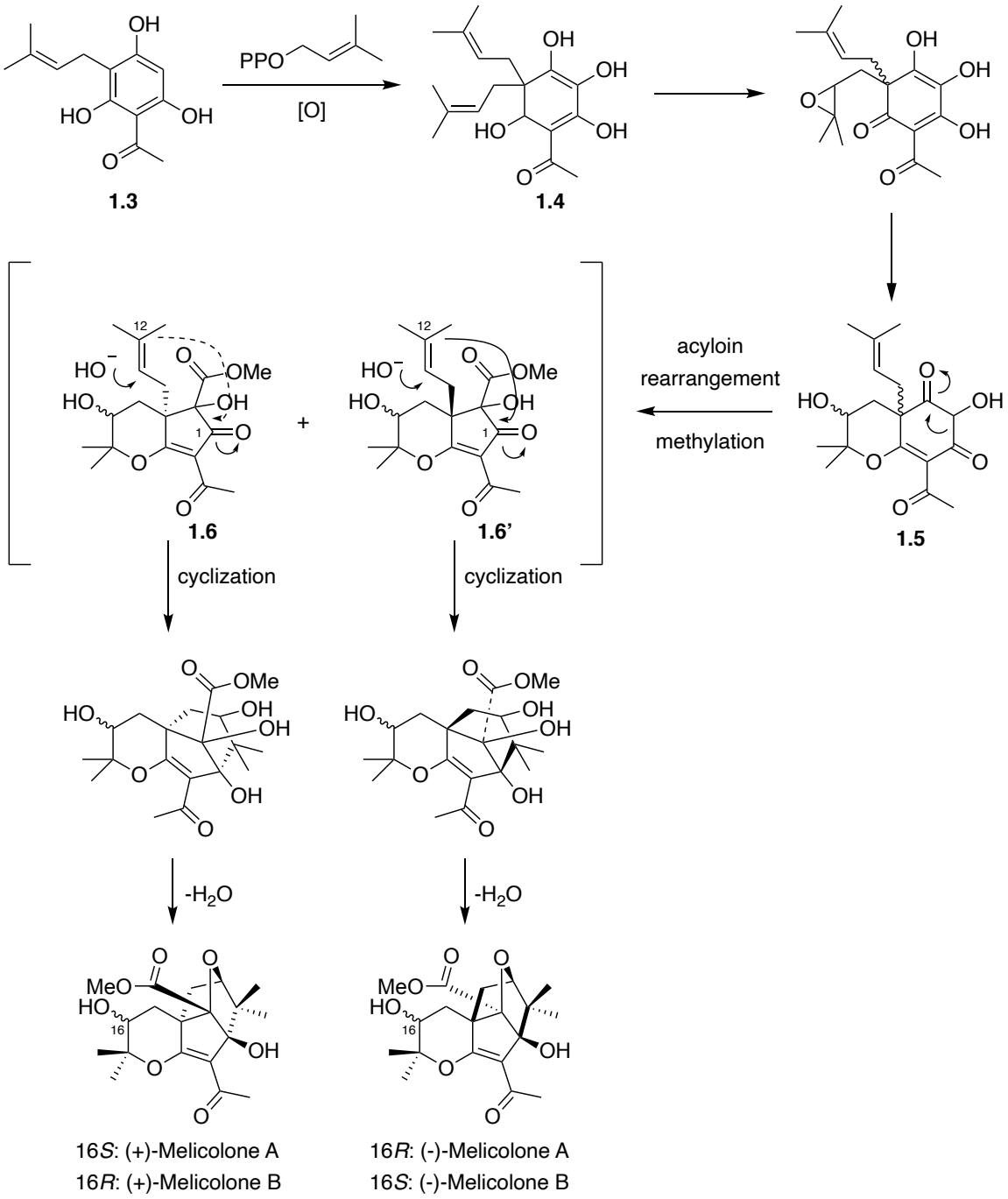

Scheme 1.1. Proposed biosynthesis of (±)-melicolone A (**1.1**) and (±)-melicolone B (**1.2**).

Previous studies have revealed the antioxidant activities from the leaves of *Melicope ptelefolia*, and further studies by Luo and Kong groups demonstrated that both

enantiomers of (±)-melicolone A and (±)-melicolone B have protective effects against oxidative stress induced by high glucose level.[10,11]

In 2019, Luo and Kong group reported the isolation of melicolones C-K (**1.7**-**1.15**) from the leaves of *Melicope Ptelefolia* (Figure 1.2).[12] Specifically, melicolones G-K (**1.11**-**1.15**) share the unprecedented 9-oxatricyclo[3.2.1.1] nonane core structure found in melicolones A (**1.1**) and B (**1.2**). Melicolone C (**1.7**) is an acetophenone analogue sharing a novel spirocyclic skeleton, and melicolones D-F (**1.8**-**1.10**) bear an unusual octalactone moiety. The putative biosynthetic pathways to all melicolone compounds were also proposed starting with the same acetophenone precursors that generated three different types of carbon scaffolds via different biosynthetic pathways (Scheme 1.2). The inhibitory effects of **1.11**-**1.15** against multidrug resistance were also evaluated using 3-(4,5-dimethylthiazol-2-yl)-2,5-diphenyltetrazolium bromide (MTT) method in MCF-7 (Michigan Cancer Foundation-7)/ADR cells.[12]

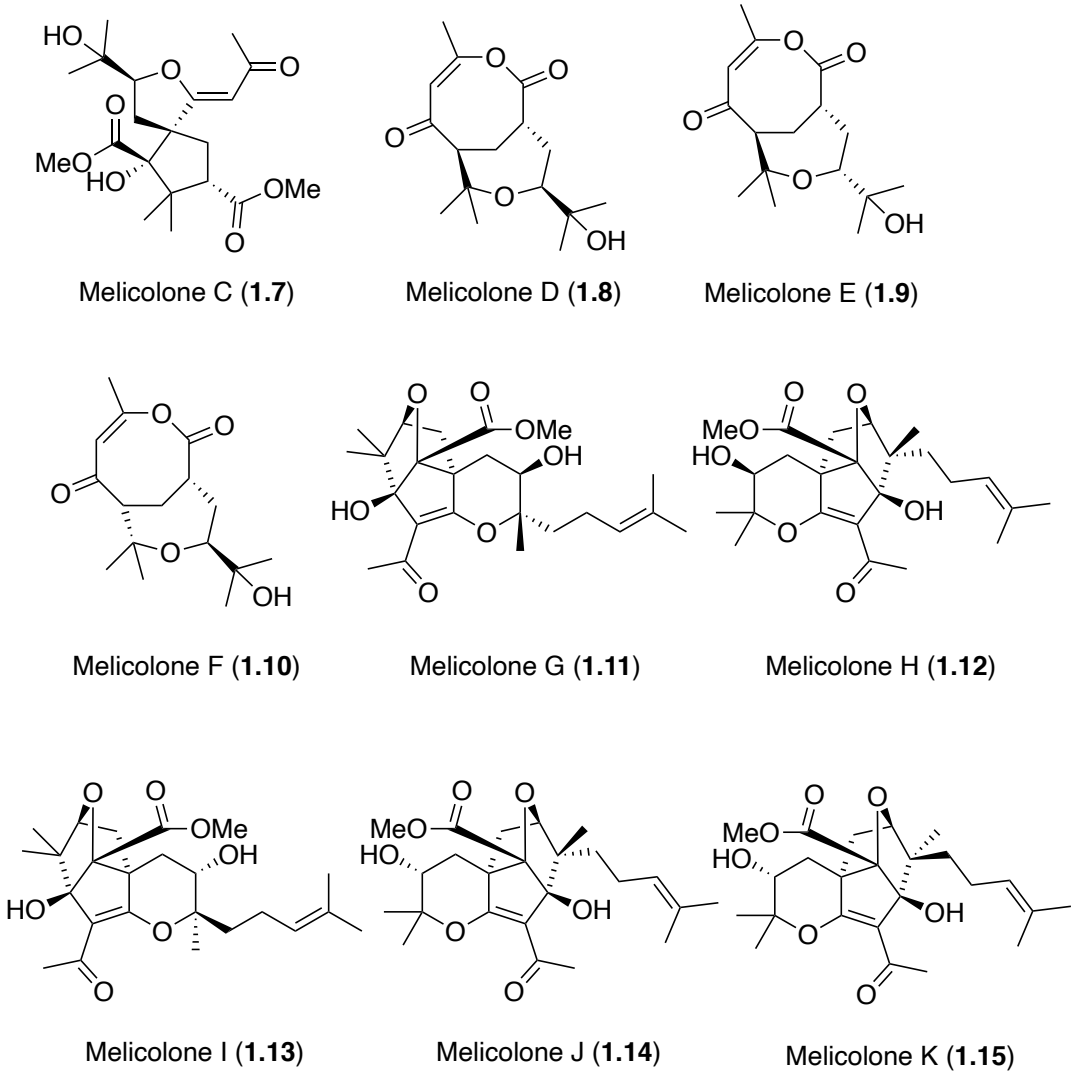

Figure 1.2. Chemical structures of melicolones C-K (**1.7**-**1.15**).

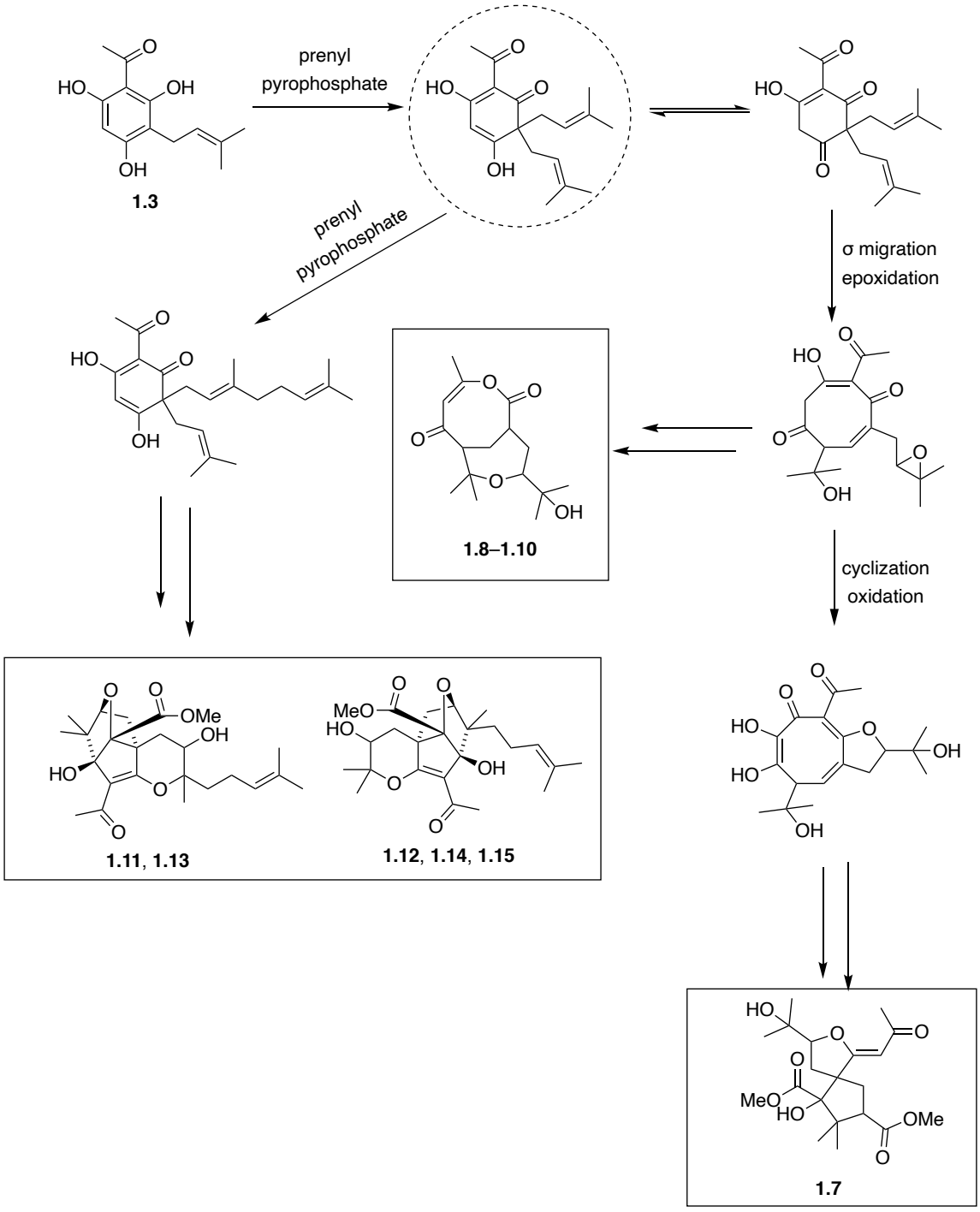

Scheme 1.2. Proposed biosynthetic pathways to the diverse acetophenone derivatives.

1.2 MARTIN GROUP APPROACH TO (±)-MELICOLONES A AND B

Martin group has long been focused in the total syntheses of novel bioactive natural products, and we were intrigued by the remarkable structures and interesting bioactivities of the melicolone natural products. Herein, we decided to develop the total syntheses of melicolones A and B. Considering the multiple melicolone family natural products share the same unprecedented 9-oxatricyclo[3.2.1.1] nonane core structures, we were interested to develop an unified approach to construct the core structure and potentially accomplish the syntheses of multiple melicolones natural products from the same intermediate.

To our knowledge, there was no report of any synthetic work diverted toward any melicolone natural products when we started, although we became aware that multiple groups were working in the area.[13,14] We envisioned that a racemic mixture of melicolones A and B can be formed from **1.16** via the sequential epoxidation of the alkene of the prenyl group and an acid catalyzed regioselective epoxide opening with the enol hydroxyl group (Scheme 1.3). **1.16** would be accessible from cycloadduct **1.17** with the transformation of stereoselective prenylation of the carbon α to the vinylogous ester followed by a base catalyzed aldol cyclization. Oxabicycloheptane **1.17** would be generated from a novel intermolecular dipolar cycloaddition of the dipolarophile **1.17** and the cyclic carbonyl ylide **1.19**, which would be generated *in situ* by the rhodium(II)-catalyzed cyclization of the diazo compound **1.20**. Cycloadditions of carbonyl ylides are well known in previous literature, but the intermediate carbonyl ylides are generally formed by cyclization of a metallocarbene with the carbonyl oxygen atom of a ketone, ester or amide.[15-23] We are aware of only two examples involving the same aliphatic aldehyde.[24,25] Another unusual aspect of the proposed cycloaddition of **1.18** and **1.19** is the predicted regiochemistry. Based upon the usual electronic effects that dictate these cycloadditions, we would predict the formation of the opposite isomer as the preferred product. However, we reasoned that

steric effects between the geminal dimethyl groups and the vinylogous ester group would control the formation of **1.17** as the preferred regioisomer. We envisioned that **1.20** would be accessible from the inexpensive starting material hydroxy pivalic acid **1.22**. **1.22** would undergo malonic ester synthesis conditions to form 1,3 dicarbonyl compounds which was subsequently treated with diazo transfer reagent to generate diazo intermediate. Finally, the hydroxyl group in the diazo intermediate can be oxidized to form the diazo aldehyde **1.20**. Vinylogous ester **1.18** would be prepared from the commercially available methyl carbonate **1.21**. The ketone carbonyl of **1.21** would first be protected as vinyl methyl ether in the presence of acid, and the ester moiety would be transformed to its Weinreb amide followed by a vinyl Grignard addition to generate **1.18**. We also envisioned that cycloadduct **1.17** would be able to serve as the unified intermediate to synthesize other melicolone family natural products such as melicolones G (**1.11**) and I (**1.13**). Moreover, chiral rhodium catalysts have been developed to construct oxabicycloheptane structures enantioselectively, which maps with the core structure of proposed cycloadduct **1.17**, thus providing the possibility to synthesize melicolone natural products enantioselectively.[26,27]

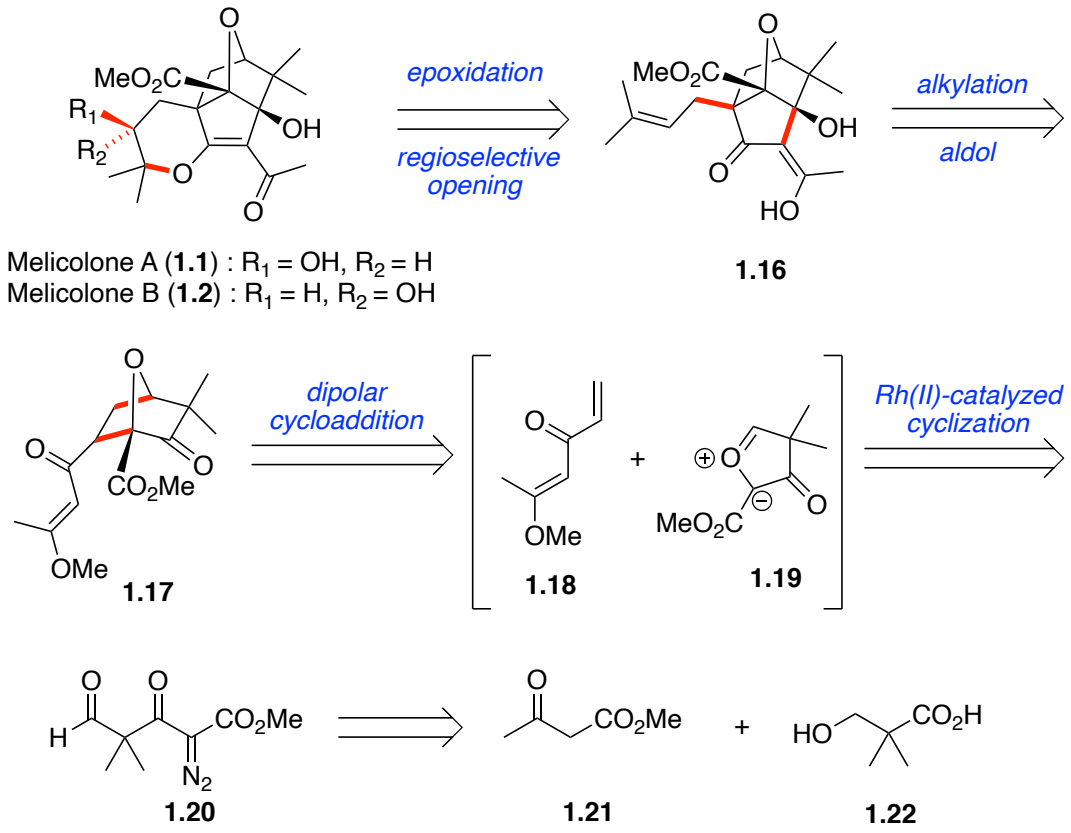

Scheme 1.3. Retrosynthetic analysis for the syntheses of (±)-melicolones A (**1.1**) and B (**1.2**).

1.3 SYNTHESIS OF THE DIAZO ALDEHYDE

We initiated our synthesis with the preparation of the key diazo aldehyde **1.20**. We were inspired by a similar procedure reported by Hashimoto, who started with the activation of the carboxylic acid **1.23** with carbonyl diimidazole (CDI) followed by the reaction with the dianion formed by the treatment of mono malonic ester with base to afford β-carbonyl ester **1.24** (Scheme 1.3).[28] Finally, the diazo transfer reaction of **1.24** with methanesulfonyl azide (MsN_3) in the presence of base furnished diazo carbonyl species **1.25**.

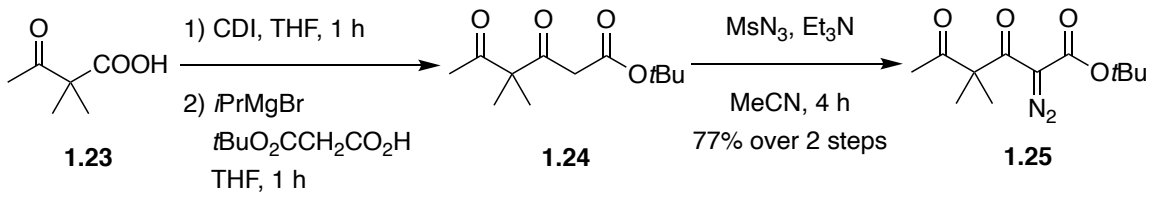

Scheme 1.4. Reported procedure of the preparation of diazo carbonyl compounds.

With this precedented procedure, we sought to prepare our diazo aldehyde **1.20** in a similar fashion. Starting the synthesis with commercially available hydroxy pivalic acid **1.22**, we were concerned the free primary hydroxyl group in **1.22** could cause side reactions in the transformation with CDI. However, in a reported procedure by Heng, the primary hydroxyl carboxylic acid **1.26** was activated by CDI in the presence of a primary hydroxyl group, followed by the treatment with dianion generated from mono ethyl malonate to yield β-ketoester **1.27** in good yields (Equation 1.1).[29] However, when we attempted the same transformation with the starting material hydroxyl pivalic acid **1.22**, the reaction gave a complex mixture (Equation 1.2). We decided to break down the reaction sequence and analyze the reaction mixture after the treatment of **1.22** with CDI (Equation 1.3). The LCMS result gave several major masses that correspond to the intermediate that were formed by the reaction of CDI with both the primary alcohol and carboxyl group. The primary hydroxyl group was identified as the cause of the side reactions, so we sought to protect the primary alcohol.

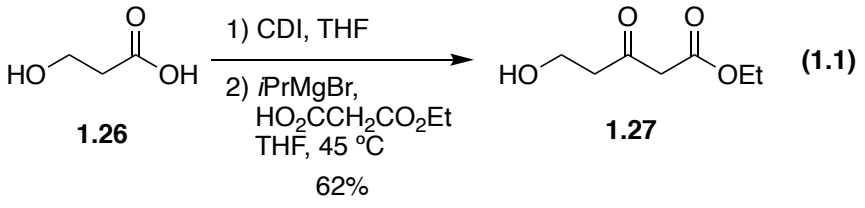

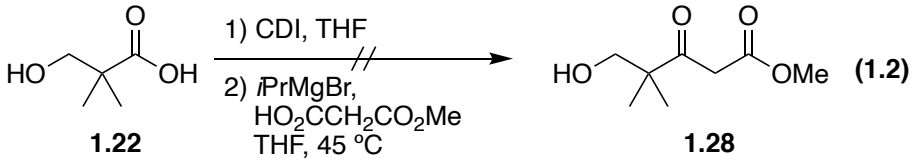

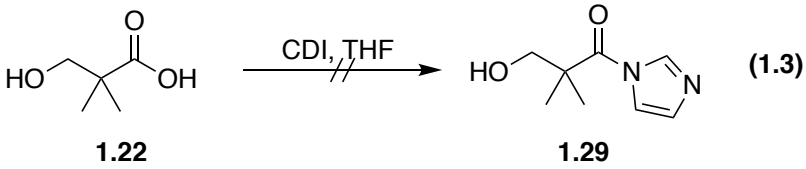

We turned our attention to picking the protecting group for the primary hydroxyl group in **1.22**. We favored the protection of this alcohol with the triethylsilyl (TES) ether group, due to the effective methods of protection and deprotection as well as its relatively robust nature in the following transformation steps. Another promising feature of TES ether group is that can be removed and oxidized in one step.[30] Hydroxyl pivalic acid **1.22** was treated with chlorotriethylsilane (TESCl) in pyridine to afford TES ether **1.30** in 95% yield (Equation 1.4).[31] The yield slightly dropped to 88% in multigram scale reactions.

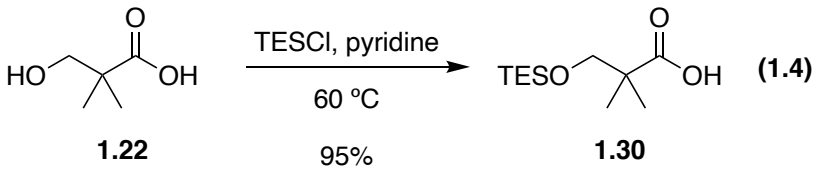

With TES ether **1.30** in hand, we treated **1.30** with CDI in THF, and we confirmed the clean generation of imidazolide on the carboxyl group with NMR analysis. Subsequently we treated the imidazolide with the dianion which was generated from the

treatment of methyl hydrogen malonate with *i*PrMgBr at 45 ºC, and the solution was stirred at room temperature overnight. To our delight, after the reaction completed, β-ketoester **1.31** and its enol tautomer **1.31'** were isolated in 65% yield with a ratio of 3 :1 (Equation 1.5). When the reaction was conducted on multigram scale, we isolated a mixture of **1.31** and **1.31'** in 62% yield with a ratio of 3.5 :1.

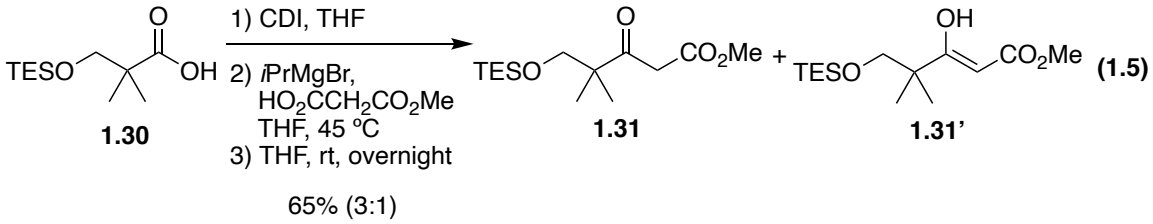

With β-ketoester **1.31** in hand, we investigated the diazo transfer reaction. The most commonly used diazo transfer reagents include *p*-toluenesulfonyl azide (TsN_3), methanesulfonyl azide (MsN_3), trifluoromethanesulfonyl azide (TfN_3) and imidazole-1-sulfonyl azide hydrochloride.[32-35] TsN_3 was found to be the most utilized diazo transfer reagent with a long history, but difficulties have been reported in the chromatographic separation of the desired product from excess reagent and *p*-toluenesulfonamide following the reactions.[36] While as an alternate to TsN_3, MsN_3 was reported to have an easier separation by using 10% NaOH aqueous solution, as well as an efficient diazo transfer rate.[37] TfN_3 is easy to separate but it has a relative poor shelf live, which necessitates its preparation in solution prior to use, and more significantly, the expense of trifluoromethanesulfonyl anhydride that is used to prepare TfN_3 prohibits its use in large scale reactions.[38] Imidazole-1-sulfonyl azide hydrochloride was developed as an alternate to TfN_3, and it is more widely used in the conversion of amine to azide.[38] Based on the research, we started our investigation with MsN_3 and TsN_3 as the diazo transfer reagents. The preparations of MsN_3 and TsN_3 are fairly straightforward, and the treatment of MsCl

and TsCl with NaN_3 gave MsN_3 and TsN_3 in 92% and 93% yield, respectively (Equations 1.6 and 1.7).[36,37]

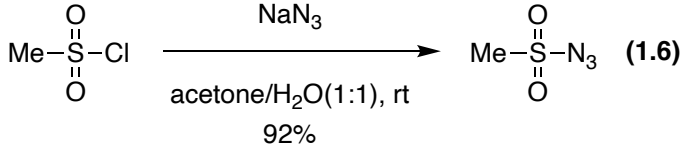

(1.6)

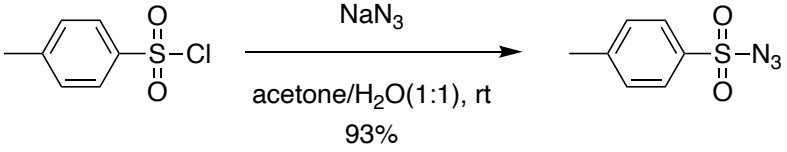

(1.7)

We started our condition screening by treating β-ketoester **1.31** with MsN_3 (1.1 eq.) and Et_3N (1.4 eq.) in MeCN, and the solution was stirred at room temperature overnight (Table 1.1 entry 1). Contradictory to what has been reported, the reaction was very sluggish and only afforded a 1:10 mixture of **1.32** and **1.31**. We also tried to prolong the reaction time to 48 h, but only 42% of **1.32** with 45% of unreacted **1.31** was isolated (Entry 2). Increasing the equivalents of MsN_3 and Et_3N gave better conversion, but starting materials were still isolated (Entry 3). We then tried using the similar amount of TsN_3 as the diazo transfer reagent, and to our delight, starting material was fully consumed when excess TsN_3 (1.5 eq.) and Et_3N (2.0 eq.) were used, and we obtained 94% of the desired diazo compound **1.32** (Entry 5). We then carried out the reaction in a multigram scale which afforded **1.32** in 90% yield.

Table 1.1. Reaction conditions screening of the diazo transfer reaction.

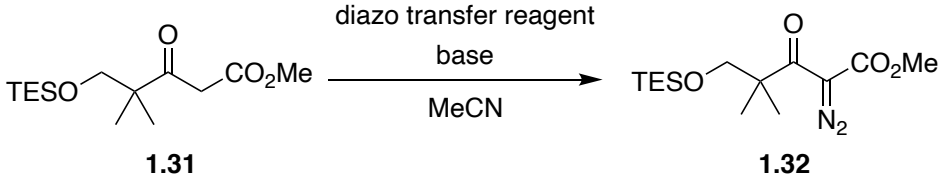

1.31 **1.32**

entry	diazo transfer reagent	base	% yield **1.32**[a]	% recovered **1.31**[a]
1	1.1 eq MsN_3	1.4 eq Et_3N	7	79
2	1.1 eq MsN_3	1.4 eq Et_3N	45[b]	42[b]
3	1.5 eq MsN_3	2.0 eq Et_3N	42	45
4	1.1 eq TsN_3	1.4 eq Et_3N	73	20
5	1.5 eq TsN_3	2.0 eq Et_3N	94	0

[a] Isolated yield after chromatographic purification for reacting overnight. [b] Isolated yield after chromatographic purification for reacting for 48h.

With **1.32** in hand, we started investigating the conditions of deprotecting the TES ether protecting group. Spur group reported that primary TMS and TES ethers could be selectively deprotected and oxidized to afford aldehydes or ketones in one pot using the Swern oxidation.[39] Encouraged by the promising precedents, we initiated our investigation on oxidative deprotection of the TES ether **1.32** using a Swern oxidation. We treated **1.32** with the premixed solution of oxalyl chloride and DMSO at -78 ºC, followed by the addition of Et_3N before slowly warming it to room temperature over the course of 30 min

(Equation 1.8). Unfortunately, we only observed trace amounts of the desired aldehyde **1.20** with most **1.32** unreacted. However, we found after the addition of **1.32** at -78 ºC, warming the reaction up to – 40 ºC was essential to help facilitate the deprotection of TES ether group prior to the formation of alkoxysulfonium ion, which further underwent intramolecular deprotonation upon addition of Et_3N to deliver aldehydes **1.20** in 75% yield (Equation 1.9).

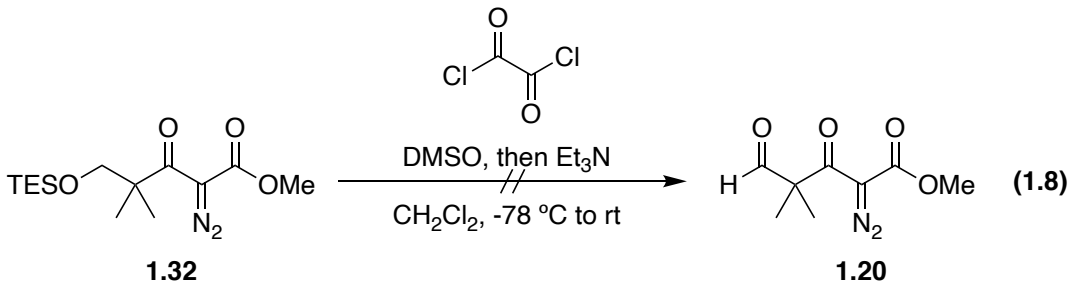

1.32 **1.20**

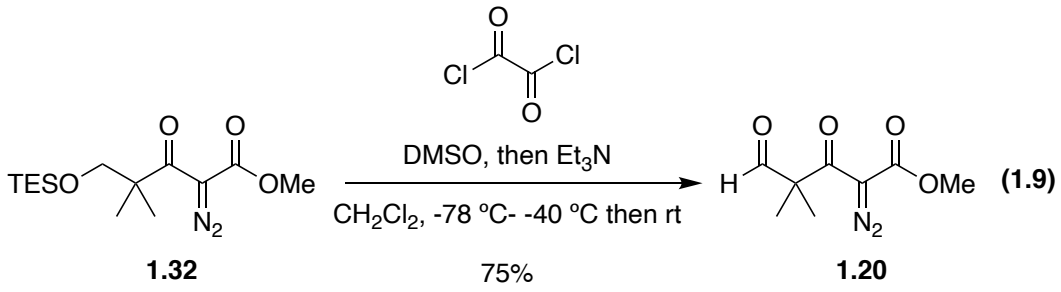

1.32 75% **1.20**

However, with **1.20** obtained via the Swern oxidation, we found that residual Me_2S generated in the Swern oxidation was difficult to remove in reactions over 200 mg scale. Unfortunately, Me_2S would consequently poison the Rh(II) catalysts used in the subsequent dipolar cycloaddition reaction.[40] This difficulty occurred consistently when we conducted the Swern oxidation on a 200-mg scale, thereby limiting the feasibility of the reaction. In order to quickly scale up the preparation of **1.20**, this particular issue led us to seek alternative approach to remove the TES group.

CrO_3/pyridine has been reported by Muzart to convert TES ethers when α to aryl rings as well as double, or triple bonds.[41] We investigated this transformation of TES ether to aldehyde method by treating **1.32** with CrO_3 and pyridine in CH_2Cl_2 at room temperature for 72 h, which afforded **1.20** in 63% yield. The **1.20** thus obtained could be used to generate carbonyl ylide in the presence of Rh(II) catalysts without any issue (Equation 1.10). However, the reaction was relatively sluggish, and the yield was modest, so we decided to examine alternative conditions. Conditions reported by Wu group were found to be efficient at transforming the TES ether **1.32** to diazo aldehyde **1.20**.[42] Namely treatment of TES ether **1.32** in the presence of 2-iodoxybenzoic acid (IBX) in DMSO and H_2O at room temperature afforded **1.20** in 89% yield, providing scalable and reliable conditions for generating the diazo aldehyde **1.20** for the subsequent Rh(II) catalyzed cycloaddition reaction (Equation 1.11).

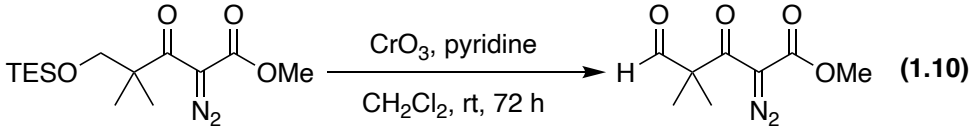

1.32 63% **1.20** **(1.10)**

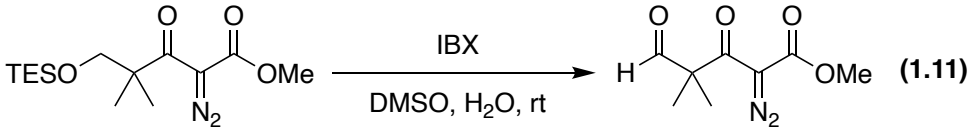

1.32 89% **1.20** **(1.11)**

1.4 RHODIUM(II) CATALYZED CARBONYL YLIDE CYCLOADDITION

1.4.1 Rh(II) Catalyzed Carbonyl Ylide Cycloaddition

The Rh(II)-catalyzed formation of carbonyl ylides have played an important role in expanding the scope and utility of the 1,3-dipolar cycloaddition reactions as means to

effectively construct heterocyclic ring systems in natural product total syntheses.[43-46] The carbonyl ylide cycloaddition reactions have been known since as early as 1885; however, before the introduction of the concept of 1,3-dipoles, these reactions were considered to proceed through a diradical mechanistic pathway. [47,48] The Huisgen group was the first group to examine the reaction in detail by trapping a carbonyl ylide with various reagents, including carbonyl compounds, to generate dioxolanes.[49] In their early studies, dimethyl diazomalonate (**1.33**) was treated with benzaldehyde in the presence of catalysts including $Rh_2(OAc)_4$, $Cu(acac)_2$, and CuOTf to furnish a mixture of isomeric 1,3-dioxolanes **1.34** (Figure 1.3A). Doyle and coworkers reported the selective formation of a dioxolane **1.35** or an epoxide **1.36** via influencing the stability of the intermediate carbonyl ylide species in their follow-up studies to the early Huisgen publication (Figure 1.3B).[50,51] Ibata and coworkers first demonstrated the utility of intramolecular carbonyl ylide formation by studying the Cu(II) catalyzed decomposition of o-alkoxycarbonyl-α-diazo-acetophenone **1.37** in the presence of different dipolarophiles (Figure 1.3C).[52,53] The utility of the carbonyl ylide formation-cycloaddition sequence was further extended by the intramolecular trapping of the carbonyl ylide with a C-C double bond within the molecule.[54] The Rh(II) catalyzed decomposition of diazo ketone **1.39** followed by carbonyl ylide formation was then trapped by the olefin forming the final cycloadduct **1.40** (Figure 1.3D).

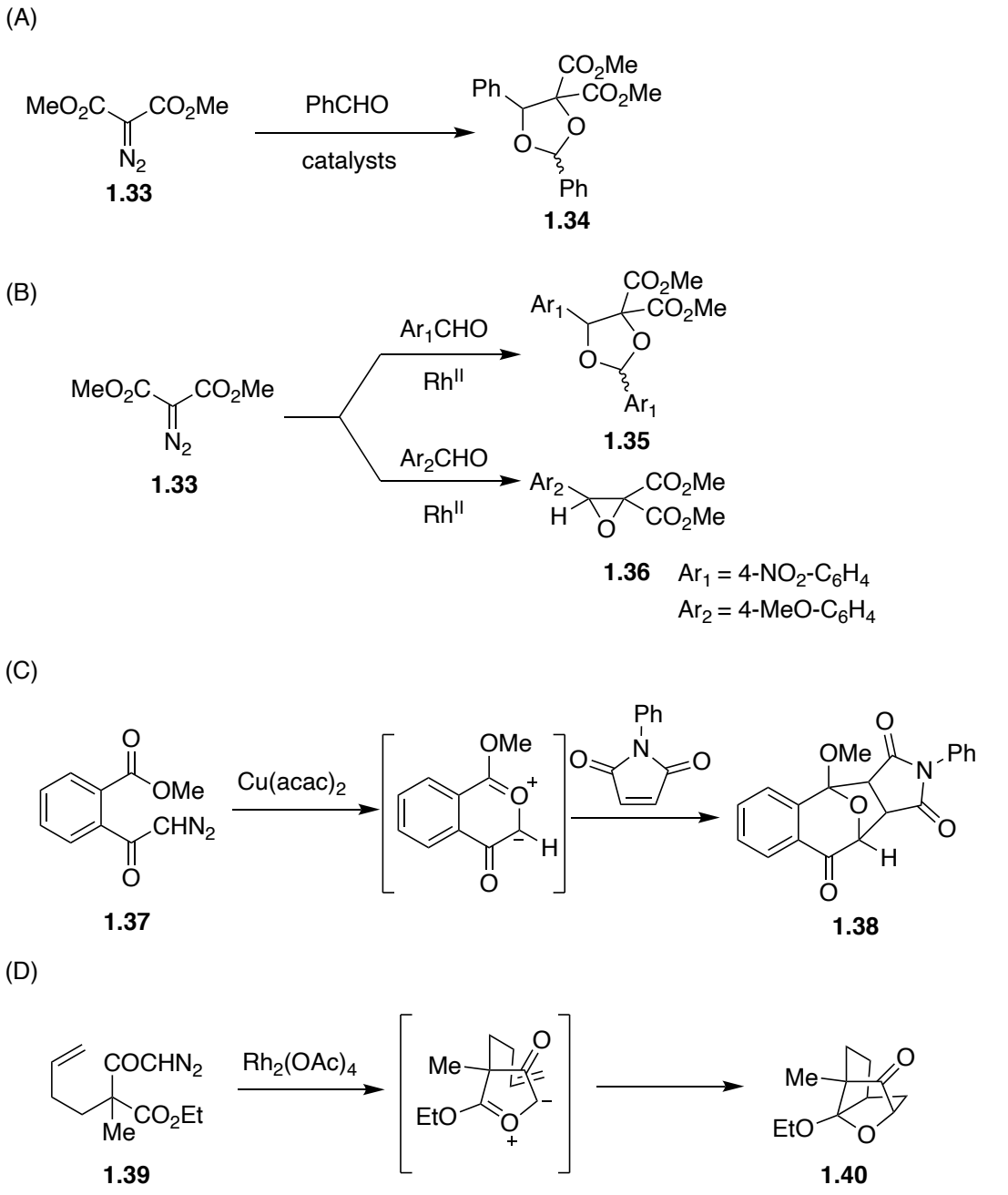

Figure 1.3. Early examples of carbonyl ylide formation.

Common methods to generate carbonyl ylides include the thermolysis or photolysis of epoxides with electron-withdrawing functional groups or the thermal extrusion of nitrogen from 1,3,4-oxadiazolines.[55-58] One of the simplest methods is the addition of a

metallocarbene onto the oxygen atom of a carbonyl compound, especially after the advent of the rhodium(II) catalysts for generating carbenoids from the decomposition of α-diazo carbonyl compounds.[59,60] Rhodium mediated carbenoid generation generally proceeds under milder reaction conditions compared with Cu and its complexes. Carbonyl ylides readily react with π-bonds via an addition to generate wide range of cycloadducts. An attractive feature of the tandem carbonyl ylide formation-cycloaddition method is the opportunity to control the stereochemistry of the product at several centers. The final product represents a highly functionalized cyclic intermediate that can be further subjected to synthetic elaborations. Padwa and co-workers have made pioneering contributions to the field of synthetic application of the tandem carbonyl ylide cyclization-cycloaddition sequence.[19] Indeed, a wide variety of oxapolycyclic ring systems have been prepared by Padwa featuring the tandem carbonyl ylide cyclization-cycloaddition sequence. Inspired by this highly effective synthetic method, we intended to utilize it constructing the tricyclic core structure in the melicolone natural products.[61-68]

1.4.2 Rh(II) Catalyzed Carbonyl Ylide Cycloaddition Model Studies

With cycloaddition precursor **1.20** in hand, we initiated the 1,3-dipolar cycloaddition studies. Most precedents of carbonyl ylide generation involve cyclization of ketones, esters, and amides with a metallocarbene.[24,25,59] Precedents of intermolecular cycloaddition of carbonyl ylides generated from alkyl aldehydes were limited, so we decided to start with simplified model studies to demonstrate the reactivity of **1.20** (Table 1.2).[15] We used dimethyl acetylenedicarboxylate (DMAD) as the dipolarophile to react with the carbonyl ylide generated from **1.20**, since it is highly electrophilic, and the cycloaddition product would not have regioisomers or diastereoisomers thus simplifying the analysis. In terms of catalysts, we tested both $Rh_2(OAc)_4$ and $Rh_2(OPiv)_4$ as they were

each reported to promote 1,3-dipolar cycloaddition reactions with diazo compounds. $Rh_2(OPiv)_4$ was shown to have better solubility in the solvents for same type of reactions. As for solvents, both CH_2Cl_2 and toluene were tested since they were commonly used in 1,3-dipolar cycloadditions. We started with $Rh_2(OAc)_4$ in CH_2Cl_2 at room temperature, but no product was isolated (Entry 1). Switching the catalyst from $Rh_2(OAc)_4$ to $Rh_2(OPiv)_4$ afforded the desired product **1.41** at room temperature in toluene and CH_2Cl_2 (Entries 2 and 3). When reactions were heated, they proceeded much faster in toluene and CH_2Cl_2 and provided higher yields (Entries 4-7). The best result was obtained by refluxing the solution **1.20** and DMAD in CH_2Cl_2 in the presence of $Rh_2(OPiv)_4$ for 6 h to afford **1.41** in 87% yield (Entry 6). These results indicated that the diazo aldehyde **1.20** cyclized to a carbonyl ylide in the presence of Rh(II) catalyst and that this ylide further reacts with dipolarophiles such as DMAD to form cycloaddition products.

Table 1.2. Condition screening of the cycloaddition reaction of **1.20** and DMAD.

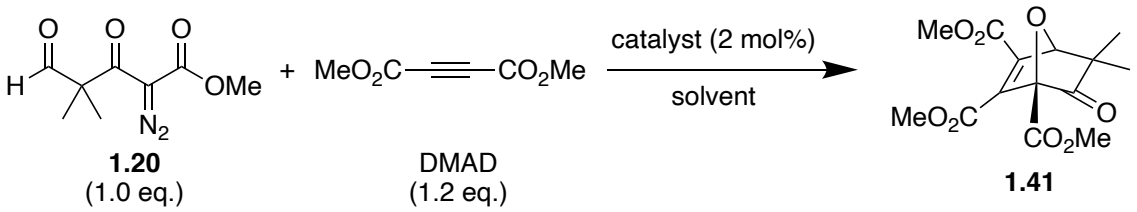

entry	catalyst	solvent	temperature	time	% yield[a]
1	$Rh_2(OAc)_4$	CH_2Cl_2	rt	overnight	NR
2	$Rh_2(OPiv)_4$	toluene	rt	overnight	42
3	$Rh_2(OPiv)_4$	CH_2Cl_2	rt	overnight	20
4	$Rh_2(OAc)_4$	toluene	100 ºC	1 h	26
5	$Rh_2(OPiv)_4$	toluene	100 ºC	1 h	52
6	$Rh_2(OAc)_4$	CH_2Cl_2	reflux	6 h	87
7	$Rh_2(OPiv)_4$	CH_2Cl_2	reflux	6 h	58

[a] *yields are based upon products purified by column chromatography*

Another aspect of the proposed 1,3-dipolar cycloaddition we needed to address was the regioselectivity of the reaction. The regioselectivity of Rh(II) catalyzed 1,3-dipolar cycloadditions is largely determined by electronic properties of the dipole and dipolarophile, and one of the easiest ways to predict the regioselectivity for the cycloaddition reaction is via the polarization analysis of carbonyl ylides and the dipolarophiles.[69] FMO theories were also employed to explain the regioselectivity of the reactions.[70,71]

Based on the precedents, the regioselectivity can be varied by using different dipolarophiles (Figure 1.4). For electron deficient dipolarophiles such as methyl propiolate **1.43**, cyclopentenone **1.45**, and cyclohexanone **1.47**, the carbonyl ylide generated from **1.42** reacts with the dipolarophile to afford a single regioisomer (Figure 1.4A-C).[72,73] When the same carbonyl ylide generated from **1.42** reacts with more electron rich dipolarophiles such as methyl propargyl ether **1.49**, the opposite regioisomer was obtained as the dominant product (Figure 1.4D).[72] A similar regioselective outcome was also obtained when **1.51** reacts with chloropropene **1.52** (Figure 1.4E).[74]

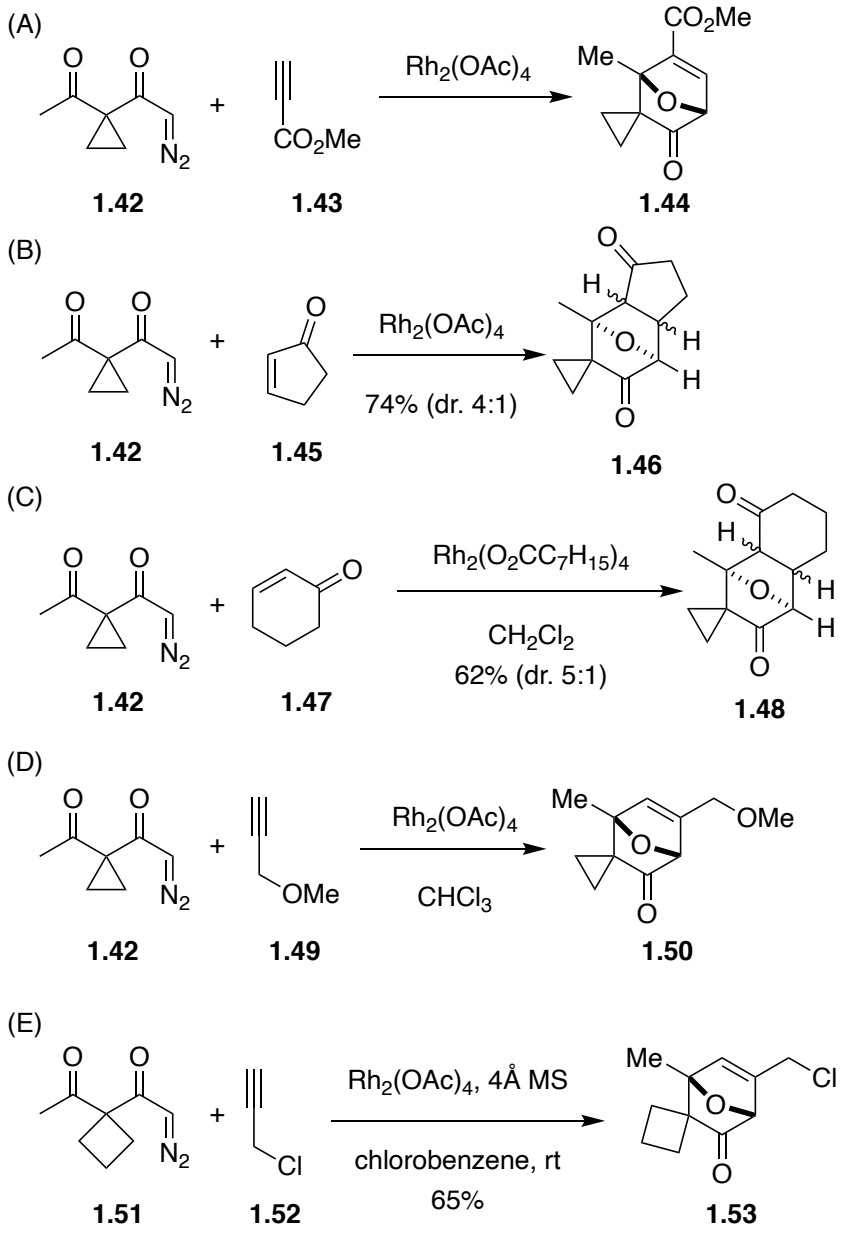

Figure 1.4. Examples of different regioselectivity outcomes of 1,3-dipolar cycloadditions.

Based on the analysis of regioselective outcomes of known 1,3-dipolar cycloaddition reactions with various dipolarophiles, we decided to initiate our investigation using the relative electron rich dipolarophile allyl methyl ether **1.58**, since desired

regioselectivities were obtained in reported examples of 1,3-dipolar cycloadditions with electron rich dipolarophiles.[72,74] The allyl methyl ether **1.58** was synthesized following a reported procedure by Deslongchamps (Scheme 1.5).[75] The synthesis commenced with methyl acetoacetate (**1.21**), which underwent ketal formation with ethylene glycol giving ketal **1.54** in 73% yield. Reduction of ester **1.54** with LAH afforded alcohol **1.55** in 89% yield, and the oxidation with IBX furnished aldehyde **1.56** in 88% yield. However, the aldehyde **1.56** was found to be unstable, so it was directly treated with vinyl magnesium bromide to afford allyl alcohol **1.57** in 79% yield. Finally, the methylation of **1.57** with MeI and NaH yielded target allyl methyl ether **1.58** in 96% yield.

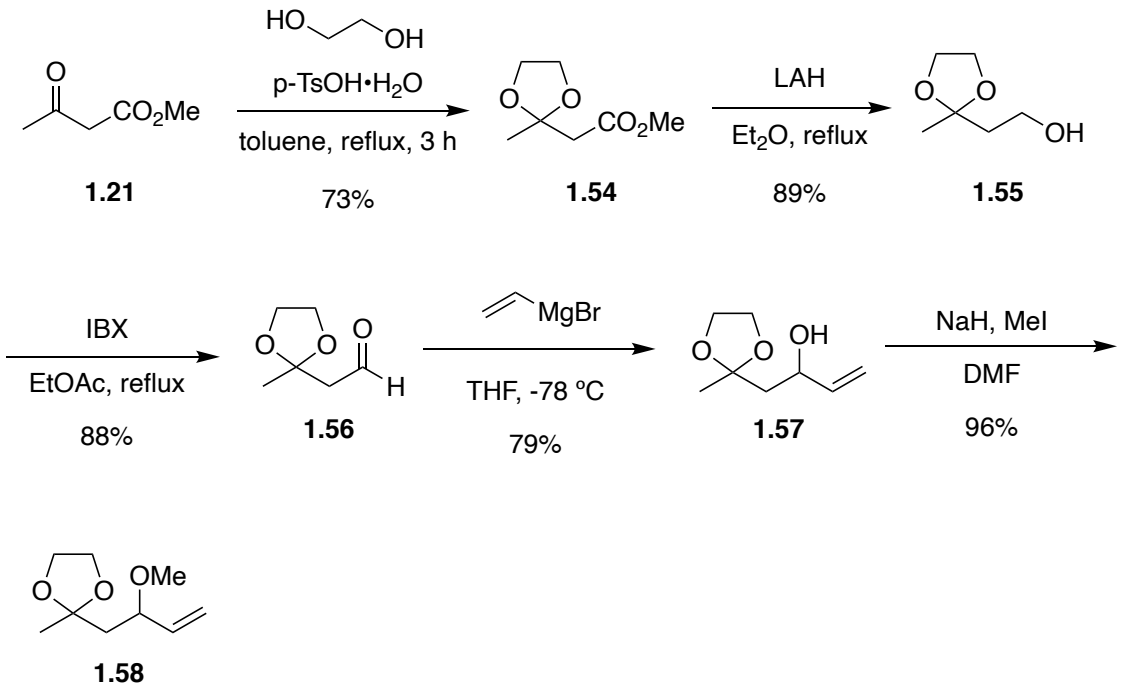

Scheme 1.5. Synthesis of dipolarophile **1.58**.

With the allyl methyl ether **1.58** in hand, we investigated the cycloaddition of diazo aldehyde **1.20** with **1.58** in the presence of Rh(II) catalysts (Equation 1.12). With reaction

of **1.20** and **1.58** in the presence of 2 mol% $Rh_2(OAc)_4$ in CH_2Cl_2 at room temperature only afforded trace amounts of product **1.59**. To our delight, when we heated the solution of **1.20** and **1.58** under reflux with 2 mol% $Rh_2(OAc)_4$ in CH_2Cl_2, **1.59** was isolated in 50% yield. We were able to confirm the structure of **1.59** based on 2D NMR spectra (HSQC, HMBC and COSY). When the solution of **1.20** and **1.58** in the presence of $Rh_2(OAc)_4$ or $Rh_2(OPiv)_4$ was heated under reflux in toluene, similar yields of **1.59** in 48 and 55% were obtained.

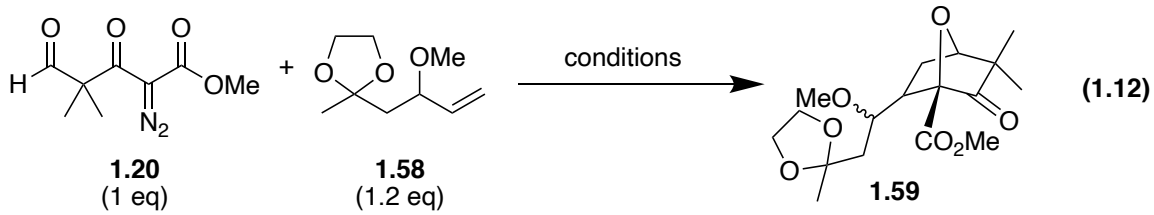

1.20 (1 eq) + **1.58** (1.2 eq) → **1.59** **(1.12)**

conditions	% yield
2 mol% $Rh_2(OAc)_4$, CH_2Cl_2, rt	trace
2 mol% $Rh_2(OAc)_4$, CH_2Cl_2, reflux	50
2 mol% $Rh_2(OAc)_4$, toluene, reflux	48
2 mol% $Rh_2(OPiv)_4$, toluene, reflux	55

The structure assignment of **1.59** is based upon extensive evidence derived from 2D NMR spectra (HSQC, HMBC, and COSY). The characteristic peak having a chemical shift of δ 4.29 ppm, which is a doublet, arises from the bridgehead proton at C1 (Figure 1.5). This assignment is made based upon the HMBC spectrum, in which correlations between C1-H and C2, C3, C4 are observed (Figure 1.6). HMBC typically shows correlations between protons and carbons that are one, two and sometimes in conjugated system three atoms away; C1-H and C4 are two atoms removed through the oxygen bridge.

The correlations between C1-H and both C2 and C3 indicate C2 and C3 are within two C atoms from C1-H. There is no correlation between C1-H and C5 because C5 is three atoms away from C1-H in **1.59**, whereas in the other regioisomer it would be two atoms removed. This observation supports the regiochemistry of the major product as being **1.59**.

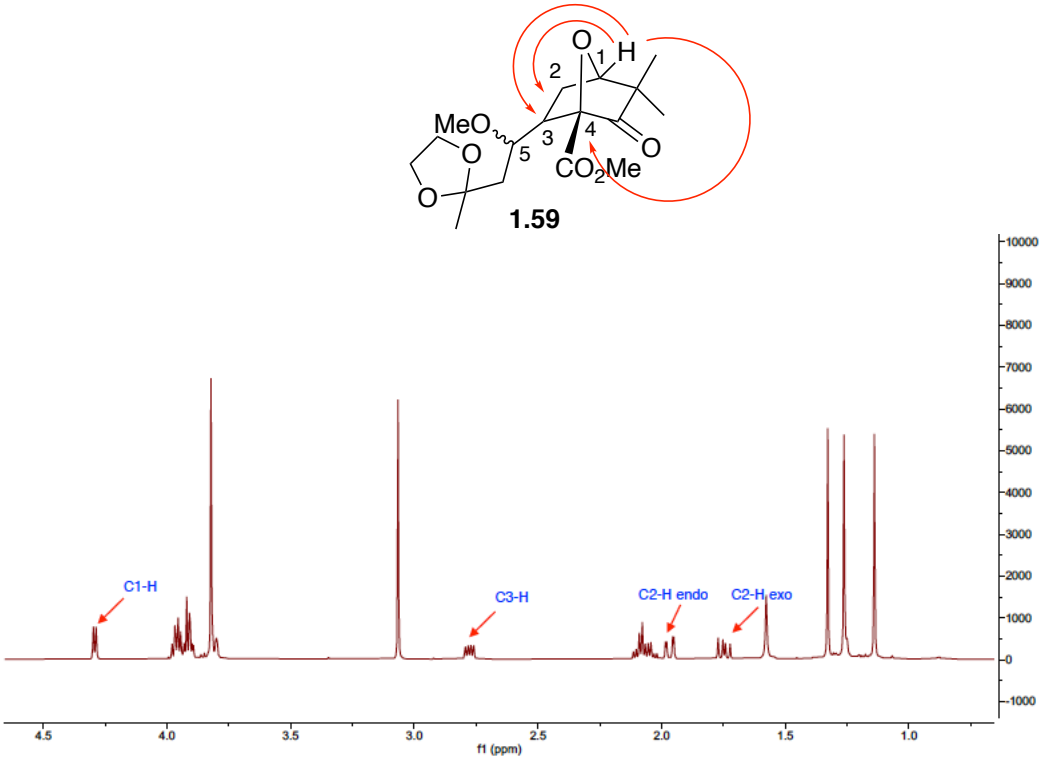

Figure 1.5. Key assignments of **1.59** on ^{1}H spectrum.

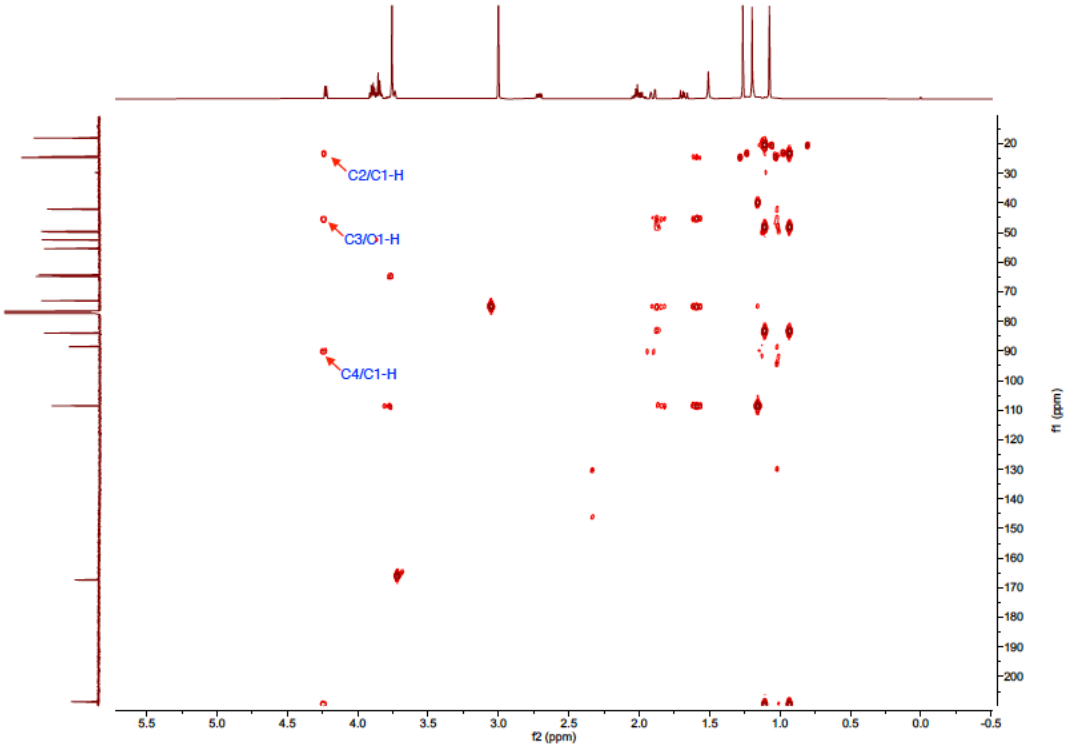

Figure 1.6. Key HMBC correlations of **1.59**.

With these encouraging results, we next attempted to simplify the synthetic route by using alternative dipolarophiles. The allyl methyl ether **1.58** in model system study was synthesized in over five steps, and we will have to deprotect the methyl ether group in later stage of the synthesis, which could be potentially problematic. Although we were not aware of any reports on the cycloaddition reaction with allyl alcohol dipolarophiles, we were interested in the cycloaddition with allyl alcohol **1.57** as the dipolarophile. Allyl alcohol **1.57** which was the intermediate used to prepare **1.58**, requires one less step to make, and it has a similar polarity distribution as the dipolarophile **1.58**. The solution of **1.20** with **1.57** in toluene was heated under reflux in the presence of 2 mol% Rh_2OAc_4, but to our surprise, we only isolated hemi ketal cycloadduct **1.60**.

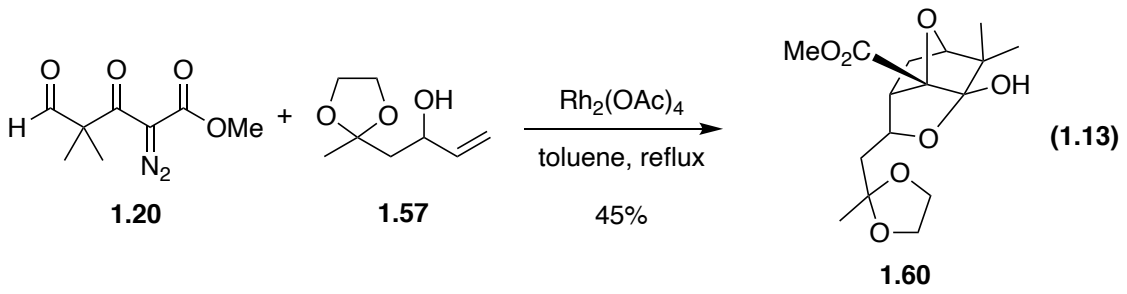

Since hemiacetals and hemiketals have been reported to undergo oxidation with PDC to form the corresponding aldehyde or ketone, we attempted to convert **1.60** to **1.61** using these conditions.[76] However, the desired ketone **1.61** was not isolated by the oxidation of **1.60** by PDC in CH_2Cl_2; only starting material **1.60** was recovered (Equation 1.14).

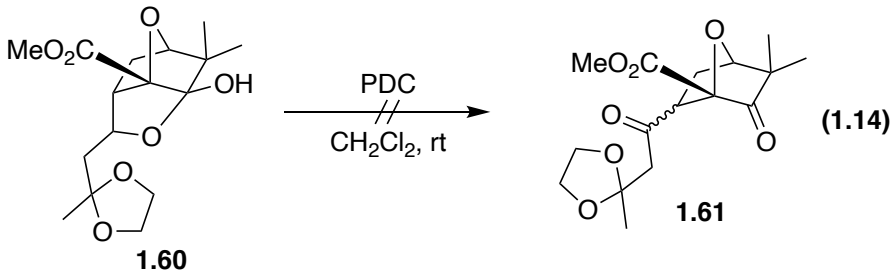

Because the hemiketal **1.60** formed from the cycloaddition reaction was generated from a very sterically hindered ketone, we wondered whether lowering the reaction temperature could potentially suppress the formation of hemiketal **1.60** and generate **1.62**. To test this hypothesis, we treated **1.20** with **1.57** in the presence of 2 mol% $Rh_2(OAc)_4$ in toluene at 40 ºC, and we isolated 20% of the desired product **1.62** (Equation 1.15). We also tested the reaction of **1.20** with **1.57** in the presence of 2 mol% $Rh_2(OAc)_4$ in CH_2Cl_2 under reflux, and the desired product **1.62** was isolated in 45% yield, with another 15% inseparable mixture with correct mass on LCMS (Equation 1.16).

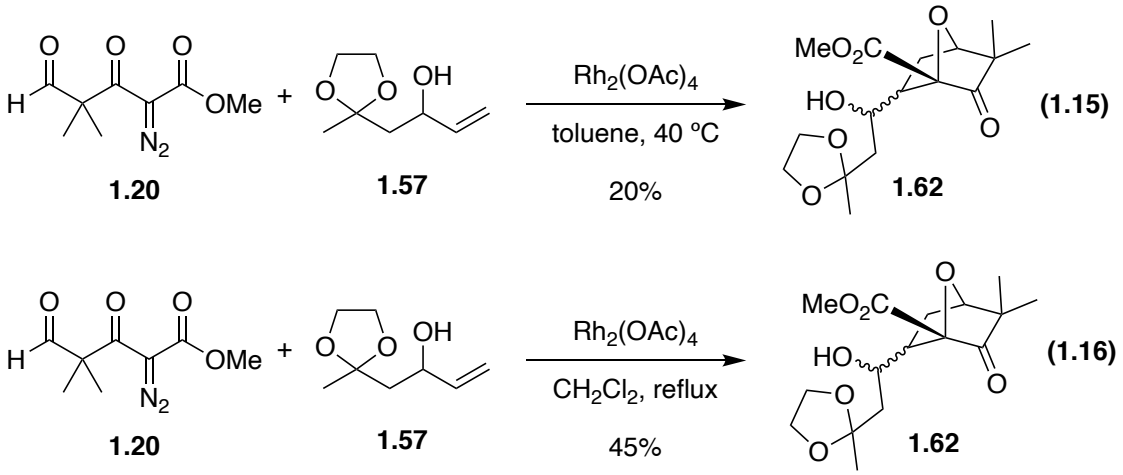

1.20 1.57 1.62

1.20 1.57 1.62

With **1.62** in hand, we attempted to oxidize alcohol **1.62** to ketone **1.61**. Toward the end, a solution of **1.62** with IBX in EtOAc was heated under reflux but desired product **1.61** was not formed. Gratifyingly, when we switched to the Swern oxidation condition, desired ketone **1.61** was obtained in 42% yield as a single diastereomer (Equation 1.17).

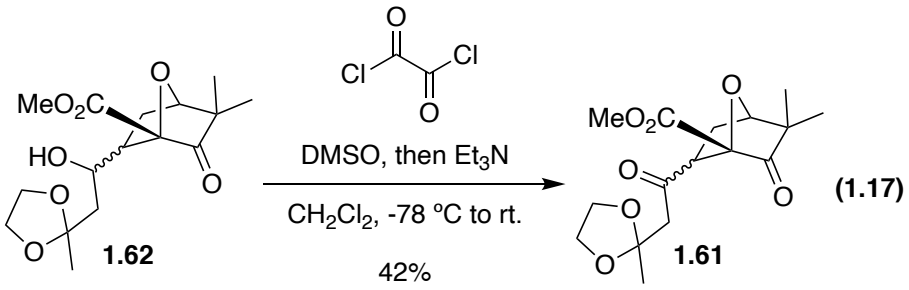

1.62 1.61

At this juncture, we sought to further simplify the sequence. Accordingly, we explored the 1,3-dipolar cycloaddition between **1.20** and enone **1.63**, even though neither the regioselectivity analysis based on polarity, nor the relevant precedents indicated the desired regioisomer would be the major product.[73,77] However, we anticipated that the geminal dimethyl group present in the carbonyl ylide intermediate would have steric

interactions with the ketal moiety of **1.63** in the transition state of the cycloaddition reaction, thus disfavoring the formation of the undesired regioisomeric cycloadduct and favoring the desired cycloadduct. Moreover, we were also interested to have more insights into the determining factors in the regioselectivity of the 1,3-dipolar cycloadditions in general. The synthesis of enone dipolarophile **1.63** was fairly straightforward, and it was readily available from direct oxidation of allyl alcohol **1.57** by Jones reagent in 45% yield (Equation 1.18).

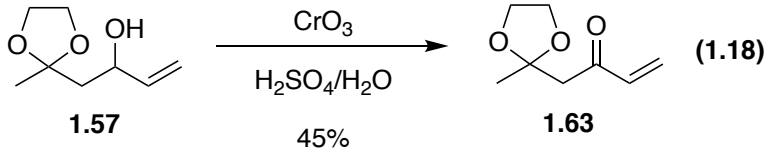

1.57 **1.63** **(1.18)**

With enone **1.63** in hand, we next investigated the carbonyl ylide cycloaddition of **1.20** and **1.63**. A solution of **1.20** and **1.63** in toluene was heated under reflux in the presence of 2 mol% $Rh_2(OAc)_4$ (Equation 1.19). To our delight, we isolated three pure diastereomers **1.64** (35%), **1.65** (4%), and **1.66** (3%) from the reaction mixture. All three structures have been confirmed by ^1H NMR, ^{13}C NMR, HSQC, HMBC, COSY, and NOESY characterization. The regioselective outcome of this 1,3-dipolar cycloaddition was relatively unexpected based on the fact that almost all similar reactions gave the regioselectivity outcomes consent to the polarity analysis. However, as we anticipated, the regioselective outcome of this 1,3-dipolar cycloaddition reaction appears to be controlled by the steric interactions discussed before. With the quick access to grams of cycloadduct **1.64** and **1.65** via the conditions we developed, we were able to move forward to explore the alkylation of the cycloadduct.

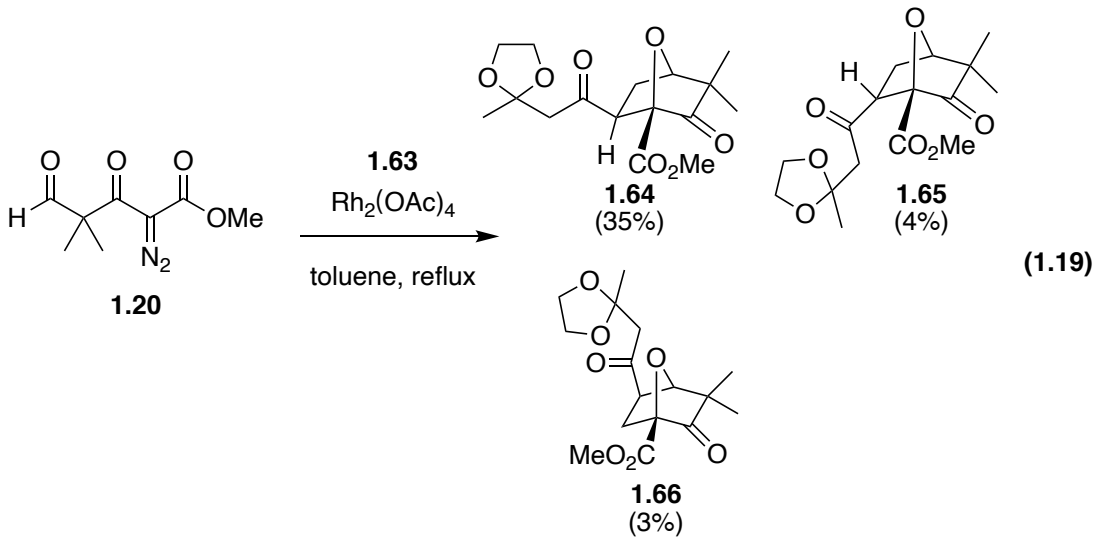

The structure assignment of **1.64** is based upon extensive evidence derived from 2D NMR spectra (HSQC, HMBC, COSY and NOESY). The characteristic peak having a chemical shift of δ 4.47 ppm, which is a doublet, arises from the bridgehead proton at C1 (Figure 1.7). This assignment is made based upon the HMBC spectrum, in which correlations between C1-H and C2, C3, C4 are observed (Figure 1.8). HMBC typically shows correlations between protons and carbons that are one, two and sometimes in conjugated system three atoms away; C1-H and C4 are two atoms removed through the oxygen bridge. The correlations between C1-H and both C2 and C3 indicate C2 and C3 are within two C atoms from C1-H. There is no correlation between C1-H and C5 because C5 is three atoms away from C1-H in **1.64**, whereas in the regioisomer **1.66** it would be two atoms removed. This observation supports the regiochemistry of the major product as being **1.64**.

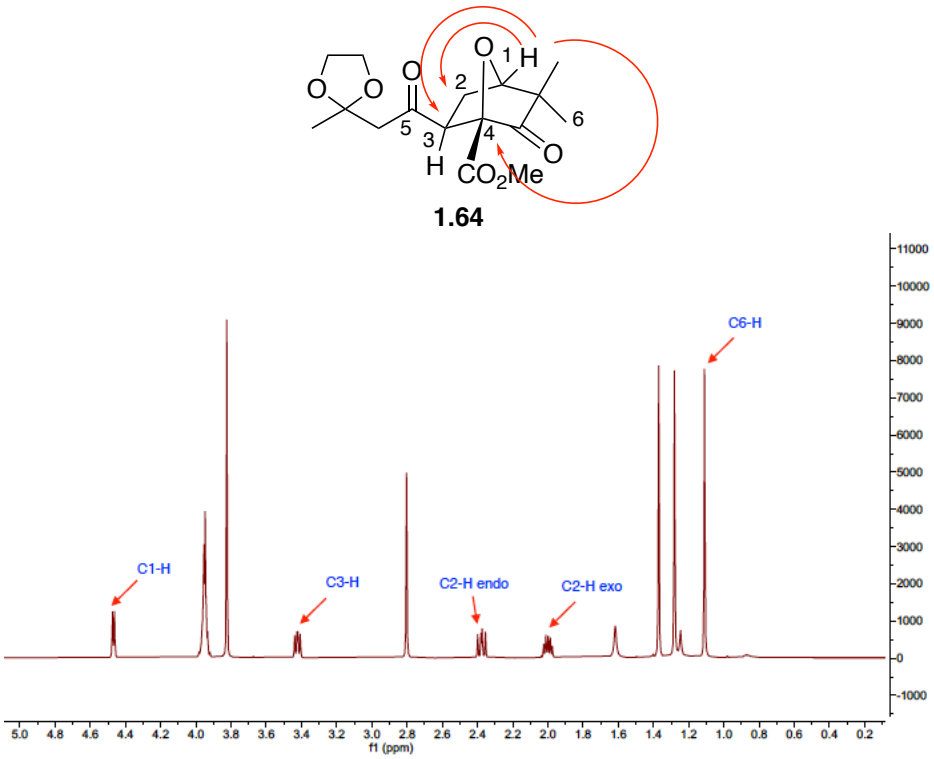

Figure 1.7. Key assignments of **1.64** on ^{1}H spectrum.

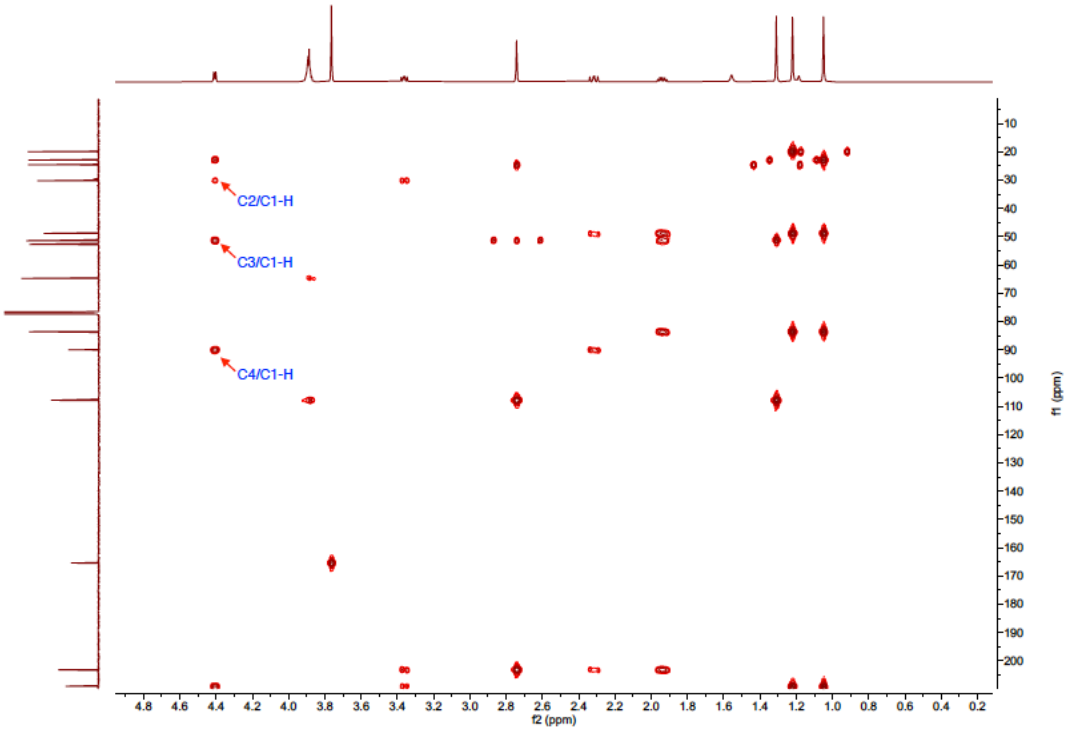

Figure 1.8. Key HMBC correlations of **1.64**.

The NOESY spectrum of **1.64** was also used to support its structural assignment (Figure 1.9). Of particular importance are the observed correlations between C2-H and C6-H, C2-H and C3-H. The NOESY correlation between the proton on C2 and the C6-CH_3 *gem*-dimethyl group suggests this proton is *endo*, because there would be no correlation of this proton with either of the *gem*-dimethyl groups if it were *exo*. The correlation between the *endo*-proton at C2 with the proton at C3 suggests that the C3-H is also *endo*. Moreover, the coupling constant between C3-H and the assigned *endo* C2-H is 9.4 Hz that is greater than that of C3-H and the assigned *exo* C2-H which is 6.4 Hz.These observations support the stereochemical assignment at C3 of **1.64**.

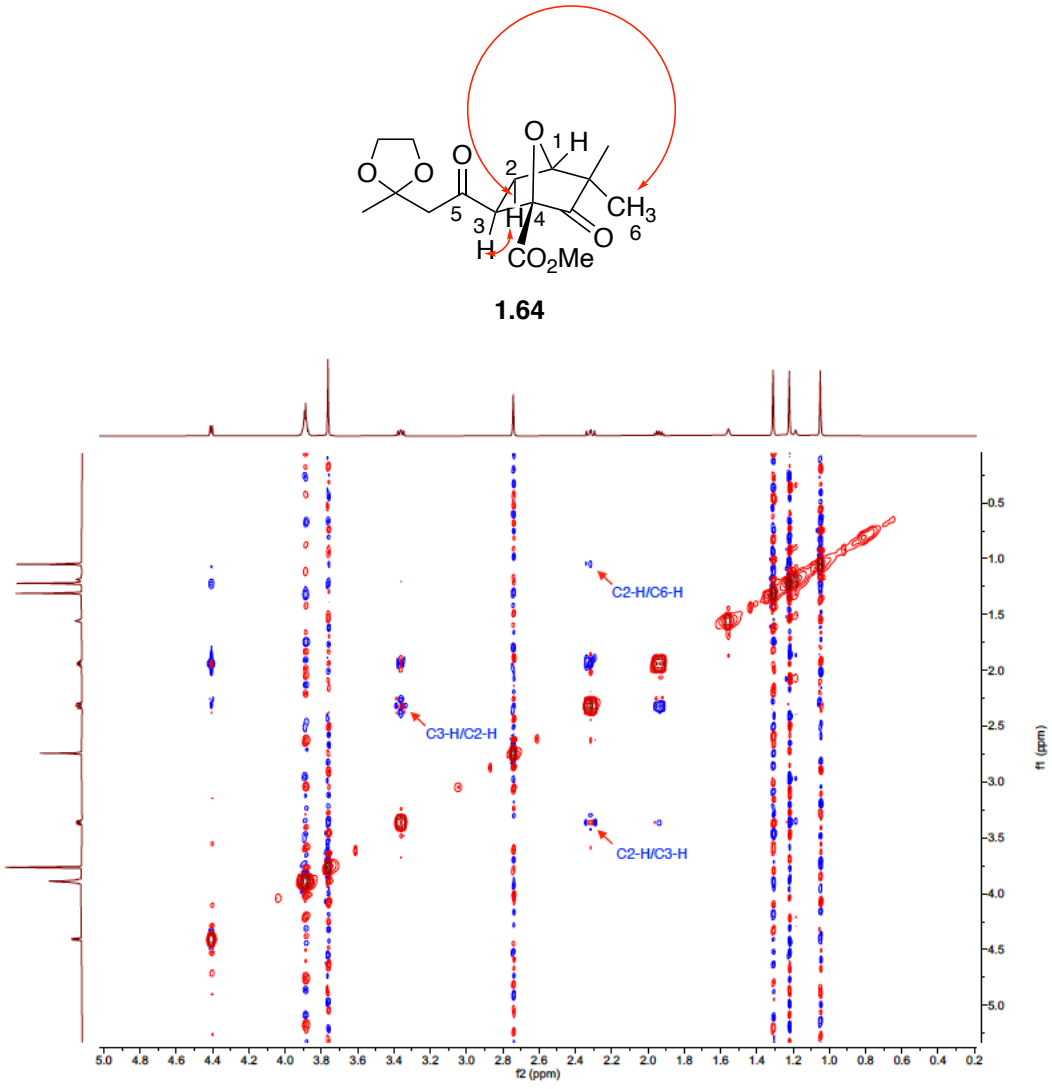

Figure 1.9. Key NOESY correlations of **1.64**.

The structure assignment of **1.65** is based upon extensive evidence derived from 2D NMR spectra (HSQC, HMBC, COSY and NOESY). The characteristic peak having a chemical shift of δ 4.39 ppm, which is a doublet, arises from the bridgehead proton at C1 (Figure 1.10). This assignment is made based upon the HMBC spectrum, in which correlations between C1-H and C2, C3, C4 are observed (Figure 1.11). HMBC typically shows correlations between protons and carbons that are one, two and sometimes in

conjugated system three atoms away; C1-H and C4 are two atoms removed through the oxygen bridge. The correlations between C1-H and both C2 and C3 indicate C2 and C3 are within two C atoms from C1-H. There is no correlation between C1-H and C5 because C5 is three atoms away from C1-H in **1.65**, whereas in the regioisomer **1.66** it would be two atoms removed. This observation supports the regiochemistry of the major product as being **1.65**. The stereochemistry was not able to assigned from NOESY due to the overlap of both protons on C2; However, with the extensive evidence to confirm the stereochemistry of **1.64**, we therefore assigned **1.65** as the epimer of **1.64**.

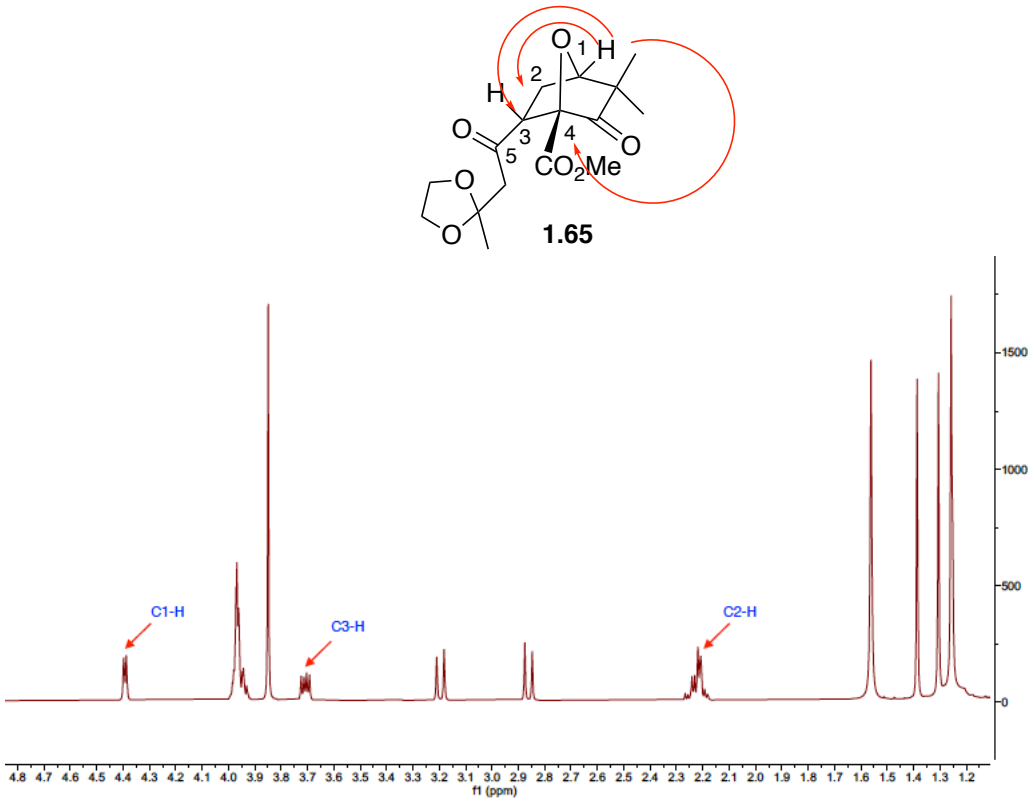

Figure 1.10. Key assignments of **1.65** on ^{1}H spectrum.

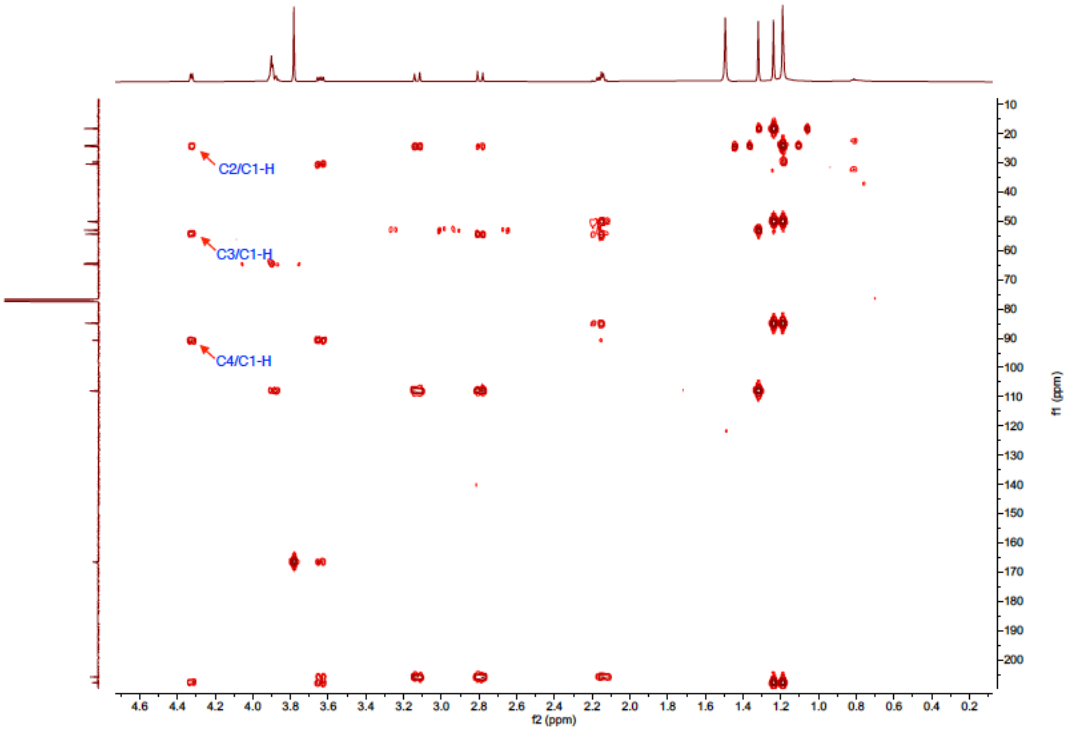

Figure 1.11. Key HMBC correlations of **1.65**.

The structure assignment of **1.66** is based upon extensive evidence derived from 2D NMR spectra (HSQC, HMBC, COSY and NOESY). The characteristic peak having a chemical shift of δ 4.68 ppm, which is a singlet, arises from the bridgehead proton at C1 (Figure 1.12). This assignment is made based upon the HMBC spectrum, in which correlations between C1-H and C2, C3, C4, C5 are observed (Figure 1.13). HMBC typically shows correlations between protons and carbons that are one, two and sometimes in conjugated system three atoms away; C1-H and C4 are two atoms removed through the oxygen bridge. The correlations between C1-H and C2, C3, C5 indicate C2, C3 and C5 are within two C atoms from C1-H, whereas in the regioisomers **1.64** and **1.65**, C5 would be three atoms removed. This observation supports the regiochemistry of the major product as being **1.66**.

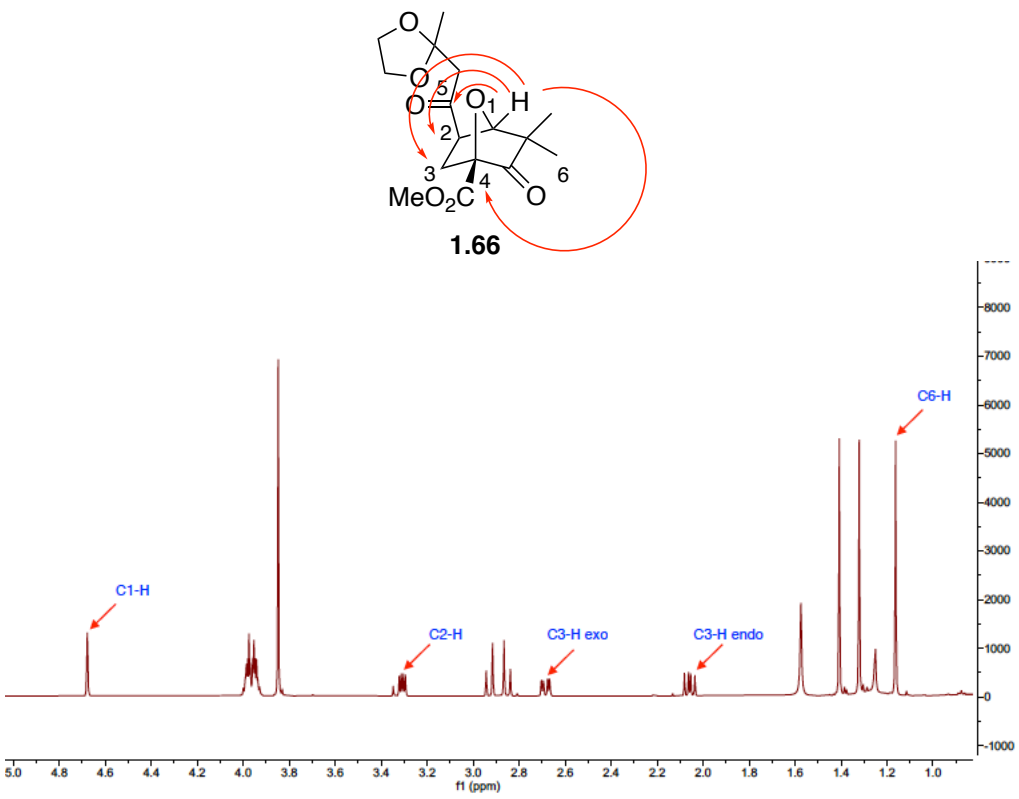

Figure 1.12. Key assignments of **1.66** on ^{1}H spectrum.

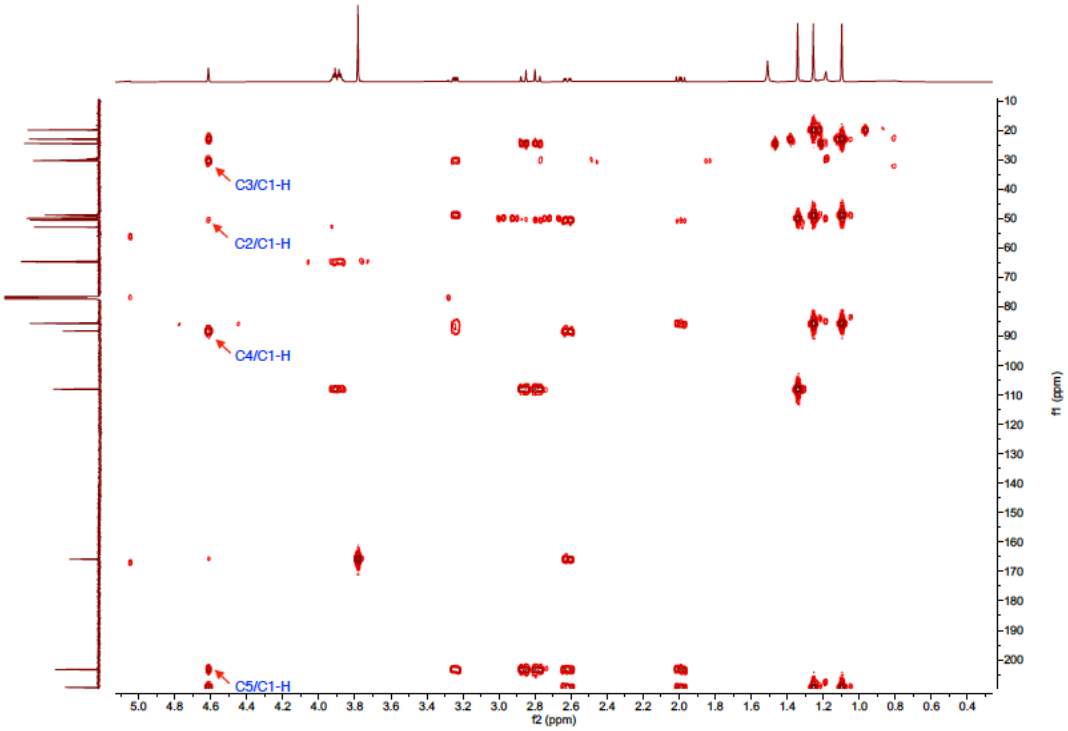

Figure 1.13. Key HMBC correlations of **1.66**.

The NOESY spectrum of **1.66** was also used to support its structural assignment (Figure 1.14). Of particular importance is the observed correlation between C2-H and C6-H. The NOESY correlation between the proton on C2 and the C6-CH_3 *gem*-dimethyl group suggests this proton is *endo*, because there would be no correlation of this proton with either of the *gem*-dimethyl groups if it were *exo*. Moreover, the coupling constant between C2-H and the assigned *endo* C3-H is 9.0 Hz that is greater than that of C2-H and the assigned *exo* C3-H which is 4.6 Hz. These observations support the stereochemical assignment at C2 of **1.66**.

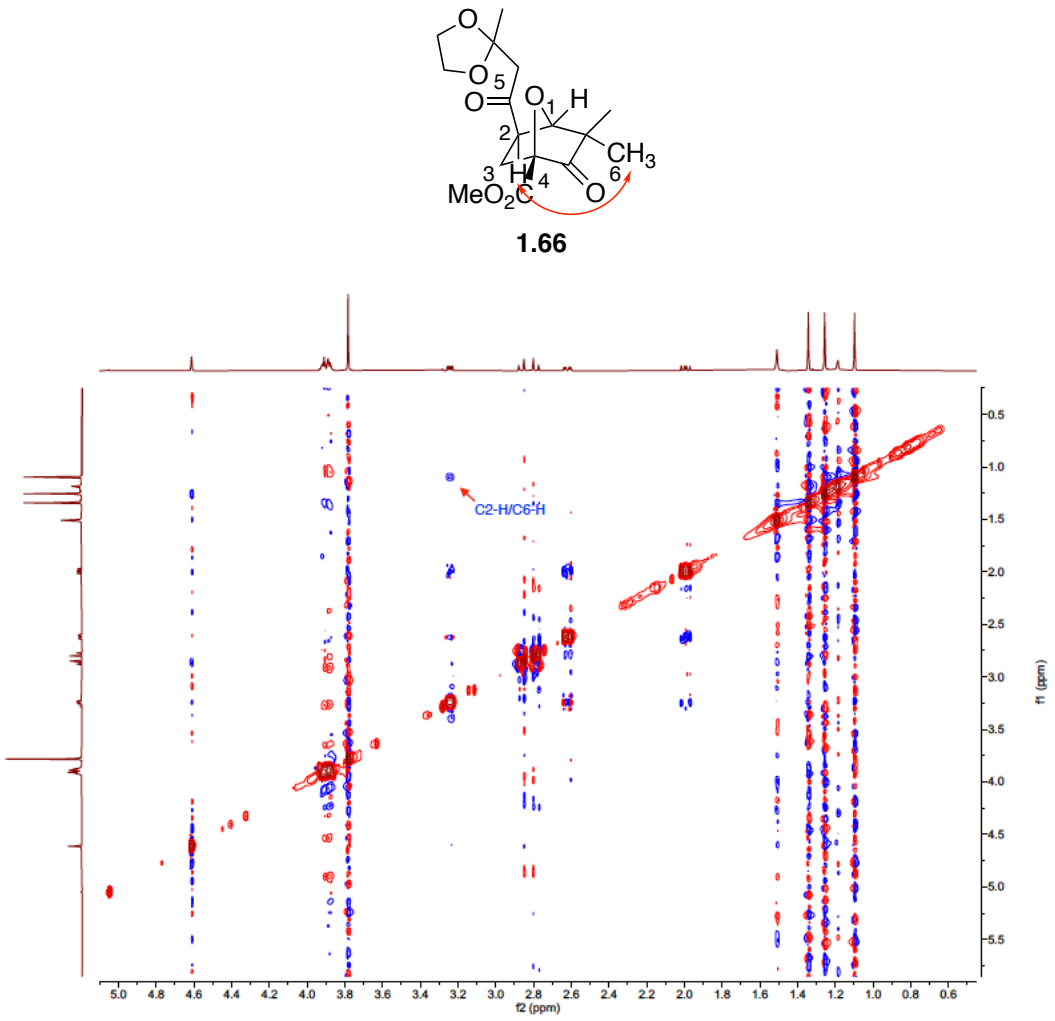

Figure 1.14. Key NOESY correlations of **1.66**.

1.5 STUDIES TOWARDS REGIOSELECTIVE GENERATION OF ENOLATES

With cycloadduct **1.64** and **1.65** in hand, we next investigated the stereoselective prenylation of the tertiary α-carbon of the cycloadduct. In order to successfully form the prenylated product, we need to selectively generate the desired enolate under basic conditions (Equation 1.20). In cycloadduct **1.64**, there are two different sets of α-protons on C-1 and C-2. However, we hoped we could use a suitable strong base to selectively deprotonate the α-proton at C-1 over C-2. We were cognizant of the rather speculative

nature of our hypothesis, but the experiments were easy to try. The subsequent addition of alkylating reagent would furnish the alkylation product **1.67**.

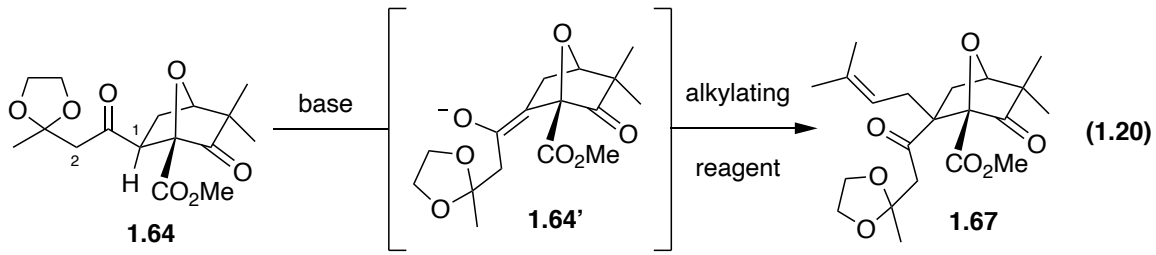

There was problem associated with enolate generation that involved β-elimination. For example, Padwa reported examples of base-induced β-elimination of the oxa-tricyclic species **1.68** and **1.70**.[73,78] They found that a carbanionic center adjacent to the oxy bridge of **1.68** led to the ring opening process in their studies towards the total synthesis of illudins (Equation 1.21).[73] A similar reaction pathway was observed when treating **1.70** with KHMDS in the synthesis towards pterosin family sesquiterpenes (Equation 1.22).[78]

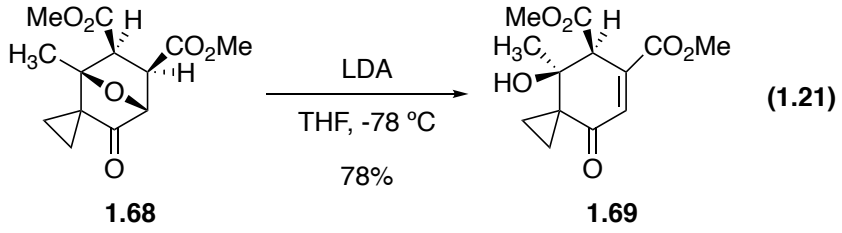

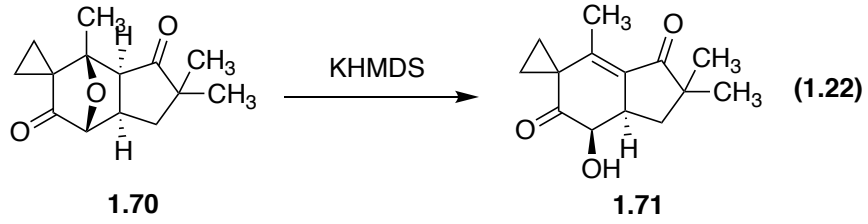

With further analyses, we decided to initiate our investigations by screening conditions to generate desired enolate first (Table 1.3). We first treaed cycloadduct **1.64** with LDA, which was generated *in situ* by treating diisopropylamine with *n*-BuLi in THF, and the solution was stirred at -78 ºC for 30 min before being quenched by the addition of D_2O (Entry 1). The reaction mixture was worked up and analyzed by NMR, but no desired deuterium incorporation was observed; rather starting material **1.64** was recovered. We next tried treating **1.64** with LDA in THF at -78 ºC followed by warming the reaction up to -40 ºC, but only a complex mixture was obtained after D_2O quenching (Entry 2). We next screened common strong bases such as $LiNEt_2$, $LiNMe_2$, NaHMDS, KHMDS; however, we were not able to obtain the desired deuterium incorporation products. Instead, by treatment of **1.64** with $LiNEt_2$ at -78 ºC, a mixture of **1.64**, **1.64''** and **1.64'''** was obtained after 60 min (Entry 3). Treatment of **1.64** with $LiNMe_2$ furnished a complex mixture, whereas treatment of **1.64** with NaHMDS and KHMDS both furnished formation of **1.64'''** (Entries 4-6).

Table 1.3. Deuterium incorporation studies of cycloadduct **1.64**.

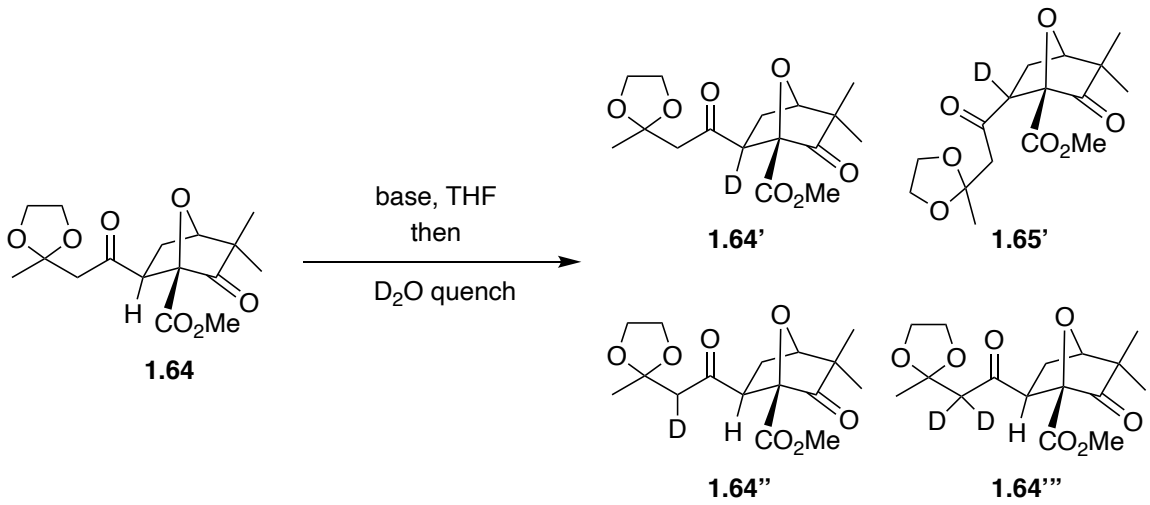

entry	base	temperature	time	result
1	LDA	-78 ºC	60 min	**1.64**
2	LDA	-78 ºC to -40 ºC	30 min	complex
3	$LiNEt_2$	-78 ºC	60 min	**1.64 1.64'' 1.64'''**
4	$LiNMe_2$	-78 ºC	30 min	complex
5	NaHMDS	-78 ºC	30 min	**1.64'''**
6	KHMDS	-78 ºC	30 min	**1.64'''**

With the extensive studies of the regioselective deprotonation of **1.64** with various bases, we were still unable to find out the optimal conditions to selectively generate the desired enolate. Ultimately, we proposed alternative cycloaddition and alkylation sequences to solve this problem.

1.6 ALTERNATIVE CYCLOADDITION & ALKYLATION SEQUENCE

1.6.1 Weinreb Amide Cycloadduct Transformation Sequence

With the regioselective enolate formation step being problematic, we proposed an alternative route to tackle the problem (Scheme 1.6). Instead of using a ketal protection group, we proposed to have the Weinreb amide cycloadduct **1.73**, which only has single α-proton thus making the enolate generation and alkylation steps more straightforward. Moreover, the Weinreb amide moiety can be further converted towards the natural product.

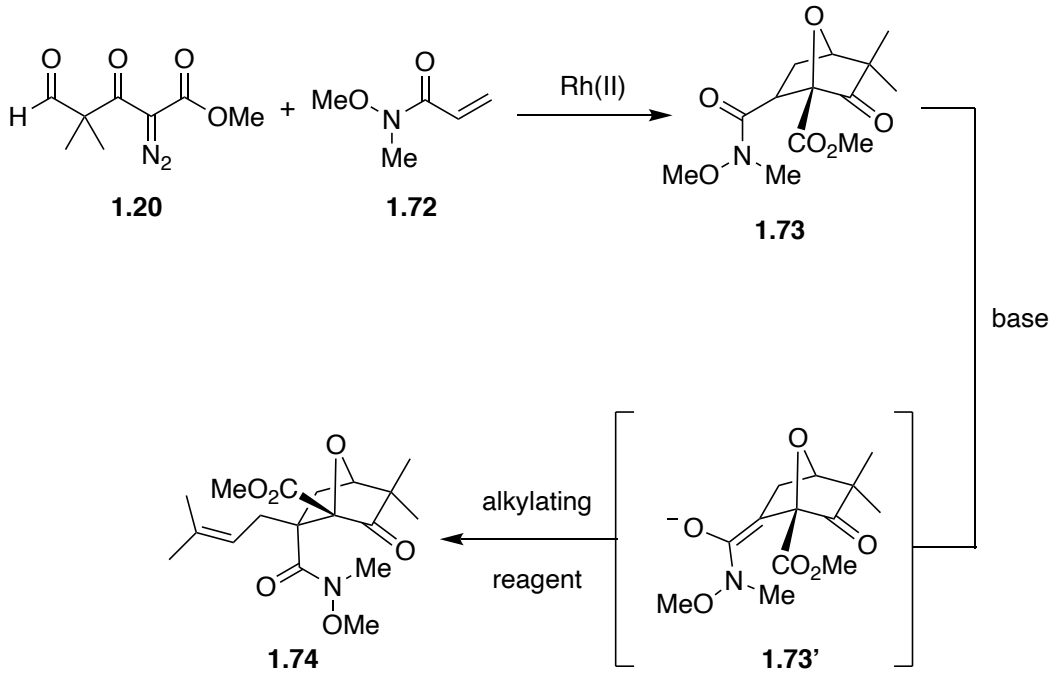

Scheme 1.6. Proposed alternative route to prenylated cycloadduct **1.74**.

1.6.1.1 Synthesis of the Weinreb Amide Cycloadduct

To explore the feasibility of the proposed alternative route, we initiated our investigation by synthesizing the Weinreb amide dipolarophile **1.72** (Scheme 1.7). Acryloyl chloride (**1.75)** was treated with N,O-dimethylhydroxylamine and $NaHCO_3$ in

CH_2Cl_2 to prepare Weinreb amide **1.72** in 70% yield. Subsequently, the 1,3-dipolar cycloaddition of **1.72** and **1.20** in the presence of $Rh_2(OAc)_4$ furnished cycloadduct **1.73** in 47% yield after isolation. The structure assignment of **1.73** is based upon extensive evidence derived from 2D NMR spectra (HSQC, HMBC, COSY and NOESY). The structures of **1.76** and **1.77** are putative based on the characteristic peaks of the C1 bridge head proton on the NMR of crude mixture of **1.73**, **1.76**, and **1.77**, and the yields of **1.76** and **1.77** are calculated based on the ratio of C1 protons of **1.73**, **1.76**, and **1.77** (Figure 1.15). The putative C1 proton of **1.76** having a chemical shift of 4.42. The peak is a doublet, which arising from the splitting between C1-H and *exo* C2-H. The endo C2-H typically doesn't split with C1-H due to the torsional angle close to 90 ºC. The putative C1 proton of **1.77** having a chemical shift of 4.58. The peak is a singlet, since the *endo* C2-H typically doesn't split with C1-H due to the torsional angle close to 90 ºC. The putative structures of **1.76** and **1.77** with the yields calculated from the ratio of C1-H account for the regio and stereoselectivity that is consistent with the result we obtained from similar 1,3-dipolar cycloadditions of **1.20** with enone dipolarophiles such as **1.18** and **1.63**.

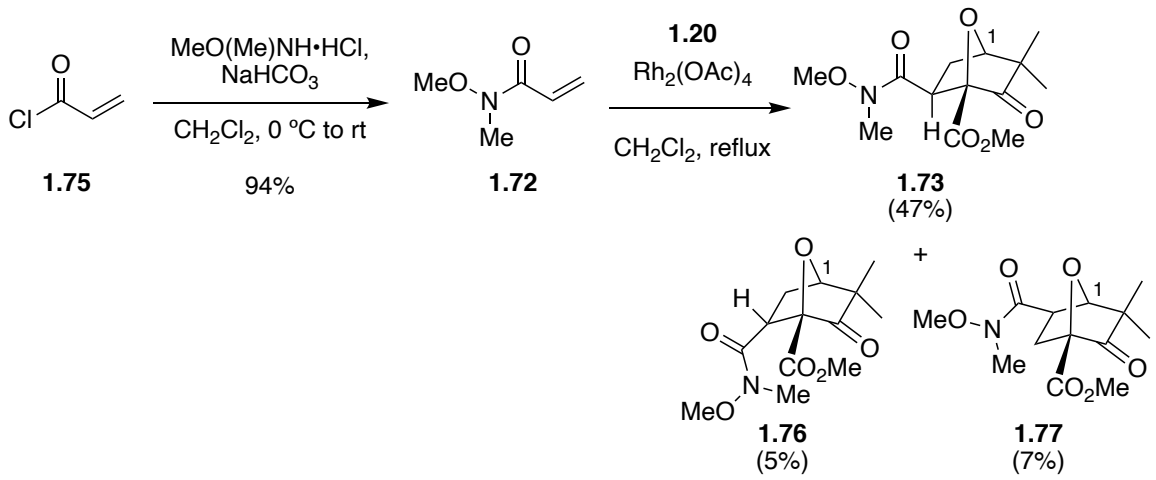

Scheme 1.7. Synthesis of Weinreb amide cycloadduct **1.73**.

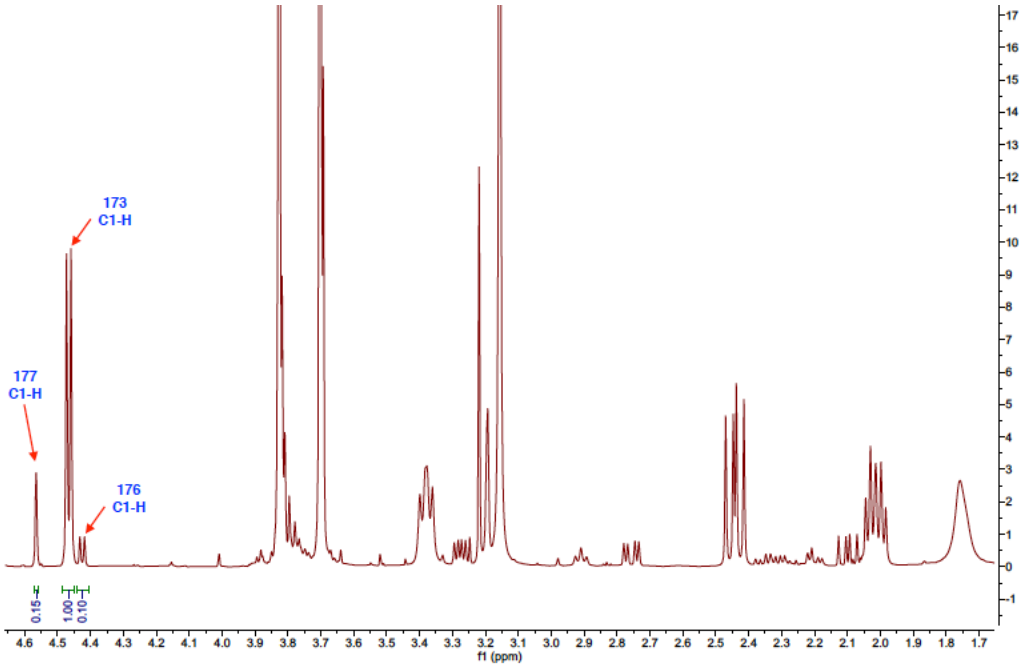

Figrue 1.15. NMR of crude mixture of **1.73**, **1.76**, and **1.77**.

The structure assignment of **1.73** is based upon extensive evidence derived from 2D NMR spectra (HSQC, HMBC, COSY and NOESY). The characteristic peak having a chemical shift of δ 4.47 ppm, which is a doublet, arises from the bridgehead proton at C1

(Figure 1.16). This assignment is made based upon the HMBC spectrum, in which correlations between C1-H and C2, C3, C4 are observed (Figure 1.17). HMBC typically shows correlations between protons and carbons that are one, two and sometimes in conjugated system three atoms away; C1-H and C4 are two atoms removed through the oxygen bridge. The correlations between C1-H and both C2 and C3 indicate C2 and C3 are within two C atoms from C1-H. There is no correlation between C1-H and C5 because C5 is three atoms away from C1-H in **1.73**, whereas in the regioisomer **1.77** it would be two atoms removed. This observation supports the regiochemistry of the major product as being **1.73**.

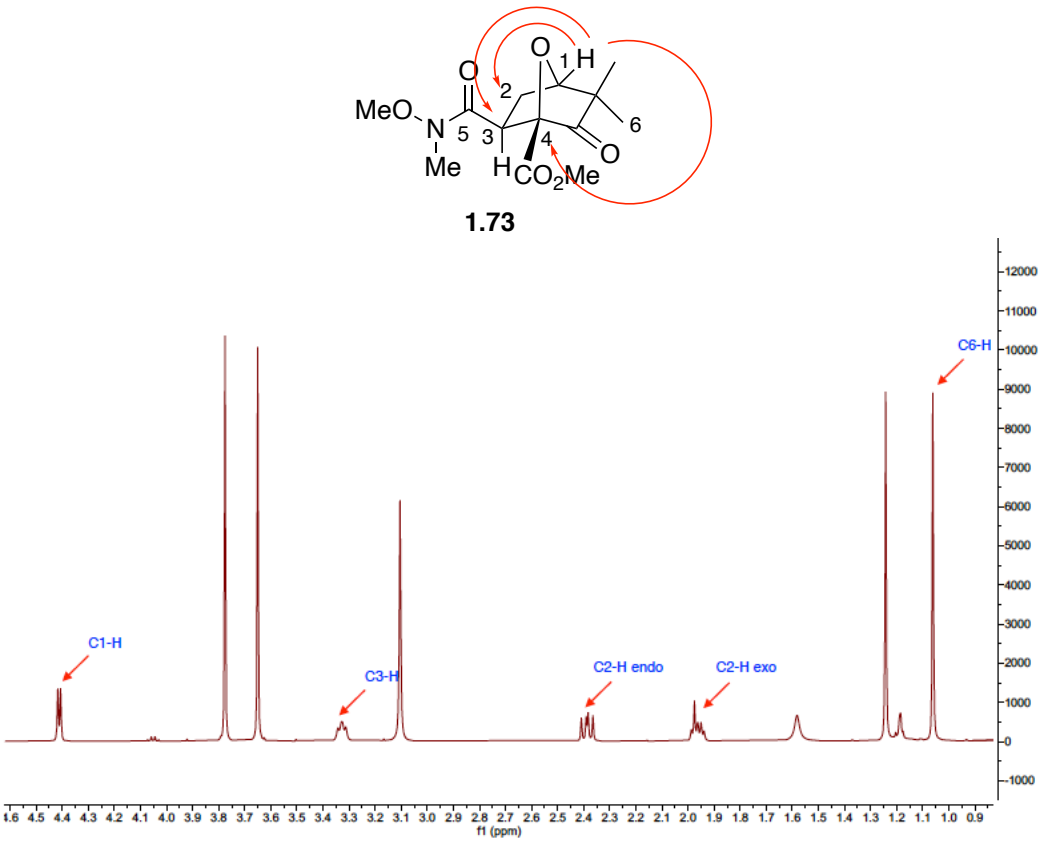

1.73

Figure 1.16. Key assignments of **1.73** on ^{1}H spectrum.

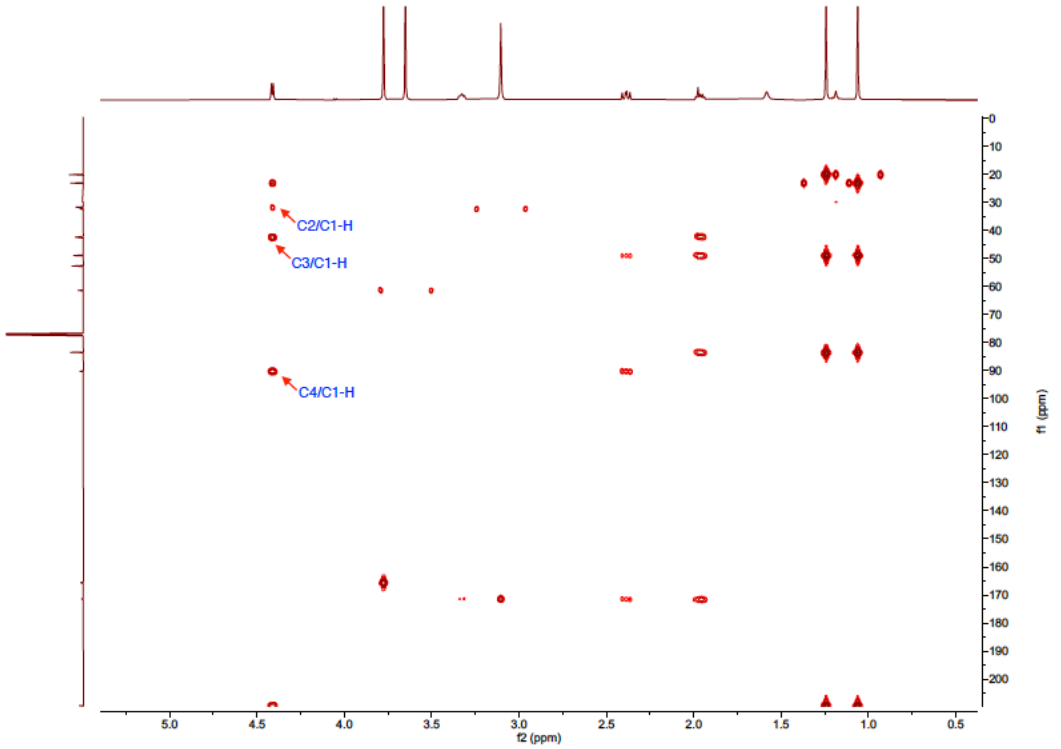

Figure 1.17. Key HMBC correlations of **1.73**.

The NOESY spectrum of **1.73** was also used to support its structural assignment (Figure 1.18). Of particular importance are the observed correlations between C2-H and C6-H, C2-H and C3-H. The NOESY correlation between the proton on C2 and the C6-CH_3 *gem*-dimethyl group suggests this proton is *endo*, because there would be no correlation of this proton with either of the *gem*-dimethyl groups if it were *exo*. The correlation between the *endo*-proton at C2 with the proton at C3 suggests that the C3-H is also *endo*; there is no NOESY correlation between the *exo*-proton at C2 with C3-H. These observations support the stereochemical assignment at C3 of **1.73**.

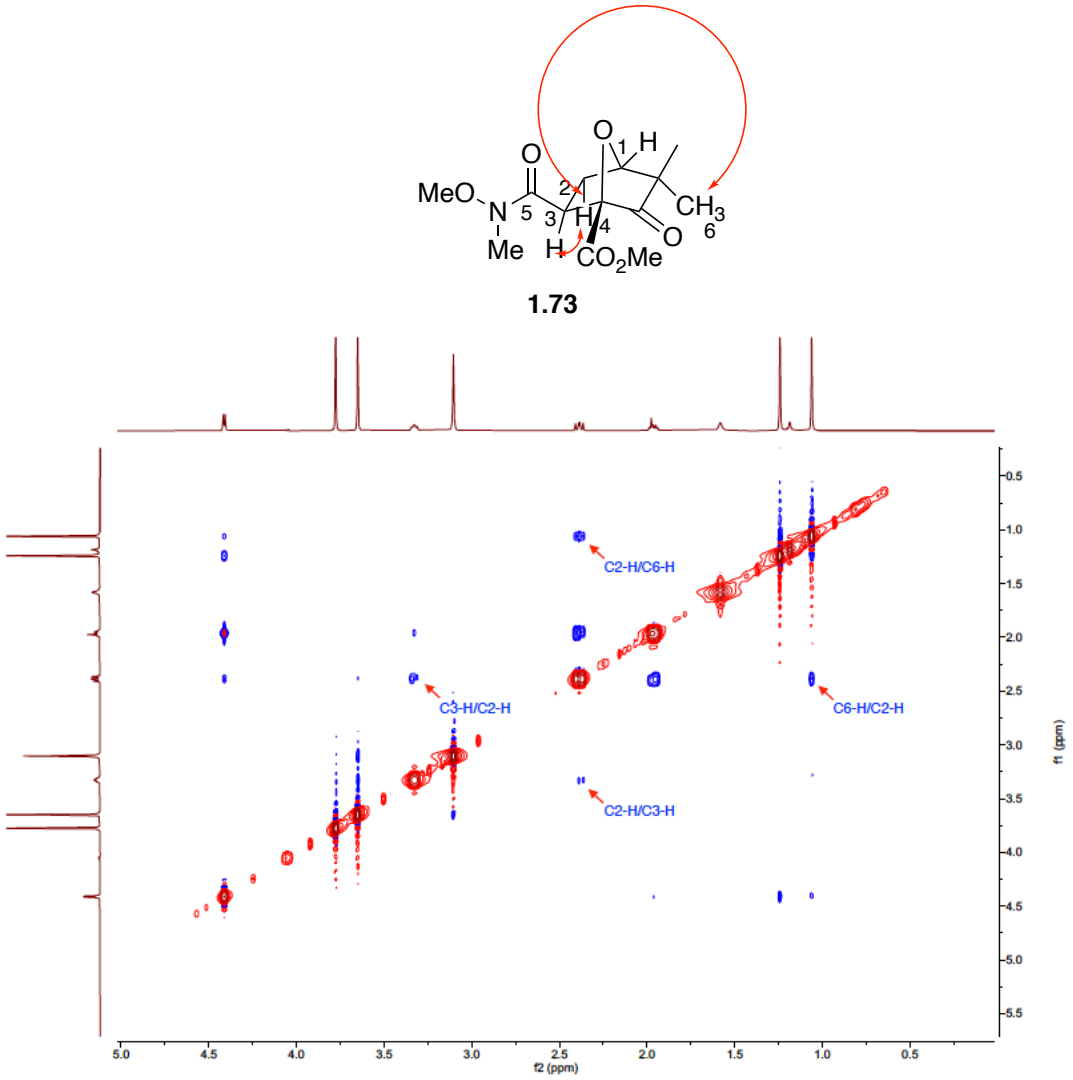

Figure 1.18. Key NOESY correlations of **1.73**.

1.6.1.2 Enolate Generation Studies of cycloadduct 1.73

With cycloadduct **1.73** in hand, we started the investigated the feasibility of generating the proposed enolate **1.73'** by deuterium incorporation studies (Scheme 1.8). The cycloadduct **1.73** was treated with various strong base in THF at -78 ºC followed by D_2O quenching, and the reaction mixture was analyzed via NMR to determine whether the desired enolate had been generated. Unfortunately, we screened commonly used strong base such as LDA, $LiNEt_2$, $LiNMe_2$, and NaHMDS, and all of them gave returned starting material **1.73** except for $LiNMe_2$, which furnished complex mixture. We rationalized the observation from a stereoelectronic perspective. Namely due to the steric repulsion between the substituent on Weinreb amide nitrogen atom in **1.73** and the CO_2Me group, the α proton was not aligned perpendicular to the carbonyl group which is required for efficient enolate generation. Moreover, the pKa of amides in DMSO is 35, whereas esters are around 29.

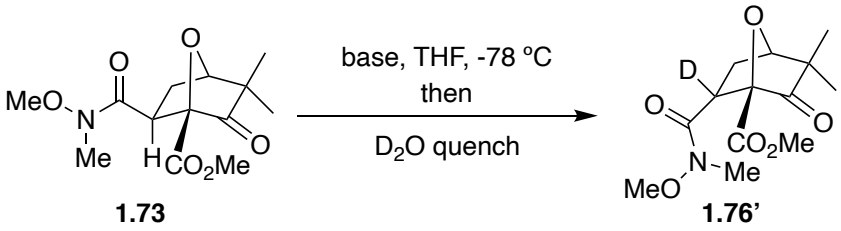

1.73 **1.76'**

base	result
LDA	**1.73**
$LiNEt_2$	**1.73**
$LiNMe_2$	complex
NaHMDS	**1.73**

Scheme 1.8. Deuterium incorporation studies of cycloadduct **1.73**.

1.6.2 Vinylogous Ester Cycloadduct Transformation Sequence

1.6.2.1 Synthesis of Vinylogous Ester Dipolarophile 1.18

We were thus forced to develop another route to the prenylated cycloadduct **1.78**, and we examined the cycloaddition of **1.20** and **1.18** (Scheme 1.9). Instead of using Weinreb amide dipolarophile, the vinylogous methyl ester **1.18** which would serve as the dipolarophile. Enolate generation from the proposed cycloadduct **1.17** was anticipated to be more straightforward, considering that there is only single proton α to the carbonyl, and it could be aligned perpendicular to the carbonyl which would be required for the enolate generation stereoelectronically. Moreover, the α proton of this ester cycloadduct is more acidic than that of the Weinreb amide.

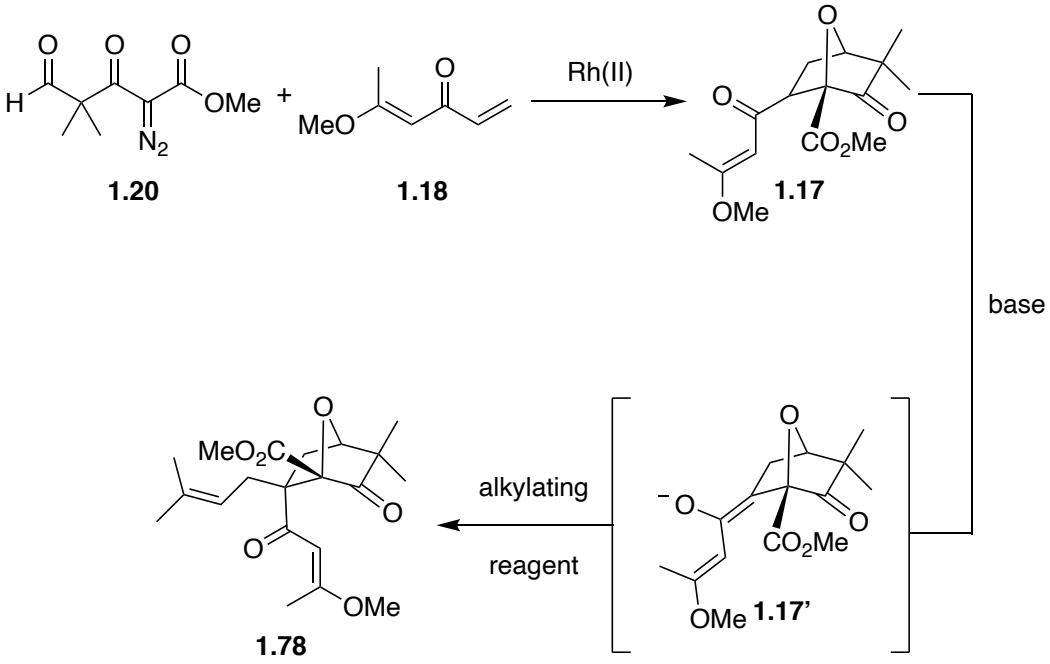

Scheme 1.9. Proposed route to prenylated cycloadduct **1.78**.

To investigate the alternative route, the vinylogous ester dipolarophile **1.18** was prepared according to a literature procedure (Scheme 1.10).[79] Starting from commercially available methyl acetoacetate (**1.21**), treatment with $CH(OMe)_3$ with catalytic amount of concentrated H_2SO_4 afforded vinylogous carbonate **1.79** in 85% yield.[80] **1.79** was converted to its Weinreb amide **1.80** in 70% yield by treatment with N,O-dimethylhydroxylamine and trimethyl aluminum. The addition of vinyl Grignard reagent to the Weinreb amide afforded the desired dipolarophile **1.18** in 82% yield.

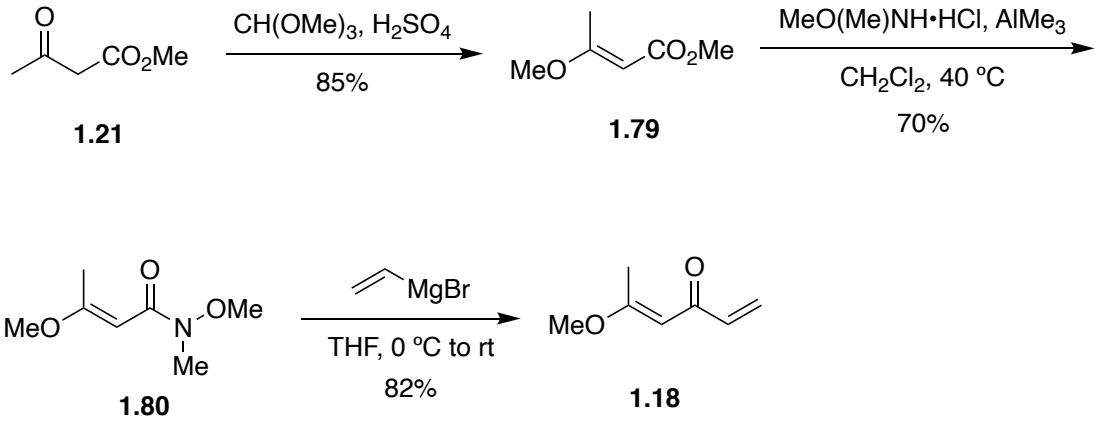

Scheme 1.10. Synthesis of vinylogous methyl ester dipolarophile **1.18**.

1.6.2.2 1,3-Dipolar Cycloaddition of 1.20 and 1.18

With **1.18** in hand, we turned our attention to the 1,3-dipolar cycloaddition reaction of **1.20** and **1.18**. We extensively screened catalysts, catalyst loading, solvents and reaction temperature for the reactions, and we listed some of the representative conditions and the yields related (Table 1.4). We initiated our investigation by refluxing the solution of **1.20** and **1.18** in the presence of 2 mol% $Rh_2(OAc)_4$ in CH_2Cl_2 overnight, and the reaction furnished a mixture of two diastereo-isomer **1.81** (44%) and **1.82** (5%) with regio isomer **1.83** (5%) (Entry 1). We also increased the catalyst loading to facilitate the product

formation as well as increase the yield (Entry 2). We observed the reaction completed in only 2 h, while the yield did not change much compared with lower catalyst loading. We have also investigated different Rh(II) catalysts, as ligands was reported impacting the chemoselectivity of the metallocarbene reactivity based on literature report.[81,82] We explored using 2 mol% $Rh_2(OPiv)_4$ as the catalyst, but unfortunately we did not detect any formation of the product, and decomposition product was detected instead (Entry 3). Then we tested $Rh_2(NHAc)_4$ as the catalyst, which we first tested refluxing the solution of **1.20** and **1.18** in the presence of 2 mol% of $Rh_2(NHAc)_4$ in CH_2Cl_2 that afforded **1.81** (34%), **1.82** (3%) and **1.83** (3%) (Entry 4). Treatment of **1.20** and **1.18** in the presence of 2 mol% of $Rh_2(NHAc)_4$ in toluene under reflux overnight afforded 44% of **1.81**, 3% of **1.82** and 3% of **1.83** (Entry 5). After further condition screening, we found that treatment of **1.20** and **1.18** in the presence of 2 mol% of $Rh_2(NHAc)_4$ in toluene at 100 ºC for 1 h furnished the best combined overall yield of **1.81** and **1.82** in 65% with 15:1 dr accompanied with 4% of undesired regioisomer **1.83** (Entry 6). The structure of cycloadduct **1.81** was exclusively confirmed by X-ray crystallography.

Table 1.4. Selected conditions screening for the cycloaddition of **1.20** and **1.18**.

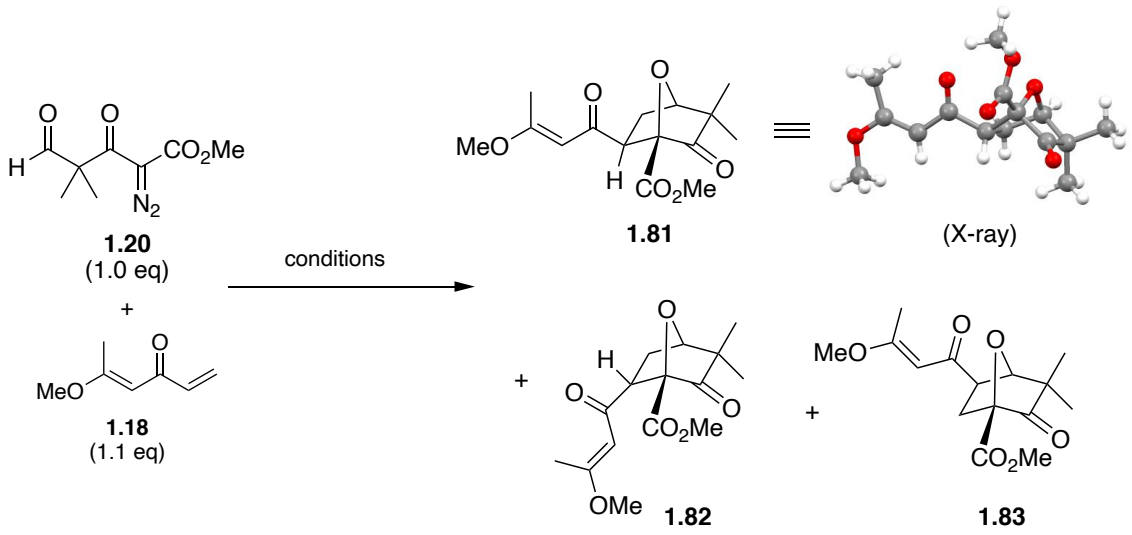

entry	catalyst loading	catalyst	solvent	T (ºC)	time (h)	% yield (**1.81**, **1.82**, **1.83**)
1	2 mol%	$Rh_2(OAc)_4$	CH_2Cl_2	reflux	overnight	44, 5, 5
2	5 mol%	$Rh_2(OAc)_4$	CH_2Cl_2	reflux	2	42, 5, 4
3	2 mol%	$Rh_2(OPiv)_4$	CH_2Cl_2	reflux	overnight	NA
4	2 mol%	$Rh_2(NHAc)_4$	CH_2Cl_2	reflux	overnight	34, 3, 3
5	2 mol%	$Rh_2(NHAc)_4$	toluene	100	overnight	44, 3, 3
6	2 mol%	$Rh_2(NHAc)_4$	toluene	100	1	61, 4, 4

The structure assignment of **1.81** is based upon extensive evidence derived from 2D NMR spectra (HSQC, HMBC, COSY and NOESY). The characteristic peak having a

chemical shift of δ 4.48 ppm, which is a doublet, arises from the bridgehead proton at C1 (Figure 1.19). This assignment is made based upon the HMBC spectrum, in which correlations between C1-H and C2, C3, C4 are observed (Figure 1.20). HMBC typically shows correlations between protons and carbons that are one, two and sometimes in conjugated system three atoms away; C1-H and C4 are two atoms removed through the oxygen bridge. The correlations between C1-H and both C2 and C3 indicate C2 and C3 are within two C atoms from C1-H. There is no correlation between C1-H and C5 because C5 is three atoms away from C1-H in **1.81**, whereas in the regioisomer **1.83** it would be two atoms removed. This observation supports the regiochemistry of the major product as being **1.81**.

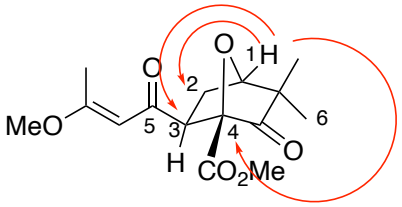

1.81

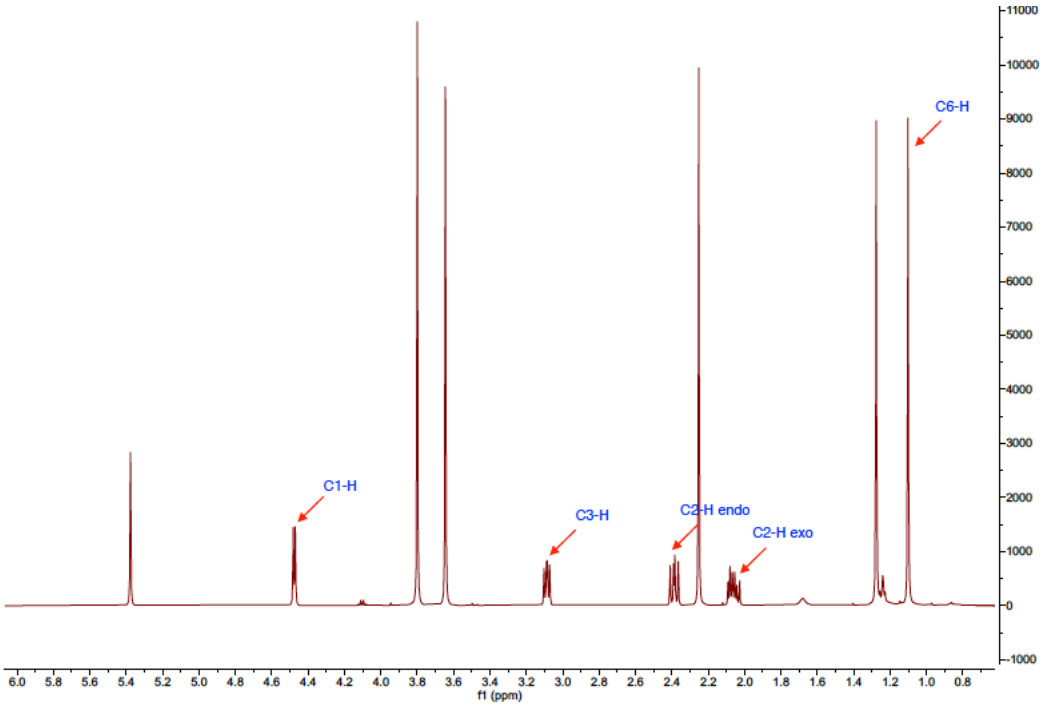

Figure 1.19. Key assignments of **1.81** on ^{1}H spectrum.

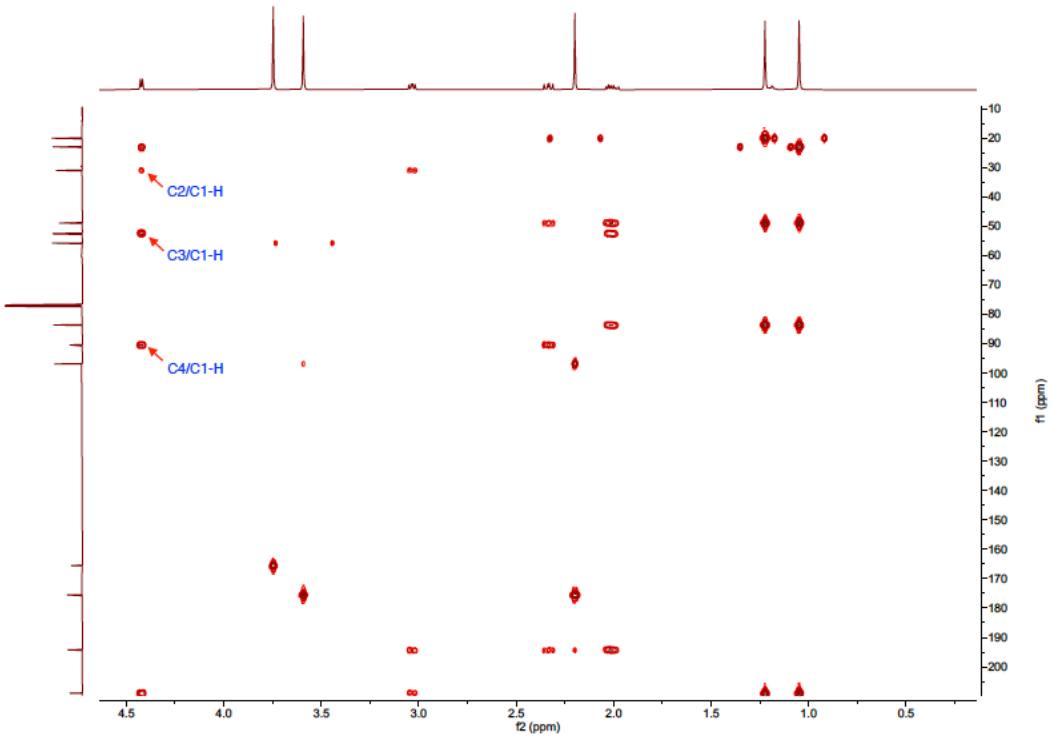

Figure 1.20. Key HMBC correlations of **1.81**.

The NOESY spectrum of **1.81** was also used to support its structural assignment (Figure 1.21). Of particular importance are the observed correlations between C2-H and C6-H, C2-H and C3-H, C3-H and C6-H. The NOESY correlation between the proton on C2 and the C6-CH_3 *gem*-dimethyl group suggests this proton is *endo*, because there would be no correlation of this proton with either of the *gem*-dimethyl groups if it were *exo*. The correlation between the *endo*-proton at C2 with the proton at C3 suggests that the C3-H is also *endo*. The correlation between the proton on C3 and the C6-CH_3 *gem*-dimethyl group further suggests both groups are *endo*. Moreover, the coupling constant between C3-H and the assigned *endo* C2-H is 9.3 Hz that is greater than that of C3-H and the assigned *exo* C2-H which is 6.3 Hz. These observations support the stereochemical assignment at C3 of **1.81**.

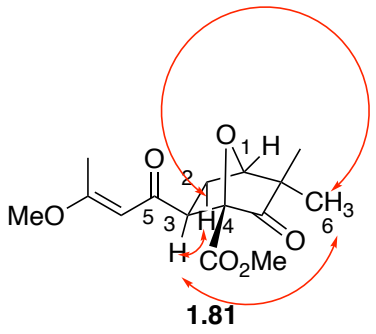

1.81

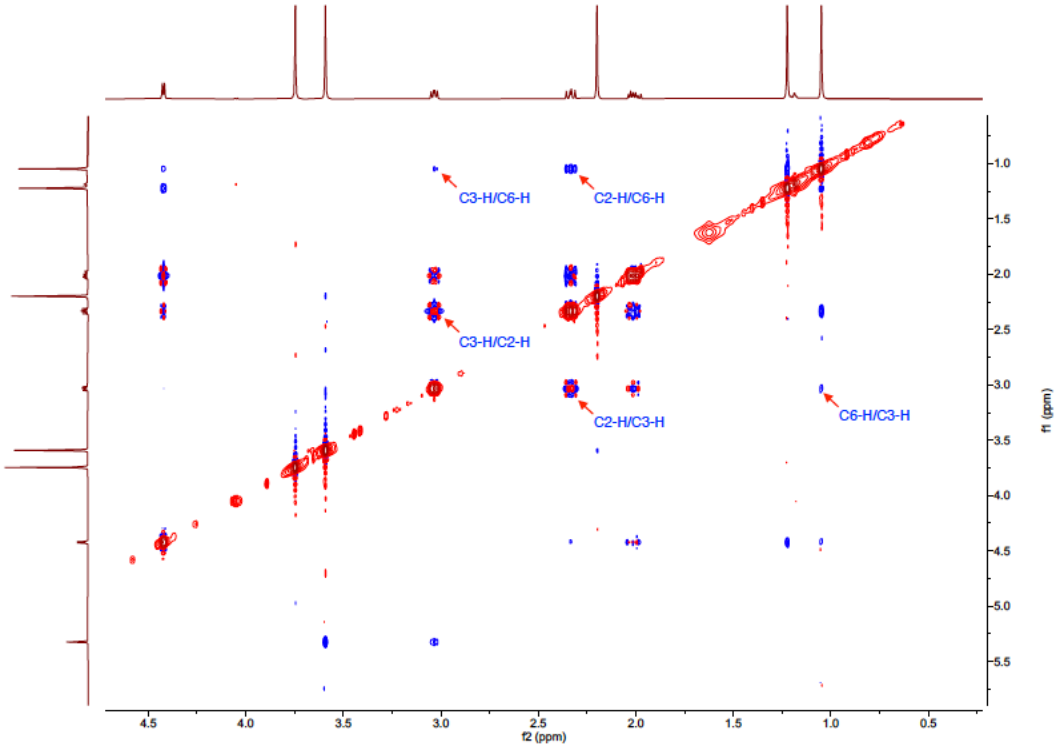

Figure 1.21. Key NOESY correlations of **1.81**.

The structure assignment of **1.82** is based upon extensive evidence derived from 2D NMR spectra (HSQC, HMBC, COSY and NOESY). The characteristic peak having a chemical shift of δ 4.38 ppm, which is a doublet, arises from the bridgehead proton at C1 (Figure 1.22). This assignment is made based upon the HMBC spectrum, in which correlations between C1-H and C2, C3, C4 are observed (Figure 1.23). HMBC typically shows correlations between protons and carbons that are one, two and sometimes in conjugated system three atoms away; C1-H and C4 are two atoms removed through the oxygen bridge. The correlations between C1-H and both C2 and C3 indicate C2 and C3 are within two C atoms from C1-H. There is no correlation between C1-H and C5 because C5 is three atoms away from C1-H in **1.82**, whereas in the regioisomer **1.83** it would be two atoms removed. This observation supports the regiochemistry of the major product as being **1.82**.

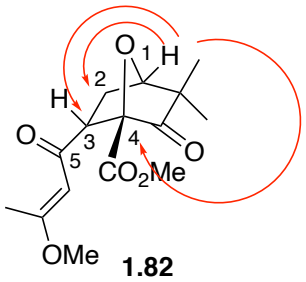

1.82

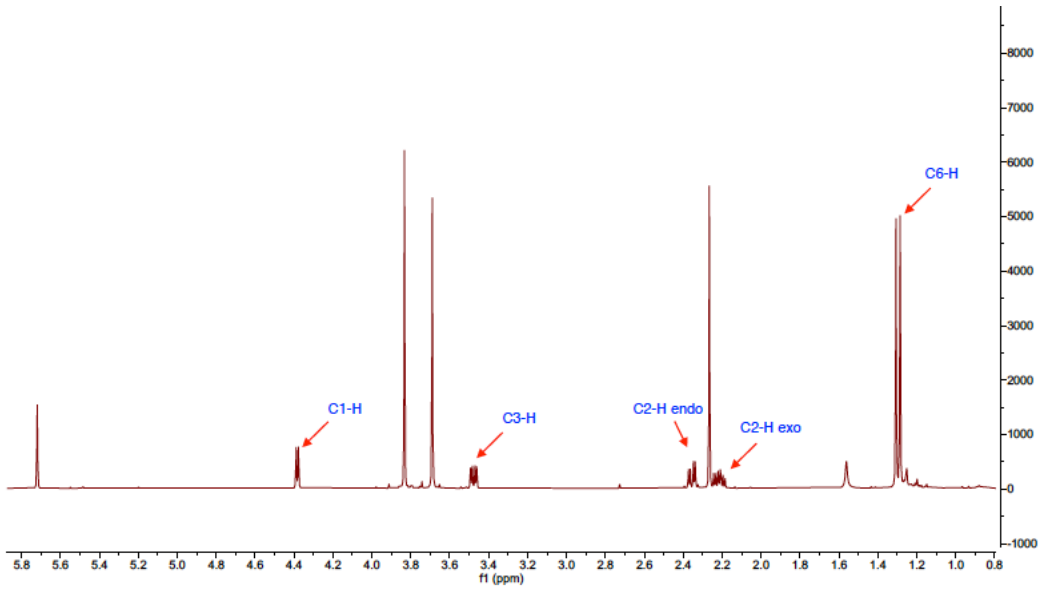

Figure 1.22. Key assignments of **1.82** on ^{1}H spectrum.

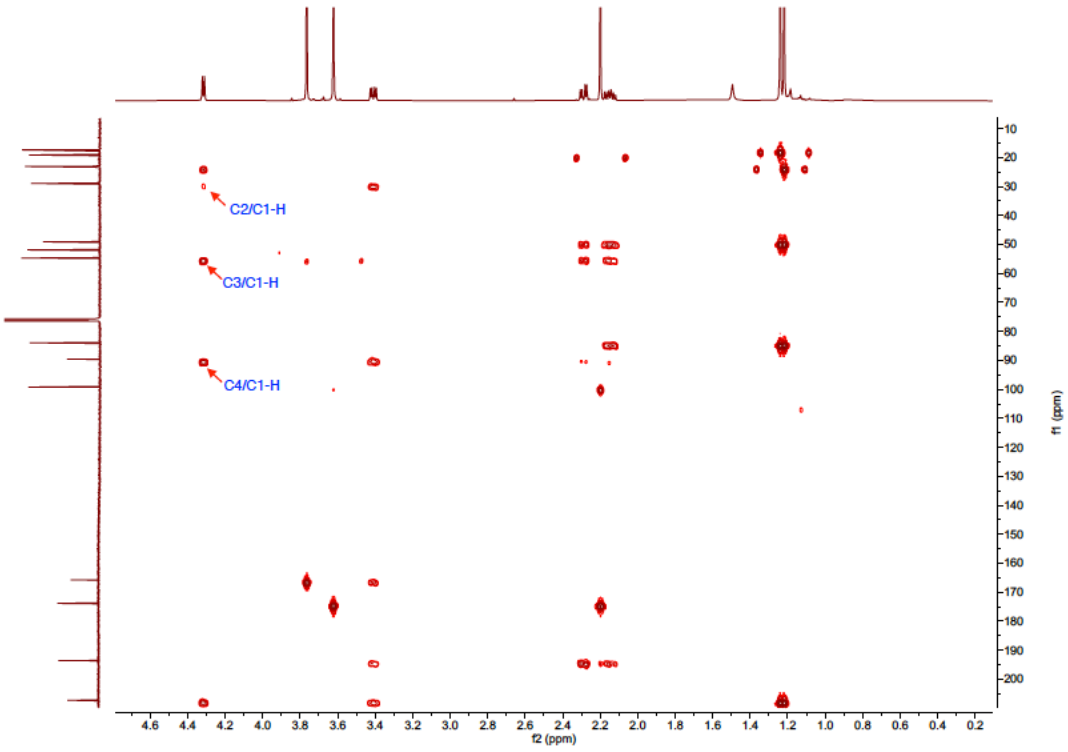

Figure 1.23. Key HMBC correlations of **1.82**.

The NOESY spectrum of **1.82** was also used to support its structural assignment (Figure 1.24). Of particular importance are the observed correlations between C2-H and C6-H, C2-H' and C3-H. The NOESY correlation between the proton on C2 and the C6-CH_3 *gem*-dimethyl group suggests this proton is *endo*, because there would be no correlation of this proton with either of the *gem*-dimethyl groups if it were *exo*. The correlation between the *exo*-proton at C2 with the proton at C3 suggests that the C3-H is *exo*. Moreover, the coupling constant between C3-H and the assigned *exo* C2-H is 11.2 Hz that is greater than that of C3-H and the assigned *endo* C2-H which is 4.6 Hz. These observations support the stereochemical assignment at C3 of **1.82**.

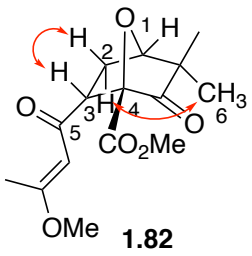

1.82

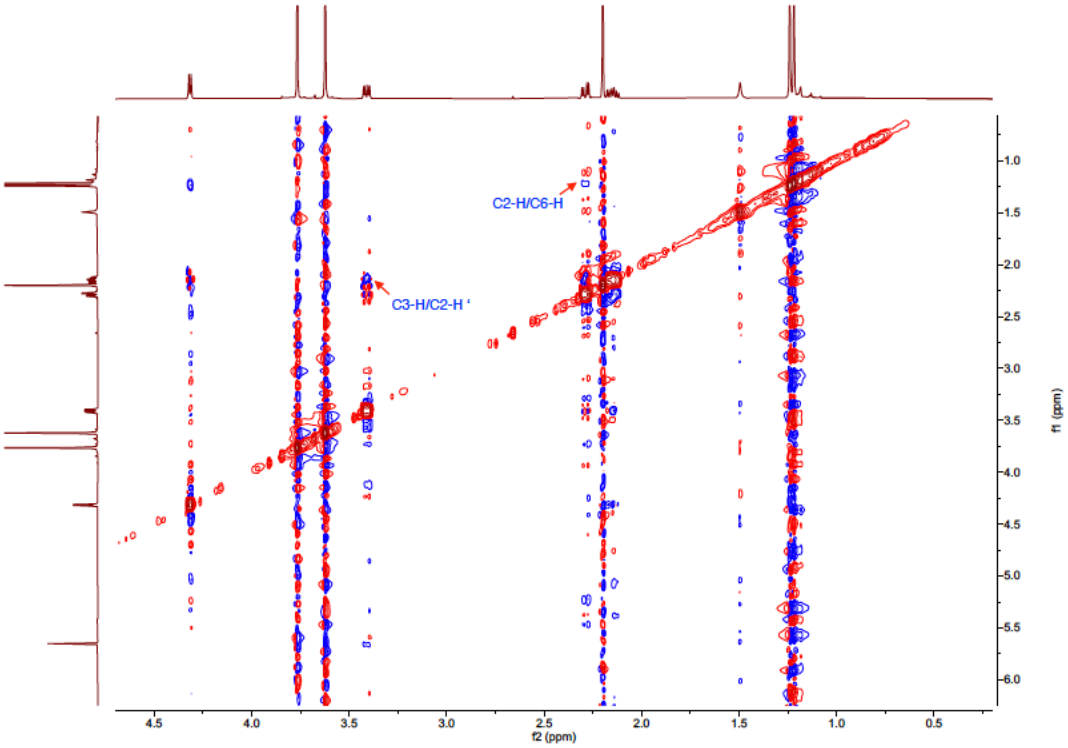

Figure 1.24. Key NOESY correlations of **1.82**.

The structure assignment of **1.83** is based upon extensive evidence derived from 2D NMR spectra (HSQC, HMBC, COSY and NOESY). The characteristic peak having a chemical shift of δ 4.65 ppm, which is a singlet, arises from the bridgehead proton at C1 (Figure 1.25). This assignment is made based upon the HMBC spectrum, in which correlations between C1-H and C3, C4, C5 are observed (Figure 1.26). HMBC typically shows correlations between protons and carbons that are one, two and sometimes in conjugated system three atoms away; C1-H and C4 are two atoms removed through the oxygen bridge. The correlations between C1-H and C3, C5 indicate C3 and C5 are within two C atoms from C1-H, whereas in the regioisomers **1.81** and **1.82**, C5 would be three atoms removed. This observation supports the regiochemistry of the major product as being **1.83**.

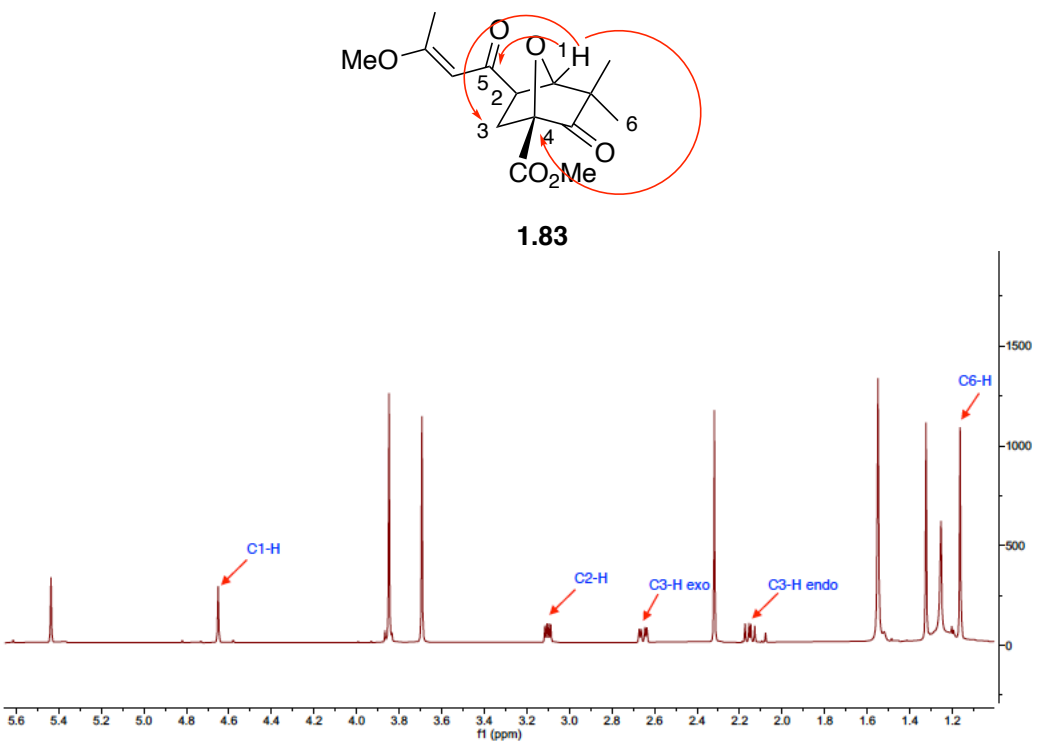

Figure 1.25. Key assignments of **1.83** on ^{1}H spectrum.

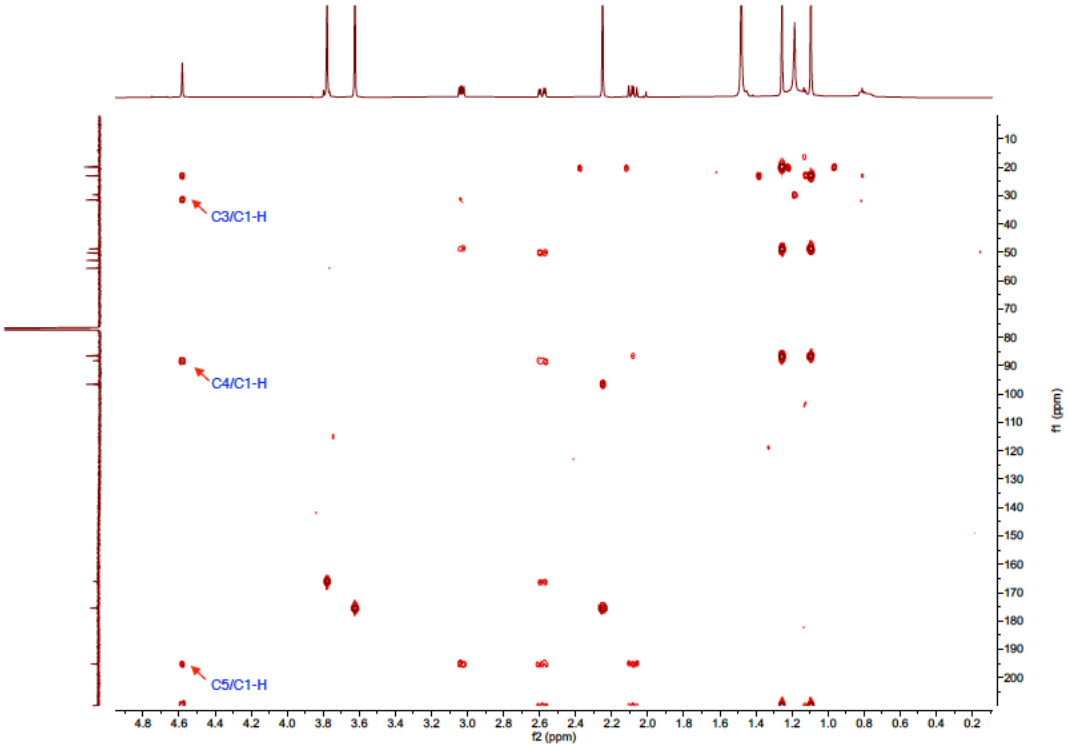

Figure 1.26. Key HMBC correlations of **1.83**.

The NOESY spectrum of **1.83** was also used to support its structural assignment (Figure 1.27). Of particular importance is the observed correlation between C2-H and C6-H. The NOESY correlation between the proton on C2 and the C6-CH_3 *gem*-dimethyl group suggests this proton is *endo*, because there would be no correlation of this proton with either of the *gem*-dimethyl groups if it were *exo*. Moreover, the coupling constant between C2-H and the assigned *endo* C3-H is 9.1 Hz that is greater than that of C2-H and the assigned *exo* C3-H which is 4.5 Hz. These observations support the stereochemical assignment at C2 of **1.83**.

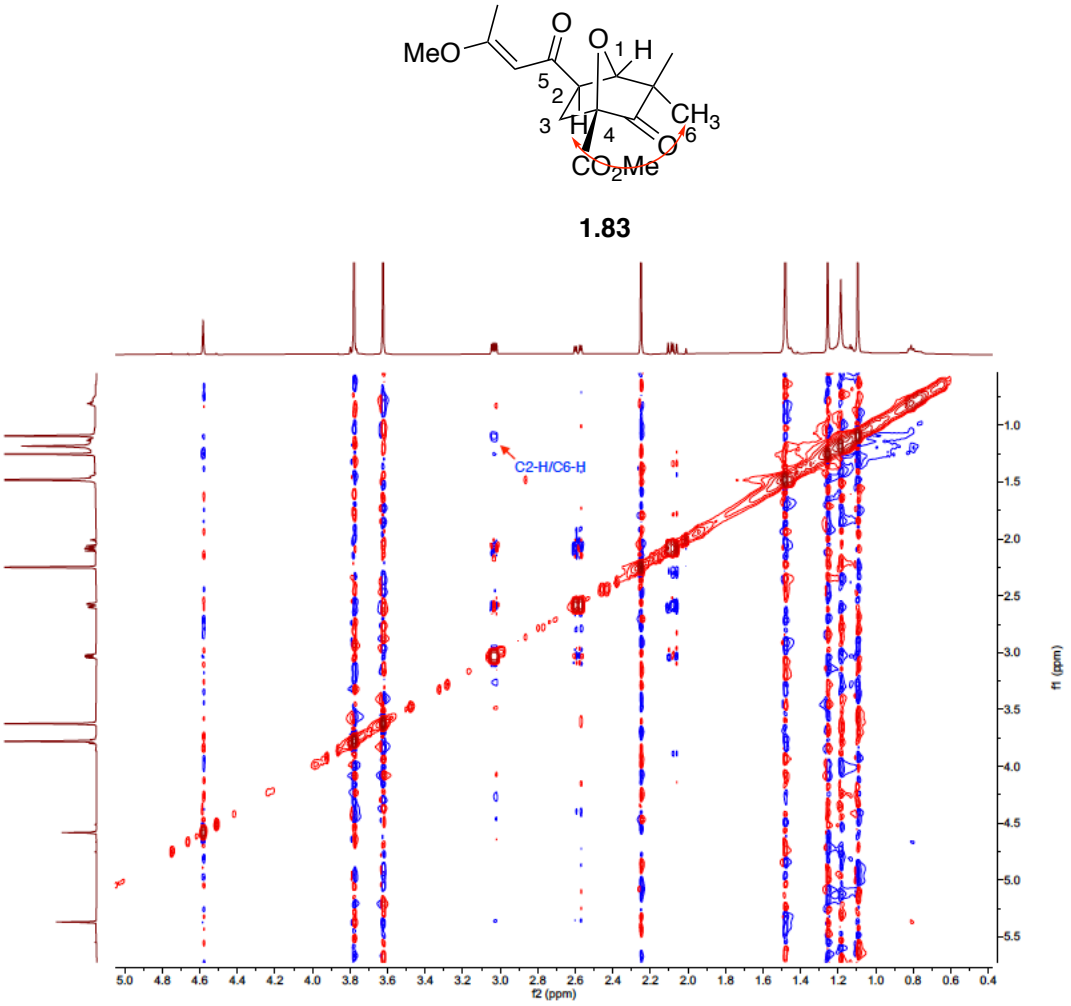

Figure 1.27. Key NOESY correlations of **1.83**.

1.6.2.3 Stereoselective Prenylation of 1.81

With **1.81** in hand, we investigated the stereoselective prenylation. We first screened conditions to generate the desired enolate intermediate. We treated cycloadduct **1.81** with various strong bases in THF at -78 ºC, followed by quenching with D_2O to analyze deuterium incorporation via NMR. We screened commonly used strong bases such as LDA, $LiNEt_2$, $LiNMe_2$, NaHMDS on deprotonation of **1.81**, and we found that both LDA and NaHMDS converted **1.81** to **1.82'** efficiently without the formation of β-

elimination product based on NMR results (Scheme 1.11). This indicated successful formation of the desired enolate intermediate as well as the highly stereoselective protonation of the enolate. For $LiNEt_2$ and $LiNMe_2$, both bases yielded a complex mixture.

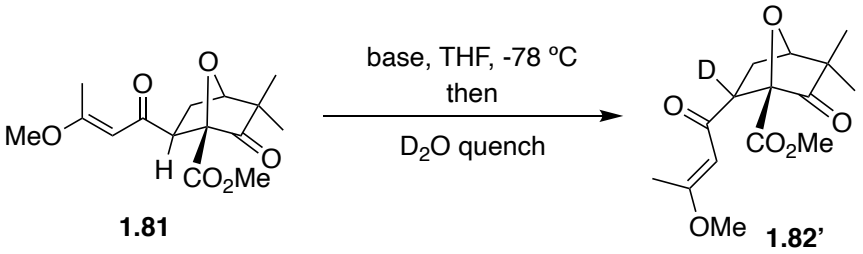

1.81 **1.82'**

base	result
LDA	**1.82'**
$LiNEt_2$	complex
$LiNMe_2$	complex
NaHMDS	**1.82'**

Scheme 1.11. Deuterium incorporation studies of **1.81**.

With effective formation of the desire enolate intermediate, we next turned our attention to alkylating the enolate with prenyl halide reagents. We initiated our investigation using commercially available prenyl bromide as the alkylating reagent. We first treated **1.81** with LDA in THF at –78 ºC for 30 min, whereupon freshly distilled prenyl bromide was added. The solution was stirred at -78 ºC for over 2 h; however, no new product was formed based on TLC analysis. Instead of directly terminating the reaction, we added D_2O to quench the reaction. We found no alkylation product **1.78** in the reaction mixture, and deuterium incorporated **1.82'** was found instead which indicated no alkylation occurred on the enolate (Equation 1.24).

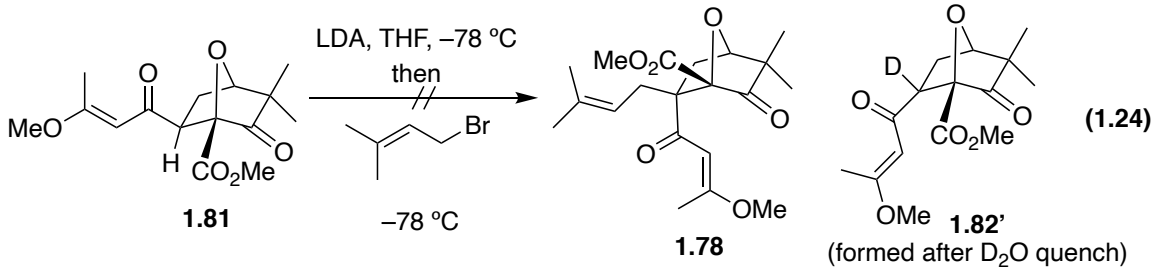

(1.24)

In order to facilitate the alkylation process, we could increase the nucleophilicity of the enolate and the electrophilicity of the alkylating reagent. As for increasing the nucleophilicity of the enolate, we tested adding dissociating reagent hexamethylphosphoramide (HMPA) with prenyl bromide after successful generation of the enolate. We initially added 10% HMPA with the prenyl bromide which only observed small amount of conversion of **1.81** to **1.78** accompanied with **1.82'** after D_2O quench. We next increased the amount of HMPA to 23% and prolonged the reaction time to 2 h at –78 ºC. However, there were still significant amounts of deuterium incorporated **1.82'** isolated (45%) after the reaction was quenched with D_2O (Equation 1.25).

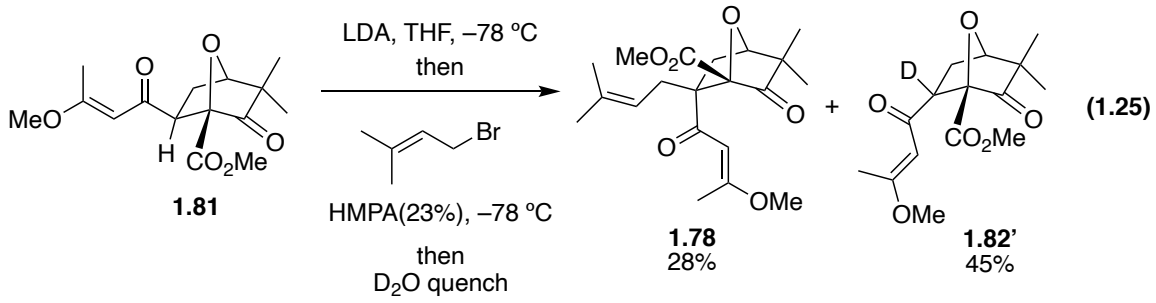

(1.25)

At the same time, we examined different alkylating reagent to facilitate the alkylation process. For example, we converted prenyl bromide (**1.84**) into prenyl iodide (**1.85**) by treatment of NaI in acetone (Equation 1.26). Without further purification, prenyl iodide **1.85** was directly added with HMPA into a solution of freshly generated enolates in

THF at –78 ºC, and the solution was stirred at –78 ºC for 1 h (Equation 1.27). Gratifyingly, we observed the complete conversion of the enolate into its prenylation product **1.78** in 45% yield without isolation of any epimeric prenylation product after the D_2O quench.

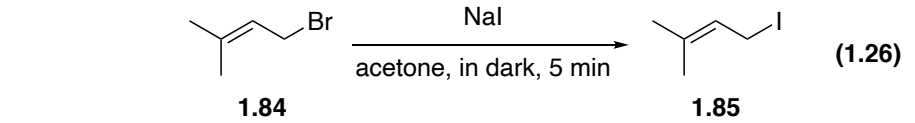

1.84 **1.85** **(1.26)**

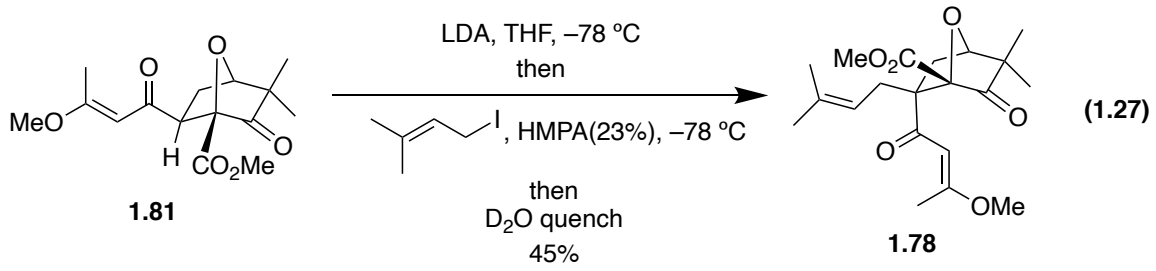

1.81 **1.78** **(1.27)**

With further experimentation, we found treating **1.81** with NaHMDS in THF at –78 ºC for 30 min followed by the treatment of enolate with freshly prepared prenyl iodide at –78 ºC for 30 min afforded **1.78** in 65% yield (Equation 1.28). At meantime, we also alkylated the diastereoisomer **1.82** using the same reaction condition to obtain 66% of **1.78** (Equation 1.29). The combined yield of **1.78** from **1.81** and **1.82** was 68%.

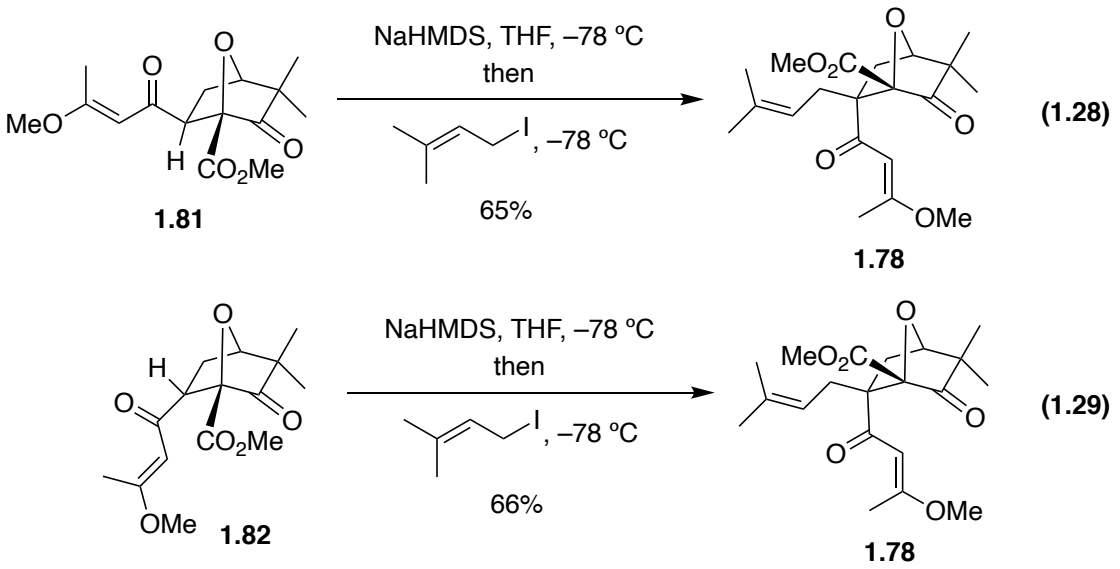

1.7 STUDIES OF ENANTIOSELECTIVE 1,3-DIPOLARCYCLOADDITION

1.7.1 Enantioselective 1,3-Dipolar Cycloaddition

With the successful approach to the core oxa-tricyclo structure and efficient installation of the prenyl group, we explored the enantioselective 1,3-dipolarcycloaddition. With extensive searching of precedents, we found three different strategies for constructing the tricyclic core structure enantioselectively. One of the strategies features a chiral Rh-catalyzed tandem carbonyl ylide formation-1,3 dipolar cycloaddition sequence, which is also the best-studied strategy among all three strategies.[27] The transition metal remains associated with the carbonyl ylide in **1.88** even after its formation, thus providing the chiral environment because the chiral ligand remains appended to the transition metal (Figure 1.28A). Hashimoto reported the 1,3-dipolar cycloaddition of α-diazo-β-ketoester **1.90** with terminal acetylenes **1.91** in the presence of N-tetrachlorophthaloyl-t-leucine ligated catalyst, Rh_2(S-TCPTTL)$_4$ afforded cycloadducts **1.93** and **1.94** with high regio- and enantioselectivities (Figure 1.28B).[83]

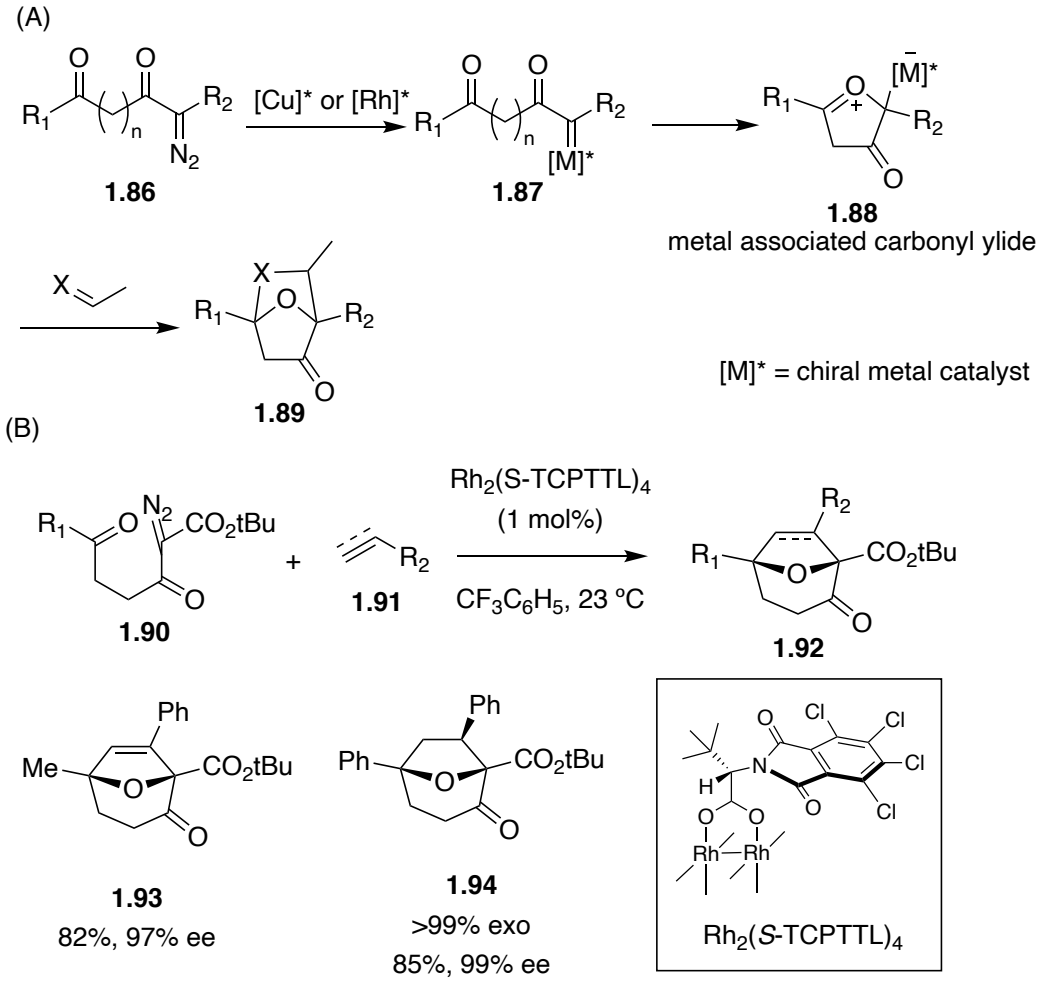

Figure 1.28. (A) Concept of chiral Rh catalyzed 1,3-dipolar cycloaddition. (B) Examples of chiral Rh catalyzed 1,3-dipolar cycloaddition.

The chiral Rh(II) catalysis builds on the formation of the Rh-associated carbonyl ylide species; however, the dissociation of the Rh(II) from the carbonyl ylide is a potential concern. To improve the chiral Rh(II) catalysts strategy, the second strategy that use of chiral Lewis acid in combination with achiral Rh catalysts were proposed and developed.[27] The Rh catalysts generate carbonyl ylide with diazo compound **1.95**, and the chiral Lewis acid either activates the carbonyl ylide species or the dipolarophile depending on the electronic nature of the substrates (Figure 1.29A). In these cases, the stereoselectivities of

the cycloadducts were determined by the chiral Lewis acid without depending on the formation of transition metal associated carbonyl ylide species. Suga group reported the example of Yb(III)/Ph-Pybox **1.100** complex promoting the 1,3-dipolar cycloaddition of diazo compound **1.98** and **1.99** to form **1.101** with high exo- and enantioselectivities (Figure 1.29B).[84]

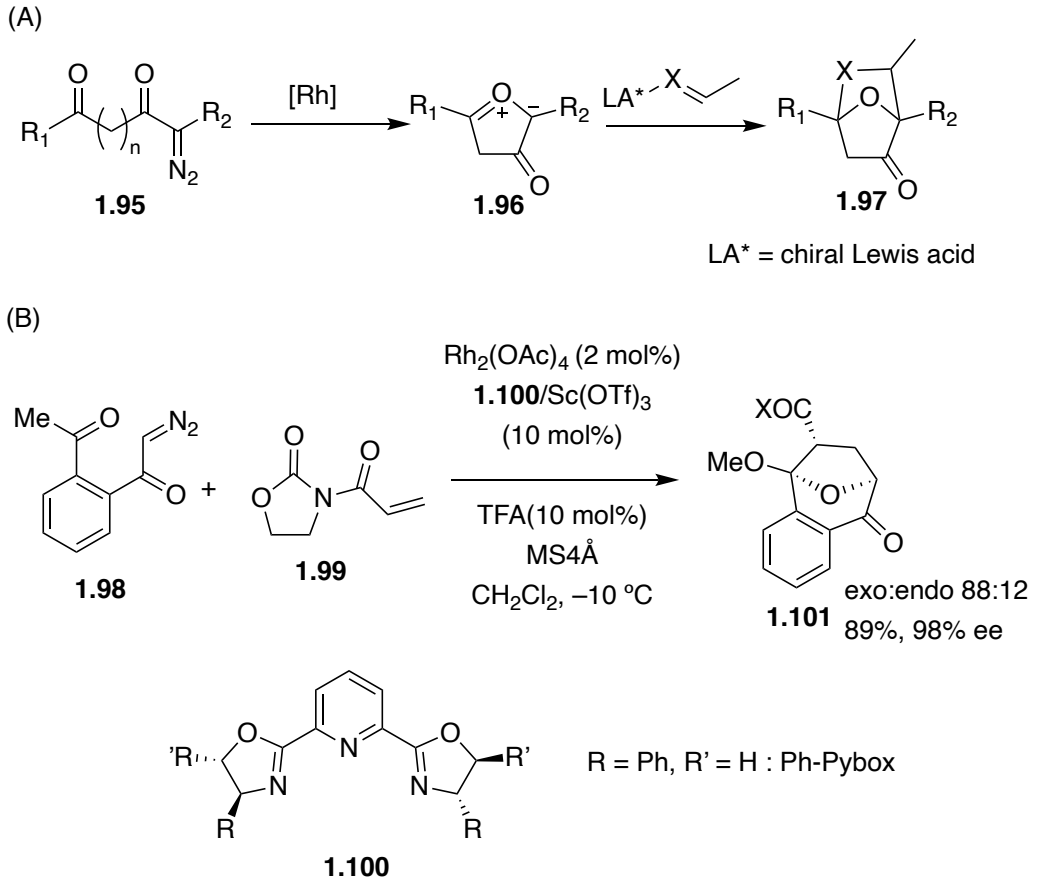

Figure 1.29. (A) Concept of chiral Lewis acid catalyzed 1,3-dipolar cycloaddition of carbonyl ylides generated by achiral Rh catalyst. (B) Examples of chiral Lewis acid catalyzed 1,3-dipolar cycloaddition.

Lastly, chiral auxiliaries were also being used in the enantioselective 1,3-dipolar cycloaddition reactions (Figure 1.30).[85] Chiral auxiliaries can be attached to the carboxyl

group to form **1.102**, which could further generate 1,3-dipoles **1.103** thus forming chiral cycloadduct **1.104**. However, we were not aware of any enantioselective carbonyl ylide cycloadditions were performed by this method, other 1,3-dipoles such as nitrones, diazoalkanes, and azomethines with chiral auxiliaries have been studied.[86-88]

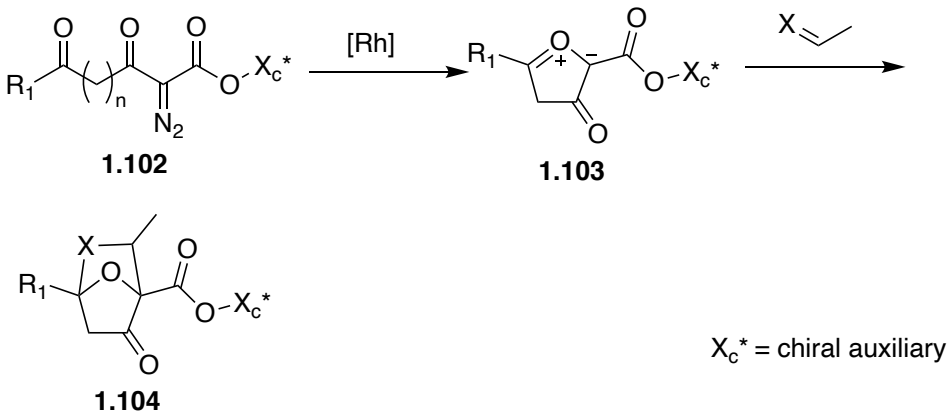

Figure 1.30. Concept of chiral auxiliary promoted enantioselective 1,3-dipolar cycloaddition of carbonyl ylides

With the knowledge of three different strategies for constructing the tricyclic core structure enantioselectively via 1,3-dipolar cycloaddition, we sought to explore the chiral rhodium catalysis since it is the best studied the method, and it would not add extra steps to our synthesis.

1.7.2 Chiral Rh-Catalyzed 1,3-Dipolar Cycloaddition

Doyle and coworkers demonstrated that the Rh(II)-catalyzed reaction of 4-nitrobenzaldehyde (**1.105**) and ethyl diazoacetate (**1.106**) afforded diastereomeric dioxolanes **1.107**, and the ratio of diastereomers depended on the ligand of the Rh(II) catalysts.[89] They postulated of the formation of Rh-associated carbonyl ylide as the intermediate, and their hypothesis led to the utilization of chiral rhodium catalyst Rh_2(4S-

MEOX)$_4$ (MEOX = methyl 2-oxooxazolidine-4-carboxylate) to form the all-cis cycloadduct as a major product with 28% ee (Figure 1.31A). Hodgson and coworkers reported the first example of catalytic asymmetric 1,3-dipolar cycloaddition of carbonyl ylide in 1997.[90] The diazo carbonyl compound **1.108** was designed to undergo 1,3-dipolar cycloaddition intramolecularly to generate **1.109**, and modest enantioselectivity was achieved by employment of chiral Rh(II) catalyst Rh_2(S-DOSP)$_4$ (Figure 1.31B). A following study of the same cycloaddition reaction revealed that using of Rh_2(R-DDBNP)$_4$ improved the enantioselectivity dramatically.[91] The strategy was then expanded to intermolecular 1,3-dipolar cycloaddition reactions. Treatment of 2-diazo-3,6-diketoester **1.110** with different dipolarophiles including styrenes, arylacetylenes, and strained alkenes afforded cycloadducts **1.113**-**1.115** with modest to good enantioselectivities (Figure 1.31C).[92-94] Cu(I)/ chiral bisoxazoline catalysts were also studied in the 1,3-dipolar cycloaddition reactions, but only slight enantioselectivities were observed.[92]

(A)

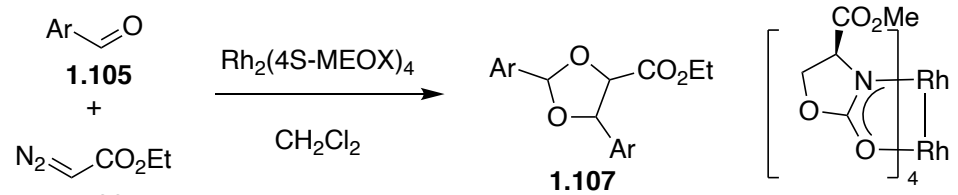
Ar
O
1.105
+
N2
CO2Et
1.106
Ar = 4-NO2C6H4
Rh2(4S-MEOX)4
CH2Cl2
Ar
O
CO2Et
O
Ar
1.107
55% (all-cis), 28% ee
CO2Me
N
Rh
O
O
Rh
4
Rh2(4S-MEOX)4

(B)

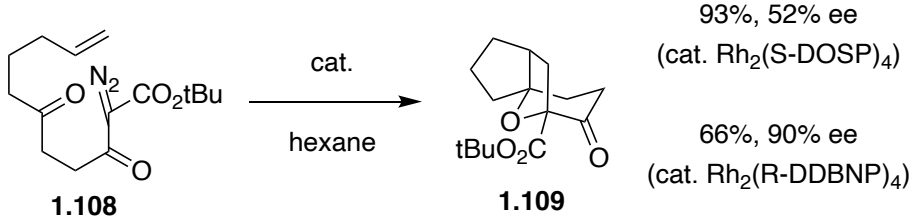
N2
CO2tBu
O
O
1.108
cat.
hexane
O
tBuO2C
O
1.109
93%, 52% ee
(cat. Rh2(S-DOSP)4)
66%, 90% ee
(cat. Rh2(R-DDBNP)4)

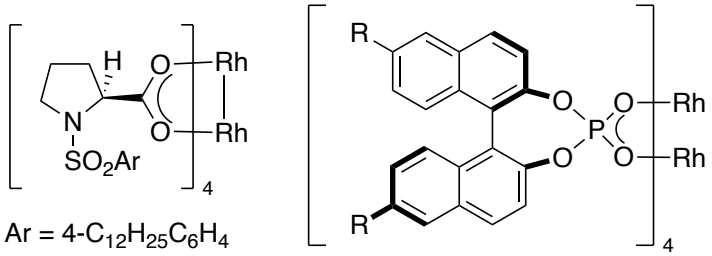
H
O
Rh
N
O
Rh
SO2Ar
4
Ar = 4-C12H25C6H4
Rh2(S-DOSP)4
R
O
O
Rh
P
O
O
Rh
R
4
R = C12H25
Rh2(R-DDBNP)4

(C)

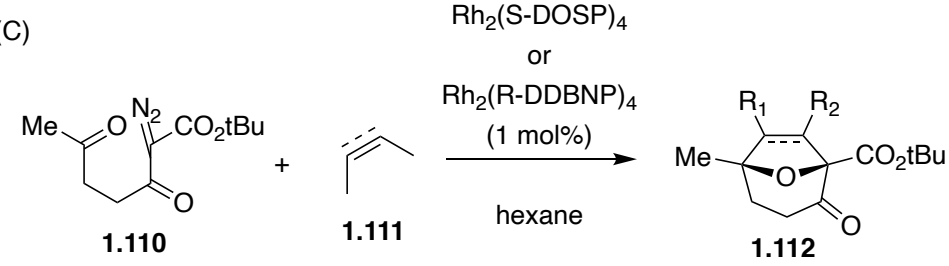
Me
O
N2
CO2tBu
O
1.110
+
1.111
Rh2(S-DOSP)4
or
Rh2(R-DDBNP)4
(1 mol%)
hexane
R1
R2
Me
O
CO2tBu
O
1.112

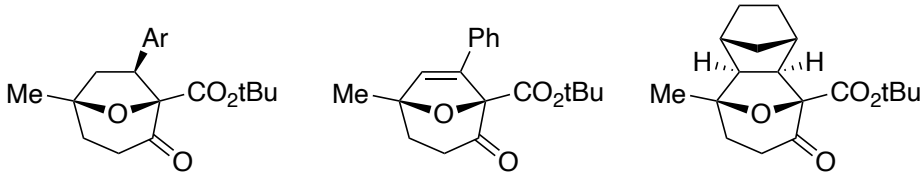
Ar
Me
O
CO2tBu
O
1.113
40%, 81% ee
Ar = 4-MeOC6H4
Ph
Me
O
CO2tBu
O
1.114
41%, 61% ee
H
H
Me
O
CO2tBu
O
1.115
49%, 92% ee

Figure 1.31. Early examples of enantioselective 1,3-dipolar cycloaddition.

Hashimoto and coworkers have done extensive pioneering studies to develop highly enantioselective 1,3-dipolar cycloaddition reactions.[27,95] The optimal chiral Rh(II) catalyst was identified by screening the amino acid residue and the aromatic moiety of the ligand.[96] They also examined the 1,3-dipolar cycloadditions of electron deficient carbonyl ylides and electron rich dipolarophiles. In the reaction of diazo carbonyl compound **1.116** with electron rich dipolarophile indole derivative **1.117**, Rh_2(S-TCPTTL)$_4$ was employed to furnish exclusive exo tetracyclic cycloadduct **1.118** with high enantioselectivities (Figure 1.32A).[28] This procedure can also be applied to formyl substituted carbonyl ylide precursor **1.120** with **1.119**, the cycloadduct **1.121** could be subsequently converted to natural product descurainin (Figure 1.32B).[15,16] Other examples including the use of indoles, or aldehydes as dipolarophile have also been reported by Hashimoto group.[97-99]

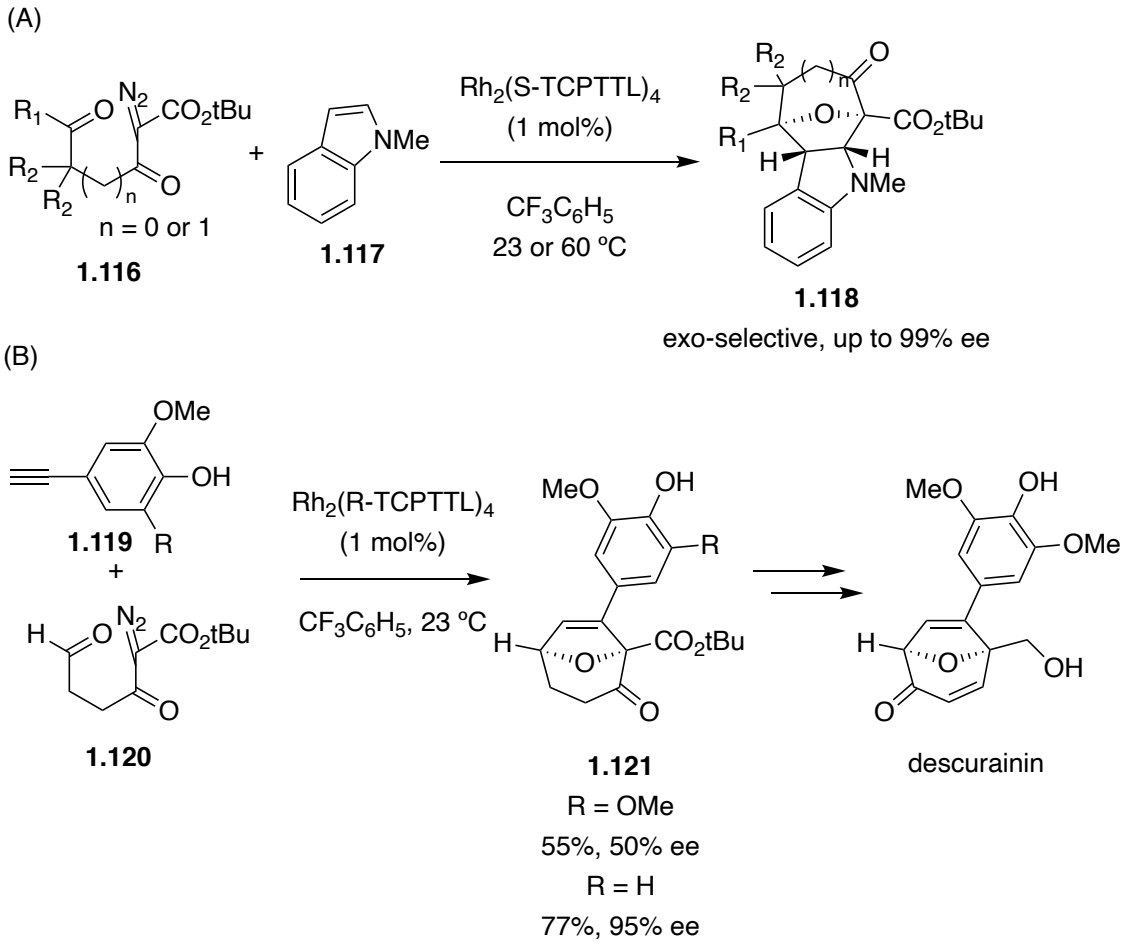

Figure 1.32. Examples of chiral Rh-catalyzed 1,3-dipolar cycloaddition of carbonyl ylides with various dipolarophiles.

1.7.3 Studies of the Chiral Rh-Catalyzed Enantioselective 1,3-Dipolar Cycloaddition

Based upon the previous studies of chiral Rh catalyzed 1,3-dipolarcycloadditions, we first examined the reaction of **1.20** with **1.18** in the presence of Rh_2(*S*-TCPTTL)$_4$ because this catalyst gave the highest enantiomeric excess (ee) in related reactions (Table 1.5).[15,16] Treatment of **1.20** and **1.18** in the presence of Rh_2(*S*-TCPTTL)$_4$ in CH_2Cl_2 at room temperature did not afford any product, starting materials were recovered instead (Entry 1). To facilitate the reaction, the solution of **1.20** and **1.18** in the presence of Rh_2(*S*-

TCPTTL)$_4$ in CH_2Cl_2 was heated under reflux which furnished 1.68 in 26% yield and 6% ee (Entry 2). Different solvents were screened including $CF_3C_6H_5$ and toluene at room temperature (Entries 3 and 4). The reaction in $CF_3C_6H_5$ did not form any cycloadduct 1.68, while the reaction in toluene furnished cycloadduct 1.68 with 38% yield and 15% ee. We next attempted to lower the reaction temperature to increase the enantioselectivity. Relatively similar yield (36%) and ee (16%) was obtained by treating the solution of **1.20** and **1.18** in the presence of Rh_2(*S*-TCPTTL)$_4$ in toluene at 0 ºC (Entry 5). The attempt to use excess of **1.18** (5 eq.) afforded **1.81** in 36% yield and 15% ee (Entry 6). Slow addition of **1.20** to the solution of **1.18** was conducted which furnished **1.81** in 40% yield and 13% ee (Entry 7). Finally we attempted increasing catalyst loading to 10 mol% which formed **1.81** in 32% yield and 12% ee (Entry 8).

Table 1.5. Selected conditions screening of the chiral Rh-catalyzed enantioselective 1,3-dipolarcycloaddition

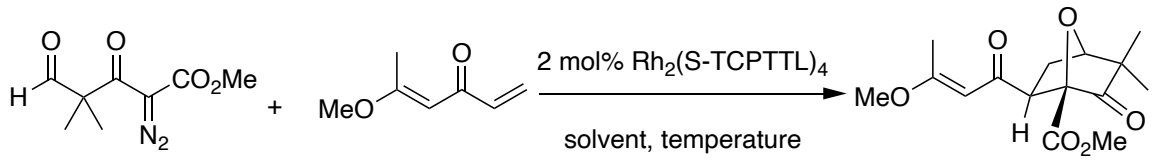

1.20 (1 eq) **1.18** (1.2 eq) **1.81**

entry	solvent	temperature	yield (%)[a]	ee (%)[b]
1	CH_2Cl_2	rt	NA	NA
2	CH_2Cl_2	reflux	26	6
3	$CF_3C_6H_5$	rt	NA	NA
4	toluene	rt	38	15
5	toluene	0 ºC	36	16
6[c]	toluene	rt	36	15
7[d]	toluene	rt	40	13
8[e]	toluene	rt	32	12

*[a] yields are based upon products purified by column chromatography but are not optimized. [b] enantiomeric excesses (ee) were determined via analytical normal phase HPLC column (CHIRALCEL® OD-H) eluting with i-PrOH/hexane (20:80, v/v). [c] 5 eq. of **1.18** was used. [d] **1.18** and catalyst were premixed in toluene, **1.20** in toluene was slowly added via syringe pump over 30 min. [e] 10 mol% was used.*

After surveying different catalyst loadings, solvents and temperatures, we discovered that treating **1.20** with **1.18** in the presence of 2 mol% Rh_2(*S*-TCPTTL)$_4$ in

toluene overnight at room temperature gave **1.81** in 38% yield in 15% ee (Table 1.5, Entry 1) (Figure 1.33).[28] Toward improving the ee of this process, we screened a series of other catalysts known to promote enantioselective dipolar cycloadditions of carbonyl ylides. Of these, Rh_2(*S*-TFPTTL)$_4$ gave **1.81** with comparable ee**,** whereas the ee obtained using Rh_2(*S*-BPTTL)$_4$ and Rh_2(*S*-TBSP)$_4$ were lower (Entries 2, 3, 4) (Figure 1.33).[95,100,101] On the other hand, no ee was observed using Rh_2(*S*-PTTL)$_4$ or Rh_2(*S*-BPTV)$_4$ (Entries 5, 6) (Figure 1.33).[101] Although these preliminary studies support the feasibility of developing new catalysts that might be used to synthesize individual enantiomers of melicolone A or B, the low ees and the fact that melicolone A or B were isolated as racemates persuaded us to continue the synthesis using racemic **1.81**.

Table 1.6. Selected catalysts screening of the chiral Rh-catalyzed enantioselective 1,3-dipolarcycloaddition

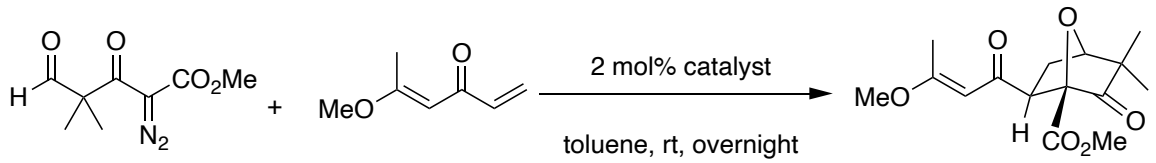

1.20 (1 eq) **1.18** (1.2 eq) **1.81**

entry	catalyst	yield (%)[a]	ee (%)[b]
1	Rh_2(*S*-TCPTTL)$_4$	38	15
2	Rh_2(*S*-TFPTTL)$_4$	32	13
3	Rh_2(*S*-BPTTL)$_4$	38	6
4	Rh_2(*S*-TBSP)$_4$	16	7
5	Rh_2(*S*-PTTL)$_4$	35	0
6	Rh_2(*S*-BPTV)$_4$	25	0

[a] yields are based upon products purified by column chromatography but are not optimized. [b] enantiomeric excesses (ee) were determined via analytical normal phase HPLC column (CHIRALCEL® OD-H) eluting with i-PrOH/hexane (20:80, v/v).

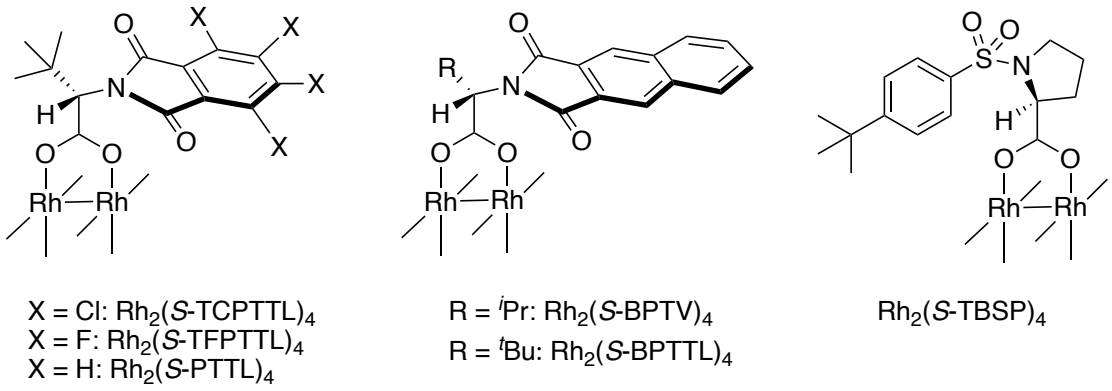

Figure 1.33. Structures of chiral dirhodium(II) complexes.

1.8 COMPLETION OF THE TOTAL SYNTHESES OF (±)-MELICOLONES A AND B

1.8.1 Base Induced Aldol Cyclization Sequence

With **1.65** in hand, we next investigated strategies to induce the aldol cyclization of the 1,3-dicarbonyl species onto the ketone carbonyl group to construct another five-membered ring. We first investigated selective removal of the methyl group on the vinylogous methyl ester to expose the 1,3-dicarbonyl moiety. However, there is another methyl ester group in **1.78**, which could potentially cause selectivity issues. Moreover, Padwa has reported the oxa-tricyclic core structure decomposes in acidic conditions.[78] Armed with this knowledges, we treated **1.78** with freshly distilled trimethylsilyl iodide (TMS-I) in $CHCl_3$ followed by the addition of MeOH (Equation 1.30). Gratifyingly, we isolated **1.122** in 62% yield after chromatography purification and another 10% inseparable mixture with the correct mass based on LCMS. We assumed the inseparable mixture to be the isomer of **1.122** which could ultimately be cyclized to aldol product as well.

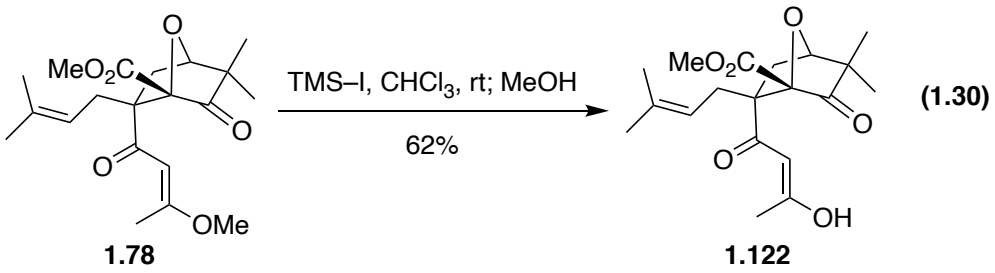

1.78 **1.122** **(1.30)**

We then investigated the base induced aldol cyclization of **1.122**. We treated **1.122** with freshly distilled 1,8-diazabicycl[5.4.0]underc-7-ene (DBU) in THF at 0 ºC for 30 min, and the reaction cleanly afforded **1.16** in 92% yield (Equation 1.31).

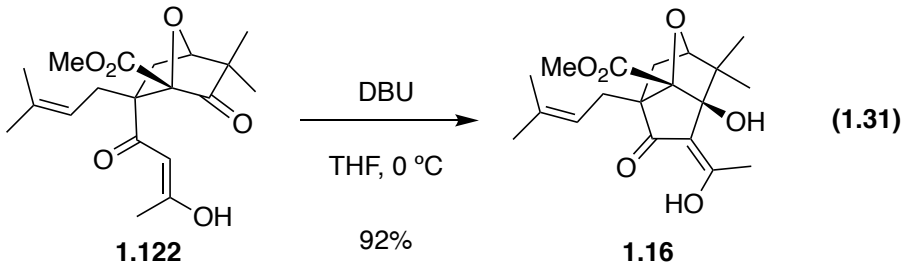

1.122 **1.16** **(1.31)**

With the successful development of a two-step sequence to prepare **1.16**, we next turned our attention to develop a one-pot procedure to convert **1.78** to **1.16**. According to the reported trimethylsilyl iodide (TMS-I) deprotection mechanism by Jung, the TMS-I first cleaves the methyl ether to afford the alkyl iodide and a trimethylsilyl ether, which was then converted to its alcohol product by the addition of methanol.[102] We proposed that after forming the trimethylsilyl ether intermediate, we should be able to directly treat the intermediate with tetrabutylammonium fluoride (TBAF) to deprotect the silyl ether and induce the aldol cyclization. To test our hypothesis, we treated **1.78** with TMS-I in MeCN at room temperature, and after forming the trimethylsilyl ether, we cooled the solution to 0 ºC and added TBAF solution (Equation 1.32). However, we were not able to isolate the

desired cyclization product, and we obtained complex mixture. We also tried directly treating the trimethylsilyl ether intermediate with DBU, but unfortunately, we were not able to observe formation of the desired product.

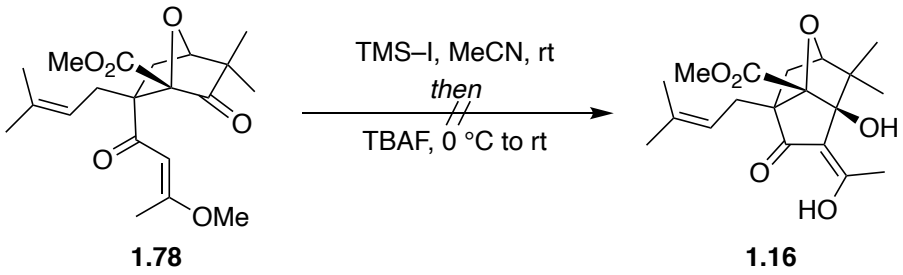

1.78 **1.16** **(1.32)**

After these unsuccessful attempts to develop a one-pot sequence to convert **1.78** to **1.16**, we developed a two-step procedure without purification of the enol intermediate. We treated **1.78** with TMS-I in $CHCl_3$, followed by the addition of MeOH to convert the trimethylsilyl ether to the corresponding enol. After working up the reaction, we directly treated the crude product with DBU in THF at 0 ºC, and then allowed the reaction to warm to room temperature. We thus isolated **1.16** via the two-step, one separation sequence in 75% yield (Equation 1.33).

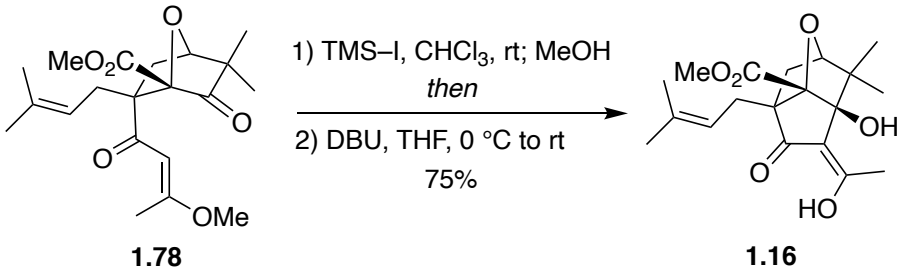

1.78 **1.16** **(1.33)**

1.8.2 Epoxide Formation and Regioselective Epoxide Opening

With **1.16** in hand, the remining step to complete the total syntheses of (±)-melicolones A and B was to construct the tetrahydropyran moiety. Such conversion has been well documented via the sequence of epoxide formation followed by hydoxy epoxide openings. We first investigated the epoxidation of **1.16** with *m*-chloroperoxybenzoic acid (*m*-CPBA) to determine if there are any substrate control present in **1.16** that would afford some facial selectivity for the epoxidation. We treated **1.16** with *m*-CPBA in CH_2Cl_2 for 30 min, and obtained the epoxide product with the dr of 1.1 : 1 in 97% yield (Equation 1.34).

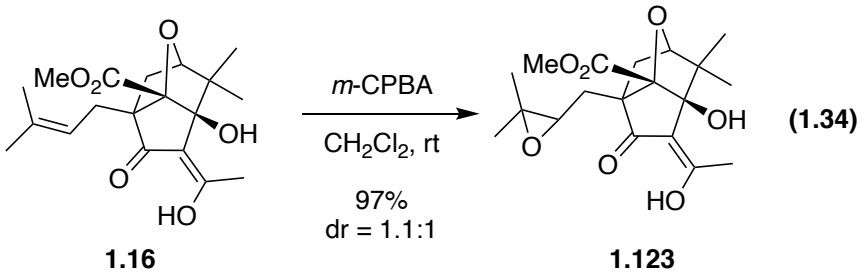

1.16 **1.123** **(1.34)**

To improve the diastereoselectivity of the epoxidation step, we turned our attention to investigate other epoxidation strategies via catalyst control. Shi reported the enantioselective epoxidation reactions of disubstituted and trisubstituted alkenes using oxone (potassium peroxymonosulfate) and the D-fructose-derived catalyst **1.124** (Equation 1.35).[103] The reaction is proposed to proceed through a dioxirane intermediate that is generated from the oxidation of the catalyst ketone by oxone. The dioxirane species would transfer oxygen to the alkene forming the epoxide.[104] Planar and spiro transition states were proposed to explain the stereoselective outcomes of the reactions, and also

trisubstituted olefins were reported to have pretty excellent outcomes under this condition.[105]

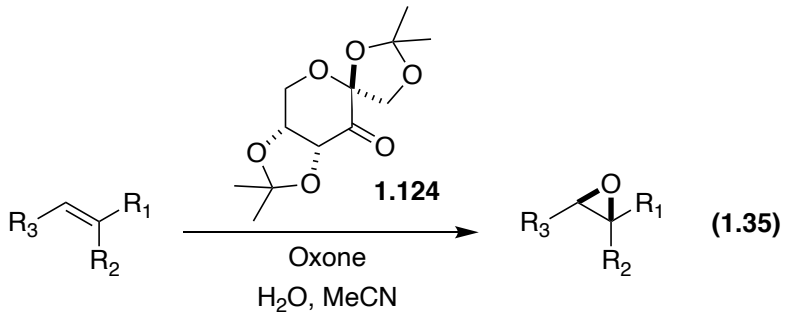

(1.35)

With the promising precedent of Shi epoxidation, we investigated the Shi epoxidation of **1.16**. Chiral ketone **1.124** was prepared from D-fructose according to the literature procedure.[103] The intermediate **1.16** was treated with chiral ketone **1.124** and oxone in the buffer solutions, but we did not isolate any of the desired epoxide products; a complex mixture was obtained instead (Equation 1.36). We have also investigated other reaction conditions Shi reported on the epoxidation of trisubstituted olefins, but we did not see any success in converting **1.16** to its epoxide **1.123** stereoselectively (Equation 1.37).

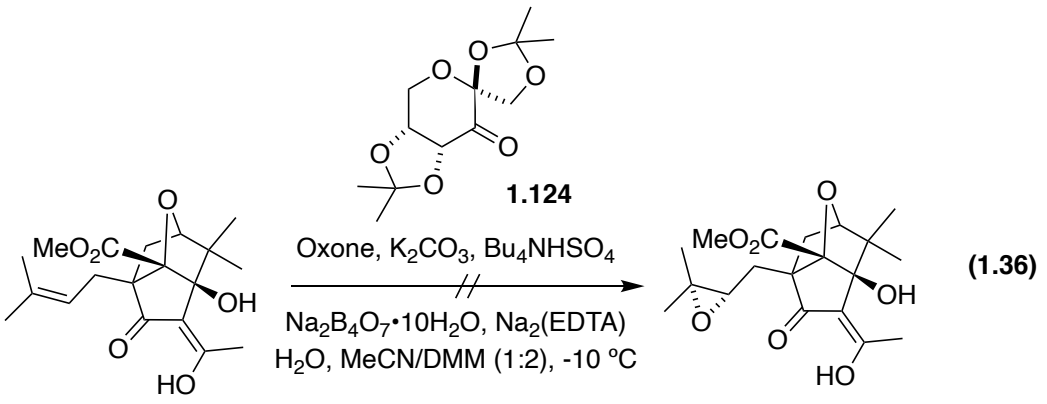

(1.36)

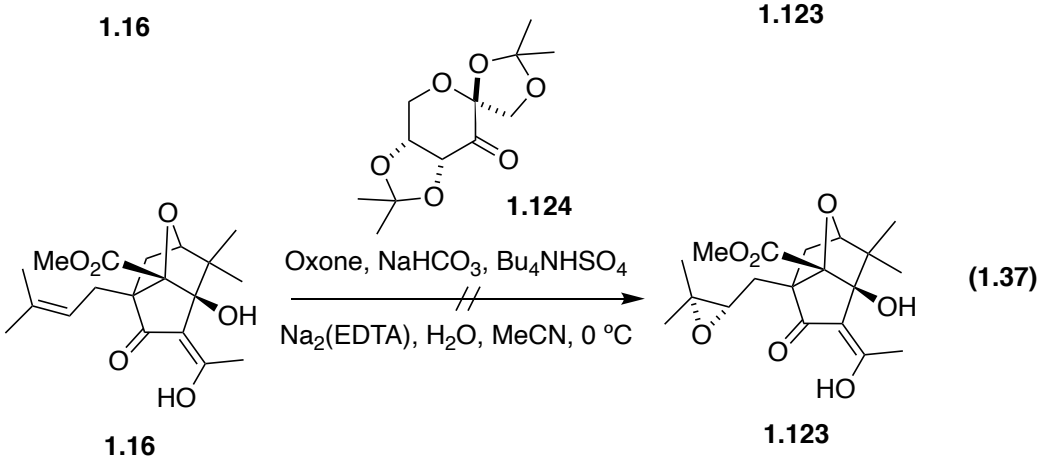

(1.37)

There are also examples of using chiral (salen)Mn (III) complexes to enantioselectively epoxidize trisubstituted olefins that have been reported by Jacobsen, so there are still potential solutions to improve the stereoselectivity of the epoxidation step.[106] However, since both epoxide isomers can be converted to melicolone natural products, and melicolones A and B were isolated as racemates, so we decided to complete the synthesis with the current epoxide mixture first.

The epoxide **1.123** was not stable at ambient temperature nor on silica gel, so we decided to use the mixture of two diastereomeric epoxides to investigate the selective epoxide opening strategies. Such selective epoxide opening in the presence of acids to form six-membered ring are well precedented in the literature (Figure 1.34).[107-109] Wang used

formic acid to promote the intramolecular cyclization of hydroxy epoxide **1.125** to form the tetrahydropyran derivative **1.126** in their total synthesis of coriandrone B (Figure 1.34A).[107] Inoue reported the use of 1N HCl in EtOH to selectively open the epoxide **1.127** to form six-membered tetrahydropyran moiety of **1.128** in the synthesis of an NG-121 model compound (Figure 1.34B).[108] Nicolaou reported the use of camphorsulfonic acid (CSA) with **1.129** to achieve the construction of the tetrahydropyran system via the intramolecular hydroxy epoxide opening to generate **1.130** (Figure 1.34C).[109] Reagent-controlled switching of 5-exo to 6-endo cyclization has also been demonstrated by Morimoto (Figure 1.34D).[110] Triisopropylsilyl trifluoromethanesulfonate (TIPSOTf) was employed to promote the cyclization of bishomoepoxy alcohols **1.131** to give TIPS ether substituted tetrahydropyran derivative **1.132**, and the formation of tetrahydrofuran derivatives was suppressed by the disfavored steric interactions of the TIPS ether and geminal dimethyl groups.[110]

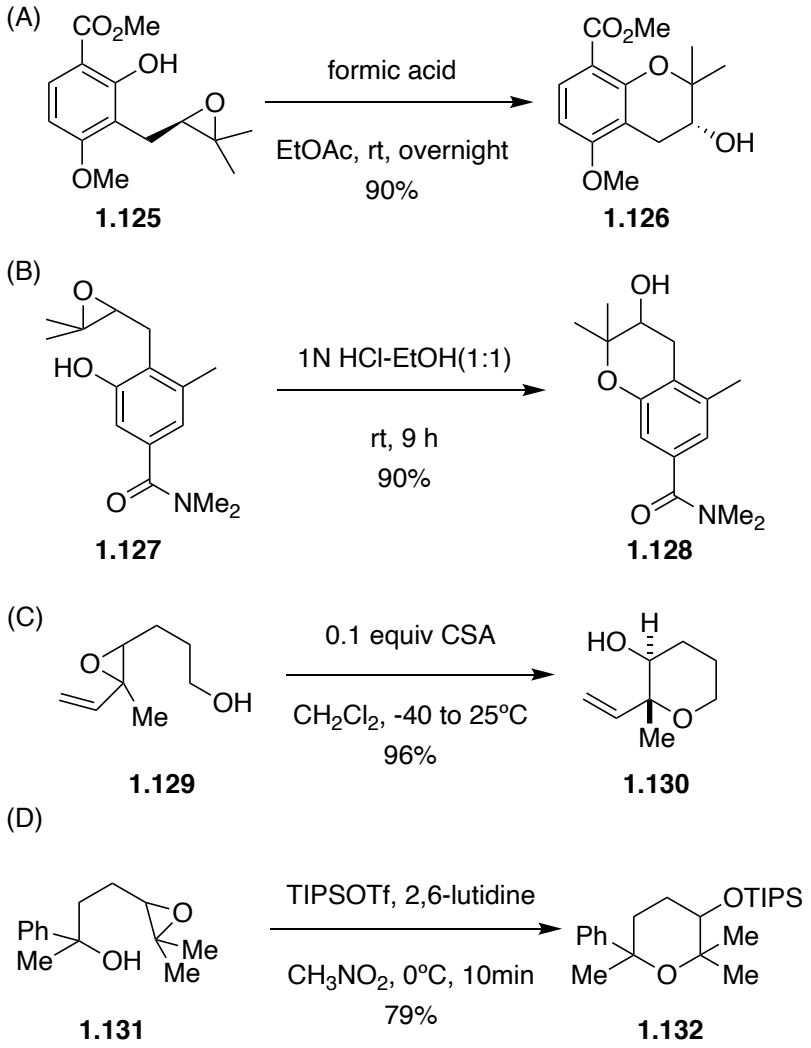

Figure 1.34. Reported examples of the selective tetrahydropyran moiety formation from the hydroxy epoxide species

Encouraged by these promising reports, we initiated our investigation of selective epoxide opening by screening acid catalyzed reaction conditions (Scheme 1.12). We first investigated the procedure reported by Wang, and treated epoxide **1.123** with formic acid in EtOAc. Unfortunately, a complex mixture was formed and the desired product was not observed.[107] The treatment of epoxide **1.123** with catalytic amount of HCl in Et_2O also failed to deliver any of the desired natural product. We also investigated the procedure

reported by Inoue, 1N HCl in EtOH at room temperature, but this reaction did not form any desired product either.[108] Gratifyingly, a reaction of epoxide **1.123** with 10 mol% CSA in CH_2Cl_2 from -40 ºC to rt, according to the procedure reported by Nicolaou, afforded a mixture of the desired final natural products **1.1** and **1.2** in 95% combined yield.[109] The mixture of **1.1** and **1.2** was not separable on silica gel chromatography, instead we developed a method on C18 column reverse phase HPLC to separate **1.1** and **1.2** effectively which ultimately afforded **1.1** in 49% and **1.2** in 45%.

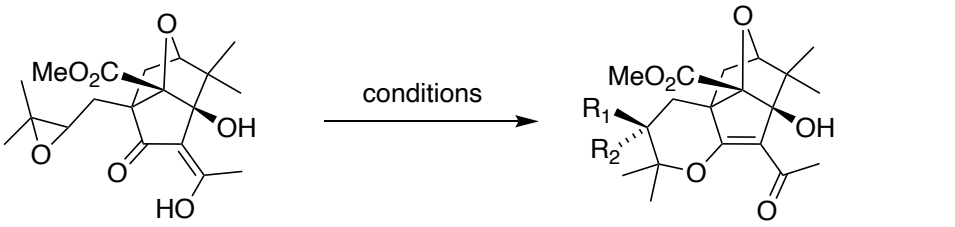

1.123

(±)-Melicolone A (**1.1**): R_1 = OH, R_2 = H
(±)-Melicolone B (**1.2**): R_1 = H, R_2 = OH

conditions	result
cat. HCOOH, EtOAc, rt	no product detected
cat. HCl, Et_2O, rt	no product detected
1N-HCl, EtOH, rt	no product detected
10 mol% CSA, CH_2Cl_2, -40 ºC to rt	95% (**1.1** and **1.2** combined)

Scheme 1.12. Selective epoxide opening of **1.123**.

With the successful formation of the melicolones A (**1.1**) and B (**1.2**) in a two-step sequence, we next turned our attention to develop a one-pot procedure for converting **1.16** to **1.1** and **1.2**. Epoxide formation and epoxide opening steps were both conducted in CH_2Cl_2, and both steps were clean and efficient. Accordingly, we treated **1.16** with MCPBA in CH_2Cl_2 at rt for 30 min whereupon the reaction mixture was cooled to –40 ºC.

CSA (10 mol%) was added, and the solution was stirred at room temperature for another 30 min. We were glad to observe the complete conversion of **1.16** to the mixture of **1.1** and **1.2**. Further purification afforded a mixture of **1.1** and **1.2** in 85% combined yield with the dr of 1.1:1 (Equation 1.38).

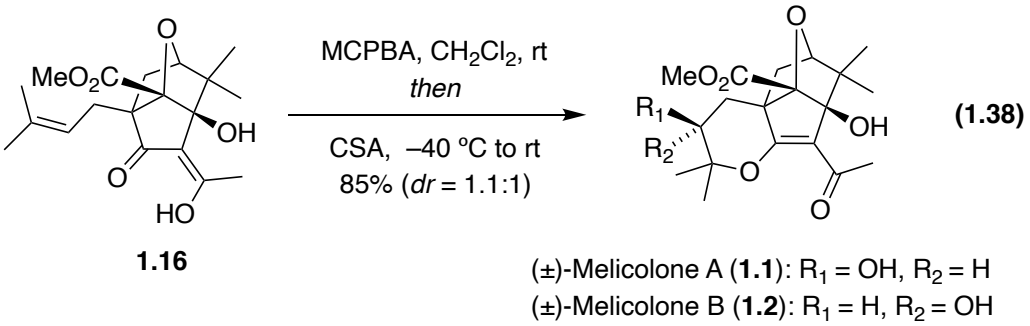

1.16

(±)-Melicolone A (**1.1**): R_1 = OH, R_2 = H
(±)-Melicolone B (**1.2**): R_1 = H, R_2 = OH

(1.38)

1.9 SUMMARY

In summary, we have accomplished the first total syntheses of (±)-melicolone A and (±)-melicolone B, which are epimeric isomers derived from rearranged acetophenones. The synthesis is remarkably concise and efficient which only requires nine longest linear steps from the commercially available starting materials and eight isolated intermediates in 12.3% combined overall yield. The synthesis features a novel rhodium(II) catalyzed 1,3-dipolar cycloaddition reactions of carbonyl ylide generated from an aliphatic aldehyde with rhodium carbene and an unsaturated vinylogous ester dipolarophile. The cycloaddition generated the oxabicycloheptane core in an unusual and highly regioselective (16:1) and stereoselective (15:1) way which could be used as the unified intermediate to approach to other melicolone natural products with the same tetracyclic core structure. The unusual regio and stereoselectivity were dominated by the steric effects instead of the more commonly observed electronic effects. Studies of enantioselective 1,3-dipolar

cycloadditions promoted by chiral rhodium(II) catalysts demonstrated the feasibility of constructing the oxabicycloheptane core enantioselectively; however, further screen of chiral catalysts are needed to improve the ee of the reaction. Stereoselective prenylation of the oxabicycloheptane cycloadduct sets the stage for the following base induced aldol cyclization to generate the penultimate tricyclic intermediate. Final epoxidation of the prenyl group and acid-catalyzed regioselective epoxide opening sequence affords a 1.1 : 1 mixture of (±)-melicolones A and B that is separated on HPLC.

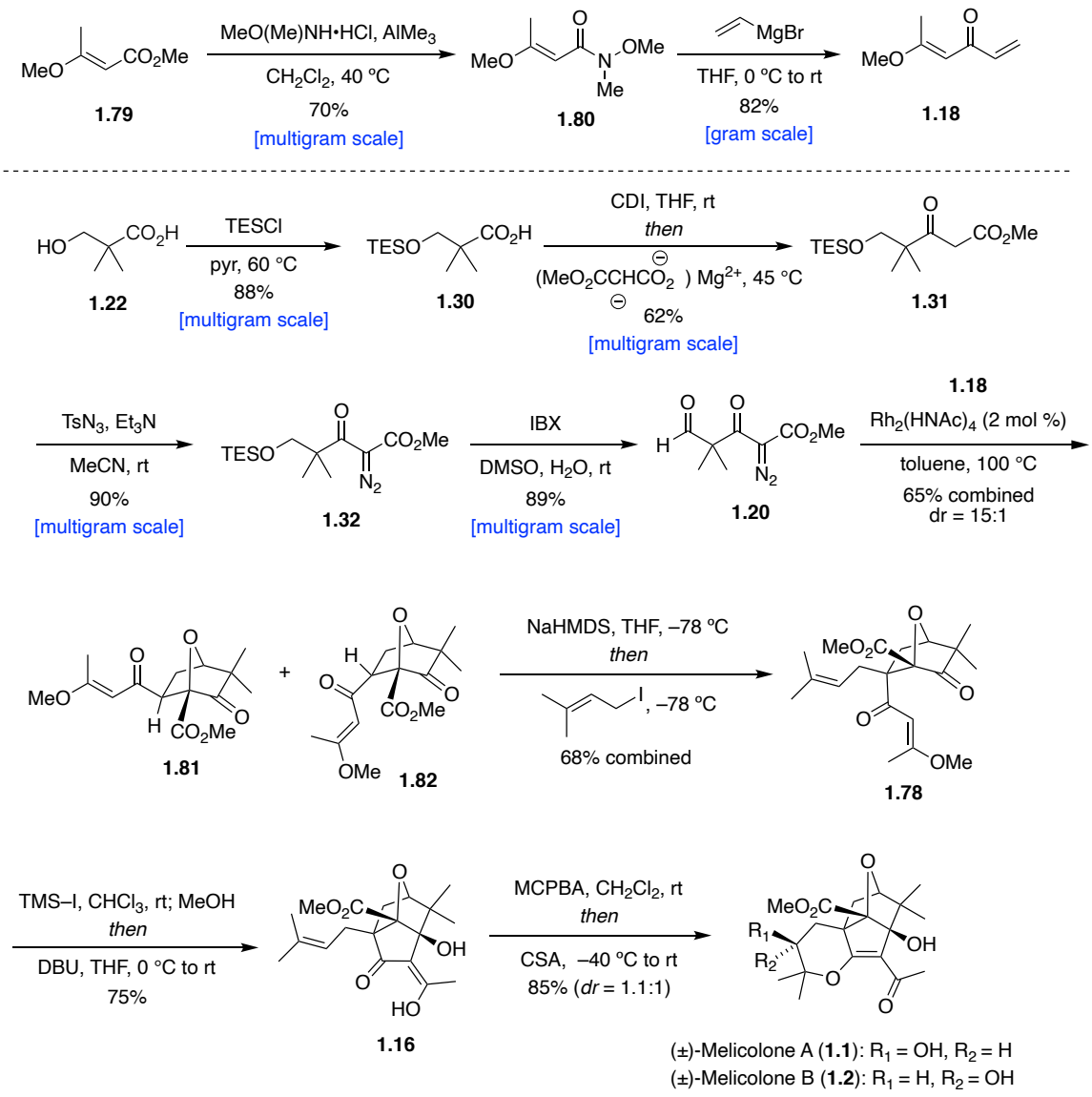

Scheme 1.13. The total syntheses of (±)-melicolone A and (±)-melicolone B

DESIGN, SYNTHESIS AND EVALUATION OF NOVEL CARBAZOLE BASED PHOTOCAGES

Chapter 2: Photocages

2.1 INTRODUCTION

Photocages are light-reactive protecting groups that can be appended to a molecule to render it chemically and biological inert. Photocages can be removed under mild conditions without the need for chemical reagents through exposure of the protected compound to light to release biologically or chemically active molecules. These unique protecting groups can be removed in a temporal and spatial controlled fashion thus releasing the active molecules.[111] Although photocages were originally designed and synthesized by synthetic chemists, the applications in synthetic chemistry are minimal. One well known example was reported by Nicolaou and coworkers in their total synthesis of calicheamicin γ1, where the *o*-nitrobenzyl group was utilized to protect a secondary amine.[112] A similar protection strategy was employed by Gareau and coworkers in their study of total synthesis of *N*-methyl leukotriene C_4.[113] In biology, the use of photocages attracted considerable interest in biology due to the precise control of the decaging process, which could enable the detailed studies of the role of bioactive molecules.[114] There are numerous applications in biology including the control of protein functions,[115] cellular stimulation,[116] regulation of gene express,[117] and neuronal stimulation or inhibition.[118]

Barltrop and Schofield reported the first example of photosensitive protecting groups in 1962 as the strategy to protect amino acids.[119] Upon irradiation with UV light, the Cbz group appended to the glycine moiety was removed from **2.1**, generating free glycine **2.2** and benzyl alcohol **2.3** (Equation 2.1). Barton, Sheehan, and Woodward later

published reports on photosensitive protecting groups followed by the original Barltrop report.[120-122]

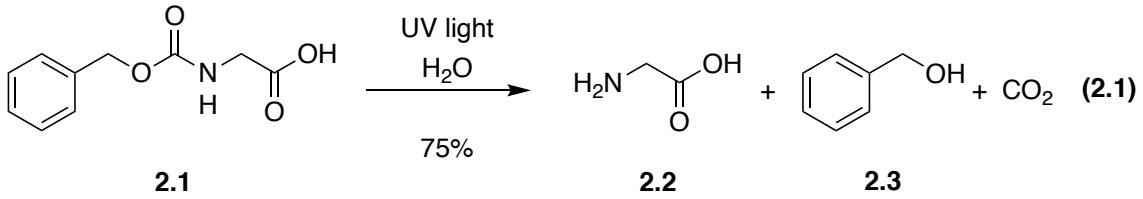

2.1 **2.2** **2.3** **(2.1)**

The term "cage" was first proposed by Hoffman in his synthesis and study of adenosine triphosphate (ATP) derivatives, even though a year earlier Engles and coworkers had synthesized a cyclic adenosine monophosphate (AMP) derivative; however, they did not use the term "cage", and decaging was not the main focus of their study.[123,124] Even though the term "cage" was coined by Hoffman, photocages were often referred to as photoremovable (or photolabile) protecting groups (PPGs).

The promising biological applications of photocages sparked the interests of chemists to develop various new photocages. The requirements for the development of a good photocage depend on the application, so it is unnecessary to fulfill all the requirements, some of which remain challenges in developing an optimal photocage.

The first requirement of a photocage is that it should have good decaging efficiencies at given wavelengths, and the wavelengths are usually above 300 nm for biological studies to avoid possible damage to the biological entity caused by the irradiation of light. The decaging efficiency of a photocage is defined as ε•Φ at a given wavelength. ε refers to the molar absorptivity of the molecule, which is relevant to the property of the chromophore moiety. Φ refers to the quantum yield of the decaging process. The quantum yield Φ is equal to the amount of released substrate, n_{rel}/mol, divided by the amount of

photons at the irradiation wavelength λ, n_p/mol (Equation 2.2). That is, the quantum yield of decaging Φ is equal to the rate constant of substrate release from the excited state (k_{rel}) divided by the sum of all of the rate constants of other potential photochemical pathways from the excited state (Σ k) (Equation 2.3). Moreover, the release of the caged molecule should also be the primary photochemical process, and it should be faster than the biological response that is under investigation. Commonly, there are multiple steps regarding ground-state and excited-state intermediates that precede the actual decaging of the target molecule, so the basic knowledge of the mechanism is necessary in the study.

$$\Phi rel = \frac{n_{rel}}{n_p} \quad \textbf{(2.2)}$$

$$\Phi rel = \frac{k_{rel}}{\Sigma\, k} \quad \textbf{(2.3)}$$

There are also other requirements for useful photocages. For example, caged molecules and their byproducts after the photochemical reaction should have good solubility in the target media (usually aqueous media for biological studies), and they should be stable in the target media and non-toxic to the biological entities under investigation.

Synthetically, caged molecules should be prepared in high yields and the purification should be facile. It is very important that caged molecules can be isolated cleanly without contamination of other uncaged substrates.

In view of the above requirements, chemists have developed various photocages with different properties that have been utilized in biological studies. Even though there is no one photocage that can meet all the requirements, depending on different purposes of biological studies, photocages have been demonstrated to be powerful and useful tools in

the biology. However, with the new demands in biological studies, scientists are still pursuing to develop novel photocages nowadays. Herein, we will briefly review some of the most common and widely utilized photocages based upon their structure features and decaging mechanisms in this chapter. Scopes and limitations of different photocages will also be presented.

2.2 NITROARYL PHOTOCAGES

2.2.1 *o*-Nitrobenzyl Photocages

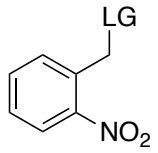

2.4
o-Nitrobenzyl photocages

λ ~ 300nm
LG = phosphates, carboxylates, carbonates,carbamates,
thiolates, phenolates, and alkoxides

The *o*-nitrobenzyl group **2.4**, is one of the most widely utilized photocage, was first used as a photocage as early as 1970, even though there were earlier reports on its photochemistry. Since then, a large number of the *o*-nitrobenzyl analogues have been synthesized and studied as photocages. Thanks to the pioneering studies by Bartlop and Woodward, *o*-nitrobenzyl photocages have been well-studied, and the decaging mechanism is well-understood.[125-129] Despite being widely used as photocages, they also have some inherent disadvantages that limit their use in some specific cases, which will be discussed later in this chapter.

The mechanism of the decaging process of *o*-nitrobenzyl groups has been studied over the years. Because of these contributions, we now have a relatively clear understanding of the decaging process (Scheme 2.1). Upon irradiation, **2.4** enters the

excited singlet state **2.5**, whereupon an intramolecular hydrogen abstraction occurs followed by internal conversion (IC) to form the *aci*-nitro tautomers **2.8** and **2.9**. The energy barrier for retautomerization of **2.8** to **2.4** is relatively low, but in some solvents (MeOH, MeCN) the equilibration between **2.8** and **2.9** is competitive with reformation of **2.4**. It is also possible for **2.5** to enter the excited triplet state through inter-system crossing (ISC), at which point an intramolecular hydrogen transfer can occur, forming the *aci*-nitro intermediate **2.8** upon ISC back to the ground state. The rate constant of decay for intermediates **2.8** and **2.9** depends heavily on aromatic ring substitution, solvent, and pH of the system. The *aci*-nitro intermediate **2.9** may undergo an irreversible cyclization to create intermediate **2.10**, which upon subsequent ring opening, forms hemiacetal **2.11**. Intermediate **2.11** collapses to form the 2-nitrosobenzaldehyde **2.12** while concomitantly releasing the leaving group, which is believed to be the rate determining step.

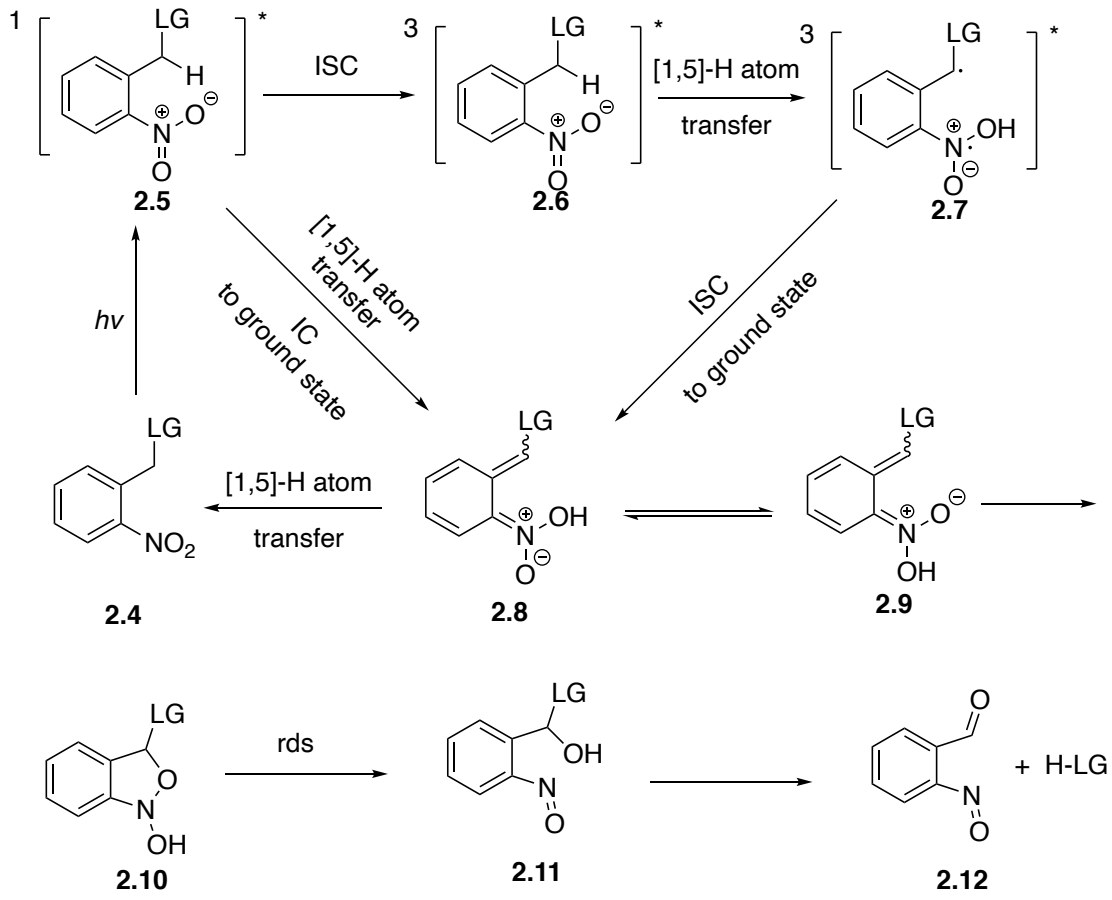

Scheme 2.1. Decaging mechanism for *o*-nitrobenzyl photocages.

There are a number of problems associated with *o*-nitrobenzyl photocages that are mostly due to the generation of the nitroso aldehyde product. The nitroso products usually have a higher molar absorptivity than the photocaged molecules at the decaging wavelength, which would adversely affect the light absorption of the photocaged compounds. Moreover, the nitroso products are generally reactive, and in some cases, the nitroso products react with the substrate itself or the decaged molecule. One example of the side reaction of nitroso products is the condensation reaction with primary amines. The undesired side reaction between nitroso product and primary amine was found by Givens and Bayley when they conducted their decaging studies of photocaged peptide.[130,131] This

raised the concern for the application of *o*-nitrobenzyl photocages for amino-containing compounds due to the potential side reactions that would diminish the efficiency of the decaging process. Furthermore, the nitroso products sometimes can be toxic toward the biological entities under investigation, which limits the application in biological studies.[114] Consequently, there have been extensive efforts to mitigate these issues. The introduction of alkyl groups at the benzylic position of the photocage resulted in enhanced uncaging rates and biologically less reactive nitroso ketones as reaction products.

One of the appealing aspects of *o*-nitrobenzyl photocages is their ability of decaging with various leaving groups such as phosphates, carboxylates, carbonates, carbamates, thiolates, phenolates, and alkoxides. However, the decaging efficiency is heavily affected by the leaving group ability. For a good leaving group such as phosphate, release of the leaving group is synchronous with the formation of the *aci*-nitro intermediate **2.9**, having a rate on the order of milliseconds. However, for a bad leaving group such as alkoxide, the decaging rate would depend on the rate of the collapse of the cyclic intermediate **2.10**. The pH was found to be important in some cases as well. At neutral pH, the decay of intermediate **2.11** was found to be significantly slower than the decay of the *aci*-nitro intermediate **2.9**. Therefore, the release of bad leaving groups is often challenging for the *o*-nitrobenzyl photocages, and other possible solutions were also proposed such as the use of carbonate linkers and carbamate linkers (Equation 2.4). They are generally better leaving groups than alkoxides and will lead to better decaging efficiencies, and subsequently the carbonates or carbamates will undergo thermal fragmentation to furnish the free alcohols or amines **2.16**.

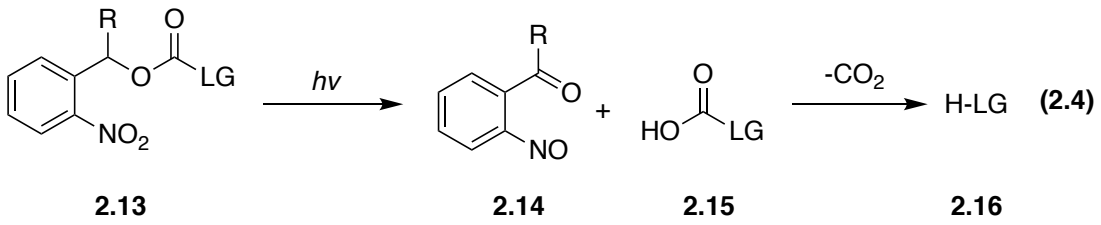

There are biological applications of the *o*-nitrobenzyl group **2.4**, due to its fast release of substrates. Deiters group, Chin group and Schutlz group have reported the collaboration studies of the photocontrol of tyrosine phosphorylation process in mammalian cells via genetic encoding of photocaged tyrosine.[132,133] Caged tyrosine derivative **2.17** was generically encoded into proteins in mammalian cells, which was then photolyzed to release free tyrosine derivative **2.18** upon irradiation of UV light (365 nm) (Figure 2.1). The released tyrosine derivative **2.18** was later found being phosphorylated in mammalian cells.

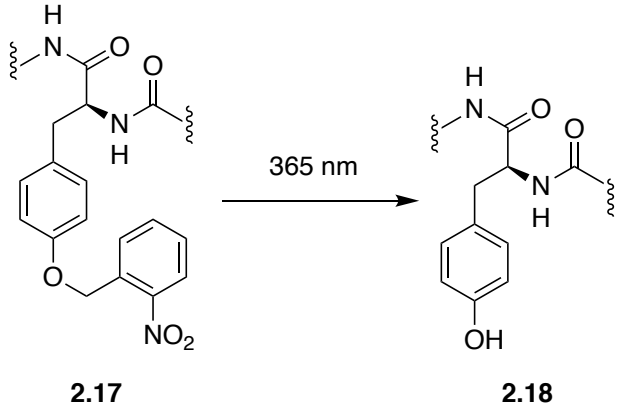

Figure 2.1. Photocaged tyrosine derivatives in biological applications.

2.2.2 *o*-Nitrobenzyl Photocage Derivatives

Since the early reports of *o*-nitrobenzyl photocages, a number of *o*-nitrobenzyl derivatives were reported. These new *o*-nitrobenzyl photocages were developed to increase the decaging efficiencies as well as to redshift the decaging wavelength. Modifications

include different substitutions at the benzylic position of the *o*-nitrobenzyl photocages and changes of the aromatic chromophores.

An early example of the modification at the benzylic position of *o*-nitrobenzyl photocages was reported by Woodward.[122] Various substituents at benzylic position were evaluated to avoid the side reactions with nitroso aldehyde products formed after decaging. One of the drawbacks of adding a substituent at the benzylic position is creating a chiral center, which would be problematic if chiral molecules have to be protected, unless the added substituent is identical to the aromatic chromophore. Photocage **2.19** fits into this category which *o*-nitrophenyl was added as the substituent at the benzylic position (Figure 2.2). Despite the chirality issue, many substituents at the benzylic position were found to be beneficial for the decaging efficiencies of the photocages. A simple addition of methyl group at the benzylic position led to a new photocage derivative 1-(2-nitrophenyl)ethyl **2.20**, which has a better quantum yield compared with *o*-nitrobenzyl cages. Reichmanis reported the examples of pivalate ester of **2.20** with $\Phi = 0.09$ in polymer and $\Phi = 0.64$ in acetonitrile compared with **2.4** with $\Phi = 0.04$ in polymer and $\Phi = 0.13$ in acetonitrile.[134,135] Other reports on the application of 1-(2-nitrophenyl)ethyl photocages including the decaging of biologically active carboxylic acids in plant cells and on solid support were published shortly after.[136,137] Specht and Goeldner proposed the introduction of an electron withdrawing group, in this case the trifluoromethyl group, at the benzylic carbon of **2.21** gave a dramatic increase in the quantum yield in the case of choline and arseniocholine ether derivatives.[138] The addition of the methyl group at the benzylic position led to the formation of nitroso ketone product instead of nitroso aldehyde, which was less reactive, thus diminishing the side reactions. They were able to be demonstrated as the efficient protecting groups for amino acids.[122]

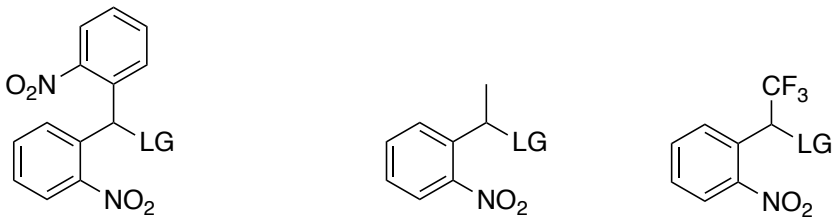

2.19
λ = 355 nm
LG = carboxylates, phosphates and carbamates

2.20
λ = 254 nm
LG = carboxylates

2.21
λ = 364 nm
LG = ethers

Figure 2.2. Select examples of *o*-nitrobenzyl photocages with substituents at benzylic position.

Due to the issues including generation of a chiral center, limited impacts on the absorbance, and synthetic challenges, modifications of the benzylic position were relatively limited compared with modifications on aromatic rings. A second electron withdrawing group was added to the aromatic ring to increase the rate of the H-abstraction process thus facilitating the formation of the *aci*-nitro intermediates (Figure 2.3). 2,6-Dinitrobenzyl derivative **2.22** was designed, and it was found to have a superior decaging efficiency compared with parent substrate.[139,140] The 6-nitroveratryl **2.23** and the related 6-nitropiperonylmethyl derivative **2.24** were designed to have a redshift of the effective irradiation wavelength, but the increased absorbance did not convert to increased decaging efficiency, and the quantum yield of 6-nitropiperonylmethyl derivatives were typically one order magnitude less than that of *o*-nitrobenzyl derivatives.[114,141] This example reveals another challenge when designing a photocage. Namely the increase in absorbance may not translate into increased efficiency of the decaging process.

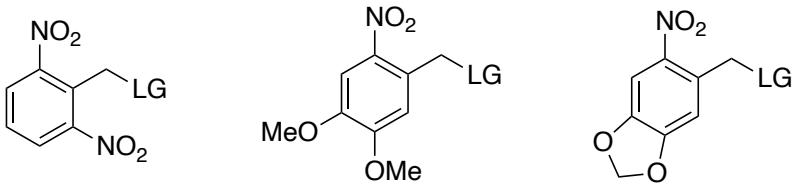

2.22
λ = 254 nm
LG = carbamates

2.23
λ = 350-420 nm
LG = carbamates

2.24
λ_{max} = 350 nm
LG = carbamates, carbonates, and ethers

Figure 2.3. Select examples of *o*-nitrobenzyl photocages with modification of aromatic rings.

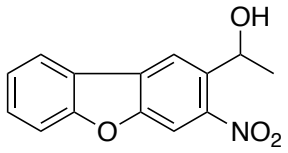

2.5
nitrodibenzofuran **(NDBF)**

Another important example of an *o*-nitrobenzyl photocage is the nitrodibenzofuran (NDBF) photocage. NDBF (**2.5**) photocage was first reported by Ellis-Davies and coworkers in 2006 belongs to the *o*-nitrobenzyl photocages group.[142] Various biological applications have been reported utilizing NDBF as the photocage, including solid phase peptide synthesis, protein function regulation, fluorescence activation, and Ca^{2+} controlled release.[143-148] The first example of NDBF was reported by Ellis-Davies and coworkers, wherein NDBF was modified with the EGTA functional group to cage Ca^{2+} ions (Figure 2.4).**Error! Bookmark not defined.** Upon irradiation of light, the EGTA group underwent fragmentation that caused the binding affinity for Ca^{2+} to drop significantly, thus releasing free Ca^{2+}. **NDBF-EGTA** caged Ca^{2+} was decaged with one-photon (350 nm) irradiation to initiate contraction of skinned guinea pig cardiac muscle. Two-photon photolysis was demonstrated in intact cardiac myocytes with irradiation at 720 nm. Viht and coworkers reported the photolysis of **NDBF-ARC** in manipulating protein functions via cAMP-

dependent protein kinase (PKA) (Figure 2.4).[149] After caging with NDBF, the 7DP-Pip moiety of a tight binding bisubstrate inhibitor (ARC), the affinity of ATP binding pocket and ARC was found to drop over 5 orders of magnitude. The inhibitory effects were illustrated in disrupting the PKA holoenzyme in cell lysates upon photolysis with a 398 nm LED light. Tampé and coworkers reported a caged glutathione derivative **NDBF-GSH** in spatially and temporally controlled 3D protein structures assemble (Figure 2.4).[150] Glutathione (GSH) was released upon irradiation with light at 365 nm with one-photon or at 730 nm with two-photon to trigger the interactions with glutathione S-transferase (GST) tagged proteins, which facilitated the 3D assembly of protein structures. Moreover, Distefano and coworkers reported NDBF caged peptide using a cysteine residue that can be decaged at 365 nm with one-photon irradiation and two-photon irradiation at 800 nm (Figure 2.4).**Error! Bookmark not defined.** The peptide that is known as the substrate for protein farnesyltransferase was released in the presence of enzyme which resulted in the formation of the farnesylated product.

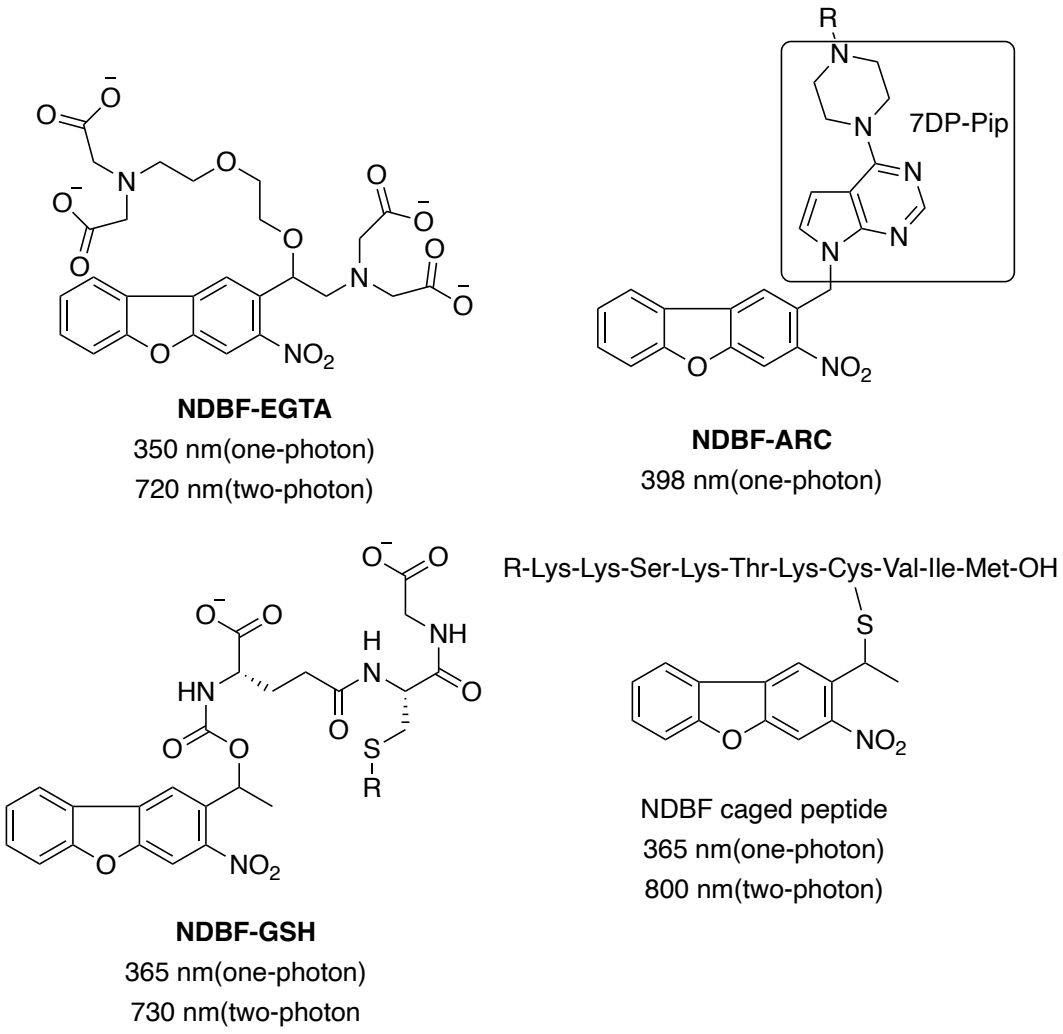

Figure 2.4. Examples of NDBF photocage in biological studies.

Modifications on NDBF were also reported to increase the decaging efficiency and solubility as well as to extend light absorption range. Substitutions on the aromatic ring were found to have impacts on absorption profiles especially the two-photon absorption (Figure 2.5). Introduction of the methoxy group at the 4-position in **MeO-NDBF** extended two-photon excitation from about 720 nm to 800 nm in releasing thiol peptides.[151] Substitution with a dimethyl amino group at the same position in **DMA-NDBF** redshifted one-photon excitation to 385 nm and two-photon excitation to 840 nm in releasing

oligonucleotides.[152] The substitution of polar functional groups such as carboxyl groups on the branch chain of **COOH-NDBF** increased the solubility of the caged molecules.[153] Moreover, different chromophores derived from NDBF were evaluated in both one-photon and two-photon irradiations. The Kobayashi group developed photocage **NPBF** from modifying the chromophore of NDBF, which has a two-photon excitation at 840 nm for the release of benzoic acids.[154] Moreover, computational studies were also exploited to direct the modification strategies.[155,156]

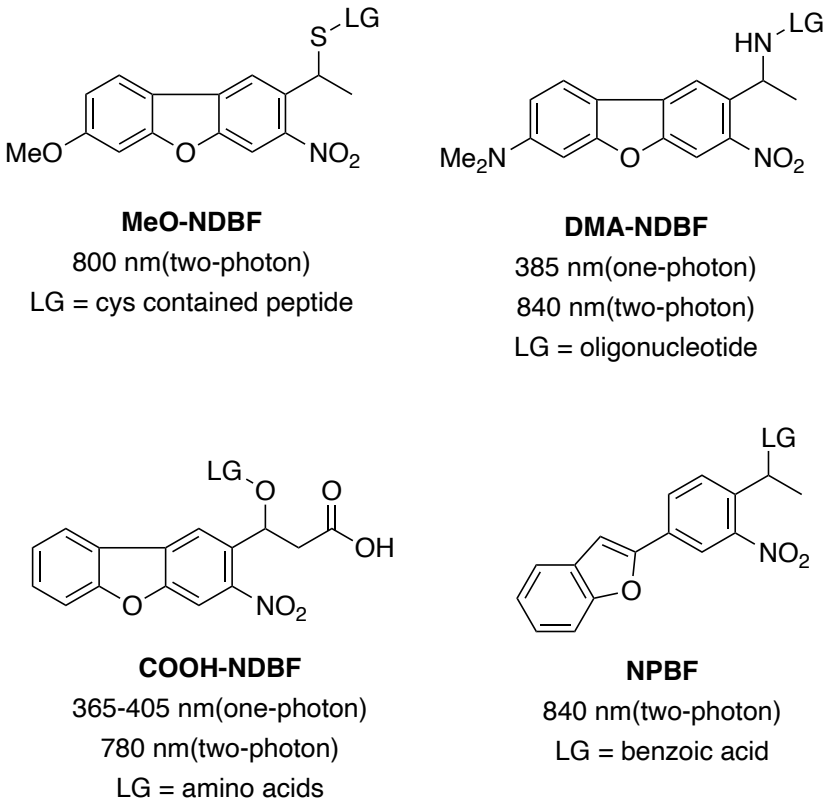

Figure 2.5. Modification attempts on NDBF photocage.

2.2.3. *o*-Nitro-(2-phenethyl)ethyl Photocages

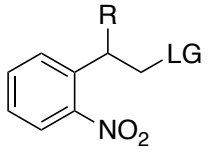

2.26 R = H
2.27 R = Me

o-Nitro-(2-phenylethyl) photocages
λ = 365 nm
LG = carbonates (nucleosides)

Hasan and coworkers developed the *o*-nitrobenzyl one homologue **2.26**, and despite the structural similarities, **2.26** has a remarkably different decaging mechanism.[157] This structural change also resulted in a slight improvement in decaging efficiencies over the *o*-nitrobenzyl counterparts. However, the addition of a methyl group to the benzylic position as shown in **2.27** led to an increase in the decaging efficiencies. For example, in a decaging study of 5'-O-nucleoside carbonates, a substrate caged with **2.26** was decaged with a slightly higher quantum yield (Φ = 0.042) than the *o*-nitrobenzyl photocage (Φ = 0.033) (Equation 2.5).[158] However, the addition of methyl group at the benzylic position in **2.27** resulting a 10-fold increase in quantum yield (Φ = 0.35). In addition, with the introduction of the methyl group, the decaging byproduct is less reactive with amine, which makes the photocage more suitable for caging amine substrates.

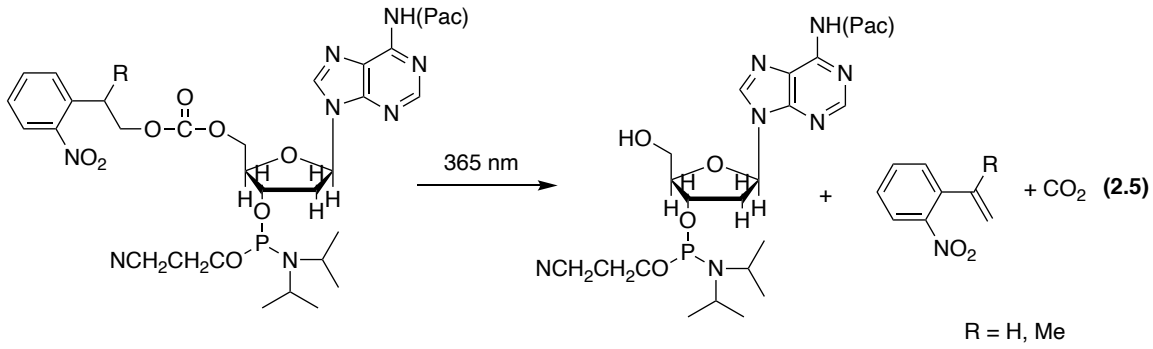

The decaging mechanism for *o*-nitro-(2-phenethyl)ethyl photocages has not been well studied, but the product **2.31** is consistent with the proposed mechanism (Scheme 2.2).[158] The decaging process starts with the irradiation of the starting material **2.28**, followed by an intramolecular hydrogen abstraction at its excited state generating the *aci*-nitro intermediate **2.29**. Deprotonation of **2.29** by solvent forms intermediate **2.30**, followed by the elimination of the leaving group and formation of nitrostyrene product **2.31**.

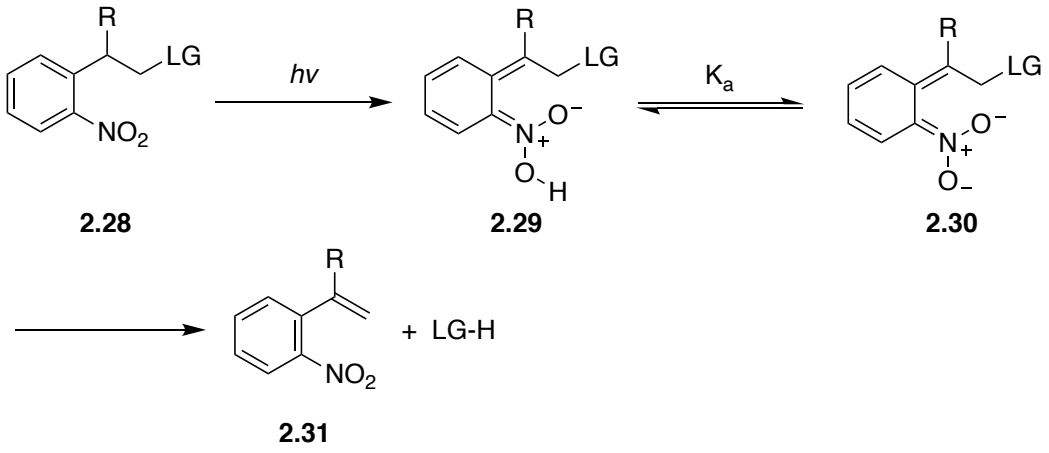

Scheme 2.2. Proposed mechanism for *o*-nitro-(2-phenethyl)ethyl photocages.

This group of photocages was later modified on its aromatic moiety to extend the absorbance, as exemplified by 2-(3,4-methyllenedioxy-6-nitrophenyl)propoxycarbonyl **2.32**.[159-161] Further modification of the backbone led to the development of biphenyl derivatives **2.33** and **2.34**.[162,163] The extension of the conjugation system helped extend the absorbance into visible light region and the two-photon absorption cross section, which has been demonstrated by Winssinger and coworkers.[164] However, there is no studies on the decaging properties of this class of photocages with bad leaving groups.

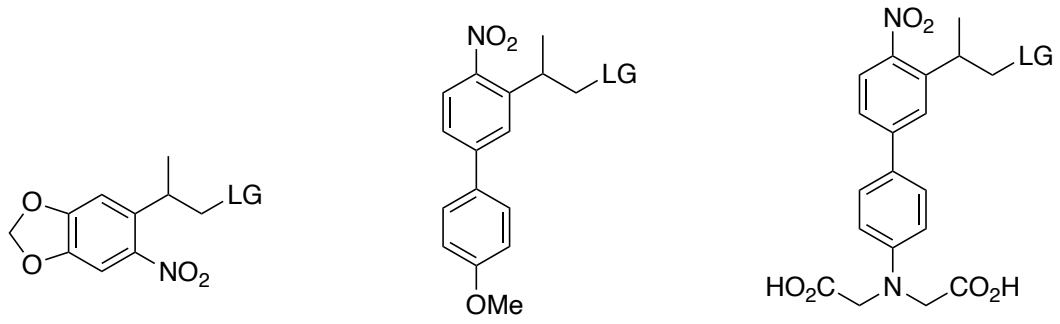

2.32
λ = 365 nm
LG = carbonates and carbamates

2.33
λ = 740 nm (two-photon)
LG = carboxylates

2.34
λ = 405 nm (one-photon)
800 nm (two-photon)
LG = carboxylates

Figure 2.6. Select examples of modification of *o*-nitro-(2-phenethyl)ethyl photocages.

The introduction of the amino group in **2.34** dramatically increased the aqueous solubility for the caged compounds, which is very helpful in biological studies. **2.35** have been applied in a recent example of the decaging of neurotransmitter GABA by Donato and coworkers (Equation 2.6).[163] GABA was released upon irradiation with light at 405 nm for one-photon and 800 nm for two-irradiation. Released GABA **2.37** was shown to activate GABA receptors in brain slices.

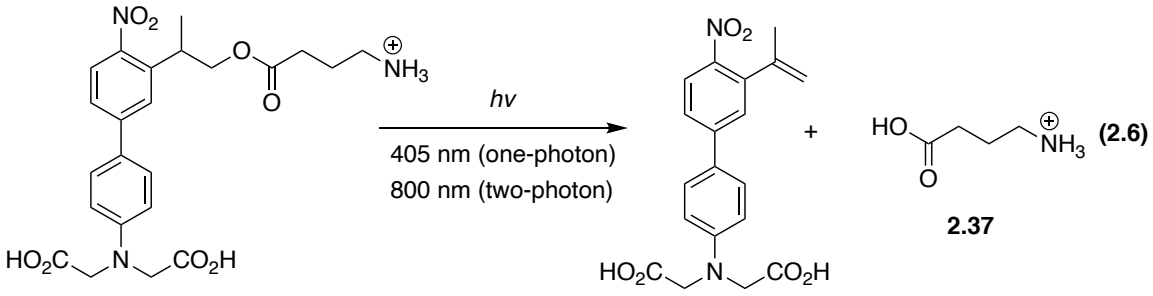

2.35

2.36

2.37

(2.6)

2.2.4 *o*-Nitroanilides Photocages

In the 1970s, *o*-nitroanilide derivative **2.38** was first reported as being photoreactive by Amit and Patchornik, and it was able to release carboxylic acids while generating different byproducts depending on reaction conditions.[165,166] Early mechanistic studies revealed the decaging reaction was a rearrangement process instead of a solvolysis. In particular, no isotopic incorporation was observed when the decaging was carried out in $H_2{}^{18}O$.[165] Cyclic derivative **2.39** was later found to be capable of decaging carboxylic acid derivative under various conditions except for in alcoholic solvents.[167] The size of the nitrogen heterocyclic ring was found to be crucial for the reactivity, and five-membered indoline derivatives **3.40** and **3.41** were found to release carboxylic acids very efficiently.[165]

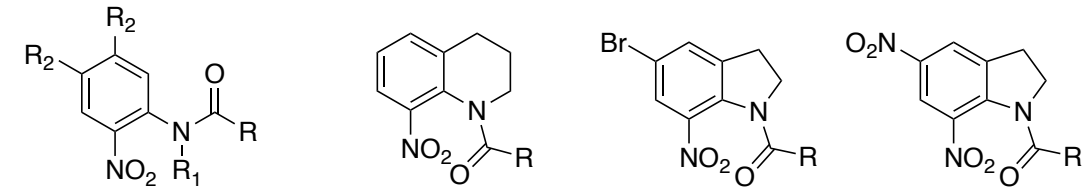

2.38
λ > 370 nm
R = Me, Ph, 2-naphthyl
R_1 = alkyl, aryl
R_2 = H, OMe

2.39
λ > 305 nm

2.40
λ > 305 nm

2.41
λ > 305 nm

Figure 2.7. Select examples of *o*-nitroanilide photocages

Corrie, Bochet, and coworkers later reported a detailed study on the reaction mechanism of caged substrate **2.42**.[168-170] The study suggested a photoinduced acyl migration from the indoline nitrogen atom to one of oxygen atoms of the nitro group, forming the reactive N-O acyl intermediate **2.43**. Interestingly, intermediate **2.43** proceed via two different pathways depending on the solvent. In moist organic solvent, intermediate

2.43 underwent a nucleophilic attack either by the solvent (alcohol or water) or by an external nucleophile releasing **2.44** with the formation of byproduct nitroindoline **2.45** (Scheme 2.3 path A). In water, deprotonation of the α position of the nitrogen released carboxylic acid **2.46** with the formation of nitrosoindole product **2.47** (Scheme 2.3 path B). Different substitution pattern on the indole aromatic ring has a certain extent of impact on the ration of the byproduct formation too.[171]

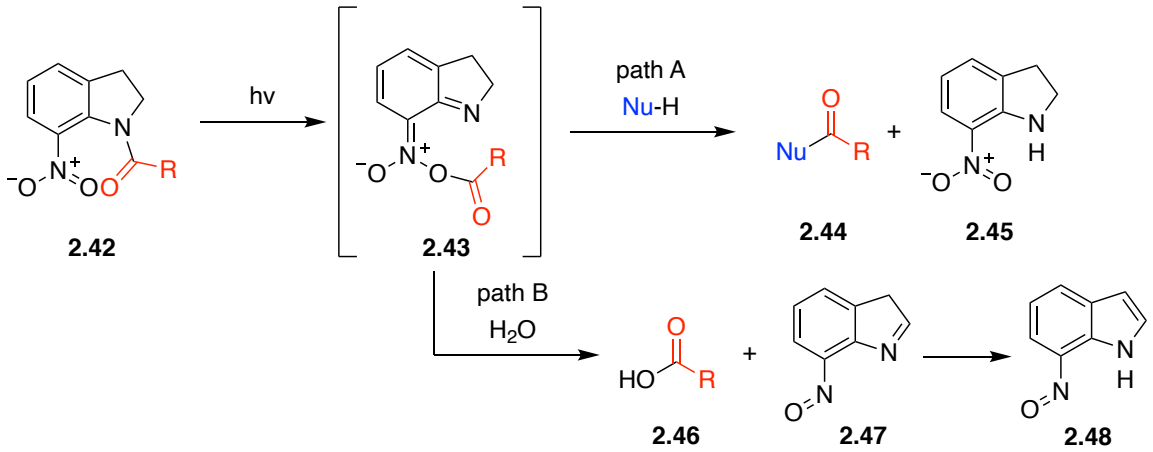

Scheme 2.3. Divergent reaction pathways for *o*-nitroanilide photocages in different solvents.

The biological applications of *o*-nitroanilide photocages are relatively limited, and in some cases, they were proved to be inferior compared with *o*-nitrobenzyl photocages.[172] In neuronal studies reported by Ellis-Davies and Kasai, the 7-nitroindoline was utilized in the decaging of glutamate and GABA with two-photon irradiation (Figure 2.8A).[173,174] Caged glutamate **2.49** was photolyzed at 720 nm with two-photon excitation, and neuron activities were demonstrated in brain cell slices. Another example is the application in photochemical synthesis of peptide.[175] Photocage **2.41** (DNI) was attached to the carboxyl group of L-leucine, and another photocage DDZ was appended to the amine group (Figure

2.8B). The photochemical acyl transfer from the DNI to an incoming nucleophilic amino group was performed with irradiation at 375 nm. Subsequently, the DDZ group was decaged at 300 nm which afforded the dipeptide **2.54**.

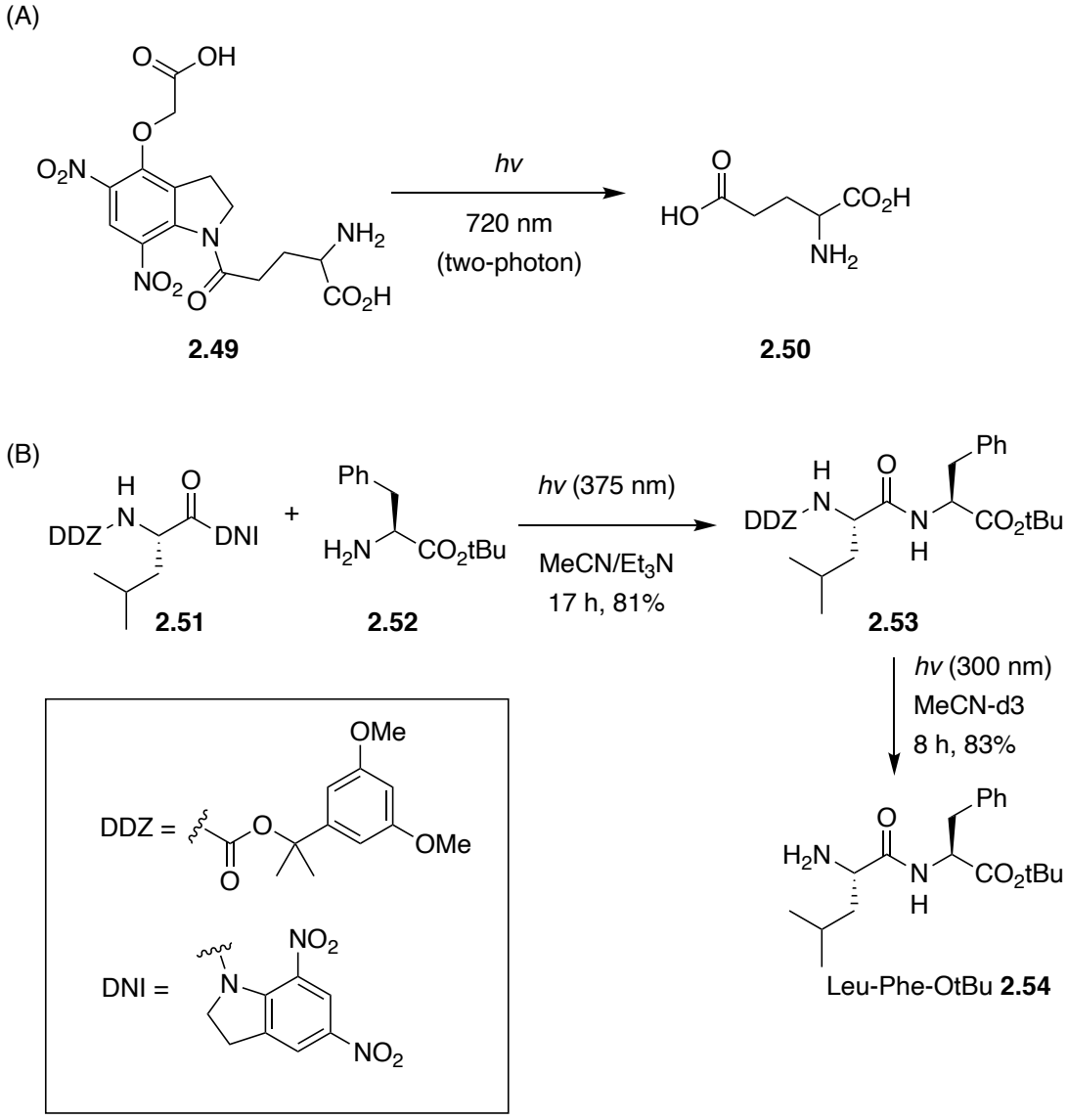

Figure 2.8. Select applications of nitroanilides photocages.

2.3 ARYLCARBONYL PHOTOCAGES

2.3.1 Phenacyl Photocages

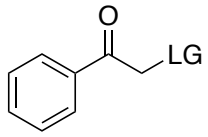

2.55
Phenacyl photocages
λ = 320 nm
LG = carboxylates, carbamates, carbonates,
sulfonates, and phosphates

The phenacyl photocages are grouped based on their structural similarity. They share the phenacyl moiety as the chromophore, and typically the leaving group is attached α to the carbonyl group. It is known that minor variations on the photocage substrate can lead to completely different decaging mechanistic pathways. Sheehan and coworkers reported the first example of phenacyl photocage **2.55** for releasing carboxylates.[176] The mechanism of the decaging process strongly depends on the leaving group, reaction conditions, and solvent.[177 - 180] For example, a mechanism that involves hydrogen abstraction from a hydrogen-atom donor by the excited state carbonyl group of phenacyl ester via a ketal ester intermediate has been confirmed by laser flash photolysis (Scheme 2.4A). In the presence of an electron donor, a different mechanism involving electron transfer from the donor to the carbonyl, followed by release of the leaving group, can also be accommodated (Scheme 2.4B).

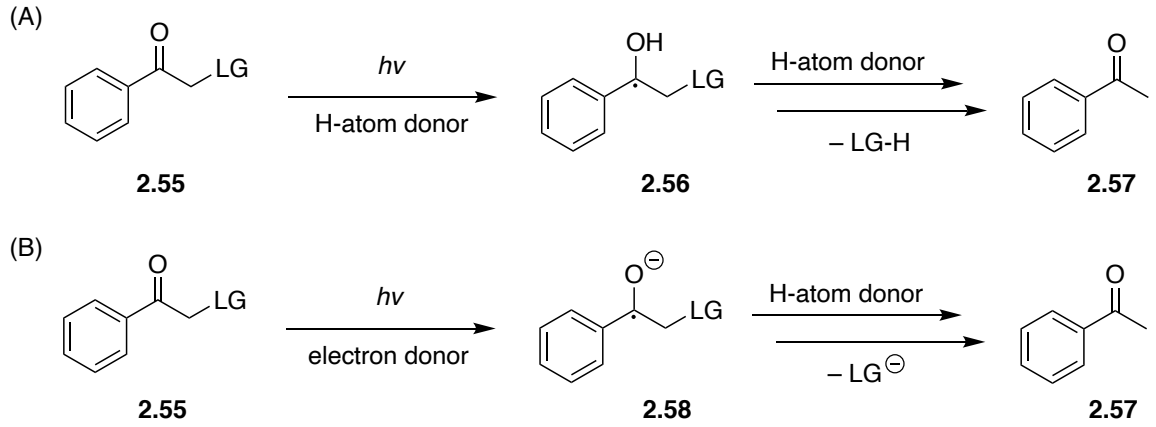

Scheme 2.4. Mechanisms of phenacyl photocages releasing a leaving group

Phenacyl photocages typically can efficiently release good leaving groups such as carbamates, carbonates, sulfonates, and phosphates. [181] Two different kinds of modifications including the substitution α to the carbonyl group such as benzoin photocages, as well as the substitution on the aromatic ring such as *p*-hydroxyphenacyl photocages have been made to improve the efficiencies of the photocages.

2.3.2 Phenacyl Derivative Photocages

2.3.2.1 Benzoin Photocages

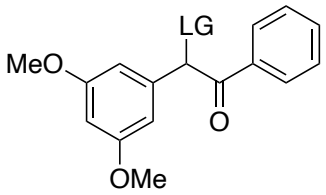

2.59
benzoin photocages
λ = 355 nm
LG = carboxylates, phosphates, amines, and fluorides

The benzoin cage **2.59**, which was first reported by Sheehan in 1970s, can be regarded as a phenacyl analogue with aryl substitution on the α-carbon atom.[176] The addition of 3,5-dimethoxyphenyl on the α-carbon atom **2.59** was found to lead to much

better decaging efficiencies compared with other substituted and unsubstituted phenyl groups. The decaging process of carboxylates and phosphates from **2.59** proceeds cleanly affording the desired substrate and the benzofuran **2.62**. Compared with the nitroso products formed from the *o*-nitrobenzyl photocages, **2.62** is chemically and photochemically inert. The decaging proceeds cleanly in both polar and nonpolar solvents, and the reaction mechanism was found to be independent of the nature of leaving groups. Poor leaving groups such as amines can also be decaged from the benzoin photocages.

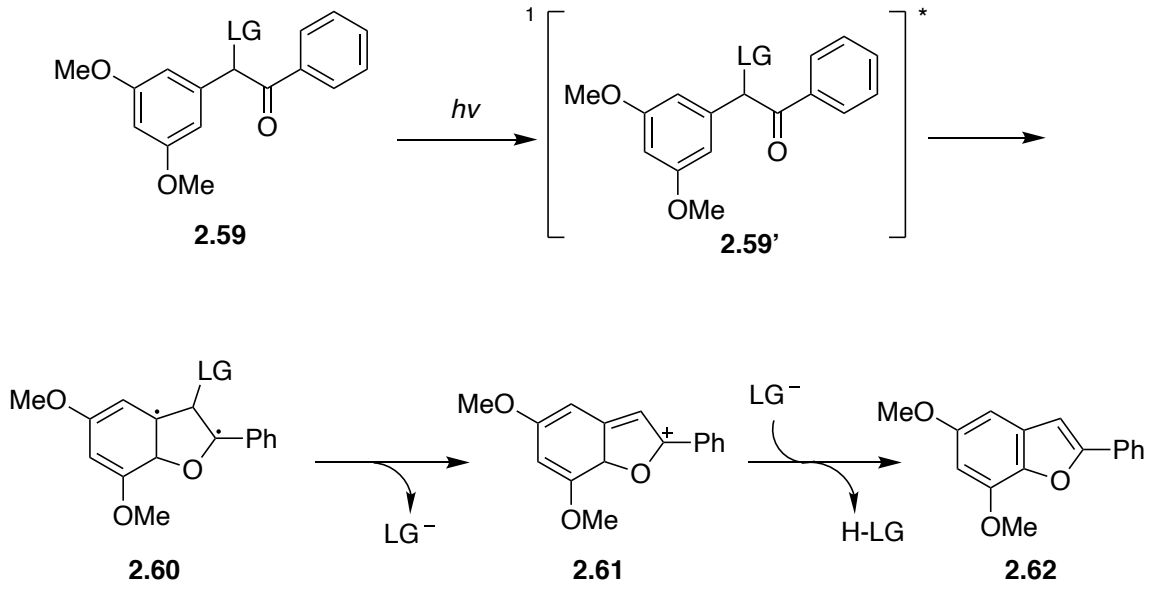

Scheme 2.5. Decaging mechanism for 3',5'-dimethoxybenzoin photocage.

2.3.2.2 p-Hydroxyphenacyl Photocages

The substitution on the aromatic ring of the phenacyl photocages also has significant impacts on the decaging process. Sheehan and Umezawa reported the *p*-methoxyphenacyl esters were more photoreactive than unsubstituted phenacyl esters.[176] Therefore, several derivatives with the substitution of methoxy and alkoxy groups on the

aromatic ring were developed and employed in the decaging of good leaving groups such as carboxylates, phosphates, carbonates, and carbamates.

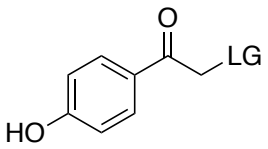

2.63
p-hydroxyphenacyl photocage
λ = 300 nm
LG = phosphates, carboxylates

Other substituents were also utilized in the development of substituted phenacyl photocages. One of the interesting examples is the *p*-hydroxyphenacyl photocage **2.63**, which was reported by Givens in 1996.[182,183] The unique aspect of *p*-hydroxyphenacyl photocage is the decaging mechanism, which is significantly different from the photoreduction mechanism for the phenacyl photocages. The decaging process starts with the irradiation of **2.63** to generate the excited triplet state **2.63'**. Subsequent formation of the spiroketone **2.64** and expulsion of the leaving group gives the spiroketone **2.64** which is prone to hydrolytic ring opening to deliver *p*-hydroxyphenyl acetic acid **2.65** (Scheme 2.6). The process to the generate the spiroketone **2.64** resembles the ground state Favorskii rearrangement of α-haloketones, so it is named the photo Favorskii rearrangement

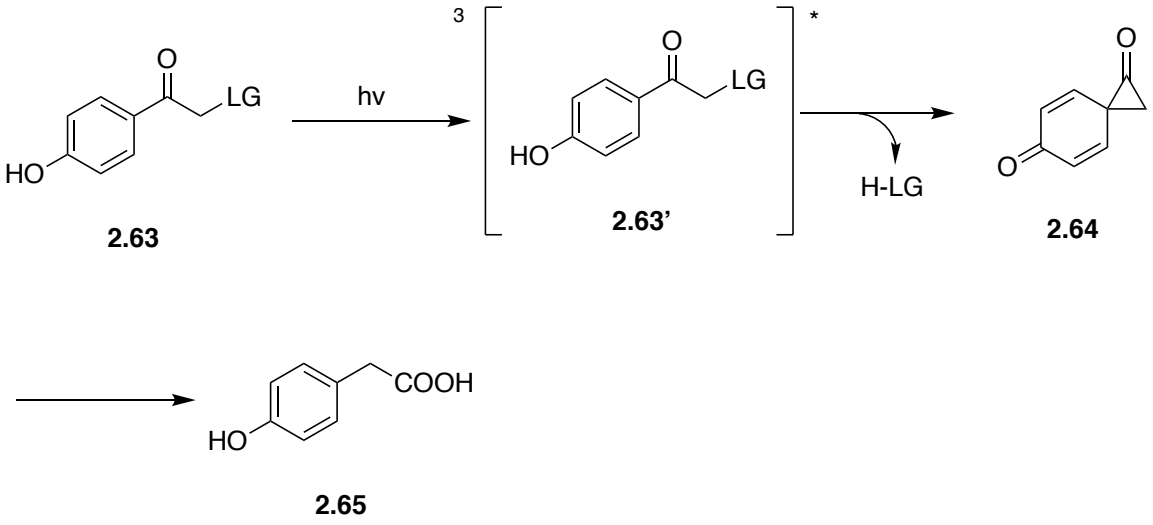

2.63 **2.63'** **2.64** **2.65**

Scheme 2.6. Decaging mechanism for *p*-hydroxyphenacyl photocage

The decaging typically proceeds with good quantum yield, which is dependent on leaving group ability. In general, the quantum yield decreases when the basicity of the leaving group increases. The quantum yield is also pH dependent, and the optimal quantum yield is typically obtained under neutral or slightly acidic conditions. Unlike the nitroso byproducts for *o*-nitrobenzyl photocages, the acid **2.65** has a drastically different UV absorption profile from the ketone **2.63**, and it does not interfere the absorbance of the starting material **2.63**. Moreover, **2.65** is photochemically stable and biologically inert, thus making **2.63** a good photocage option for biological studies. The applications of *p*-hydroxyphenacyl photocage mainly focus on the time-resolved biochemical and physiological studies due to fast decaging rates and benign biological natures of **2.65**.[181]

2.3.3 Photocages with Photoenolization Decaging Mechanism

Unlike the phenacyl photocages, this group of photocages are classified based on the similar decaging mechanism, which involves the sequence of hydrogen abstraction,

photoenolization and subsequent ground-state transformation of the enol moiety to release the substrate.

2.3.3.1 2-Alkyl Substituted Acetophenone

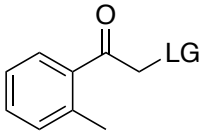

2.66
λ 254-366 nm
LG = phosphates, carboxylates, sulfonates,
carbonates, and carbamates

Klan and Wirz first reported the caging with 2-alkyl substituted acetophenones, and demonstrated the successful decaging of substrates including phosphates, carboxylates, sulfonates, carbonates, and carbamates.[184-188] With the substitutions on the aromatic ring of phenacyl photocages, the decaging mechanism changed dramatically. Upon irradiation, **2.66** is converted to its singlet excited state **2.67** that can partition in different ways (Scheme 2.7). For example, **2.67** could undergo an intersystem crossing forming the triplet excited state **2.68**, which would be transformed through the 1,5-hydrogen abstraction to generate diradical intermediate **2.70**, that could further decay to two isomeric enols **2.69** and **2.71**. The (*Z*)-photoenol **2.69** could also be generated from the singlet state intermediate **2.67** via enolization, and subsequently undergo a sigmatropic rearrangement to regenerate starting material **2.66**. The (*E*)-photoenol **2.71** would cyclize to afford **2.72** along with the release of substrate (H-LG). The leaving group is released in an intramolecular S_N2 like fashion, thus making it candidate for only caging good leaving groups.

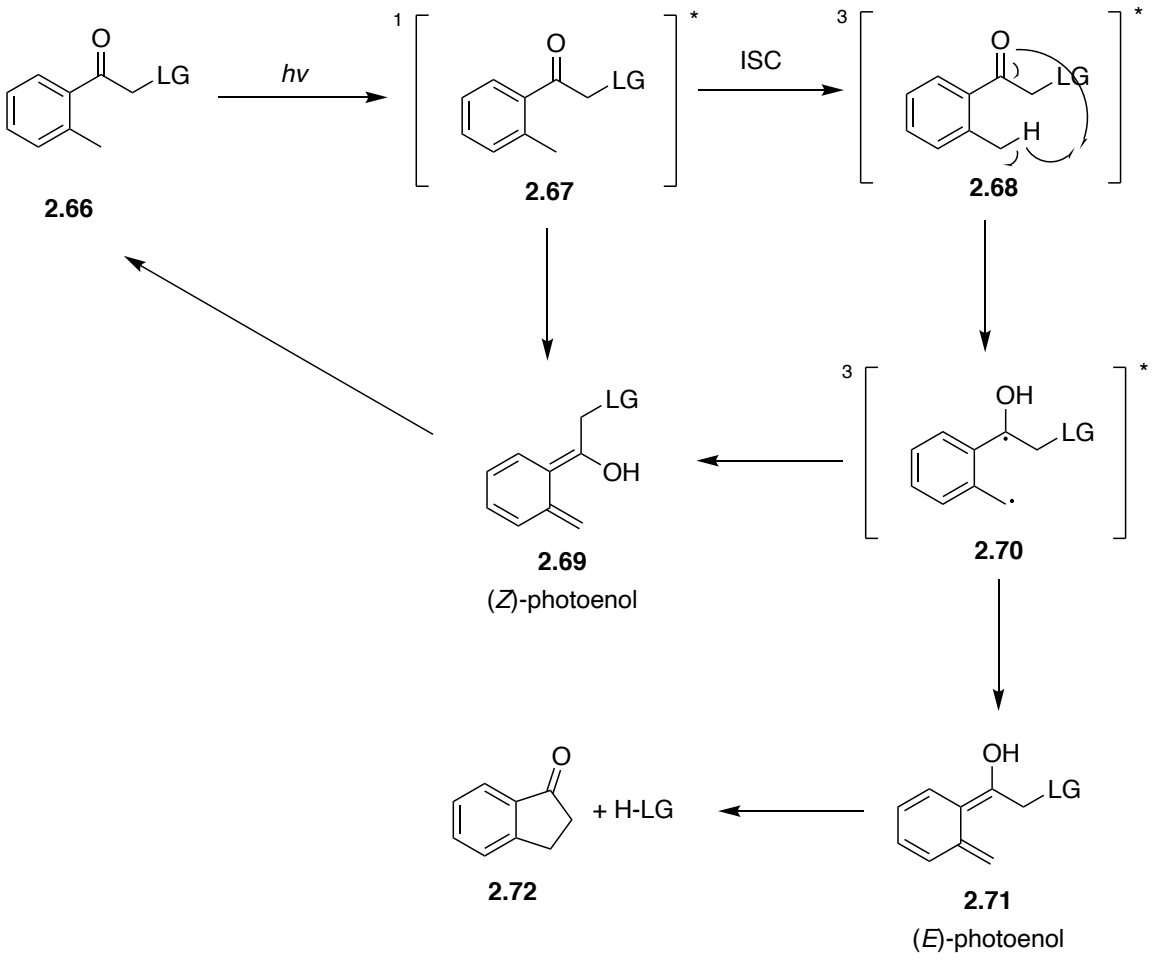

Scheme 2.7. Decaging mechanism for 2-methylacetophenone photocages.

2.3.3.2 Ethylene Substituted Acetophenone Photocages

Tseng and Ullman reported an alternative strategy on the modification of phenacyl photocages by attaching the leaving group to the substituted alkyl branch.[189] The decaging process starts with the irradiation of **2.73** leading to photoenol intermediate **2.74**, which then tautomerizes back to its keto form **2.75** while expelling the leaving group. The decaging rate is not affected by solvents, but it is usually slow with low decaging efficiency. Good decaging efficiencies can be achieved by using good leaving groups such as tosylate; however, with poor leaving groups, the final elimination step would be rate

determining and sometimes is competitive with the regeneration of **2.73**.[141] Modifications on **2.73** have been reported, but little success was achieved in increasing decaging efficiencies compared with parent photocage **2.73**.[190] Therefore, the use of this type of photocages in biological studies is rare.

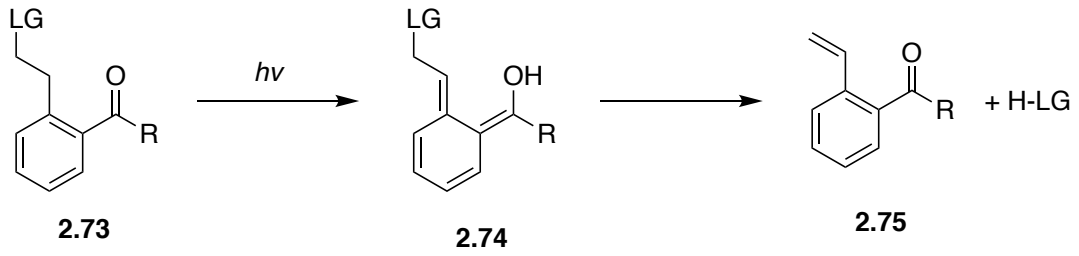

2.73 **2.74** **2.75**

Scheme 2.7. Decaging mechanism for 2-ethylene substituted lacetophenone photocages.

2.3.3.3 Intramolecular Lactonization Photocages

Gudmundsdottir and coworkers demonstrated another type of photocages directly decaging alkoxide via a sequence of photoenolization and intramolecular lactonization.[191] Upon irradiation with UV light, **2.76** undergoes photoenolization to generate **2.77** via the excited triplet state (Scheme 2.9). A [2+2] cycloaddition of **2.77** will form benzocyclobutanol **2.78**. Cyclization of **2.78** affords lactone **2.79** along with the release of alcohols in high yields. Although the direct release of alcohol substrate is a pretty rare trait in photocages, this type of photocage has not been widely used due to the low decaging efficiencies and long reaction time.

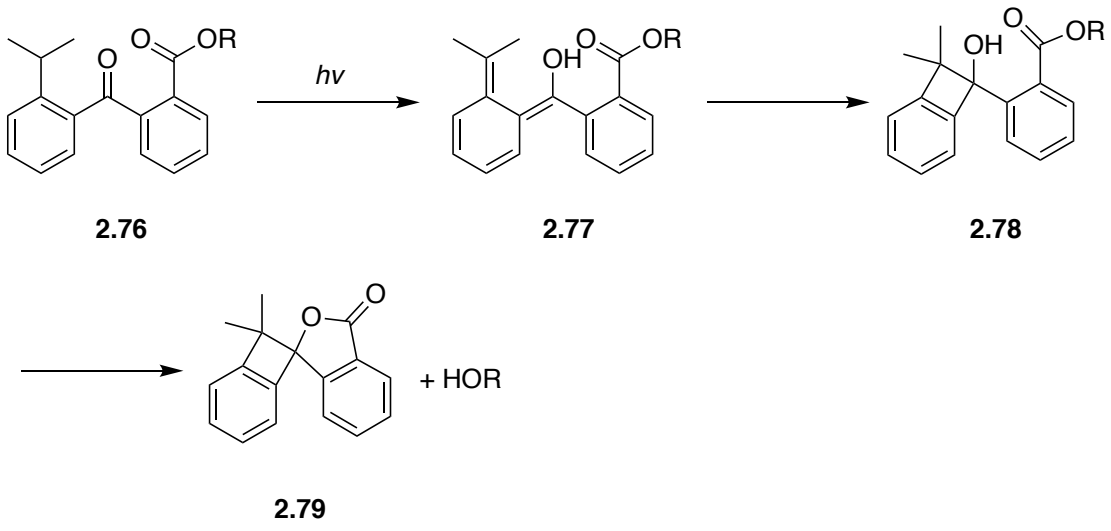

Scheme 2.8. Decaging mechanism for intramolecular lactonization photocage **2.76**.

Steinmetz and coworkers reported a different photocage that may be released by a photoenolization process, as exemplified by attaching α to the caged group ketoamide **2.80**. Upon irradiation of **2.80**, the zwitterion **2.81** is formed via photoenolization, and **2.81** releases leaving group while generating **2.82** and **2.83**. The rate determining step was found to be the release of substrate, and the decaging process was found to have a pretty good quantum yield and efficiency. However, the further modifications to expand the absorbance to longer wavelength led to the significant drops in quantum yields.[192,193]

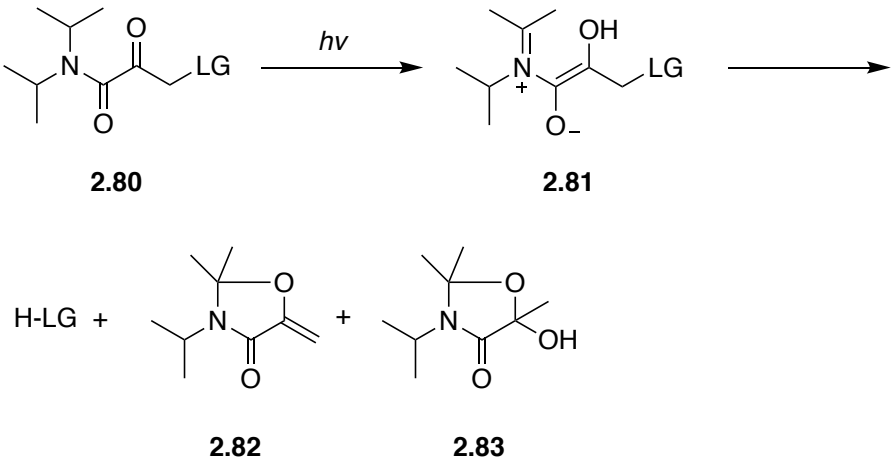

Scheme 2.9. Decaging mechanism for the intramolecular lactonization photocage **2.80**.

2.4 BENZYL BASED PHOTOCAGES

Benzyl-based photocages are benzyl substituted structures that release substrates via a photosolvolysis pathway (Figure 2.9). Upon irradiation, the starting material **2.84** is converted to its excited state **2.85**, and subsequent heterolytic cleavage or a sequence of homolytic cleavage and single electron transfer generates the benzyl cation as well as an anionic leaving group ion pair **2.87**. Subsequently, the benzyl cation is trapped by nucleophiles, generally solvent (ROH), thus releasing the leaving group **2.89**. Alternatively, the benzyl cation can recombine with the leaving group, leading to the regeneration of starting material **2.84**. Given the competitive reaction pathway, the reactions are often carried out in polar protic solvents that typically give good decaging efficiencies.

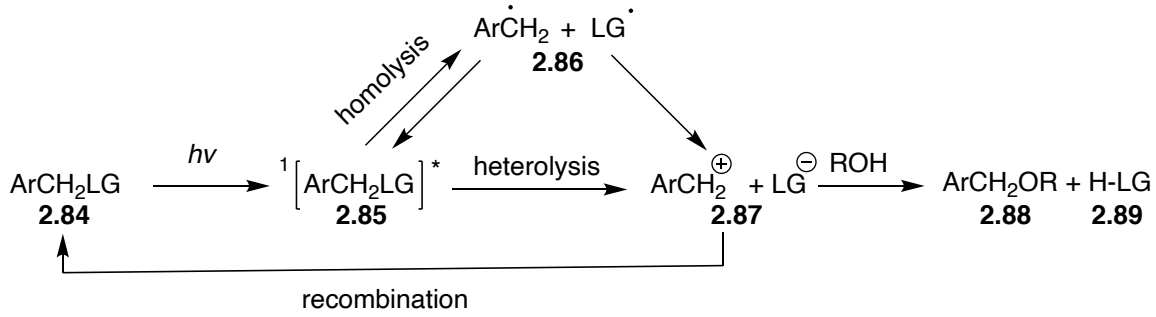

Figure 2.9. Decaging mechanism for benzyl based photocages

A number of photocages with the leaving group at the benzylic position have been developed (Figure 2.10). The 9-phenylxanthyl photocage **2.90** was reported to directly release alcohol upon irradiation with light at 254–300 nm.[194] Modifications of **2.90** with a sulfur atom gave the 9-phenylthioxanthyl photocage **2.91**, which releases primary alcohols at a longer wavelength (λ = 350 nm).[195] The anthraquinone-2-yleth-2-yl photocage **2.92**

was shown to release alcohols with carbonate linkers and carboxylic acids.[196] Applications including carbohydrates and nucleoside decaging have been reported.[197] The 3-(dimethylamino)trityl photocage **2.93** was reported to release primary alcohols at 254 nm by Wang and coworkers.[198] The major concern is the stability of trityl group in acidic conditions, as it has been traditionally used as an acid-labile protecting group in organic synthesis. Wang and coworkers later developed **2.94** for caging ketones and aldehydes.[199,200] Biological applications including neural activation and photogeneration of bases for cellular imaging have been reported on this class of photocages.[201,202]

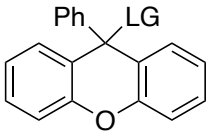

9-Phenylxanthyl photocage **2.90**
λ 254–300 nm
LG = alcohols

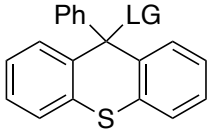

9-Phenylthioxanthyl photocage **2.91**
λ = 350 nm
LG = 1° alcohols

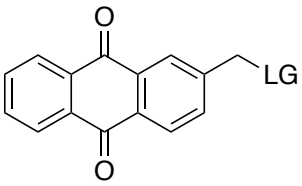

Anthraquinone-2-yleth-2-yl photocage **2.92**
λ = 350 nm
LG = carbonates, and carboxylates

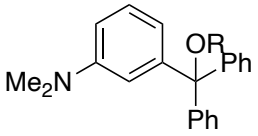

3-(Dimethylamino)trityl photocage **2.93**
λ = 254 nm
LG = 1° alcohols

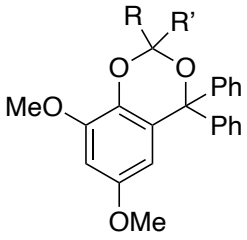

Salicyl derivative photocage **2.94**
λ < 320 nm
LG = carbonyl compound

Figure 2.10. Select examples of benzyl based photocages

2.5 COUMARIN PHOTOCAGES

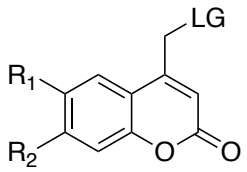

2.95
coumarin photocages
λ_{max} = 350–475 nm
LG = carboxylates, phosphates, sulfonates,
carbonates, carbamates,amines,thiols

Coumarin derivatives **2.95** were first exploited as photocages by Givens and coworkers as a means of releasing phosphates, and this report set the stage for the development of a new class of coumarin based photocages. Coumarin based photocages have attracted attention due to their superior properties including large absorption coefficients at longer wavelength (λ_{max} = 350–475 nm) and fast decaging rates. However, disadvantages including limited water solubility and relatively low quantum yields also limit their utilization. Great efforts have been made to modify the coumarin based photocages to address these limitations, and modified coumarin photocages have proven to be powerful tools in various biological studies.

The decaging mechanism for coumarin photocages is proposed to proceed via a heterolytic bond cleavage process from the excited singlet state intermediate **2.97** (Scheme 2.11).[203,204] The excited singlet state **2.97** is generated upon irradiation of **2.96**, and **2.97** can either decay back to the ground state **2.96** via fluorescence and nonradiative deactivation or undergo heterolytic cleavage to generate **2.98**. It is also possible to generate **2.98** via a homolytic cleavage of **2.97** followed by single electron transfer; however, mechanistic studies have revealed little evidence for this reaction pathway. Once ion pair **2.98** is formed, it can either recombine to regenerate starting material **2.96** or generate the

separated ion pair **2.99**. Subsequently, the ion pair **2.99** is captured by solvent generating coumarin **2.100** along with the leaving group.

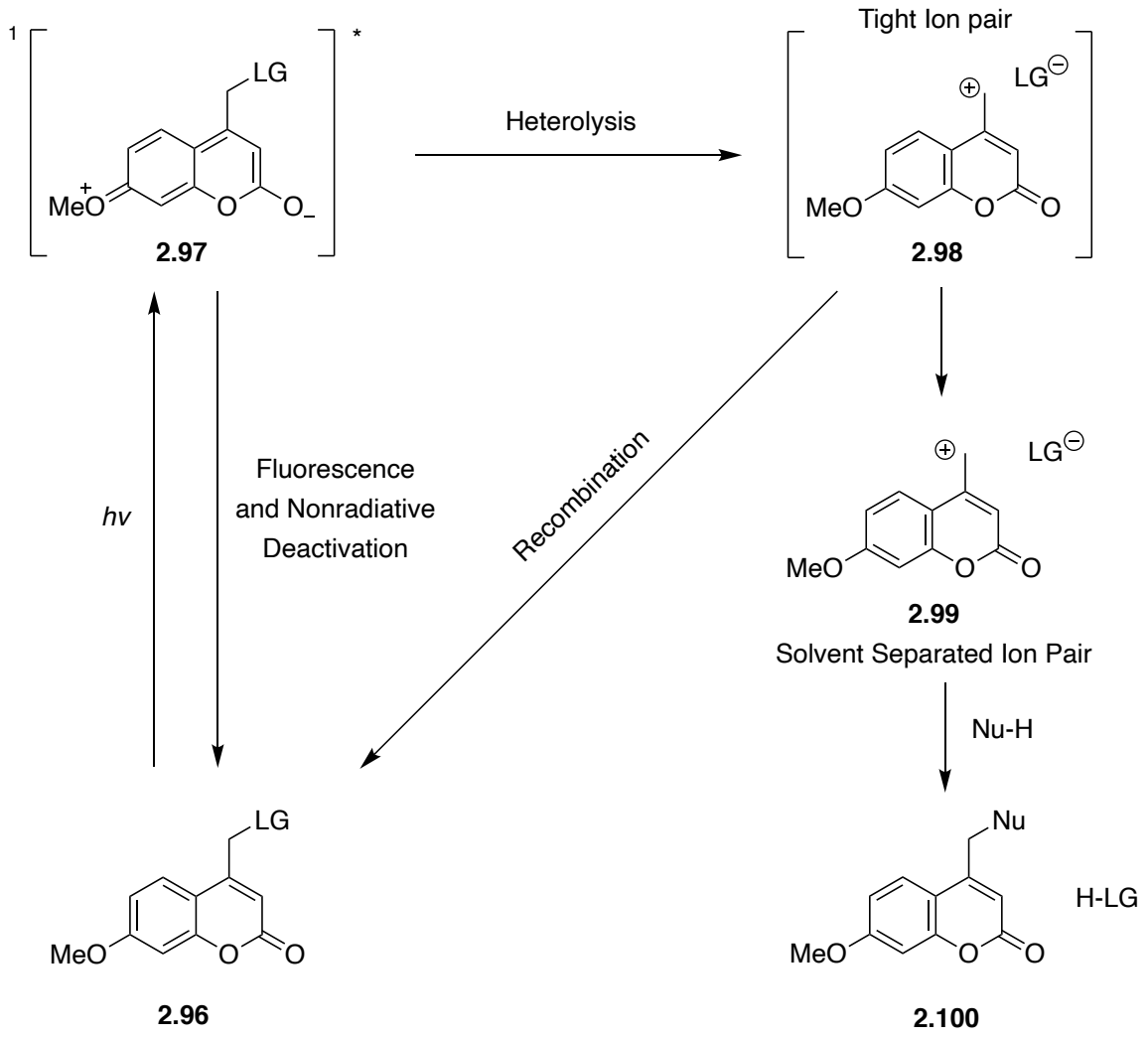

Scheme 2.10. Decaging mechanism of coumarin photocages.

One of the major disadvantages of coumarin photocages is inherent with the photosolvolysis decaging mechanism. The generation of ion pairs is offset by the quick recombination, especially for poor leaving groups such as alcohols, phenols, amines, and thiols, which can render the coumarin derivatives resistant to the heterolysis process.

Modifications including using carbonate or carbamate linkers have been adopted to increase the decaging efficiencies; however, the decomposition of the carbonate and carbamate can be slow and become the rate limiting step in the decaging process. Hence, coumarin photocages are often used for good leaving groups such as phophates and sulfonates, and the release rates are typically fast, thus making them useful photocages for studies of fast physiological events.[205]

A large number of coumarin derivative photocages have been developed in recent years (Figure 2.11). An early example of coumarin derivative photocages was 6-bromo-7-hydroxycoumarin-4-methyl (BHCM), wherein the bromo substituent lowered the pKa of the proximal phenol moiety, thus allowing full deprotonation of the phenol at physiological pH. The deprotonation of BHCM results in a dramatic increase of the aqueous solubility of caged compounds and also a 50 nm red shift of the max absorbance (λ_{max} = 370 nm) compared with MCM (λ_{max} = 320 nm). Further modification such as the introduction of the diethylamino group at the 7-position led to the significant increases on decaging efficiencies as well as the redshift of the max absorbance wavelength of DEAC. Shortly after the report of DEAC, Ellis-Davies and coworkers reported the development of DEAC450 which has the maximum absorbance (λ_{max} = 470 nm) in the visible light region due to the extended conjugation system. The thio-DEAC was reported to possess a very high absorbance in the visible light region with λ_{max} = 470 nm too. Finally, BCMAC including DEAC450 were modified with amino-dicarboxylate groups which was intended to increase the aqueous solubility of the caged compounds.[114]

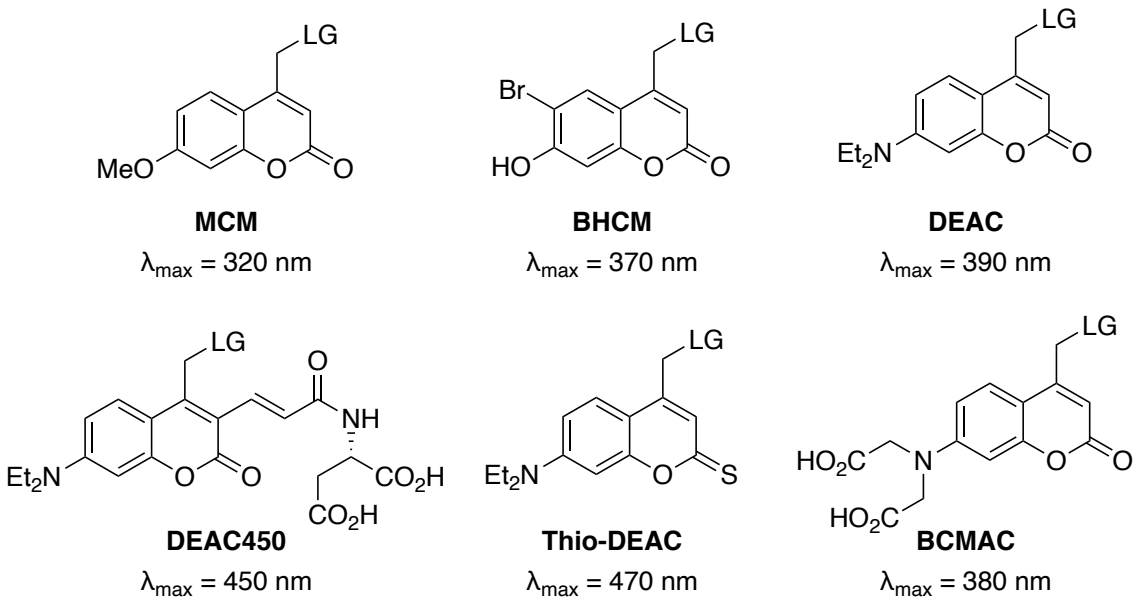

Figure 2.11. Select examples of modified coumarin photocages

Biological application such as decaging small molecule inducer cyclofen in zebra fish embryos to induce protein expression have been demonstrated with irradiation of green light (λ = 488 nm) (Figure 2.12A).[206] Feringa and coworkers illustrated the application of photocaged fluoroquinolone **2.103** in controlled bacterial patterning studies (Figure 2.12B).[207] **2.103** was incorporated into certain regions of agar-plates, which were then irradiated by UV light at 312 nm. The released fluoroquinolone inhibited the growth of *E*. coli that was applied on the same regions of agar-plates. The growth of *E*. coli outside of the regions with **2.103** was found not affected. Moreover, the growth of *M*. *luteus* was found not affected regardless of what region they were applied, since fluoroquinolone **2.104** does not show antibacterial effects against *M*. *luteus*.

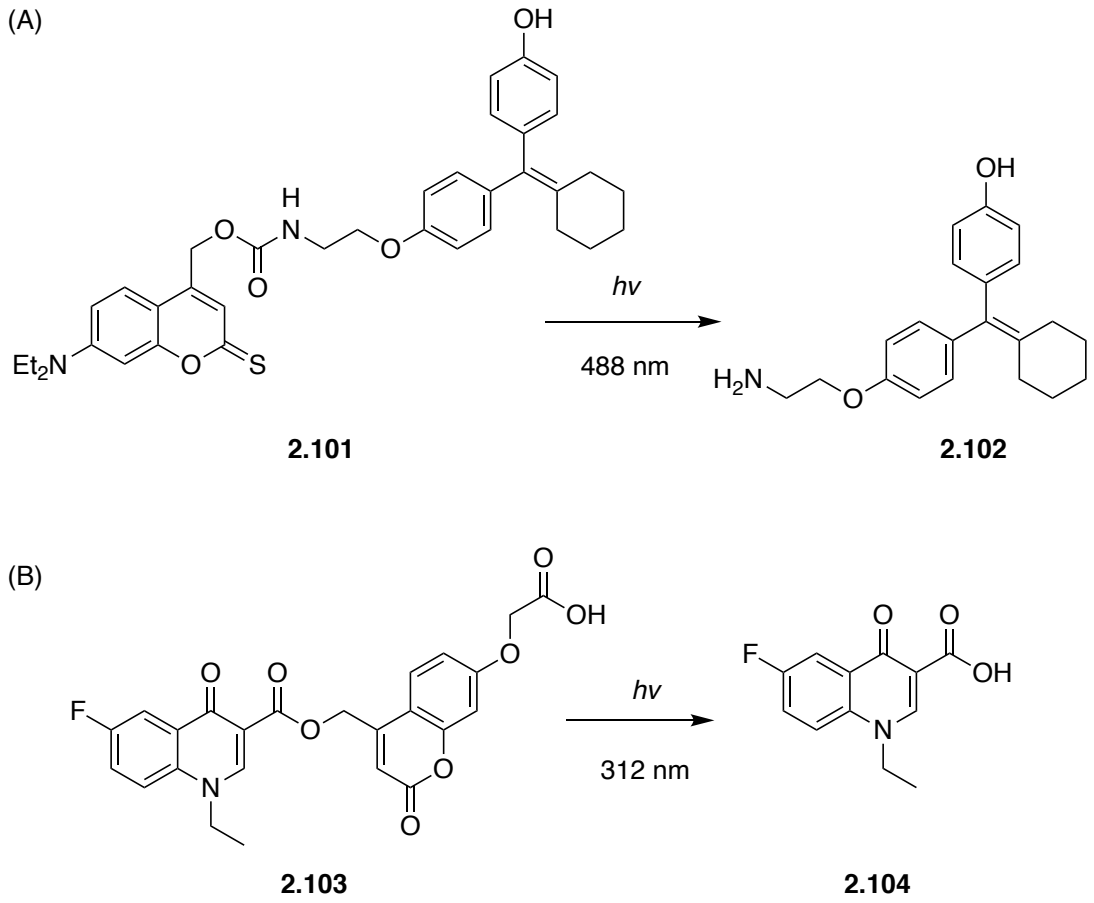

Figure 2.12. Examples of coumarin caged compounds in biological applications.

2.6 BODIPY DERIVED PHOTOCAGES

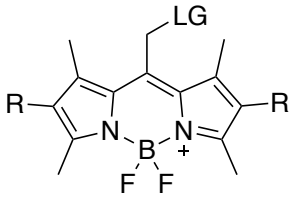

2.105

λ_{max} > 500 nm

The boron dipyrromethene (BODIPY) derivatives were introduced by Winter and Weinstain as photocages that released carboxylic acids by irradiation with green light (λ > 500 nm). [208, 209] Further studies on BODIPY involved caging substrates including

carbonates, carbamates, phenols, alcohols, and carbon monoxide.[210,211,212] It quickly became a promising photocage due to the compelling properties including narrow excitation bandwidth in visible light region, adaptable synthetic chemistry, and biocompatibility.[213] The decaging of BODIPY photocages is proposed to occur via a photosolvolysis mechanism similar to coumarin photocages (Scheme 2.12). Irradiation of **2.105** with light generates an excited state species, which undergoes heterolytic cleavage to form cation **2.106** along with expulsion of the leaving group anion. Trapping **2.106** by solvent generates **2.107**.

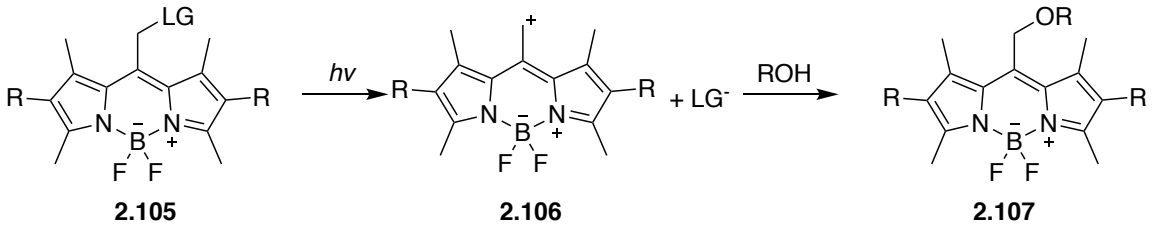

2.105 **2.106** **2.107**

Scheme 2.11. Decaging mechanism for BODIPY photocages.

A thorough structure-reactivity relationship study was carried out by the collaborative work of Weinstain, Winter, and Klán, which provided more insights into the modification strategies of BODIPY photocages (Figure 2.13).[214] The substitution of halogen atoms on 2,6-position was explored and shown to increase the quantum yield. Computation studies by Smith, Winter, and coworkers attributed this result to the increased formation of a triplet state intermediate via intersystem crossing process due to the heavy atom effect.[208] Replacement of the fluorine atoms by alkyl groups were also explored to increase the decaging efficiencies, since alkyl groups can help stabilize the carbocation intermediate **2.106**, which would facilitate the decaging process. Switching from the fluorine atoms to methyl groups was found to increase the decaging efficiency; however,

substitutions with ethyl and phenyl groups decreased the decaging efficiencies. This result was rationalized by the distortion of the planarity with the introduction of steric bulky groups. Substitution at 3,5-positions with alkyl groups stabilized the intermediate **2.106**, and increases the decaging efficiency. Extended conjugation with conjugated PMB group was found to help redshift absorption, but the decaging efficiencies dropped due the decreased quantum yields.

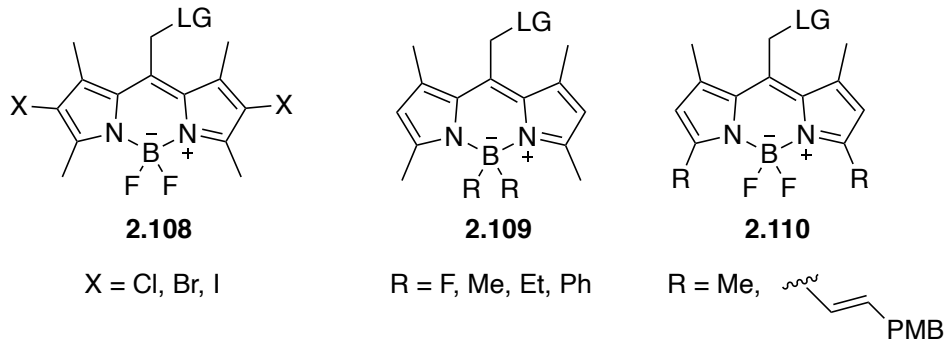

Figure 2.13. Modification strategies of BODIPY photocages.

Another interesting aspect of BODIPY photocages is that leaving groups can be attached at different positions (Figure 2.14). Urano and coworkers reported the first example of leaving group appended to the boron atom.[215] During their studies of fluorescence properties of the 4-aryloxy BODIPY derivative **2.111**, they observed cleavage of B-O bond after visible light irradiation. Following by their original study, they extended the conjugation by synthesizing **2.112**, and longer wavelength absorption was achieved along with decreasing decaging efficiencies.[215] Urano first reported the example of leaving groups appended to 2,6 position as in **2.113**, wherein fulfonamide groups were found to release amines under irradiation of visible light.[216] Zhang and coworkers later took advantage of the weak N-O bond of oxime ester and designed photocage **2.114** that was capable of releasing carboxylic acids.[217-219]

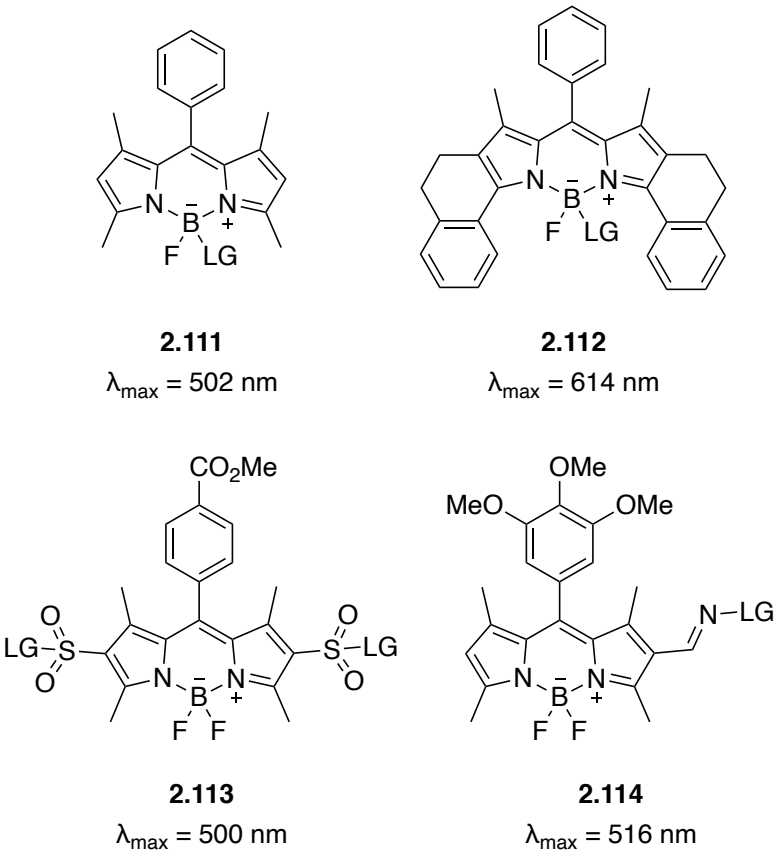

Figure 2.14. Select examples of BODIPY photocages with leaving group at different positions.

2.7 OTHER NOTABLE PHOTOCAGES

There are other reported photocages that do not belong to any of the classes discussed so far, and some notable photocages that undergo decaging under visible light irradiation will be discussed (Figure 2.15). 9-Aryl substituted xanthene derivatives are generally used as fluorophores that absorb visible light. Klán and Wirz first reported that the xanthene derivative **2.115** as the 1:1 complex with DDQ successfully release carboxylates and phosphates in aqueous solutions under irradiation of light at 546 nm.[220] Shortly after the original report, a 9-COOH xanthene derivative was shown to successfully release CO_2 when irradiated by green light in aqueous media.[221] Benzoquinone derivative

2.116 was reported by Kalow to release benzoic acid when irradiated by red light at 626nm, and a photocyclization pathway was proposed to explain the decaging process.[222-224] Benzothiadiazole derivative **2.117** is an example of photocage that takes advantage of the "*meta-ortho* effect", and carboxylic acids and alcohols are decaged at 430 nm.[225,226] Modification of fluorophore 7-hydroxyquinolines resulted in the development of photocage **2.118** which was reported to release amines via carbamate linkers with blue light irradiation.[227] Methylation of the nitrogen atom reduces the pKa of the hydroxyl group, which promotes the formation of zwitterions thus increasing absorbance and red shifting absorption wavelength.[228]

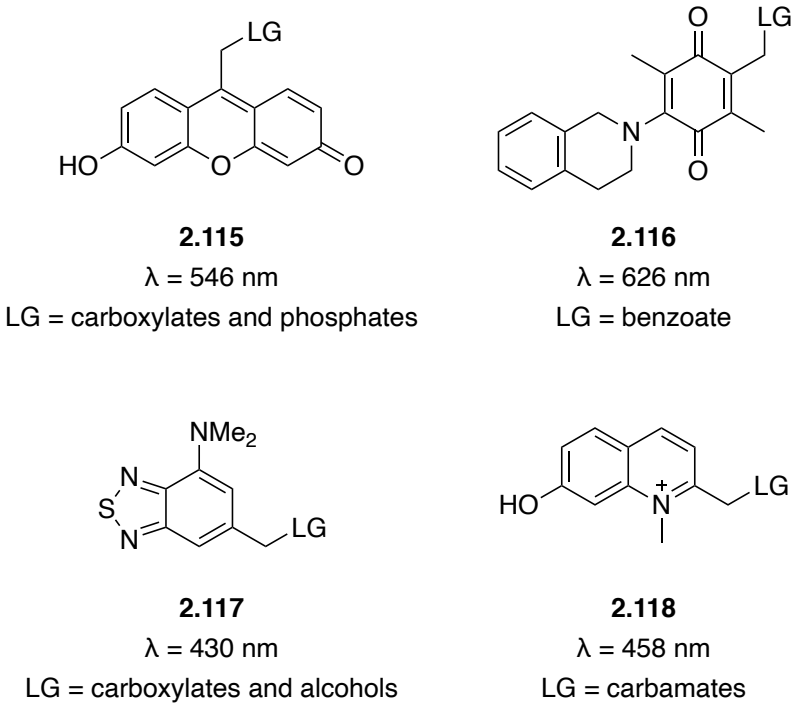

2.115
λ = 546 nm
LG = carboxylates and phosphates

2.116
λ = 626 nm
LG = benzoate

2.117
λ = 430 nm
LG = carboxylates and alcohols

2.118
λ = 458 nm
LG = carbamates

Figure 2.15. Notable photocages in visible light region.

2.8 SUMMARY OF PHOTOCAGES

Since the first report of photolytic deprotection of Cbz-glycine, the field of photocages have grown dramatically, and various application have been developed in different fields of research. A wide variety of photocages with different decaging mechanisms have been reported over the past half-century. The demands for photocages in biological applications have been the constant driving force for development of new photocages, since no one photocage fulfills every requirement in every application. However, good photocages usually share the superior properties including fast substrate release, good absorbance, adequate aqueous solubility, and good photosensitivity. It is important to have a number of photocages, so that an appropriate photocage can be used for a given application.

Some of the most commonly used photocages are shown in Figure 2.16. By far the most commonly used photocages are still *o*-nitrobenzyl derivative photocages **2.4**. Despite the apparent disadvantage of decaging under UV light, advantages including high decaging efficiencies, wide variety of leaving groups, and straightforward chemical synthesis make it highly used in various applications. NDBF **2.25** as one of the examples of *o*-nitrobenzyl photocages with superior properties is likely to be used or modified in the future studies. The *o*-nitro-(2-phenylethyl) photocages **2.27** are mechanistically related to *o*-nitrobenzyl photocages, which are shown to be particularly effective at two-photon caging. It is demonstrated that **2.34** as an example of this class of photocage has superior two-photon caging properties. Moreover, the extension of the conjugation system as well as the introduction of solubility handle make it a powerful tool in biological applications such as siRNA and peptides decaging. Phenacyl photocages **2.55** and its derivative benzoin photocage **2.59** are useful especially in photochemical physiology studies due to their fast release rates. However, applications in other fields are relatively limited due to their short

decaging wavelengths. Coumarin photocages **2.95** are one of the most promising classes of photocages due to their superior properties, including fast rate of decaging, large absorbance in visible light region, and fluorescent properties. Currently, modification efforts are focused on improving the aqueous solubility as well as further redshift its decaging wavelength. DEAC 450 which was reported by Ellis-Davies is a great example of successful modification of coumarin photocages, and it has been utilized in studies such as orthogonal decaging system. One inherent disadvantage of coumarin photocages is they are only applicable for decaging good leaving groups due to its photosolvolysis mechanism. BODIPY **2.105** as another example of photosolvolysis photocage is shown to be promising as well. The fast decaging rate and absorbance in visible light region makes it powerful in numerous biological studies.

Thanks to all the efforts toward photocage development, various photocages have been developed and utilized in biological studies; however, there are still many challenges remained to be tackled. Most *o*-nitrobenzyl photocages photolyze with near-UV light around 365 nm, which can cause damage to biological entities in studies.[229] Moreover, for *in vivo* studies, the penetration ability of UV light is limited, which would lead to low decaging efficiencies for caged compounds. For photosolvolysis photocages such as coumarin and BODIPY, caged compounds can typically be photolyzed in visible light region; however, due to the photosolvolysis mechanism, bad leaving groups cannot be released in good efficiencies. The decaging efficiencies of bad leaving groups such as alcohols, phenols can still be improved. Finally, the aqueous solubilities of many photocaged compounds are moderate, which limit the utilizations in biological studies.

To this day, research efforts continue to focus on the development of new classes photocages and modification of current photocages to better accommodate biological applications. Our group has been interested in this field for some time, and we sought to

develop new photocages with better properties. We sought to discover new photocages can release substrates in longer wavelengths, ideally visible light region. We want the new photocages that release substrates with high efficiencies, even with bad leaving groups. Moreover, we want the new photocages with good aqueous solubility, that can be widely utilized in biological studies.

o-Nitrobenzyl photocages

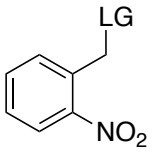

2.1

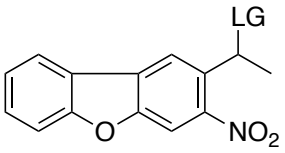

NDBF

***o*-Nitro-(2-phenylethyl) photocages**

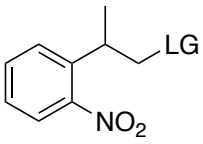

2.24

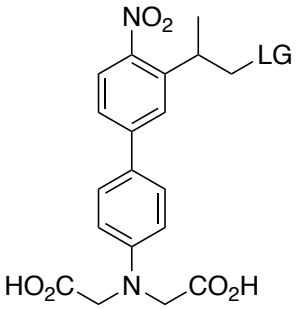

2.32

Phenacyl photocages

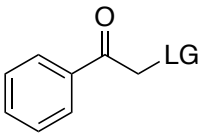

2.42

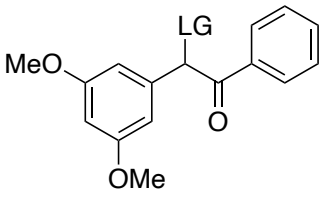

2.43

Coumarin photocages

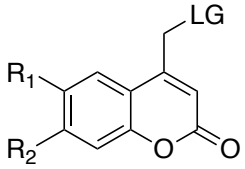

2.73

BODIPY photocages

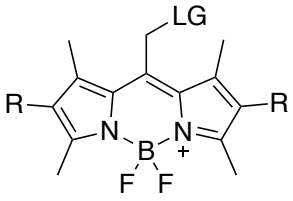

2.79

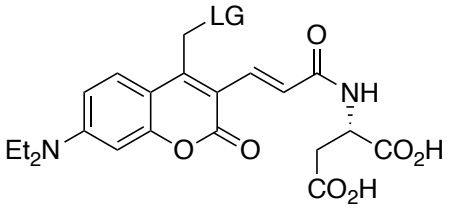

DEAC450

Figure 2.16. Summary of the most commonly used photocages.

Chapter 3: Design, Synthesis and Evaluation of Novel Carbazole Based Photocages

3.1 Design of Novel Carbazole Photocages

Different heteroatoms typically have different electronic effects on aromatic systems that would result in different UV-vis absorption properties. Wong and coworkers reported the study of photophysical and electrochemical properties of different heteroatom containing tetraphenylenes including oxygen, nitrogen, sulfur, and selenium atoms (Figure 3.1).[230] In the UV-vis absorption studies of all the tetraphenylene compounds, the incorporation of hetero atoms was shown to redshift the absorption compared with tetraphenylene without heteroatom incorporation. Moreover, the nitrogen incorporated tetraphenylene displayed the absorption with the longest wavelength among other heterocycles. The author attributed the observed redshifts to HOMO-LUMO transitions, which was the n-π transition of the lone pair electrons on the oxygen, nitrogen, sulfur, selenium atoms to the conjugated π system. Moreover, the conformation of heteroatom incorporated tetraphenylenes also played a role in determining the photophysical properties. With the knowledge of hetero atom effects on tetraphenylene species, we were curious to explore if same effects would apply to dibenzo analogues. If similar effects were observed on dibenzo analogues, we would be able to observe the change of UV-vis absorption of dibenzo analogues bearing different heteroatoms and potentially discover a new photocage with superior decaging properties.

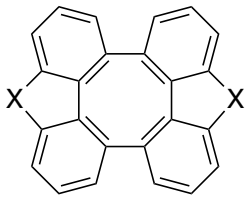

3.1

X = O, NH, S, Se

Figure 3.1. Structures of heteroatoms incorporated tetraphenylenes.

We first investigated the UV-vis spectra of the carbazole and dibenzofuran chromophores (Figure 3.2). We observed carbazole has an absorption band in longer wavelength ranging from 300 to 350 nm compared with dibenzofuran. The absorption band over 300 nm for carbazole indicated that the proposed carbazole photocages are likely to have a longer wavelength absorption than NDBF photocage.

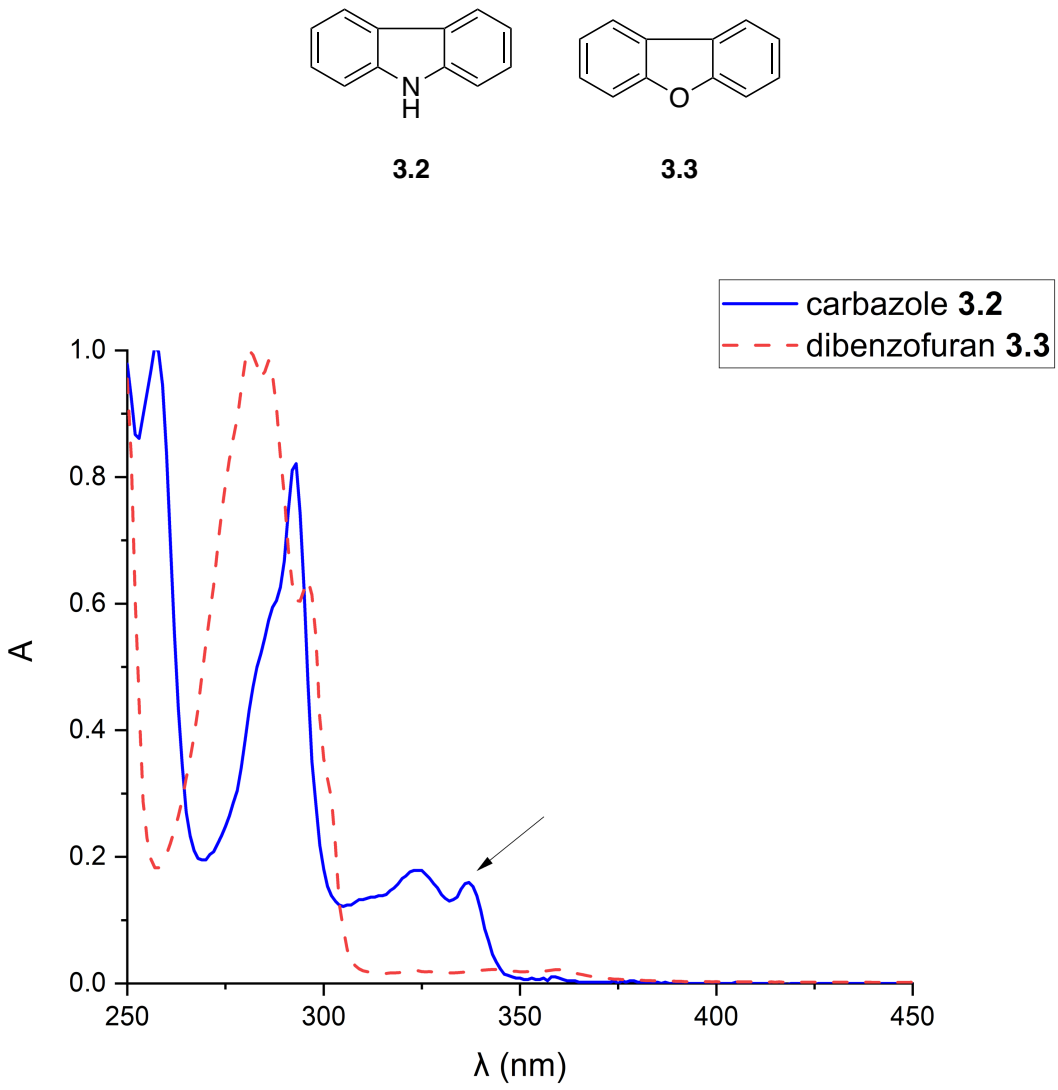

Figure 3.2. Normalized UV-vis spectra of carbazole and dibenzofuran.

We attribute the absorption band to the n-π* transition of the lone pair electrons of nitrogen atom (Figure 3.3). The electron lone pair on the nitrogen atom is higher in energy than that of the electron lone pair of the oxygen atom, because nitrogen is less electronegative than oxygen. The energies of π* orbitals are relatively the same for carbazole and nitrobenzofuran due to the similar conjugation systems. Therefore, the n-π*

transition of carbazole requires longer wavelength irradiation with lower energy compared with nitrobenzofuran, which requires shorter wavelength irradiation with higher energy.

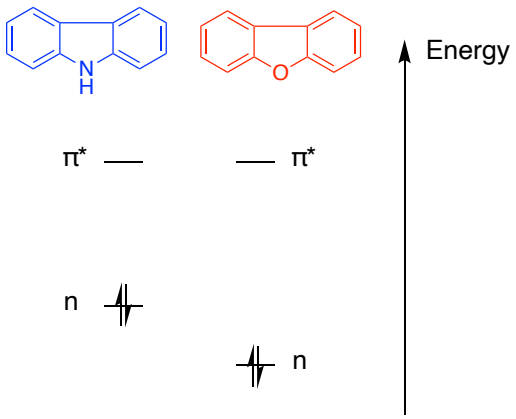

Figure 3.3. Illustration of n-π* transition of carbazole and dibenzofuran.

Our lab has been interested in the field of photocage chemistry, and we sought to develop novel photocages having better properties. Toward this goal, we designed two new *o*-nitrobenzyl photocages **3.5** and **3.6** with the carbazole chromophore but different substitution patterns (Figure 3.4). There has been no study on the effects of different substitution pattern, so we sought to get more information about it with our study of **3.5** and **3.6**, which would be insightful for developing new photocages. Moreover, we are specifically interested in carbazole chromophores since the carbazole has a free nitrogen atom present which provides the possibility for further modification such as introduction of hydrophilic functional groups.

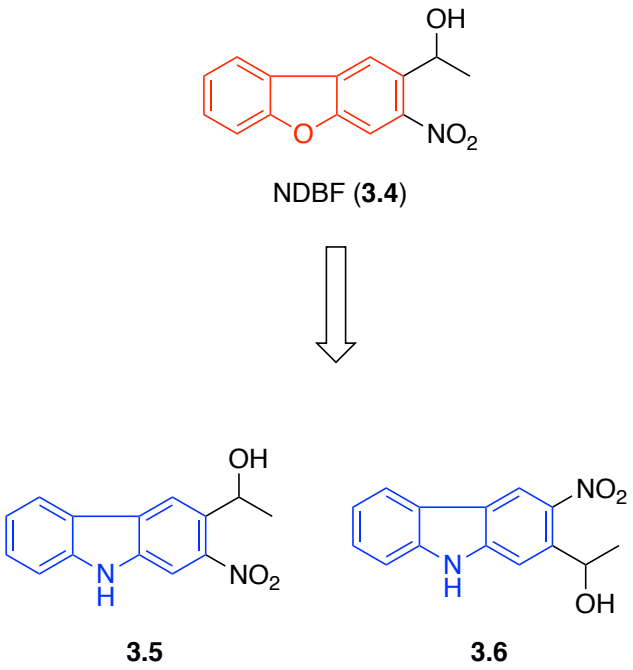

Figure 3.4. Proposed carbazole based photocages **3.5** and **3.6**.

3.2 SYNTHESIS OF CARBAZOLE PHOTOCAGES

3.2.1 Synthetic efforts toward photocage 3.5 and 3.6

The synthesis of the photocage **3.5** commenced with the triflation of 3-nitro-4-methylphenol (**3.7**) to give triflic ester **3.8** in quantitative yield (Scheme 3.1). A Buchwald-Hartwig coupling between **3.8** and aniline generated diaryl amine **3.9** in 94% yield. Unfortunately, we found the oxidative ring closure of **3.9** in the presence of $Pd(OAc)_2$ and $Cu(OAc)_2$ gave a mixture (1:5) of the desired and undesired carbazole isomers **3.10** and **3.11** in 55% yield.

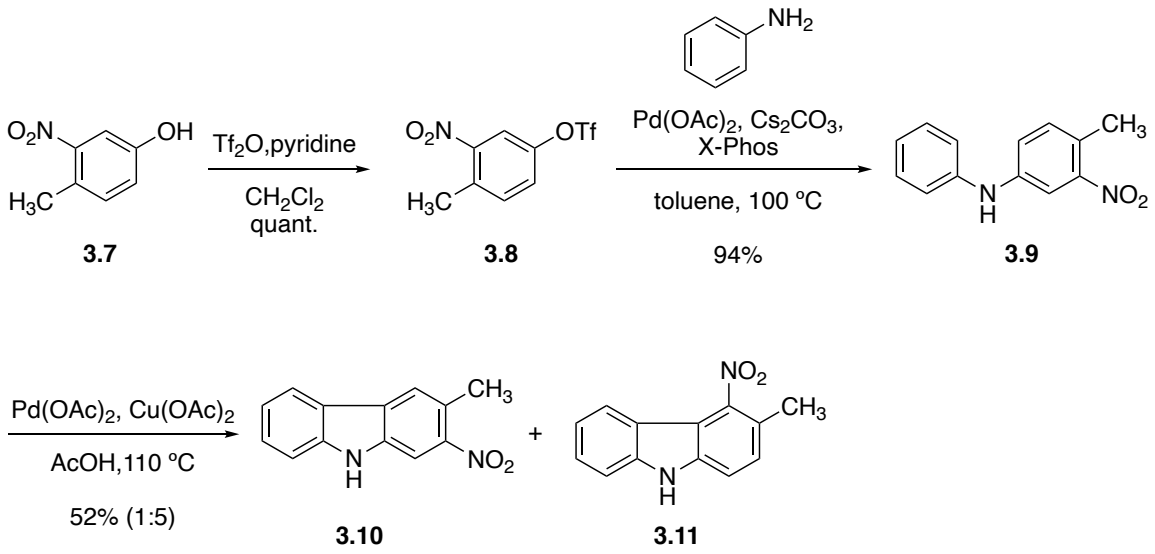

3.7 **3.8** **3.9** **3.10** **3.11**

Scheme 3.1. Synthesis toward photocage **3.5**.

With this undesired result, we decided to pursue a different strategy. We hypothesized that we could favor the formation of **3.10** in the oxidative coupling reaction by blocking the undesired reactive site on the ring by introducing a bromine atom (Scheme 3.2). Mono-brominated phenol **3.12** was obtained in 84% yield by bromination of **3.7** in the presence of tetramethylguanidine. Triflation of **3.12** with triflic anhydride afforded brominated triflic ester **3.13** in quantitative yield.

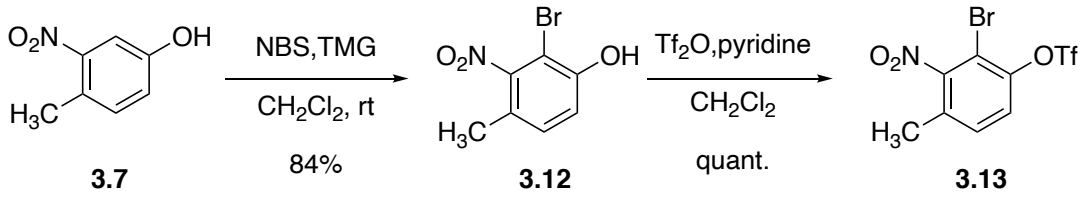

3.7 **3.12** **3.13**

Scheme 3.2. Synthesis of brominated triflic ester **3.13**.

We then investigated the generation of diaryl amine **3.15** via the Buchwald-Hartwig reaction of **3.13** and **3.14** (Scheme 3.3). We screened numerous combinations of palladium catalysts, ligands, and bases that have been reported to promote similar type of reactions,

but no product formation was observed under these conditions. All of reaction conditions we screened either only gave returned starting material brominated triflic ester **3.13** or resulted in detriflation of **3.13** to give bromophenol **3.12** as the major product.

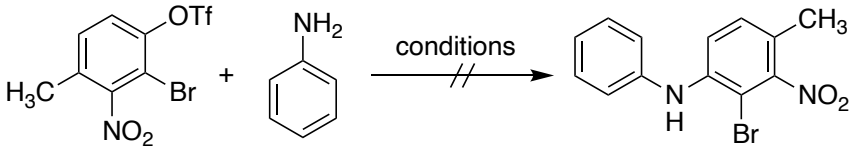

3.13 **3.14** **3.15**

conditions	result
Pd_2dba_3, BINAP, NaO*t*Bu, toluene, 100 ºC	recovered **3.13**
Pd_2dba_3, Davephos, K_3PO_4, toluene, 60 ºC	recovered **3.13**
Pd_2dba_3, Davephos, K_3PO_4, toluene, 100 ºC	recovered **3.12**
Pd_2dba_3, Davephos, NaO*t*Bu, toluene, 100 ºC	recovered **3.12**
$Pd(OAc)_2$, X-Phos, Cs_2CO_3, toluene, 100 ºC	recovered **3.13**

Scheme 3.3. Conditions screening of Buchwald-Hartwig reaction of **3.13**.

Fortunately, we found a recent report that showed the oxidative coupling reaction for a nitro-diaryl amine in pivalic acid favored the formation of the desired isomers because of steric effects.[231] Because pivalic acid coordinates to the nitro group to impede the approach of active Pd catalyst to the ortho position of the nitro group, bond formation at the *para* position is favored. Gratifyingly, the oxidative coupling reaction of **3.9** in pivalic acid afforded a mixture (1.7:1) of **3.10** and **3.11** in 55% yield (Equation 3.1). Although the regioselectivity was not ideal, we obtained a sufficient amount of desired product **3.10**, so we could complete the synthesis of proposed photocage **3.5**.

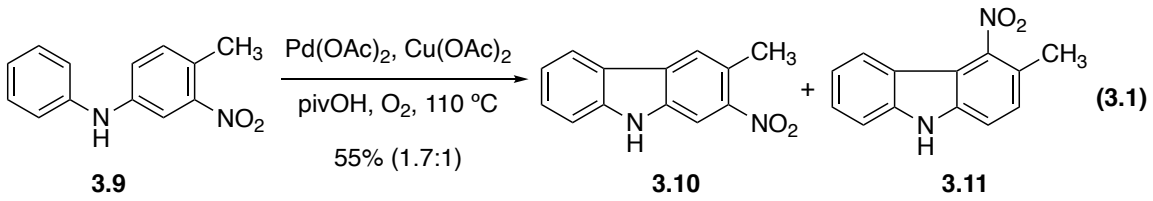

3.9 **3.10** **3.11** **(3.1)**

We next initiated a study of the oxidation of **3.10** to aldehyde **3.16**, but to our surprise, the methyl group proved to be unreactive under various conditions (Scheme 3.4). Conditions included DDQ oxidation, radical bromination, selenium oxidation, IBX oxidation, and chromium oxidation were all screened. Unfortunately, none of the reaction conditions delivered the desired product, and most conditions only resulted in returned starting material. DDQ oxidation in THF at 45 ºC and IBX oxidation at 80 ºC both furnished complex mixtures. Moreover, the radical bromination of **3.10** with NBS and AIBN at 80 ºC yielded a mixture of bromination products on the aryl moiety.

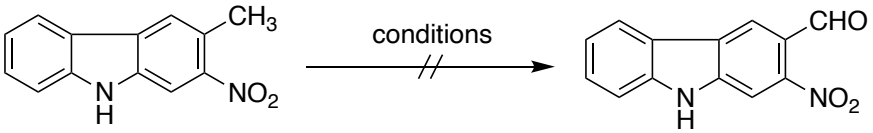

3.10 **3.16**

conditions	results
DDQ, MeOH	recovered **3.10**
DDQ, THF, 45 ºC	complex mixture
NBS, AIBN, CCl_4, hv	recovered **3.10**
NBS, AIBN, CCl_4, 80ºC	mixture of brominated products
SeO_2, 1,4-dioxane, 80 ºC	recovered **3.10**
CrO_3, DMP, DCM, – 20 ºC	recovered **3.10**
IBX, DMSO, 80 ºC	complex mixture
CrO_3, AcO_2, H_2SO_4, 0 ºC	recovered **3.10**

Scheme 3.4. Unsuccessful attempts of the oxidation of **3.10**.

We eventually found the Leimgruber-Batcho reaction with DMF-DMA and pyrrolidine in DMF converted **3.10** to an enamine intermediate **3.17**, which was then cleaved by $KMnO_4$ in THF and H_2O to yield aldehyde **3.16** in 37% yield over two steps (Scheme 3.5). Finally, the methylation of aldehyde **3.16** afforded the photocage **3.5** in 62% yield. Several methylation reagents including methyl magnesium bromide, trimethyl aluminum and methyllithium were evaluated, but methyllithium gave the best yield of 62%.

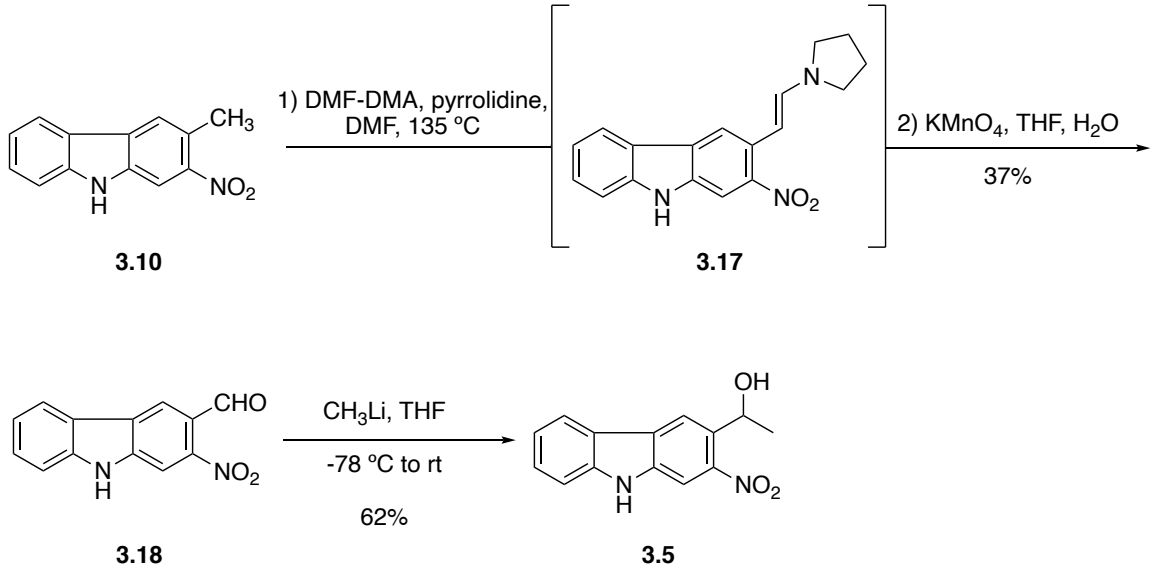

Scheme 3.5. Final steps to the synthesis of photocage **3.5**.

We next turned our attention to streamline the synthetic route. We realized the sequential cyclization of **3.9** and oxidation of **3.10** gave a relatively low yield with a mediocre regioselectivity. Fortunately, we found we could easily oxidize the diaryl amine **3.9** with the Leimgruber-Batcho reaction condition to get aldehyde **3.17** in 86% yield

(Scheme 3.6). The subsequent methylation of **3.17** with trimethyl aluminum afforded alcohol **3.18** in 89% yield, and the final cyclization of **3.18** was conducted in pivalic acid in the presence of $Pd(OAc)_2$ and $Cu(OAc)_2$ in O_2 to furnish a mixture (3:1) of **3.5** and **3.19**.

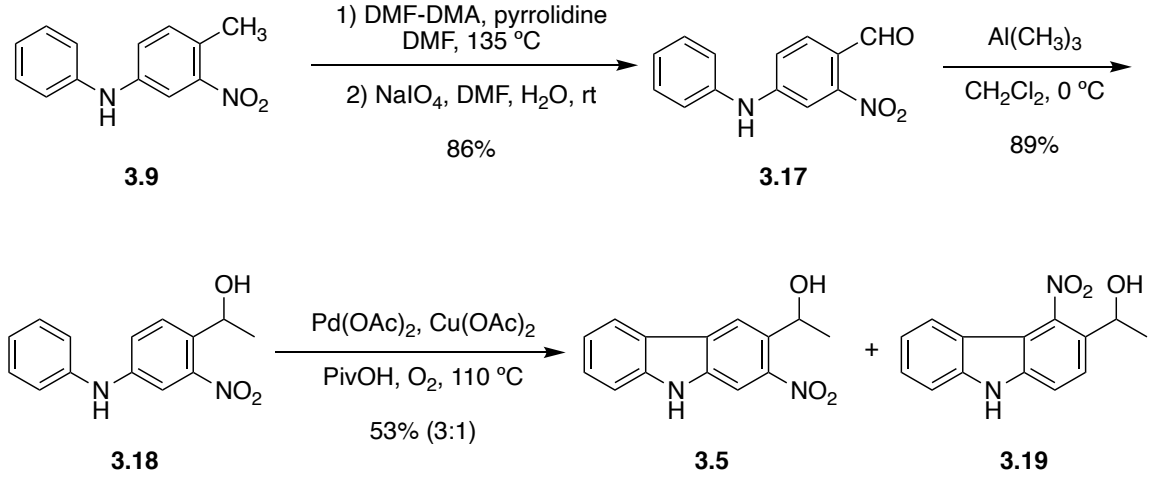

Scheme 3.6. Revised sequential steps of synthesis toward photocage **3.5**.

Synthesis of photocage **3.2** was carried out in the same transformation sequence, which would be summarized in the next section.

3.2.2 Summary of synthesis of carbazole photocages 3.5 and 3.6

The synthesis of photocage **3.5** commenced with 4-nitro-3-methyl phenol **3.7** which was converted to its triflic ester **3.8** in quantitative yield (Scheme 3.7). **3.8** was coupled with aniline in the presence of $Pd(OAc)_2$ and X-Phos to give diaryl amine **3.9** in 94% yield. The subsequent oxidation of **3.9** via a Leimgruber-Batcho reaction to afford aldehyde **3.17** in 86% yield. Aldehyde **3.17** was then methylated with trimethylaluminum to afford alcohol **3.18** in 89% yield. The final oxidative cyclization of **3.18** with $Pd(OAc)_2$ in pivalic acid afforded a mixture (3:1) of photocage **3.5** and **3.19** in 53% yield. The photocage **3.5**

was thus readily prepared in five steps with 28% overall yield from commercially available materials.

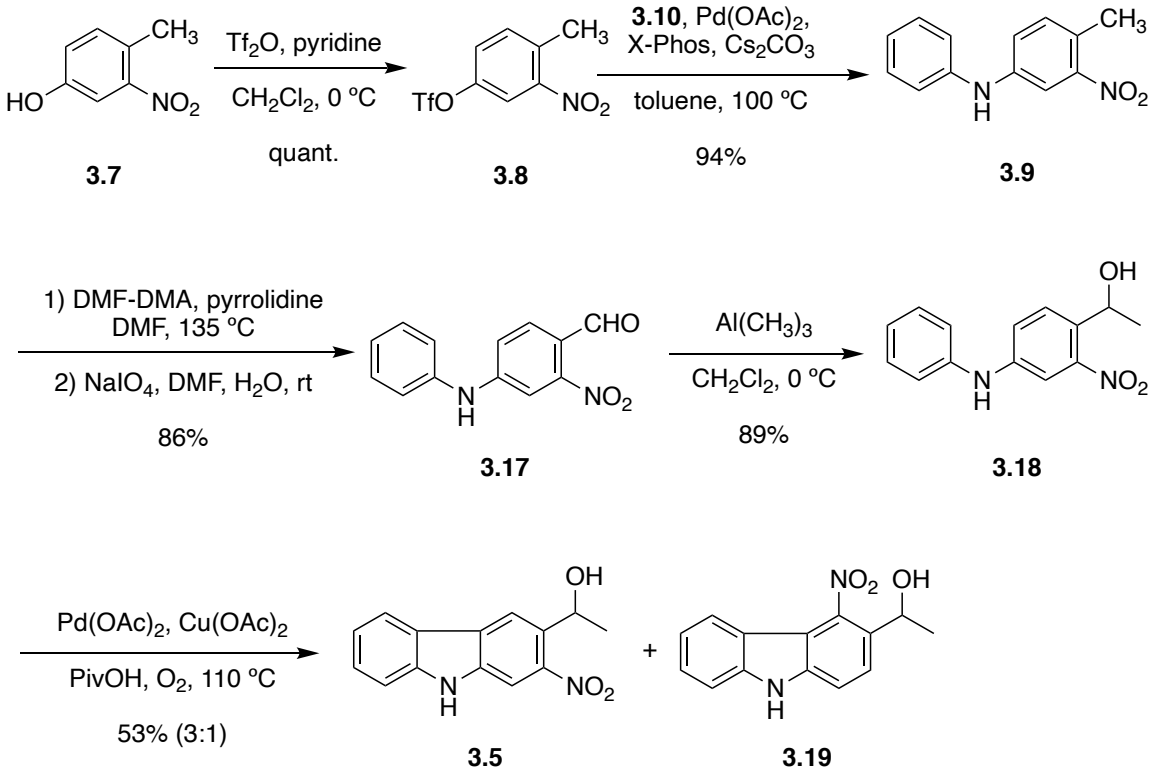

Scheme 3.7. Synthesis of photocage **3.5**.

Photocage **3.6** was prepared in an analogous manner (Scheme 3.8). Starting from 4-nitro-3-methyl phenol (**3.20**), triflation with triflic anhydride afforded **3.21** in quantitative yield. **3.21** was coupled with aniline in the presence of $Pd(OAc)_2$ and X-Phos to give diaryl amine **3.22** in 95% yield. The subsequent oxidation of **3.22** via a Leimgruber-Batcho reaction condition to give aldehyde **3.23** in 80% yield. Aldehyde **3.23** was then methylated with trimethylaluminum to afford alcohol **3.24** in 90% yield. The final

oxidative cyclization of **3.24** with $Pd(OAc)_2$ in pivalic acid afforded photocage **3.6** in five steps and 29% overall yield from **3.20**.

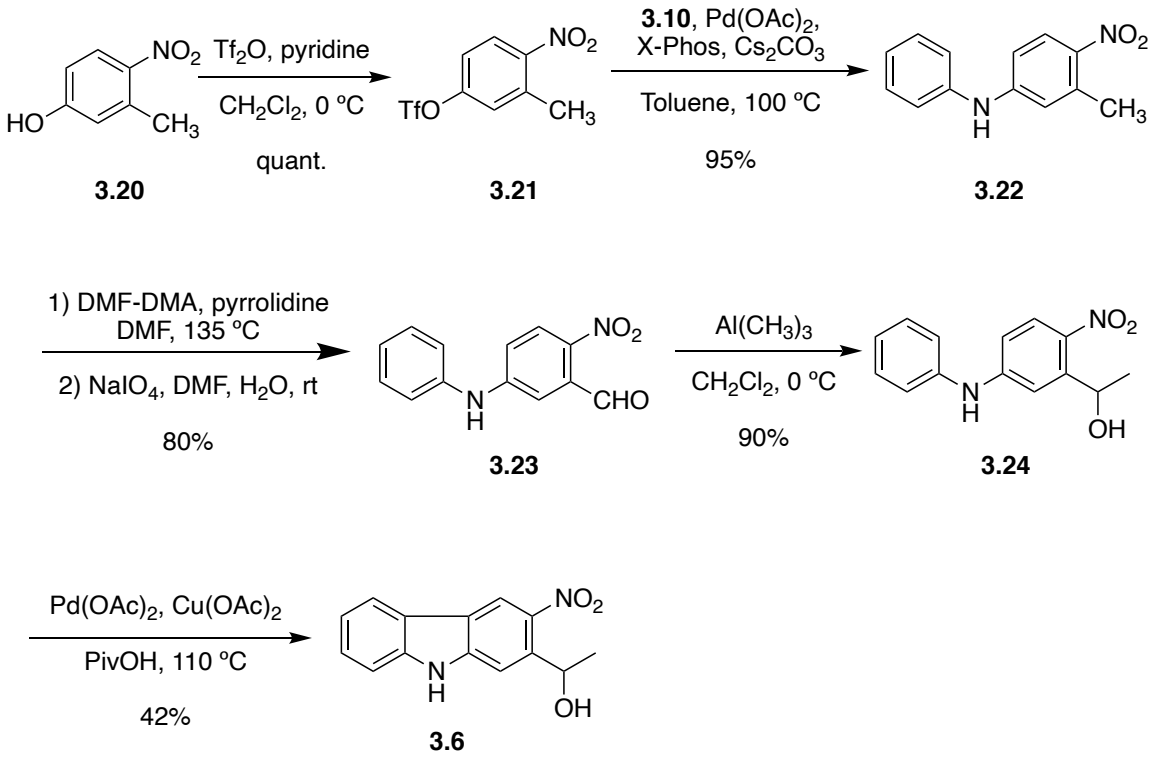

Scheme 3.8. Synthesis of photocage **3.6**.

3.3 BENZOIC ACID MODEL SYSTEM STUDY

With the novel photocages **3.5** and **3.6** in hand, we next characterized their decaging properties in a model system study; we also used a known photocage as a comparison. We selected NDBF (**3.4**) as our comparison target. We conducted the synthesis of NDBF according to the literature procedure (Scheme 3.9).[232] Starting from commercially available starting material **3.25** and **3.26**, Ullmann coupling in the presence of Cu(I) afforded diaryl ether **3.27** in 70% yield. Methylation of **3.27** with trimethylaluminum yielded alcohol **3.28** in quantitative yield, which was subsequently cyclized under Heck

reaction condition to form NDBF in 25% yield. NDBF was obtained in three steps with an overall yield of 18%.

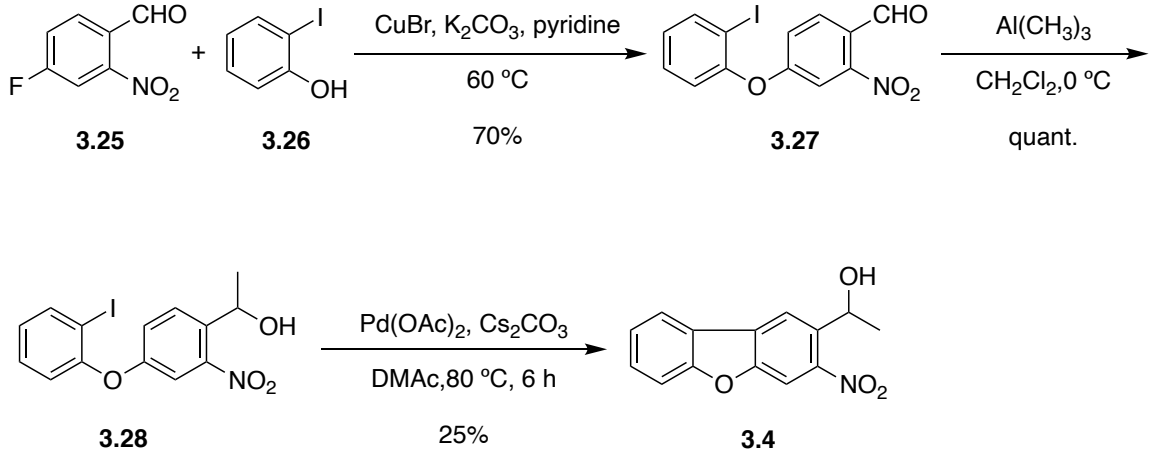

Scheme 3.9. Synthesis of photocage NDBF (**3.4**).

With NDBF in hand as the benchmark comparison, we investigated decaging properties using a benzoic acid model system. Benzoic acid is often picked as the releasing target in similar photocage evaluation studies, because it is a good leaving group.[233] Benzoic acid also has a strong UV absorption that can be easily monitored by LC after being decaged. Moreover, the chemical "caging" process was straightforward. Benzoate esters can be readily formed between benzoic acid and alcohol cages under various conditions, and typically the reactions are efficient thus affording target benzoate esters in high yield and good purity. Accordingly, we prepared the corresponding benzoate esters **3.29**–**3.32** via the Steglich esterification reactions (Equations 3.2-3.5).[234]

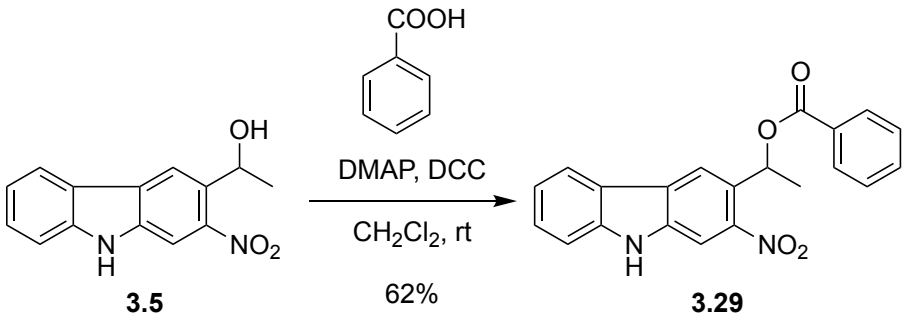

(3.2)

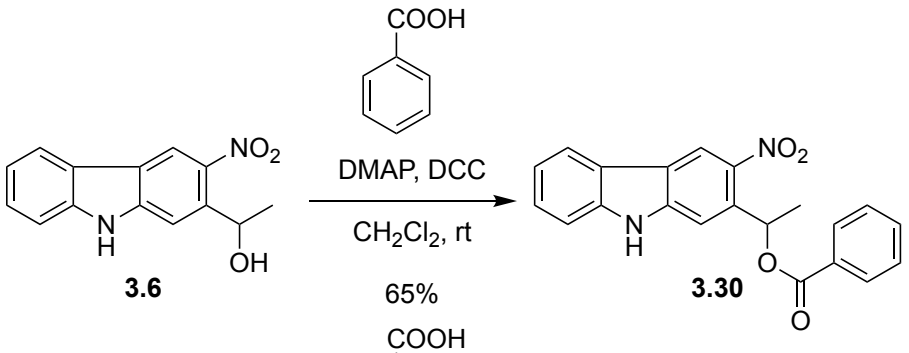

(3.3)

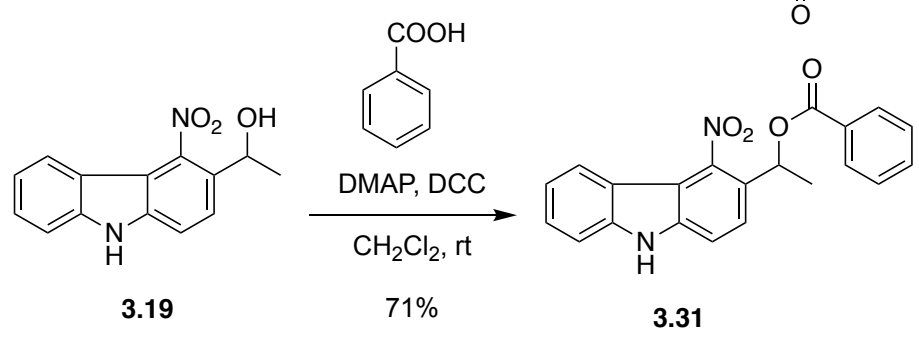

(3.4)

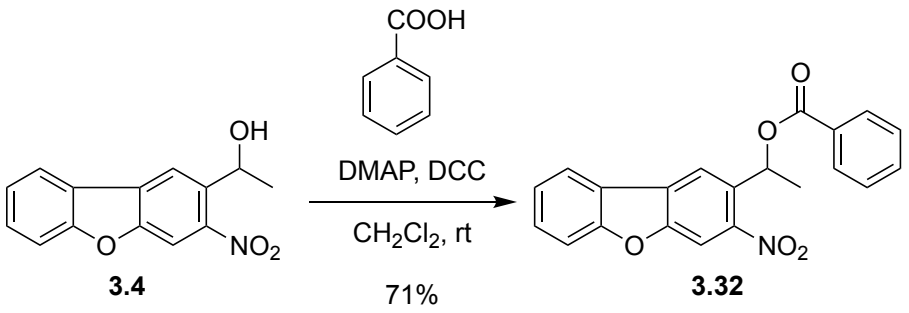

(3.5)

The UV-vis spectra of **3.29**–**3.32** were obtained at different concentrations varying from 0.01 mM to 0.1 mM in THF, and the molar absorptivity was calculated and plotted in Figure 3.5. Compounds **3.29** and **3.30** were found to have significantly longer wavelength

absorption than **3.32**. Moreover **3.29** has a moderate absorption at 420 nm. Both **3.29** and **3.30** have larger molar absorptivity values than **3.32** at wavelengths above 350 nm. However, **3.31** showed very weak absorption over 300 nm. We rationale this observance as the steric interactions between the nitro group and the benzoate group as well as the carbazole group prevent the nitro group from being coplanar with the carbazole chromophore.

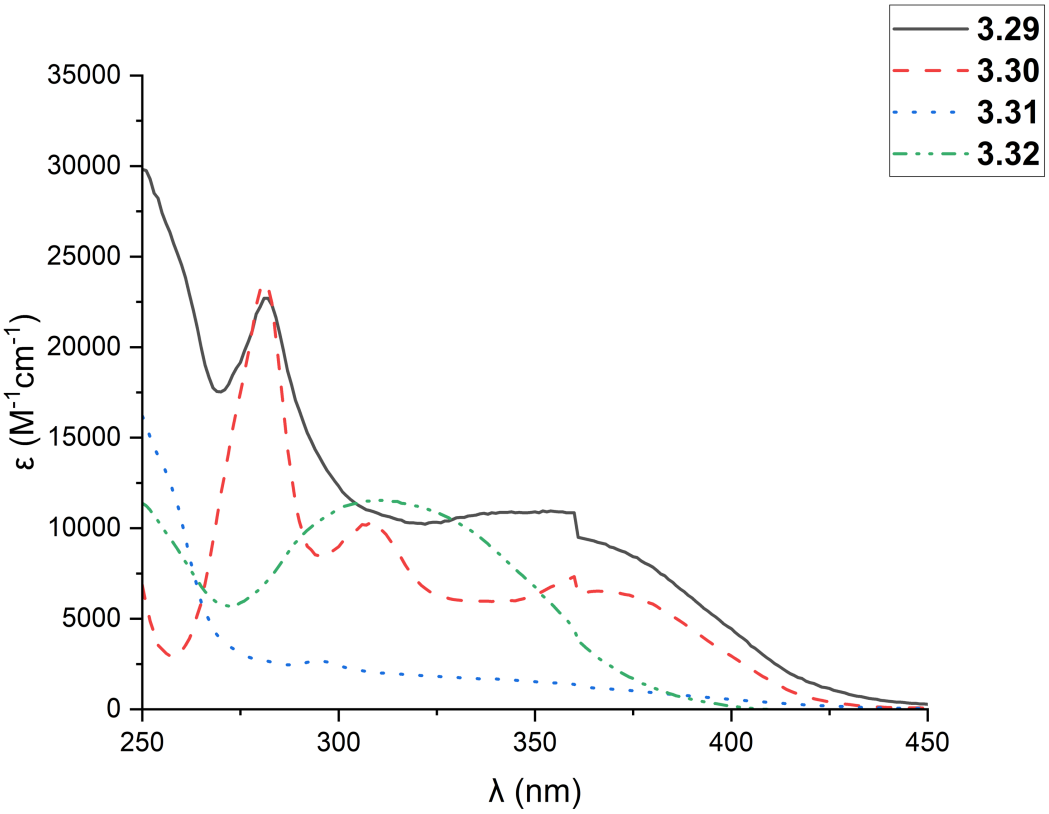

Figure 3.5. UV-vis spectra of photocaged benzoic compounds **3.29–3.32**.

Comparative decaging studies were conducted by irradiating 0.1 mM solutions of **3.29**, **3.30** and **3.32** in THF at 390 nm and 400 nm using a fluorimeter (Figure 3.6). Same

decaging study was also performed on **3.31** at 400 nm, but trace amounts of decaging were detected. Aliquots were taken every 10 min and analyzed by C18 column on reverse phase HPLC using 60% MeCN in water as the eluent. The decaging percentage was calculated based on the peak areas of the starting material, benzoic acid and the nitrosoketone product. Upon irradiation at 390 nm for 60 min, 87% of **3.29** and 70% of **3.30** were decaged**,** whereas only 42% of the NDBF analog **3.32** was decaged. A similar trend was observed upon irradiation at 400 nm where 82% of **3.29** was decaged and 42% of **3.30** was decaged, after 60 min; however, decaging of **3.32** was only 22%. These results indicate that our newly design photocage **3.5** and **3.6** can release small molecules such as benzoic acids by single photon excitation at wavelengths in the visible region more readily than their NDBF caged counterparts.

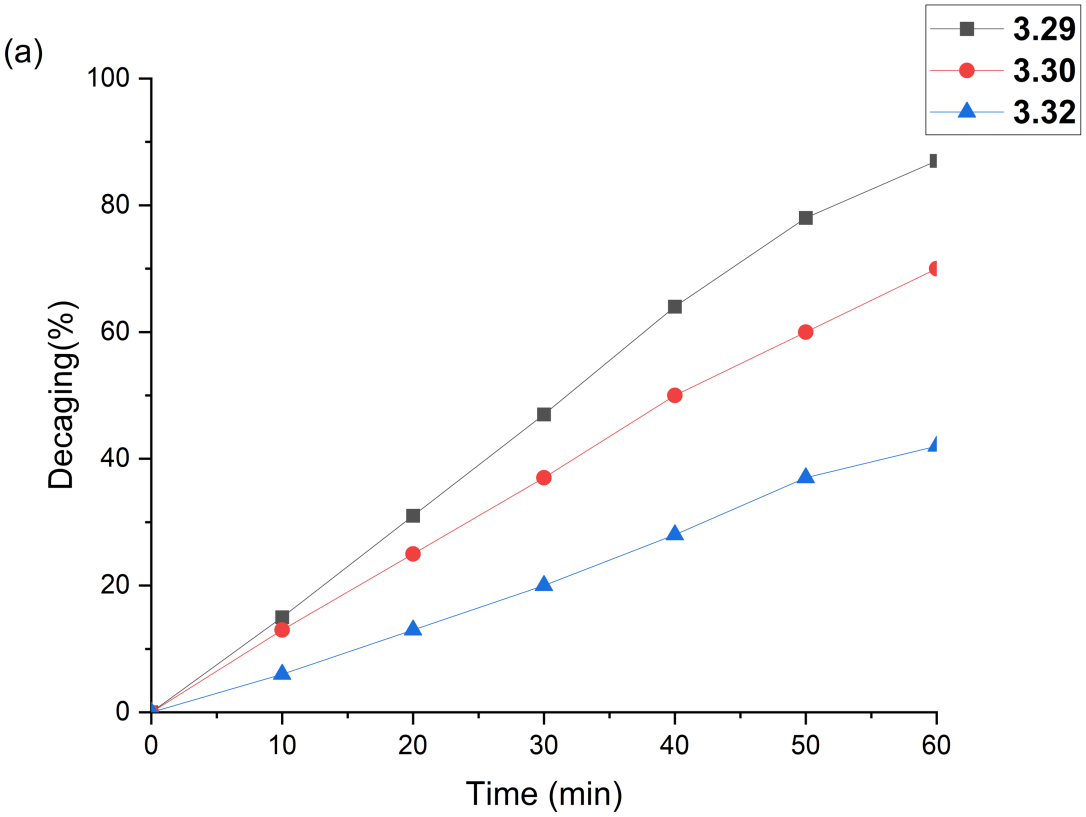
(a)
3.29
3.30
3.32
Decaging(%)
Time (min)
0
20
40
60
80
100
0
10
20
30
40
50
60

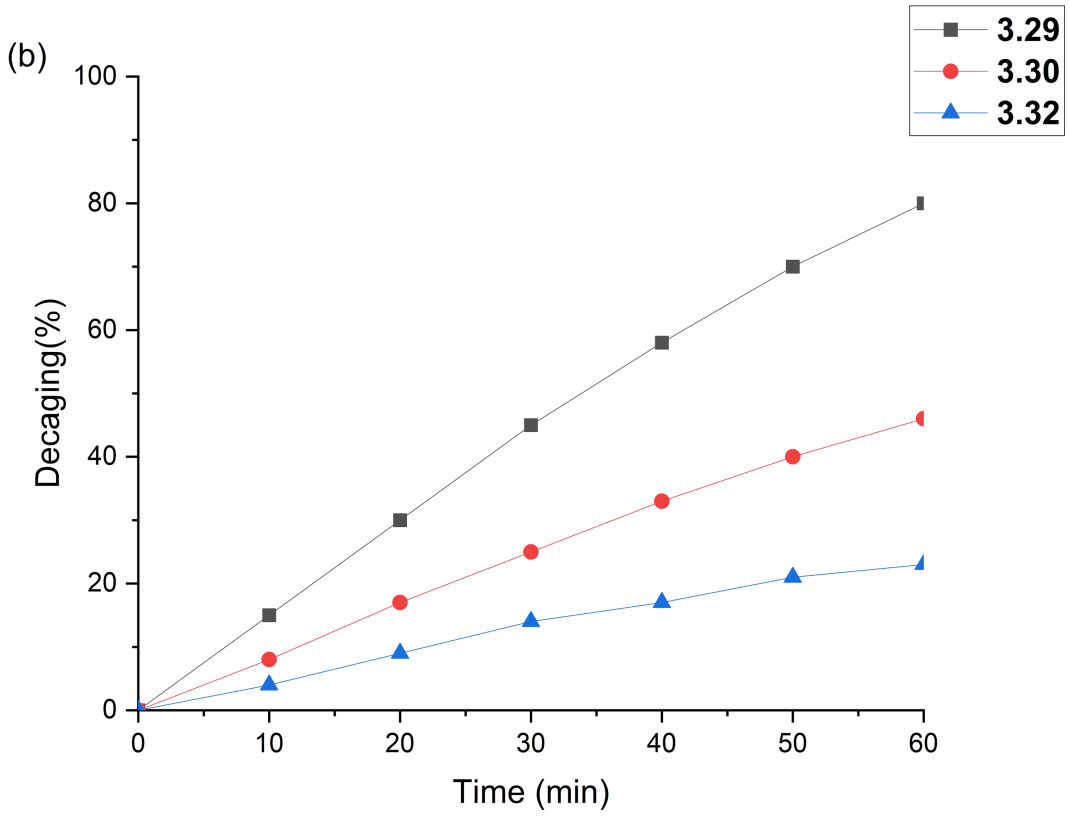

Figure 3.6. (a) Decaging of **3.29**, **3.30** and **3.32** (0.1 mM in THF) at 390 nm was measured over time by HPLC. (b) Decaging of **3.29**, **3.30** and **3.32** (0.1 mM in THF) at 400 nm was measured over time by HPLC.

Extending the absorption spectrum to longer wavelength is only one goal that needs to be addressed when developing new caging molecules. High molar extinction coefficients, ε, and quantum yields of decaging, Φ, are also important because together these parameters define decaging efficiencies, ε•Φ. The extinction coefficients of **3.29**, **3.30** and **3.32** were determined by UV-vis absorptions at different concentrations according to Lambert-Beer's law, and quantum yields were determined using ferrioxalate actinometer as the standard at excitation wavelengths (Table 3.1).[235] In the event, the decaging efficiency of **3.29** at 390 nm was 40-fold greater than **3.32**, while **3.30** was degaged 25-

fold more efficiently than **3.32**. At 400 nm, **3.29** shows a more superior efficiencies with a 150-fold increase compared with NDBF-derived compound **3.32**, while **3.30** showed moderate increase at 20-fold better than **3.32**.

Table 3.1. Photochemical properties of photocaged compounds **3.29, 3.30** and **3.32**.

Caged compound	$\varepsilon(M^{-1}cm^{-1})$ (390 nm)	Φ (390 nm)	$\varepsilon\Phi$ $(M^{-1}cm^{-1})$ (390 nm)	$\varepsilon(M^{-1}cm^{-1})$ (400 nm)	Φ (400 nm)	$\varepsilon(M^{-1}cm^{-1})$ (400 nm)
3.29	6105	0.11	672	4490	0.1	449
3.30	4727	0.09	425	2871	0.02	57
3.32	572	0.03	17	260	0.01	3

3.4 TYROSINE DECAGING STUDY

3.4.1 Introduction of caged tyrosines

With the successful demonstration of chemical caging and efficient decaging of benzoic acids with irradiation of visible light, we next investigated the decaging of different substrates with the newly designed photocage **3.5**, therefore, expanding the scope of decaging substrates of photocage **3.5**. As we have discussed previously, *o*-nitrobenzyl photocages are typically efficient at decaging good leaving groups such as carboxylic acids, phosphates, carbonates, and carbamates. However, for bad leaving groups such as phenols and alcohols, the decaging rates are moderate. The decaging of phenols and alcohols can be mitigated using the carbonate linkers, however, as we discussed previously, the decomposition of carbonate linkers can sometimes be the rate limiting steps in the decaging process. Therefore, a more direct release of phenols and alcohols would be advantageous.

Tyrosine phosphorylation is a key step in signal transductions and regulations of enzymatic activities. A phosphate (PO_4^{3-}) group is installed on the phenolic hydroxy group of amino acid tyrosine on a protein in the presence of adenosine triphosphate (ATP) through tyrosine kinases. Scientists have demonstrated the photocaged tyrosine derivatives, which are formed through formation of the phenol ether, can be powerful tools in the studies of information transduction. To illustrate the role of individual steps in information transduction, both fast reveal of protein phosphorylation sites and rapid protein kinase activation are needed. The photolysis of caged tyrosine derivatives meets both requirements thus providing the foundation of detailed studies of information transduction. Deiters group, Chin group and Schutlz group have reported the collaboration studies of the photocontrol of tyrosine phosphorylation process in mammalian cells via genetic encoding of photocaged tyrosine.[236,237] Caged tyrosine derivative **3.33** was generically encoded into proteins in mammalian cells, which was then photolyzed to release a free tyrosine derivative upon irradiation of UV light (365 nm) (Figure 3.7). The released tyrosine derivative was later phosphorylated in mammalian cells.

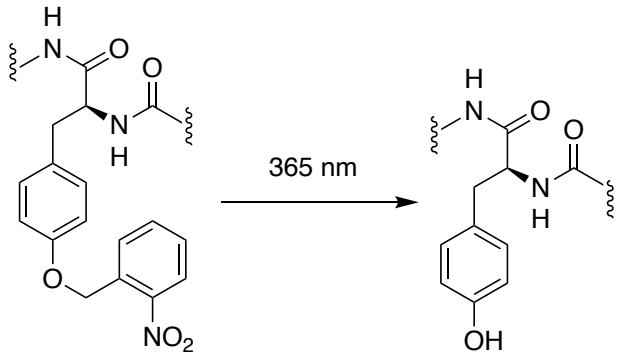

3.33 **3.34**

Figure 3.7. Photocaged tyrosine derivatives in biological applications.

We decided to showcase the utility of photocage **3.5** by caging tyrosine derivatives. *o*-Nitrobenzyl photocages typically have lower efficiencies releasing phenol derivatives than good leaving groups such as carboxylic acids. Improved decaging efficiencies of releasing phenols can be a promising trait for new photocages. Moreover, potential biological applications with caged tyrosine derivatives could be further developed based on these decaging studies of caged tyrosine.

3.4.2 Synthesis of the caged tyrosine compound

The first task was to synthesize modified tyrosine substrates. In the event, the Cbz protected tyrosine **3.35** was converted to its methyl ester **3.36** in 89% yield according to a literature procedure.[238]

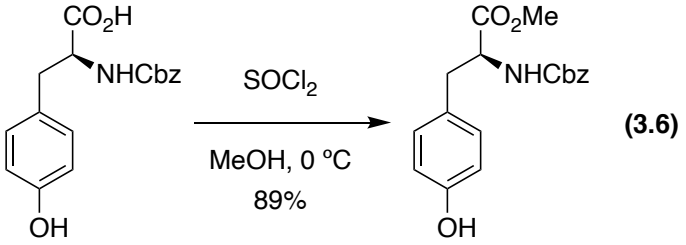

3.35 **3.36** **(3.6)**

To make photocage **3.5** more useful in biological applications, further modifications are needed to improve its water solubility. To achieve this objective, hydrophilic functional groups such as carboxylic acids can be attached to the carbazole nitrogen atom. One of the most commonly used hydrophilic groups to increase water solubility is the amino dicarboxylate functional group, and it could be readily appended to the nitrogen atom of photocage **3.5** via a simple substitution reaction with bromo substituted amino dicarboxylate **3.38**, which was prepared by the literature procedure.[239]

Namely, a solution of **3.37** and *t*-butyl bromoacetate in the presence of Hunig's base (N,N-diisopropylethylamine) in DMF was stirred overnight at room temperature to generate **3.38** in 89% yield (Equation 3.7).

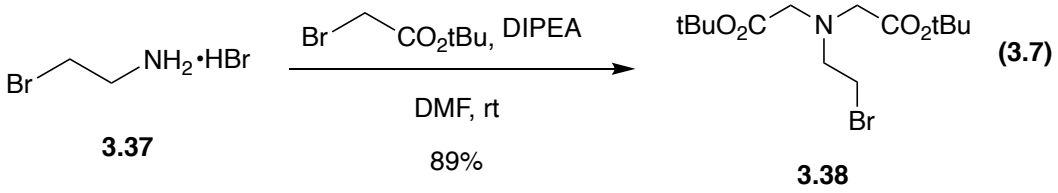

(3.7)

A solution of **3.5** was then treated with NaH at 0 ºC to deprotonate the nitrogen atom, and **3.38** was added to generate **3.39** in 73% yield.

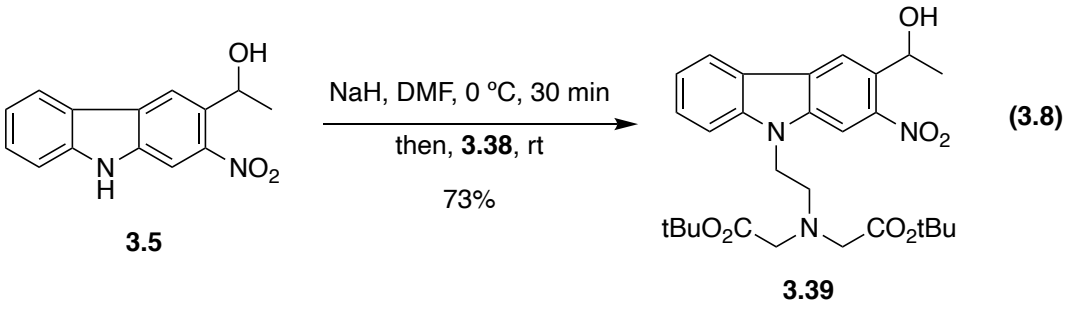

(3.8)

With **3.39** in hand, we next investigated its reaction with the tyrosine derivative **3.36**. We intended to first convert alcohol **3.39** to its corresponding methanesulfonic ester, which would be further substituted with the tyrosine hydroxyl group. However, treatment of **3.39** with methanesulfonyl chloride (MsCl) in the presence of Et_3N in CH_2Cl_2 did not generate mesylate **3.40**, but the chlorine derivative **3.41** was isolated in 55% instead (Equation 3.9).

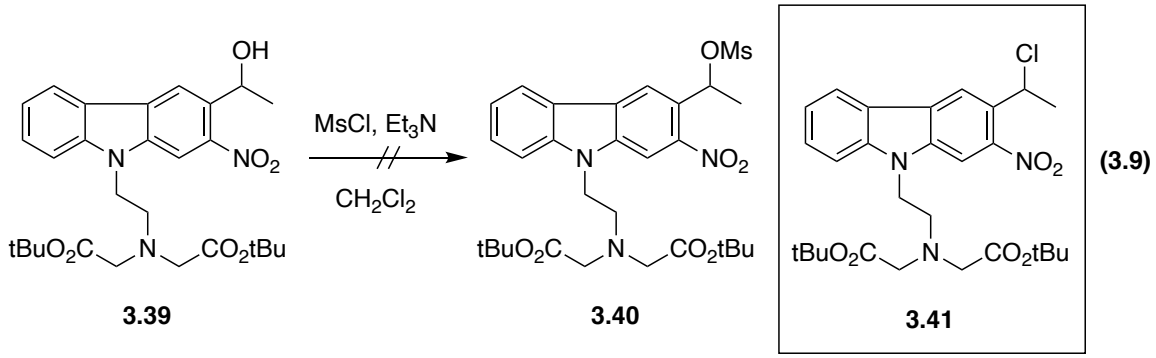

Examples of chlorine derivatives being formed by treating benzyl alcohols with tosyl chloride (TsCl) have been reported in literature.[240] Similarly, mesylate would be possible to be further replaced by chlorides in solutions to generate **3.41**. To avoid this side reaction, we decided to use mesyl anhydride (Ms_2O) instead of mesyl chloride. Ms_2O was readily prepared by treating methanesulfonic acid with phosphorous pentoxide (P_2O_5).[241] A solution of **3.39** was treated with Ms_2O in the presence of Et_3N to furnish **3.40** in 77% yield (Equation 3.10).

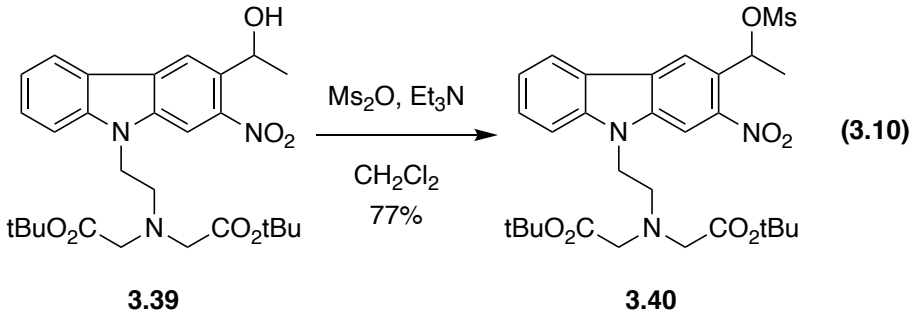

With **3.40** in hand, we investigated the reaction of **3.40** with **3.36**. A solution of **3.40** and **3.36** containing K_2CO_3 in DMF was stirred at 80 ºC overnight (Equation 3.11). Unfortunately, only trace amounts of **3.41** were observed on LCMS, and the hydrolysis product **3.39** was isolated as the major product.

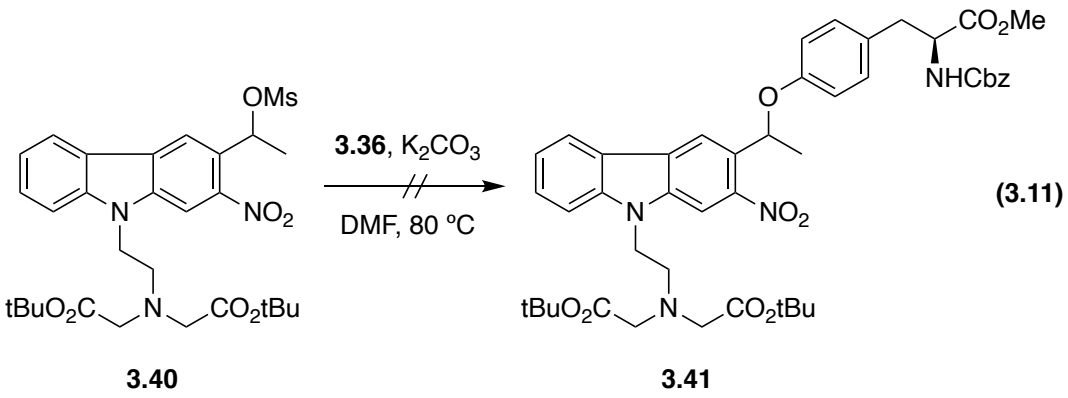

We then turned our attention to the Mitsunobu reaction to form ether **3.41** (Equation 3.12). We first treated **3.39** and **3.36** with Ph_3P and diethyl azodicarboxylate (DEAD) in THF at 0 ºC, and the solution was stirred overnight at room temperature. However, only unreacted **3.39** was recovered after the reaction. Unreacted **3.38** was also recovered from the reaction of **3.39** and **3.36** with Ph_3P and DEAD in toluene at room temperature. Gratifyingly, a solution of **3.36** and **3.40** in the presence of Bu_3P and 1,1'-(azodicarbonyl)dipiperidine (ADDP) in CH_2Cl_2 furnished ether **3.41** in 63% yield (Equation 3.12).

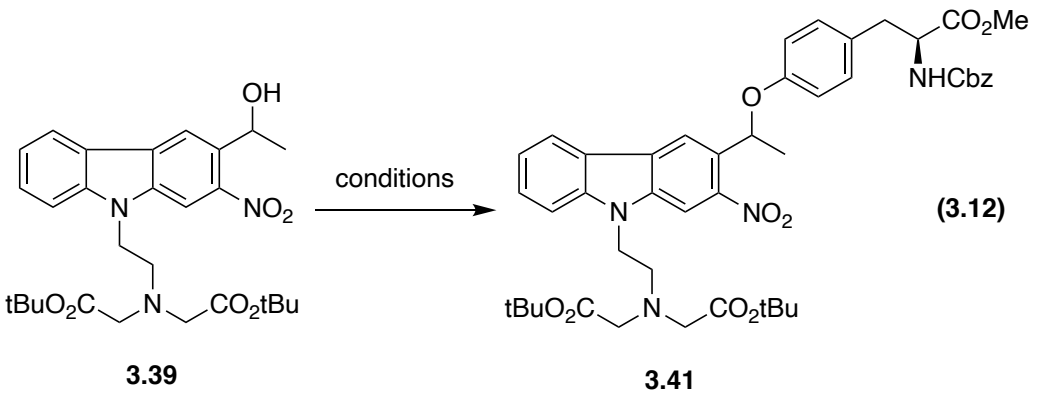

conditions	results
3.36, Ph_3P, DEAD, THF, 0 ºC to rt	recovered **3.39**
3.36, Ph_3P, DEAD, toluene, rt	recovered **3.39**
3.36, Bu_3P, ADDP, CH_2Cl_2, rt	**3.41** in 63%

The final deprotection of t-butyl ester group of **3.41** was conducted with the treatment of HCl in dioxane to afford **3.42** in 95% yield (Equation 3.13).

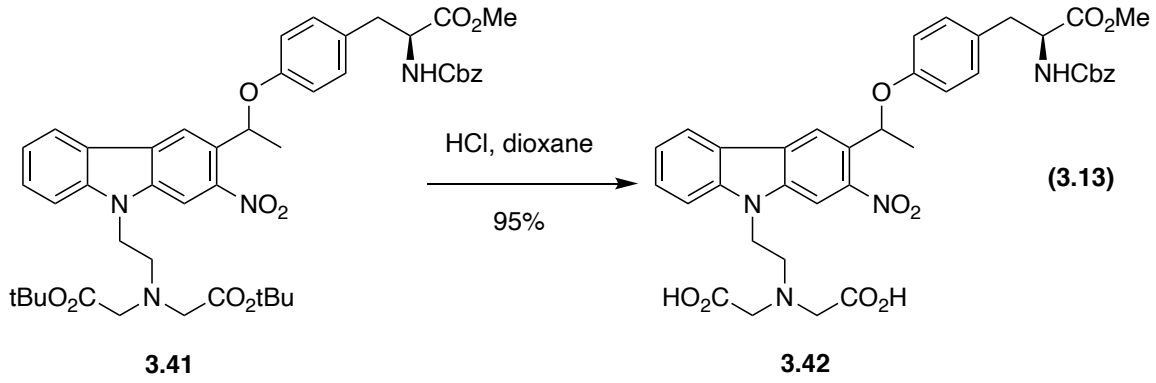

3.4.3 Decaging studies of caged tyrosine compound

Decaging studies were conducted by irradiating 0.1 mM solutions of **3.42** in H_2O at 360, 370, 380, 390, and 400 nm using a fluorimeter over 60 min (Figure 3.8). Aliquots were taken every 10 min, and these aliquots were analyzed by reverse phase HPLC with

C18 column using gradients from 0% to 100% MeCN in water over 30 min as the mobile phase. Decaging percentages were calculated based on the disappearance of **3.42** and appearance of **3.36**. We observed 81% of **3.42** was released after 60 min irradiation at 360 nm. At 370 nm, 63% decaging of **3.42** was observed after 60 min irradiation. For longer wavelengths, 45% decaging was detected at 380 nm, 26% at 390 nm, and 16% at 400 nm after 60 min respectively.

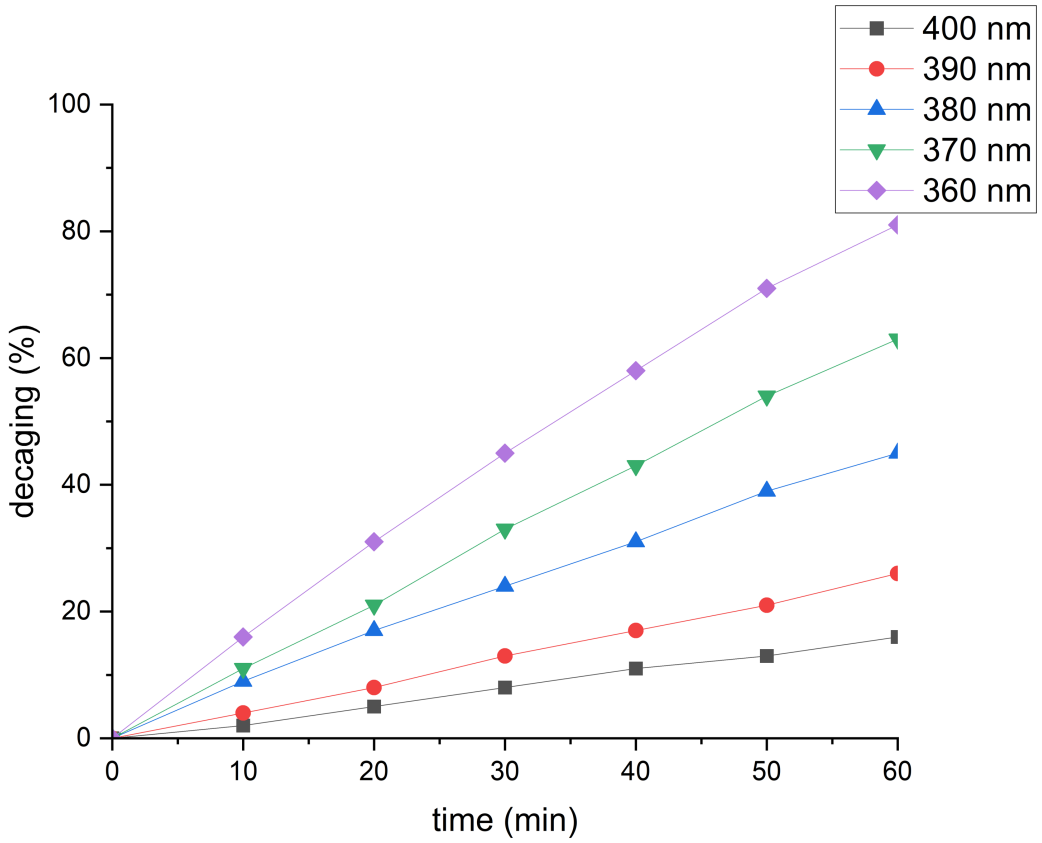

Figure 3.8. Decaging of **3.42** (0.1 mM in H_2O) from 360–400 nm was measured over time by HPLC.

The decaging results of the photocaged tyrosine derivative indicate the release of bad leaving group phenol derivatives is less efficient than releasing good leaving groups

such as carboxylic acids. In order to achieve an ideal decaging outcome (over 80% decaging) over 60 min, irradiation at 360 nm was needed. Although, the decaging of tyrosine derivatives at wavelengths near visible light region were not as fast as we expected, the successful decaging are still promising results for potential applications which do not require ultra-fast decaging rates.

3.5 FLUOROQUINOLONE DECAGING STUDY

3.5.1 Introduction of fluoroquinolone and its applications with photocages

With the successful demonstration of decaging benzoic acids and tyrosine derivatives, we turned our attention to explore the application of newly designed photocage in biological studies.

Since their discovery in the early 1960s, quinolone derivatives have generated considerable clinical and scientific interests owing to their use as antibiotics to treat bacterial infections.[242] The early modification of introducing a fluorine atom onto the ring dramatically increased the potency of quinolone derivatives that were later classified as fluoroquinolone derivatives. Fluoroquinolone antibiotics are widely utilized due to their ideal attributes including high potency, good bioavailability, oral and intravenous formulation and low side effects. Since the first derivative nalidixic acid was developed in 1960s, four generations of fluoroquinolones have been developed based on their spectra of activities, and multiple derivatives have been marketed since 1960s (Figure 3.9).[243]

First generation:

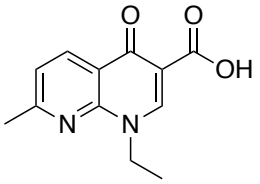

Nalidixic acid

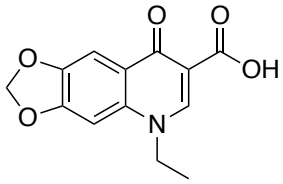

Oxolinic acid

Second generation:

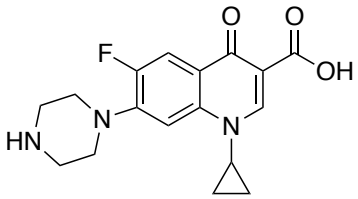

Ciprofloxacin (Ciloxan)

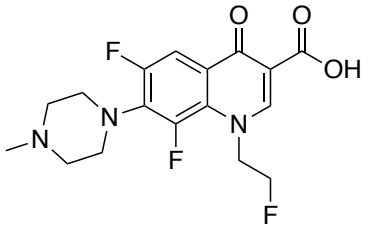

Fleroxacin (Quinodis, Megalocin)

Third generation:

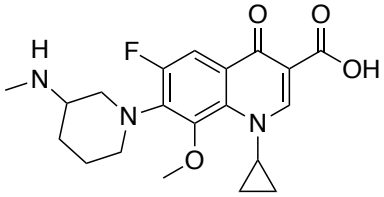

Balofloxacin (Q-Roxin)

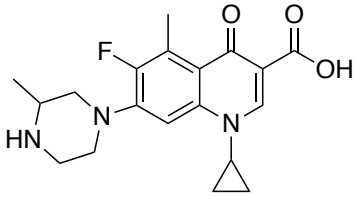

Grepafloxacin (Raxar)

Fourth generation:

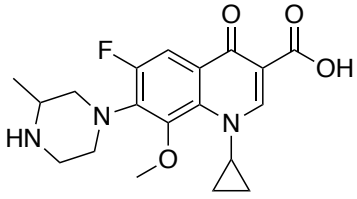

Gatifloxacin (Gatiflo, Tequin, Zymar)

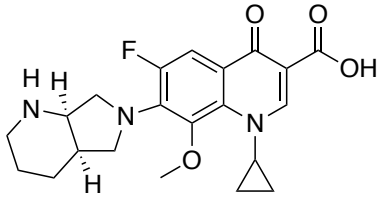

Moxifloxacin (Acelox, Vigamox)

Figure 3.9. Select examples of quinolone derivatives of each generation and their trade names.

The mechanism of action of fluoroquinolone derivatives are well studied.[244,245] Fluoroquinolones function by inhibiting the replication and transcription process of bacterial DNA that is required for the proper functioning of the bacteria. During replication and transcription, duplex DNA uncoils into a single-stranded structure by the DNA gyrase or DNA topoisomerase enzymes. DNA gyrase, which contains two A subunits (gyr A) and two B subunits (gyr B), is a critical enzyme to prevent the detachment of gyrase from the DNA. Fluoroquinolone derivatives inhibit this enzyme by binding gyr A and prevent bacteria from replicating or even synthesizing proteins.

The structure-activity relationships of quinolone derivatives have been well-studied.[246] Figure 3.10 shows the core structure of fluoroquinolone derivatives and positions that can be modified to manipulate the activities. Among them, positions 2,3 and 4 are of the great importance. Position 3 must be a carboxyl group and position 4 must be an oxygen atom because these groups are essential for gyrase binding and bacterial transport. At position 2, a hydrogen atom was found optimal, because any larger group at this position creates a disfavored steric hinderance to the adjacent 3 and 4 positions. The fluorine at position 6 was one of the earliest modifications, which resulted in a 10-fold increase in gyrase inhibition, and 5 to 100-fold improvement in MIC compared with any other halogen atoms. Substitutions on positions 1,5 and 7 were found to have moderate effects on antibacterial potency. At position 8, a carbon atom and associated substituents identify the quinolone derivatives, whereas the presence of a nitrogen atom identifies the naphthyridones.

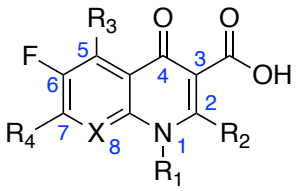

Figure 3.10. The structures of quinolone antibiotics.

As mentioned previously, the presence of a carboxyl group at position 3 is essential for the antibacterial effect of fluoroquinolone derivatives. Hence the generation of ester with this carboxyl group has been employed as the strategy to suppress the activities. In the field of photocage chemistry, photocages were appended to the carboxyl group to render it biologically inert. After irradiation, the ester bond was cleaved to release fluoroquinolone derivatives with a free carboxyl group which restored antibacterial effects. Feringa and coworkers illustrated the application of photocaged fluoroquinolone **3.43** in controlled bacterial patterning studies (Figure 3.11A).[247] **3.43** was incorporated into certain regions of agar-plates, which were then irradiated by UV light at 312 nm. The released fluoroquinolone inhibited the growth of *E*. coli that was applied on the same regions of agar-plates. The growth of *E*. coli that was outside of the regions with **3.43** was not affected. Moreover, the growth of *M*. *luteus* was not affected, regardless of what region they were applied, since fluoroquinolone **3.44** does not show antibacterial effects against *M*. *luteus*. In another example from Feringa, the photocaged fluoroquinolone **3.45** and photocaged benzylpenicillin **3.46** were demonstrated in the application of orthogonal control of bacterial growth by light (Figure 3.11B).[248] **3.45** released fluoroquinolone, which can inhibit the growth of *E*. *coli* upon irradiation of light at 380 nm. **3.46** released benzylpenicillin, which can inhibit the growth of *S. aureas* upon irradiation of light at 312 nm. When a mixture of **3.45** and **3.46** was added into a mixture solution of *E*. *coli* and *S. aureas. E*. *coli* can be selected out of the mixture by the means of releasing benzylpenicillin **3.47** with light at 312 nm to inhibit the growth of *S. aureas*, and vice versa.

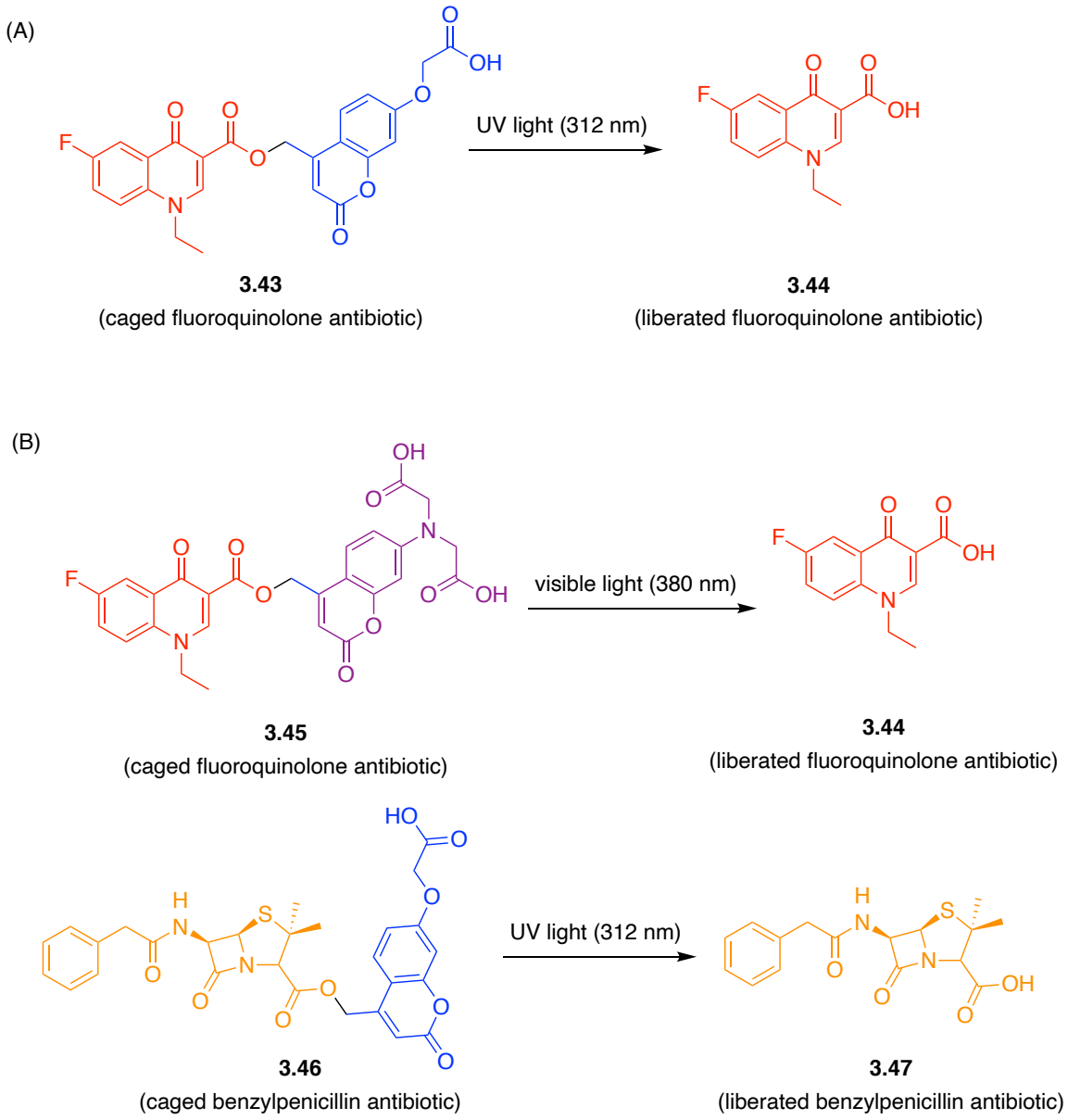

Figure 3.11. Select examples of photocaged antibiotics.

We anticipated that our modified photocage **3.39** would be able to effectively cage fluoroquinolone via esterification reactions to form **3.48**. Subsequently, fluoroquinolone **3.44** would be liberated from **3.48** with irradiation of visible light around 400 nm. The aliquot was taken from the solution and then incubated with *E. coli* solution Furthermore,

a bacterial growth inhibition assay can be conducted with **3.48** to illustrated the potency of modified photocage **3.39** in biological studies.

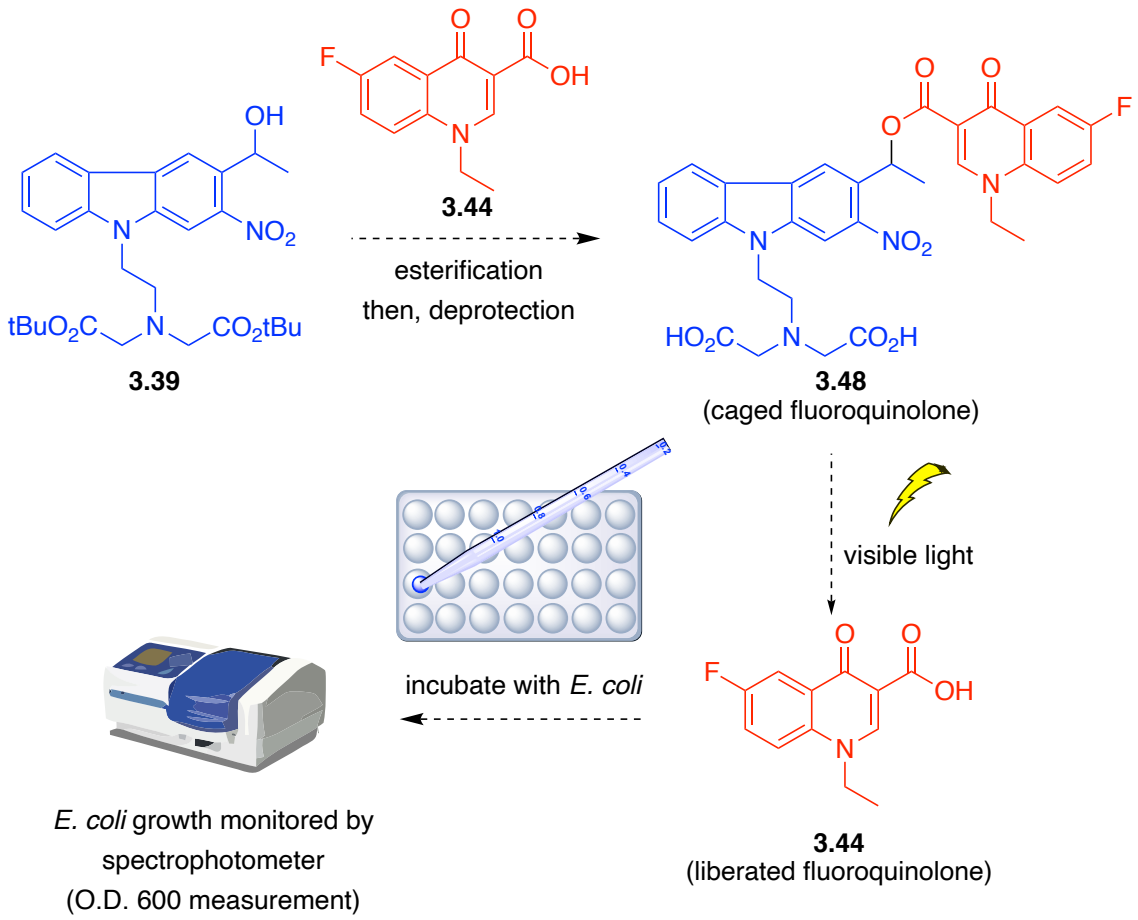

Figure 3.12. Proposed bacterial growth inhibition assay with photocaged fluoroquinolone.

3.5.2 Synthesis of the caged fluoroquinolone compound

We started our investigation by synthesizing a photocaged fluoroquinolone antibiotic. Fluoroquinolone **3.44** was first synthesized according to the literature procedure (Scheme 3.10).[247] Namely, the condensation of 4-fluoroaniline (**3.49**) with diethyl ethoxy methylene malonate (**3.50**) at 80 ºC afforded **3.51** in 99% yield. A solution of **3.51** in phenyl

ether was heated under reflux to generate **3.52** in 80% yield. Alkylation of **3.52** with ethyl bromide in the presence of K_2CO_3 in DMF at 80 ºC gave **3.53** in 67% yield. The final saponification of **3.53** with NaOH in ethanol at 70 ºC furnished fluoroquinolone **3.54** in 66% yield.

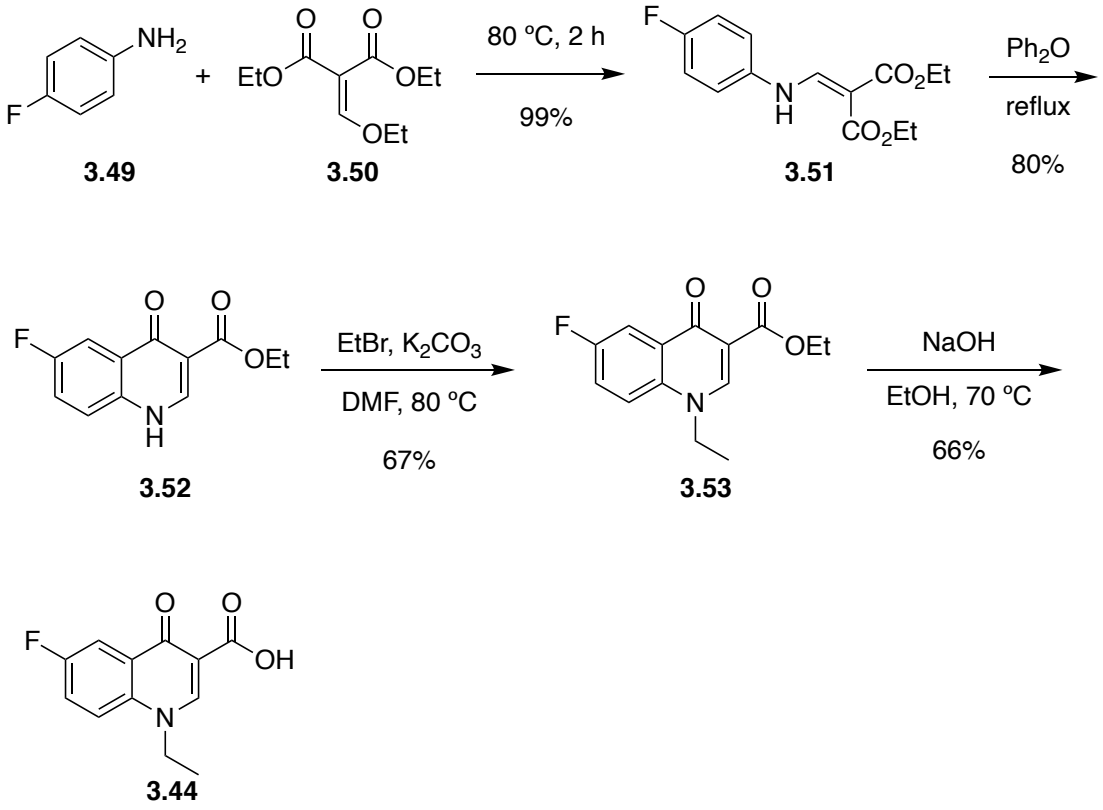

Scheme 3.10. Synthesis of fluoroquinolone **3.44**.

We next investigated the reaction of the modified photocage **3.39** with fluoroquinolone **3.44** to generate **3.48**. The ester formation, to our surprise, is not easy to promote, and we screened various reaction conditions (Scheme 3.11). We first examined the Steglich esterification reaction by treating **3.39** and **3.44** in the presence of 4-dimethylaminopyridine (DMAP) and N,N'-dicyclohexylcarbodiimide (DCC) in CH_2Cl_2 at

room temperature, but we only recovered **3.39** and **3.44**. Heating the solution of **3.39**, **3.44,** DMAP and DCC in CH_2Cl_2 under reflux to promote the formation of ester **3.48**, but again only returned staring material **3.39** was isolated. The same reaction in DMF at 80 ºC afforded a complex mixture. We next converted **3.44** to its acid chloride by reacting with $SOCl_2$, followed by the addition of photocage **3.39**. We were able to confirm the successful formation of acid chloride by LCMS, but the acid chloride did not react with **3.48** to give **3.48** in CH_2Cl_2 at room temperature or in DMF at 100 ºC. **3.39** was recovered under both reaction conditions. We also investigated the Yamaguchi esterification reaction by treating **3.44** with **3.54** to generate a mixed anhydride followed by the treatment with **3.39**; however, no product formation was observed, and **3.39** was recovered. Finally, we discovered heating the solution of **3.39** and **3.44** in the presence of 1-(3-dimethylaminopropyl)-3-ethylcarbodiimide hydrochloride (EDCI•HCl) and DMAP in DMF at 70 ºC for 24 h furnished desired ester **3.48** in 55% yield.

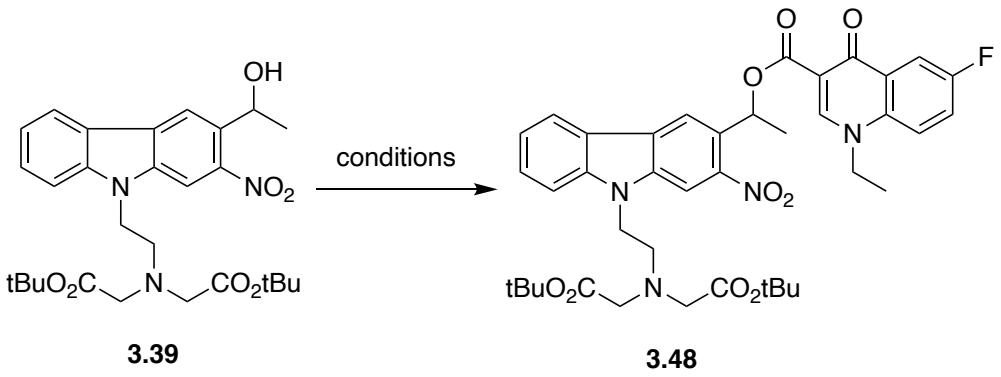

3.39 **3.48**

conditions	results
3.44, DMAP, DCC, CH_2Cl_2, rt	recovered **3.39**
3.44, DMAP, DCC, CH_2Cl_2, reflux	recovered **3.39**
3.44, DMAP, DCC, DMF, 80 ºC	complex mixture
3.44, $SOCl_2$, cat. DMF, reflux, then **3.34** Et_3N, DMAP, CH_2Cl_2, rt	recovered **3.39**
3.44, $SOCl_2$, cat. DMF, reflux, then **3.34** Et_3N, DMF, 100 ºC	recovered **3.39**
3.54, Et_3N, DMAP, THF, rt	recovered **3.39**
3.44, EDCI•HCl, DMAP, DMF, 70 ºC, 24 h	**3.48** in 55%

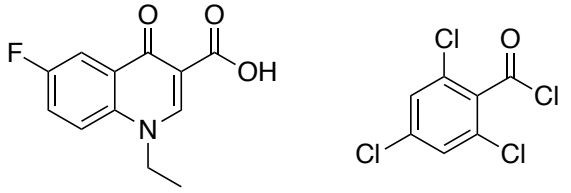

3.44 **3.54**

Scheme 3.11. Conditions screening of forming caged fluoroquinolone.

Deprotection of *t*-butyl ester groups of **3.48** in 4M HCl in dioxane for 8 h afforded **3.55** in 97% yield (Equation 3.14).

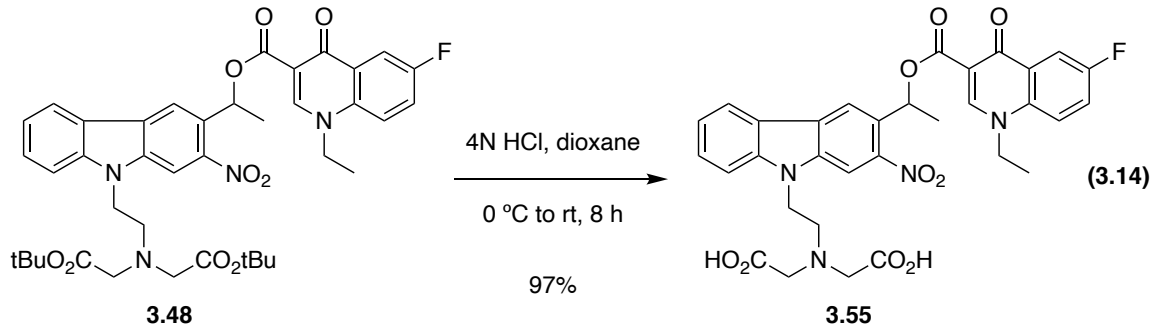

3.5.3 Decaging studies of the caged fluoroquinolone

With caged fluoroquinolone **3.55** in hand, we investigated its decaging at 400 nm. Decaging studies were conducted by irradiating 0.01 mM solutions of **3.55** in H_2O at 400 nm using a fluorimeter over 12 and 30 min, respectively (Figure 3.13). For 12 min irradiation experiment, aliquots were taken every 2 min, and for 30 min irradiation experiments, aliquots were taken every 5 min. Aliquots were analyzed using reverse phase HPLC with C18 column using gradient eluents from 0% to 100% MeCN in water over 30 min as the mobile phase. Decaging percentages were calculated based on the disappearance of **3.55** and appearance of **3.48**. We observed 58% of **3.55** was released after 30 min irradiation (Figure 3.13a). 22% decaging of **3.55** was observed after 12 min irradiation (Figure 3.13b).

(a)

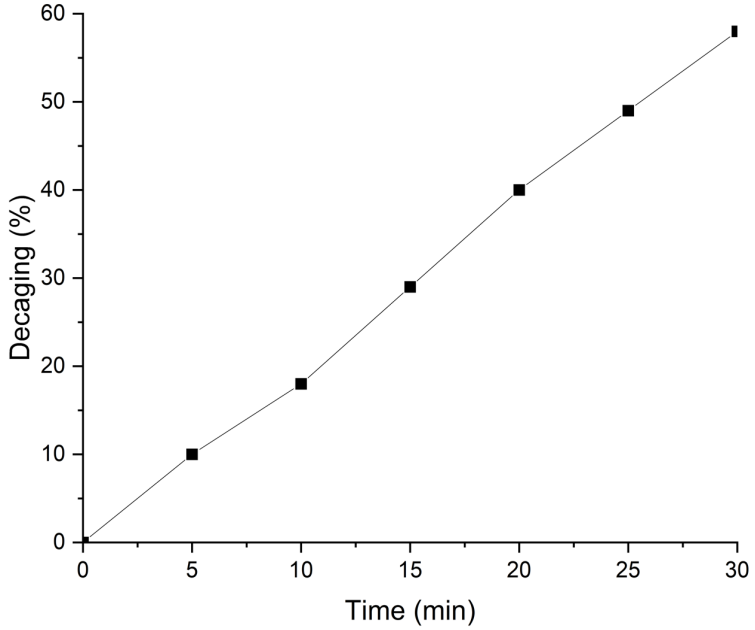
Decaging (%)
Time (min)
0
10
20
30
40
50
60
0
5
10
15
20
25
30

(b)

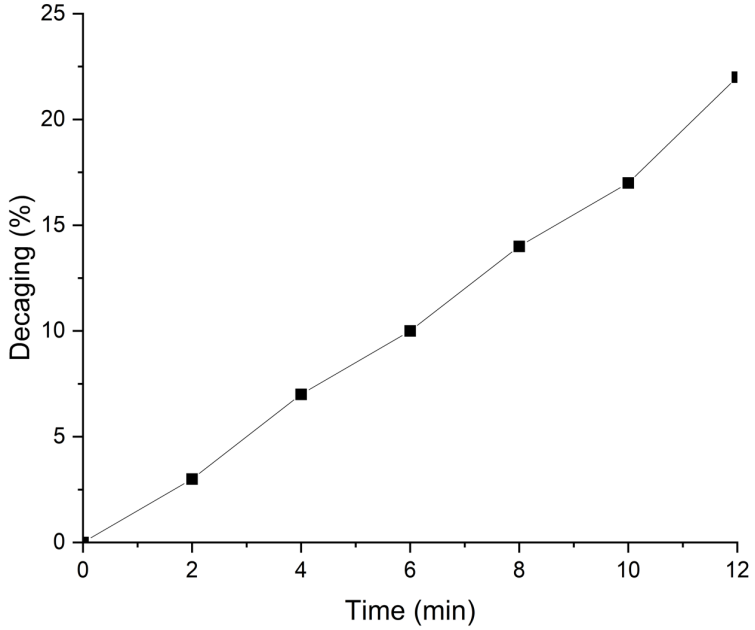
Decaging (%)
Time (min)
0
5
10
15
20
25
0
2
4
6
8
10
12

Figure 3.13. (a) Decaging of **3.55** (0.01 mM in H_2O) at 400 nm over 30 min. (b) Decaging of **3.55** (0.01 mM in H_2O) at 400 nm over 12 min.

3.5.4 Bacterial growth inhibition assay

With the demonstration of successful decaging of fluoroquinolone **3.48** from the **3.55**, we next conducted the bacterial growth inhibition assay. First, we investigated the concentration of fluoroquinolone **3.48** that effectively inhibits the growth of *E. coli.* Saturated *E. coli* solution was prepared by incubating the *E. coli* (BL21 (de3)) with Luria Broth Base medium (5 g/L yeast extract; 10 g/L casein peptone; 10 g/L NaCl) at 37 ºC overnight. The overnight cultures of *E. coli* were diluted with LB medium to an $O.D._{600}$ of 0.1, and 100 μL of this cell suspension was added to 100 μL medium containing antibiotics ranging from 1 μM to 4 μM. The control group was set by adding 100 μL of cell suspension with an $O.D._{600}$ of 0.1 to 100 μL medium without antibiotics. Cells were grown in a microtiter plate at 37 °C and cell density (O.D. at 600 nm) was measured every 10 min for 6 h, with a 15 sec shaking step before each measurement, in a microplate reader. Graphs were background-corrected by subtracting the $O.D._{600}$ at time. The $O.D._{600}$ changes were plotted in Figure 3.14. Bacterial growths were partially inhibited at concentrations ranging from 1 μM to 3 μM compared with control group, and complete inhibition occurred at 4 μM (Figure 3.14).

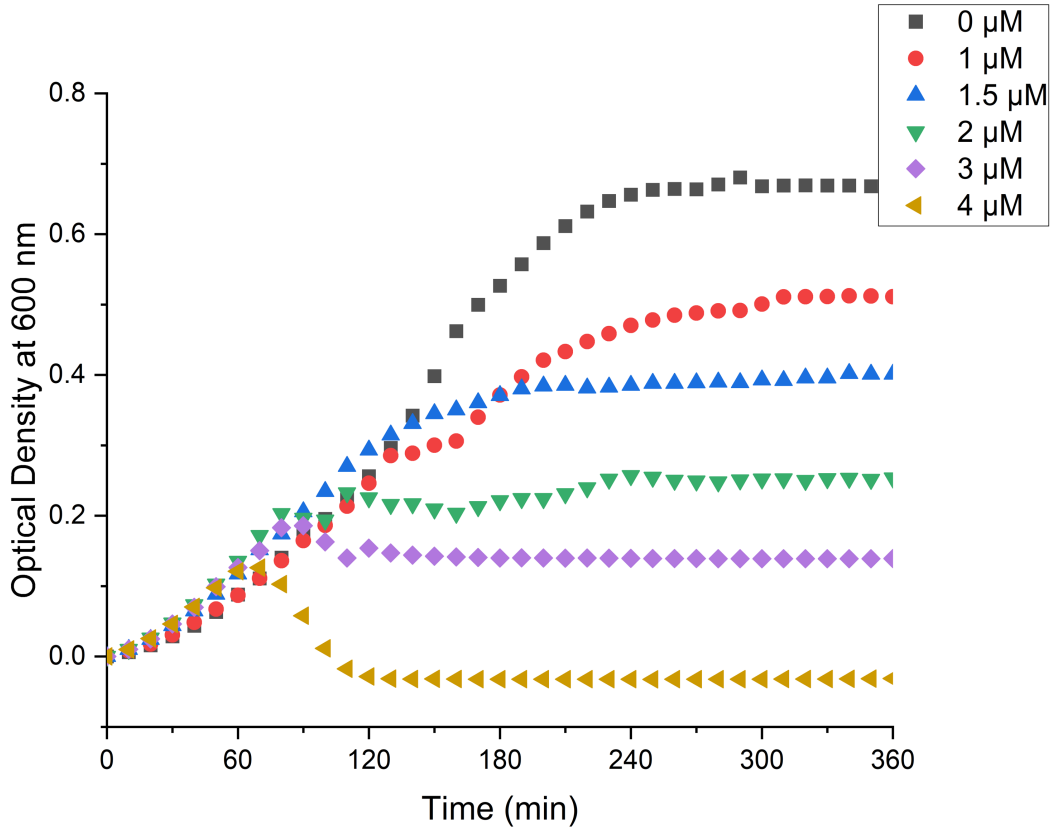

Figure 3.14. Time curves for growth of *E. coli* at different concentrations (0, 1, 1.5, 2, 3, and 4 μM) of **3.55**.

We investigated the inhibitory effects of the solution of **3.55** after irradiation with light at 400 nm. An aqueous solution of **3.55** (0.01 mM) was irradiated at 400 nm, and 100 μL of aliquots were taken after 1, 2, 5 and 10 min. 100 μL of the cell suspension with an $O.D._{600}$ of 0.1 in Luria Broth Base medium was added to each of the aliquots taken after 1, 2, 5 and 10 min irradiation. The control group was set by adding 100 μL of cell suspension with an $O.D._{600}$ of 0.1 to 100 μL solution of **3.55** (0.01 mM) without irradiation of light. Cells were grown in a microtiter plate at 37 °C, and cell density (O.D. at 600 nm) was measured every 10 min for 6 h, with a 15 sec shaking step before each measurement, in a microplate reader. Graphs were background-corrected by subtracting the $O.D._{600}$ at time.

The O.D.$_{600}$ changes were plotted in Figure 3.15. First, no inhibitory effect was observed in the control group, where the solution of **3.55** was not irradiated (Figure 3.14 curve 0 min). The result from the control group indicates after forming the ester **3.55**, the antibacterial effects of quinolone derivative **3.48** was completely suppressed. Partial inhibitory effects were observed for groups with aliquots that were irradiated for 1,2, and 5 mins at 400 nm (Figure 3.15 curve 1, 2, 5 min). Moreover, complete inhibition was observed for the group with aliquots that were irradiated for 10 min (Figure 3.15 curve 10 min).

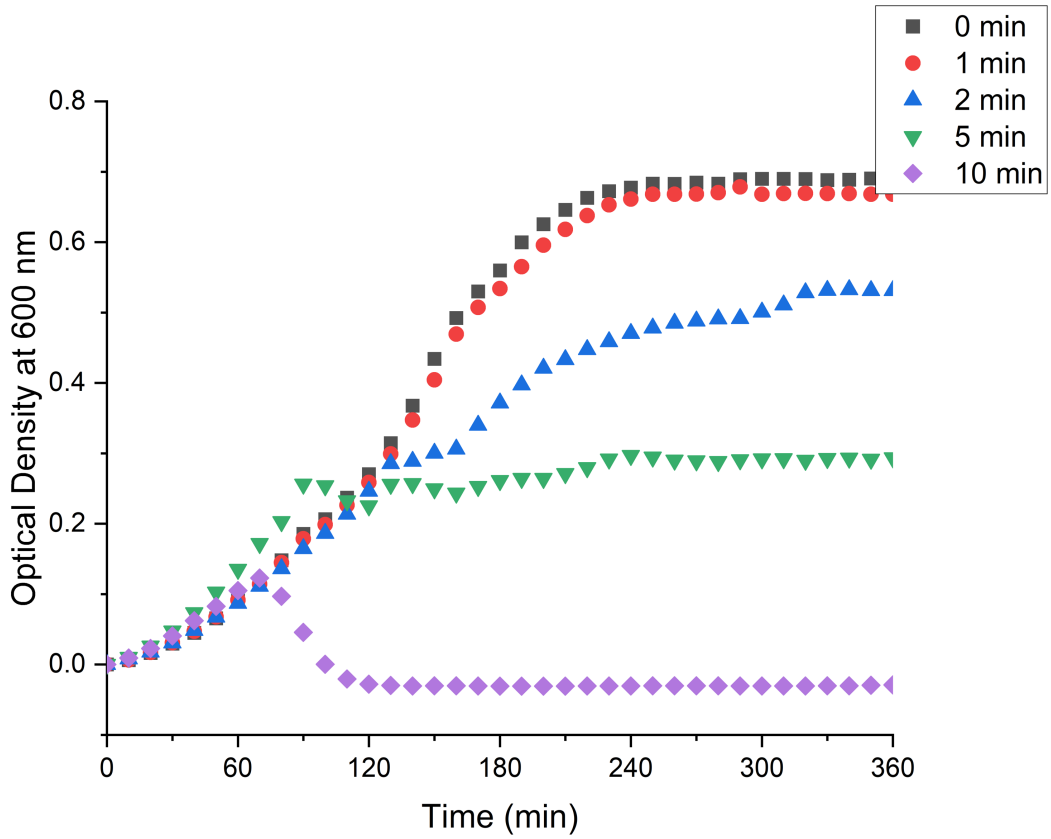

Figure 3.15. Time curves for growth of *E. coli* when incubated with a solution (0.01 mM in H_2O) of **3.55** that had been irradiated for 1, 2, 5, and 10 min.

3.5.5 Summary of caged fluoroquinolone studies

In summary, we synthesized caged fluoroquinolone **3.55** from modified photocage **3.39** in two steps. The decaging studies of **3.55** in H_2O were conducted to demonstrate the efficient release of fluoroquinolone **3.48** at 400 nm. The biological application of **3.55** was also demonstrated by the bacterial growth inhibition assay. Antibacterial effects of **3.48** were suppressed after forming caged fluoroquinolone **3.55**. Fluoroquinolone **3.48** was then released from **3.55** after irradiation with light at 400 nm, and antibacterial effects were restored as demonstrated by the inhibitory effects on the bacterial growth.

3.6 SUMMARY

We have successfully developed two new carbazole photocages **3.5** and **3.6** to tackle the challenges existing in the field of photocage chemistry. Namely, the challenges are decaging of substrates in visible light region, efficiently release poor leaving groups, and possess adequate aqueous solubility. We were able to demonstrate the superior decaging properties of **3.5** and **3.6** compared with reported NDBF photocage as was illustrated by the benzoic acid model system study. Caged benzoic acid **3.29** underwent decaging to release benzoic acid at 400 nm with great efficiency. Whereas **3.30** released benzoic efficiently at 390 nm. NDBF caged benzoic acid **3.32** only had moderate decaging percentage at both 400 and 390 nm over 60 min. Photophysical properties including extinction coefficients, ε, quantum yields of decaging, Φ, and decaging efficiencies, $\varepsilon \bullet \Phi$. of **3.29** and **3.30** both showed improvement compared with NDBF derivative **3.32**. To demonstrate the ability to release bad leaving groups, modified photocage **3.39** was caged with phenol derivatives. A caged tyrosine derivative **3.42** was synthesized and the decaging properties were evaluated at wavelength from 360 nm to 400 nm. Efficient decaging was achieved at 360 nm over 60 min, and moderate decaging was observed from 370 nm to 400

nm over 60 min. Although no kinetic studies of releasing tyrosine have been reported, most applications with caged tyrosine were performed in UV light region. The decaging profile of **3.42** from 360 to 400 nm provides the foundation for future biological applications with caged tyrosine compounds. Lastly, a caged fluoroquinolone was evaluated to demonstrate the potency of modified photocage **3.39** in biological applications. Caged fluoroquinolone **3.55** was successfully synthesized, and decaging properties were evaluated with irradiation at 400 nm. The antibacterial effects of caged fluoroquinolone **3.44** were evaluated before and after irradiation with *E. coli* solution. No inhibitory effects were against bacterial growth observed before irradiation, and partial to complete inhibitory effects were observed after irradiation for 1 min to 10 min.

Chapter 4 Experimental Procedures

4.1 General Experimental Methods

Solvents were purified unless otherwise noted before use as follows. Tetrahydrofuran (THF) was dried by filtration through two columns of activated neutral alumina prior to use. Acetonitrile (MeCN) was dried by filtration through two columns of activated molecular sieves. Toluene was filtered through one column of activated neutral alumina and Q5 reactant. Methylene chloride (CH_2Cl_2), pyridine (pyr.), and triethylamine (Et_3N) were freshly distilled over CaH_2. Trimethylsilyl iodide (TMS-I) was freshly distilled prior to use. All other reagents and solvents were reagent grade and were purchased and used as received unless otherwise noted. Reactions were performed under a nitrogen or argon atmosphere in round-bottom flasks sealed under rubber septa with magnetic stirring, unless otherwise noted. Water sensitive reactions were performed with flame-dried glassware, stir-bars, and steel needle. Reaction temperatures are reported as the temperatures of the bath surrounding the vessel. Sensitive reagents and solvents were transferred using plastic syringes and steel needles using standard techniques.

Proton nuclear magnetic resonance (^{1}H NMR) and carbon nuclear magnetic resonance (^{13}C NMR) spectra were acquired in $CDCl_3$ unless otherwise noted. Chemical shifts are reported in parts per million (ppm, δ), downfield from tetramethylsilane (TMS, δ=0.00ppm) and are referenced to residual solvent ($CDCl_3$, δ = 7.26 ppm (^{1}H) and 77.16 ppm (^{13}C)). Coupling constants (*J*) are reported in hertz (Hz) and the resonance multiplicity abbreviations used are: s, singlet; d, doublet; t, triplet; q, quartet; p, pentet; dt, doublet of triplets; dd, doublet of doublets; ddd, doublet of doublet of doublets; dddd, doublet of doublet of doublet of doublets; m, multiplet; comp, overlapping multiplets of magnetically non-equivalent protons. The abbreviation br stands for broad. Infrared (IR) spectra were

obtained with a thermo scientific Nicolet 380 spectrometer. Thin-layer chromatography (TLC) was performed on EMD 60 F254 glass-backed pre-coated silica gel plates and were visualized using one or more of the following methods: UV light (254 nm) and staining with basic potassium permanganate ($KMnO_4$) acidic *p*-anisaldehyde (PAA) or CAM. Flash chromatography was performed using glass columns and with Silicycle® SiliaFlash F60® (40-63 μm) silica gel eluting with the solvents indicated according to the procedure of Still.[249]

Methyl (*E*)-3-methoxybut-2-enoate is commercially available from Synthonix or can be prepared according to literature procedure.[250] *p*-Toluenesulfonyl azide was prepared according to the literature procedure and the ^1H and ^{13}C spectra were consistent with those previously reported.[251]

4.2 EXPERIMENTAL PROCEDURES FOR CHAPTER 1

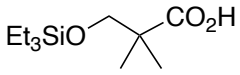

1.30

2,2-Dimethyl-3-((triethylsilyl)oxy)propanoic acid (1.30). zw-4-meli1. Et_3SiCl (6.700 g, 44.45 mmol) was added to a solution of hydroxy pivalic acid (**1.22**) (5.000 g, 42.33 mmol) in pyridine (100 mL) at 60 ºC. The solution was stirred at 60 ºC for 8 h. After cooling to room temperature, the solvent was removed under reduced pressure. The residue was dissolved in CH_2Cl_2 (100 mL), washed with 1 N HCl solution (3 x 50 mL), H_2O (3 x 50 mL), and brine (50 mL). The organic fraction was dried (Na_2SO_4), filtered, and concentrated under reduced pressure to give crude **1.30** as colorless oil. The crude material was purified via flash column chromatography eluting hexanes : EtOAc (10:1) to give 8.657 g (88%) of **1.30** as colorless oil. ^1H NMR (500 MHz, $CDCl_3$) δ 3.60 (s, 2 H), 1.19

(s, 6 H), 0.96 (t, J = 8.0 Hz, 9 H), 0.62 (q, J = 8.0 Hz, 6 H); ^{13}C NMR (126 MHz, $CDCl_3$) δ 188.6, 174.7, 138.7, 125.5, 97.9, 55.5, 20.0; IR (neat) ν_{max} 2957, 1703, 1101, 904, 818, 725 cm^{-1}; HRMS (ESI) *m*/*z* calcd for $C_{11}H_{24}O_3SiNa^+$ $(M+Na)^+$, 255.1387; found 255.1390.

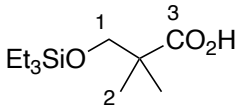

1.30

NMR Assignment. ^{1}H NMR (500 MHz, $CDCl_3$) δ 3.60 (s, 2 H, C1-H), 1.19 (s, 6 H, C2-H), 0.96 (t, J = 8.0 Hz, 9 H, Et_3Si), 0.62 (q, J = 8.0 Hz, 6 H, Et_3Si).

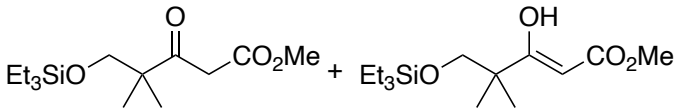

1.31 **1.31'**

Methyl 4,4-dimethyl-3-oxo-5-((triethylsilyl)oxy)pentanoate (**1.31**). **zw-4-meli2**. Carbonyl diimidazole (CDI) (2.698 g, 16.64 mmol) was added to the solution of **1.30** (3.516 g, 15.13 mmol) in THF (50 mL). The solution was stirred at room temperature for 1 h. In a separate flask, *i*-PrMgBr (16.64 mL, 49.93 mmol) was added dropwise to a solution of monomethyl malonate (2.680 g, 22.70 mmol) in THF (50 mL) at 0 ºC. The solution was stirred at 0 ºC for 30 min, room temperature for 30 min and 45 ºC for 1 h. The solution of monomethyl malonate dianion was added dropwise to the solution of acyl imidazolide at 0 ºC, and the resulting mixture was stirred overnight at room temperature. Aqueous 10% citric acid (30 mL) was added, and the aqueous layer was separated and extracted with CH_2Cl_2 (3 x 30 mL). The combined organic fractions were washed with H_2O (3 x 30 mL) and brine (30 mL), dried (Na_2SO_4), and concentrated under reduced pressure to give crude **1.31** as colorless oil. The crude material was purified via flash

column chromatography eluting hexanes : CH_2Cl_2 (5:1) to give 2.706 g (62%) mixture of **1.31** as a mixture (3.5:1) of keto-enol tautomers as colorless oil. ^{1}H NMR (500 MHz, $CDCl_3$) δ 12.24 (s, 0.22 H), 5.09 (s, 0.22 H), 3.73 (s, 0.66 H), 3.72 (s, 2.34 H), 3.62 (s, 1.56 H), 3.57 (s, 1.56 H), 3.54 (s, 0.44 H), 1.13 (s, 4.7 H), 1.10 (s, 1.3 H), 0.96-0.91 (comp, 9), 0.61-0.53 (comp, 6 H); ^{13}C NMR (126 MHz, $CDCl_3$) δ 207.7, 183.6, 173.6, 168.5, 87.7, 70.0, 69.3, 52.3, 51.3, 50.1, 45.9, 42.5, 22.3, 21.4, 6.87, 6.85, 4.5, 4.4; IR (neat) ν_{max} 2955, 1746, 1709, 1437, 1321, 1239, 1146, 1098, 1005, 906, 804, 727 cm^{-1}; HRMS (ESI) *m/z* calcd for $C_{14}H_{28}O_4SiNa^+$ $(M+Na)^+$, 311.1649; found 311.1659.

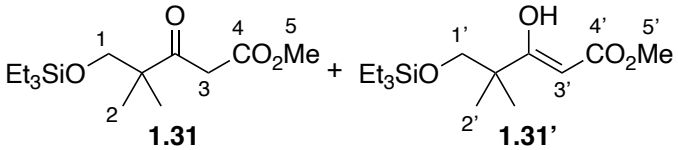

NMR Assignment. ^{1}H NMR (500 MHz, $CDCl_3$) δ 12.24 (s, 0.22 H, -OH), 5.09 (s, 0.22 H, C3'-H), 3.73 (s, 0.66 H, C5'-H), 3.72 (s, 2.34 H, C5-H), 3.62 (s, 1.56 H, C1-H or C3-H), 3.57 (s, 1.56 H, C1-H or C3-H), 3.54 (s, 0.44 H, C1'-H), 1.13 (s, 4.7 H, C2-H), 1.10 (s, 1.3 H, C2'-H), 0.96-0.91 (comp, 9 H, Et_3Si), 0.61-0.53 (comp, 6 H, Et_3Si).

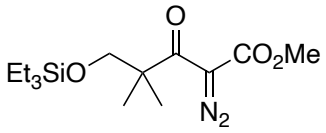

1.32

Methyl 2-diazo-4,4-dimethyl-3-oxo-5-((triethylsilyl)oxy)pentanoate (1.32). zw-4-meli3. Et_3N (1.546 g, 15.28 mmol) was added dropwise to the solution of **1.31** (2.204 g, 7.64 mmol) and TsN_3 (2.260 g, 11.46 mmol) in MeCN (35 mL) at 0 ºC. The solution was stirred at room temperature for 12 h, whereupon 10% aq. NaOH (30 mL) was added. The resulting mixture was extracted with Et_2O (3 x 30 mL), and the combined organic extracts

were washed with H_2O (3 x 30 mL) and brine (30 mL). The organic fraction was dried ($MgSO_4$), filtered and concentrated under reduced pressure to give crude **1.32** as yellow oil. The crude material was purified via flash column chromatography eluting hexanes : CH_2Cl_2 (10:1 to 5:1) to give 2.162 g (90%) of **1.32** as yellow oil. ^{1}H NMR (500 MHz, $CDCl_3$) δ 3.81 (s, 2 H), 3.80 (s, 3 H), 1.26 (s, 6 H), 0.91 (t, J = 8.0 Hz, 9 H), 0.55 (q, J = 8.0 Hz, 6 H); ^{13}C NMR (126 MHz, $CDCl_3$) δ 195.6, 161.8, 68.3, 52.3, 50.4, 21.4, 6.8, 4.4; IR (neat) ν_{max} 2955, 2877, 1704, 1365, 1230, 1098, 1004, 816, 726, 672 cm^{-1}; HRMS (ESI) m/z calcd for $C_{14}H_{26}N_2O_4SiNa^+$ $(M+Na)^+$, 337.1554; found 337.1565.

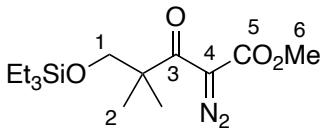

1.32

NMR Assignment. ^{1}H NMR (500 MHz, $CDCl_3$) δ 3.81 (s, 2 H, C1-H), 3.80 (s, 3 H, C6-H), 1.26 (s, 6 H, C2-H), 0.91 (t, J = 8.0 Hz, 9 H, Et_3Si), 0.55 (q, J = 8.0 Hz, 6 H, Et_3Si).

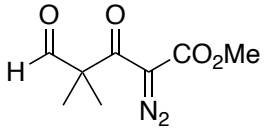

1.20

Methyl 2-diazo-4,4-dimethyl-3,5-dioxopentanoate (1.20). zw-4-meli4. IBX (7.479 g, 26.71 mmol) was added to a solution of **1.32** (2.100 g, 6.678 mmol) in DMSO (40 mL) and H_2O (601.7 mg, 33.39 mmol) at room temperature, and the solution was stirred overnight at room temperature. The reaction mixture was partitioned between Et_2O (30 mL) and H_2O (30 mL), and the organic layer was separated and washed with H_2O (3 x 20 mL) and brine (20 mL), dried ($MgSO_4$), filtered and concentrated under reduced pressure

to give crude **1.20** as yellow oil. The crude material was purified via flash column chromatography eluting hexanes : EtOAc (7:1) to give 1.178 g (89%) of **1.20** as yellow oil. ^{1}H NMR (500 MHz, $CDCl_3$) δ 9.59 (s, 1 H), 3.79 (s, 3 H), 1.39 (s, 6 H); ^{13}C NMR (126 MHz, $CDCl_3$) δ 200.4, 191.2, 161.7, 57.7, 52.5, 20.7; IR (neat) ν_{max} 2149, 1716, 1650, 1439, 1320, 1130, 1011, 905, 727 cm^{-1}; HRMS (ESI) *m/z* calcd for $C_8H_{10}N_2O_4Na^+$ $(M+Na)^+$, 221.0533; found 221.0537.

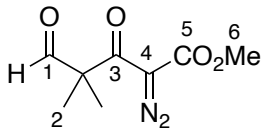

1.20

NMR Assignment. ^{1}H NMR (500 MHz, $CDCl_3$) δ 9.59 (s, 1 H, CHO), 3.79 (s, 3 H, C6-H), 1.39 (s, 6 H, C2-H).

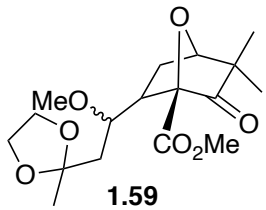

1.59

Methyl-6-(1-methoxy-2-(2-methyl-1,3-dioxolan-2-yl)ethyl)-3,3-dimethyl-2-oxo-7-oxabicyclo[2.2.1]heptane-1-carboxylate (1.59). az-3-206-1. A solution of **1.20** (20 mg, 0,10 mmol), **1.58** (21 mg, 0.12 mmol) and $Rh_2(OPiv)_4$ (1.2 mg, 0.0020 mmol) in toluene (1.5 mL) was stirred under reflux under N_2 for 1 h. The solution was cooled to rt, diluted with CH_2Cl_2 (1 mL), washed with H_2O (3 X 1mL) and brine (1 mL), dried (Na_2SO_4), filtered and concentrated in *vacuo* to give crude **1.20** as white solid. The crude material was purified via flush column chromatography eluting hexanes : EtOAc (8:1) to give 20 mg (58%) **1.59** as white solid. ^{1}H NMR (500 MHz, $CDCl_3$-d) δ 4.23 (d, 1 H, *J* = 5.4 Hz), 3.90-3.84 (m, 4 H), 3.76-3.73 (m, 4 H), 3.00 (s, 3 H), 2.71 (dd, 1 H, *J* = 11.0, 5.4

Hz), 2.05-1.95 (comp, 2 H), 1.90 (dd, 1 H, J = 14.5, 2.8 Hz), 1.68 (dd, 1 H, 14.5, 9.5 Hz), 1.26 (s, 3 H), 1.20 (s, 3 H), 1.07 (s, 3 H). ^{13}C NMR (500 MHz, $CDCl_3$-*d*) δ 208.5, 167.4, 108.5, 88.6, 84.0, 73.0, 64.8, 64.3, 55.5, 52.5, 49.8, 49.6, 42.1, 24.7, 24.4, 18.0.

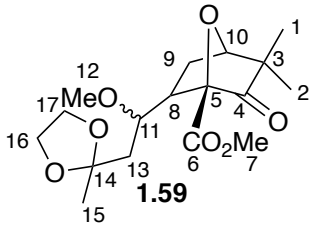

NMR Assignment. ^{1}H NMR (500 MHz, $CDCl_3$-d) δ 4.23 (d, 1 H, J = 5.4 Hz, C10-H), 3.90-3.84 (m, 4 H, C16-H), 3.76-3.73 (m, 4 H, C7-H and C11-H), 3.00 (s, 3 H, C12-H), 2.71 (dd, 1 H, J = 11.0, 5.4 Hz, C8-H), 2.05-1.95 (comp, 2 H, C9-H), 1.90 (dd, 1 H, J = 14.5, 2.8 Hz, C13-H), 1.68 (dd, 1 H, 14.5, 9.5 Hz, C13-H), 1.26 (s, 3 H, C15-H), 1.20 (s, 3 H, C1-H or C2-H), 1.07 (s, 3 H, C1-H or C2-H). ^{13}C NMR (500 MHz, $CDCl_3$-*d*) δ 208.5 (C4), 167.4 (C6), 108.5 (C14), 88.6 (C5), 84.0 (C10), 73.0 (C11), 64.8 (C16 or C17), 64.3 (C16 or C17), 55.5 (C12), 52.5 (C7), 49.8 (C3), 49.6 (C8), 42.1 (C13), 24.7 (C15), 24.4 (C1 or C2 and C9), 18.0 (C1 or C2).

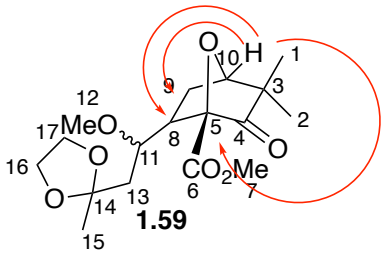

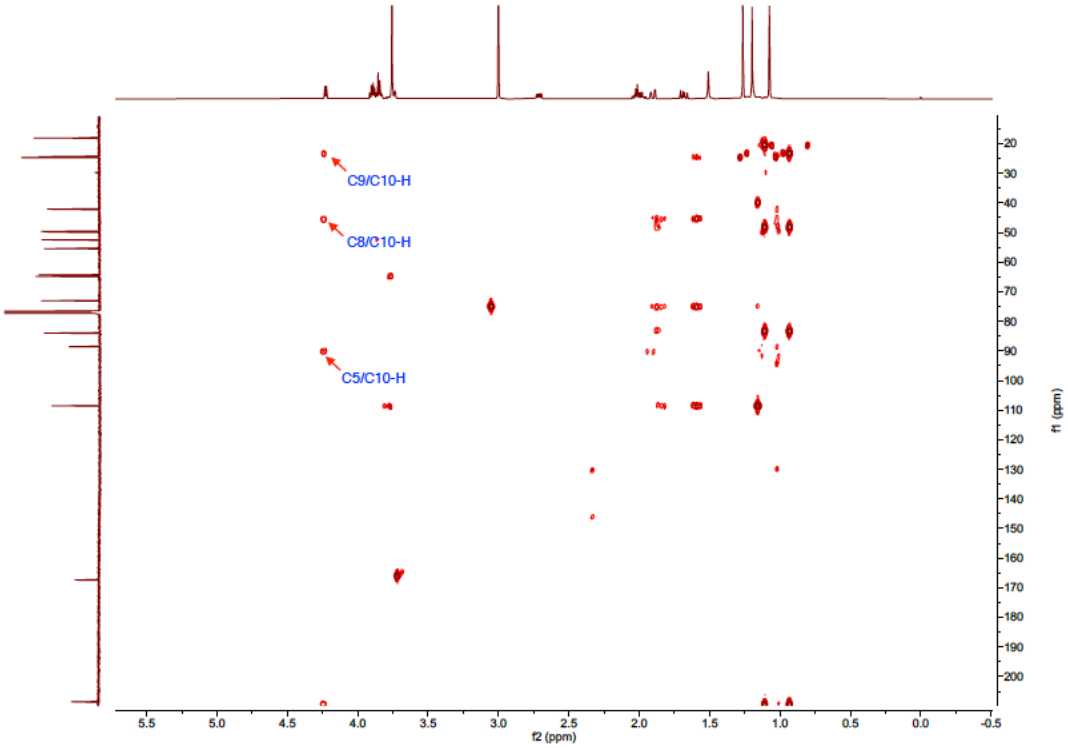

Figure 4.1. Key HMBC correlations of **1.59**.

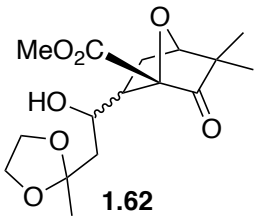

1.62

Methyl-6-(1-hydroxy-2-(2-methyl-1,3-dioxolan-2-yl)ethyl)-3,3-dimethyl-2-oxo-7-oxabicyclo[2.2.1]heptane-1-carboxylate (1.62). az-3-225-3. A solution of **1.20** (24 mg, 0.12 mmol), **1.57** (23 mg, 0.14 mmol) and Rh_2OAc_4 (1.1 mg, 0.0024 mmol) in CH_2Cl_2 (1 mL) was stirred under reflux for 3 h. The solution was cooled to rt, washed with H_2O (3 X 1 mL) and brine, dried (Na_2SO_4), filtered and concentrated in *vacuo* to give crude **1.62** as colorless oil. The crude material was purified via flush column chromatography eluting

hexanes : EtOAc (7:1) to give 18 mg (45%) **1.62** as colorless oil. ^{1}H NMR (500 MHz, $CDCl_3$-d) δ 4.56 (s, 1 H), 3.94 (s, 4 H), 3.88 (dt, 1 H), 3.78 (s, 3 H), 3.69 (t, 1 H), 1.96 (dd, 1 H), 1.80 (d, 1 H), 1.60 (m, 2 H), 1.28 (s, 3 H), 1.23 (s, 3 H), 1.04 (s, 3 H). ^{13}C NMR (500 MHz, $CDCl_3$-*d*) δ 210.9, 166.5, 110.2, 88.5, 85.5, 69.0, 64.7, 64.7, 64.4, 52.8, 48.6, 42.3, 32.3, 23.3, 19.6.

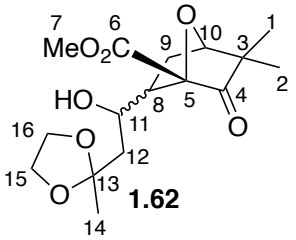

1.62

NMR Assignment. ^{1}H NMR (500 MHz, $CDCl_3$-d) δ 4.56 (s, 1 H, C10-H), 3.94 (s, 4 H, C15-H), 3.88 (dt, 1 H, C11-H), 3.78 (s, 3 H, C7-H), 3.69 (t, 1 H, C8-H), 1.96 (dd, 1 H, C9-H), 1.80 (d, 1 H, C12-H), 1.60 (m, 2 H, C9-H and C12-H), 1.28 (s, 3 H, C14-H), 1.23 (s, 3 H, C1-H or C2-H), 1.04 (s, 3 H, C1-H or C2-h). ^{13}C NMR (500 MHz, $CDCl_3$-*d*) δ 210.9 (C4), 166.5 (C6), 110.2 (C13), 88.5 (C5), 85.5 (C10), 69.0 (C8), 64.7 (C15 or C16), 64.7 (C15 or C16), 64.4 (C11), 52.8(C7), 48.6 (C3), 42.3 (C12), 32.3 (C9), 23.3 (C1 or C2), 19.6 (C1 or C2).

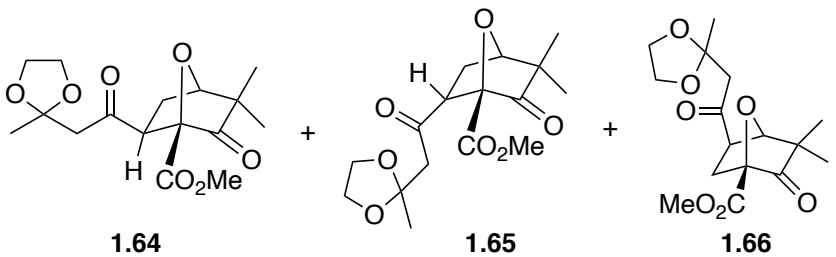

1.64 **1.65** **1.66**

Preparation of 1.64, 1.65, and 1.66. A solution of **1.20** (50 mg, 0.26 mmol), **1.63** (50 mg, 0.32 mmol) and Rh_2OAc_4 (2.2 mg, 0.0052 mmol) in CH_2Cl_2 (2 mL) was stirred under reflux under N_2 for overnight. The solution was cooled to rt, washed with H_2O (3 X

1 mL) and brine (1 mL), dried (Na_2SO_4), filtered and concentrated in *vacuo* to give crude mixture of **1.64**, **1.65** and **1.66** as colorless oil. The crude material was purified via flush column chromatography eluting hexanes : EtOAc (5:1) to give 30 mg (35%) **1.64**, 3.4 mg (4%) **1.65** and 3.0 mg (3%) **1.66** as white solid respectively.

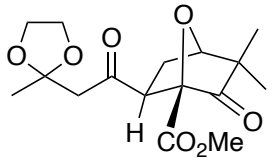

1.64

Methyl (1S,4R,6S)-3,3-dimethyl-6-(2-(2-methyl-1,3-dioxolan-2-yl)acetyl)-2-oxo-7-oxabicyclo[2.2.1]heptane-1-carboxylate (1.64). az-3-245-3. ^{1}H NMR (500 MHz, $CDCl_3$-d) δ 4.41 (d, 1 H, *J* = 5.4 Hz), 3.91-3.88 (m, 4 H), 3.76 (s, 3 H), 3.36 (dd, 1 H, *J* = 9.4, 6.4 Hz), 2.74 (s, 2 H), 2.32 (dd, 1 H, *J* = 12.7, 9.4 Hz), 1.94 (td, 1 H, *J* = 12.2, 5.9 Hz), 1.31 (s, 3 H), 1.22 (s, 3 H), 1.05 (s, 3 H). ^{13}C NMR (500 MHz, $CDCl_3$-*d*) δ 209.0, 203.2, 165.4, 107.9, 90.1, 83.6, 64.8, 64.7, 52.7, 51.4, 51.2, 48.9, 30.3, 24.6, 23.0, 20.0.

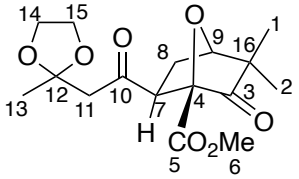

1.64

NMR Assignment. ^{1}H NMR (500 MHz, $CDCl_3$-d) δ 4.41 (d, 1 H, *J* = 5.4 Hz, C9-H), 3.91-3.88 (m, 4 H, C14-H), 3.76 (s, 3 H, C6-H), 3.36 (dd, 1 H, *J* = 9.4, 6.4 Hz, C7-H), 2.74 (s, 2 H, C11-H), 2.32 (dd, 1 H, *J* = 12.7, 9.4 Hz, C8-H), 1.94 (td, 1 H, *J* = 12.2, 5.9 Hz, C8-H), 1.31 (s, 3 H, C13-H), 1.22 (s, 3 H, C1-H or C2-H), 1.05 (s, 3 H, C1-H or C2-H). ^{13}C NMR (500 MHz, $CDCl_3$-*d*) δ 209.0 (C3), 203.2 (C10), 165.4 (C5), 107.9 (C12),

90.1 (C4), 83.6 (C9), 64.8 (C14), 64.7 (C15), 52.7 (C6), 51.4 (C7), 51.2 (C11), 48.9 (C16), 30.3 (C8), 24.6 (C13), 23.0 (C1 or C2), 20.0 (C1 or C2).

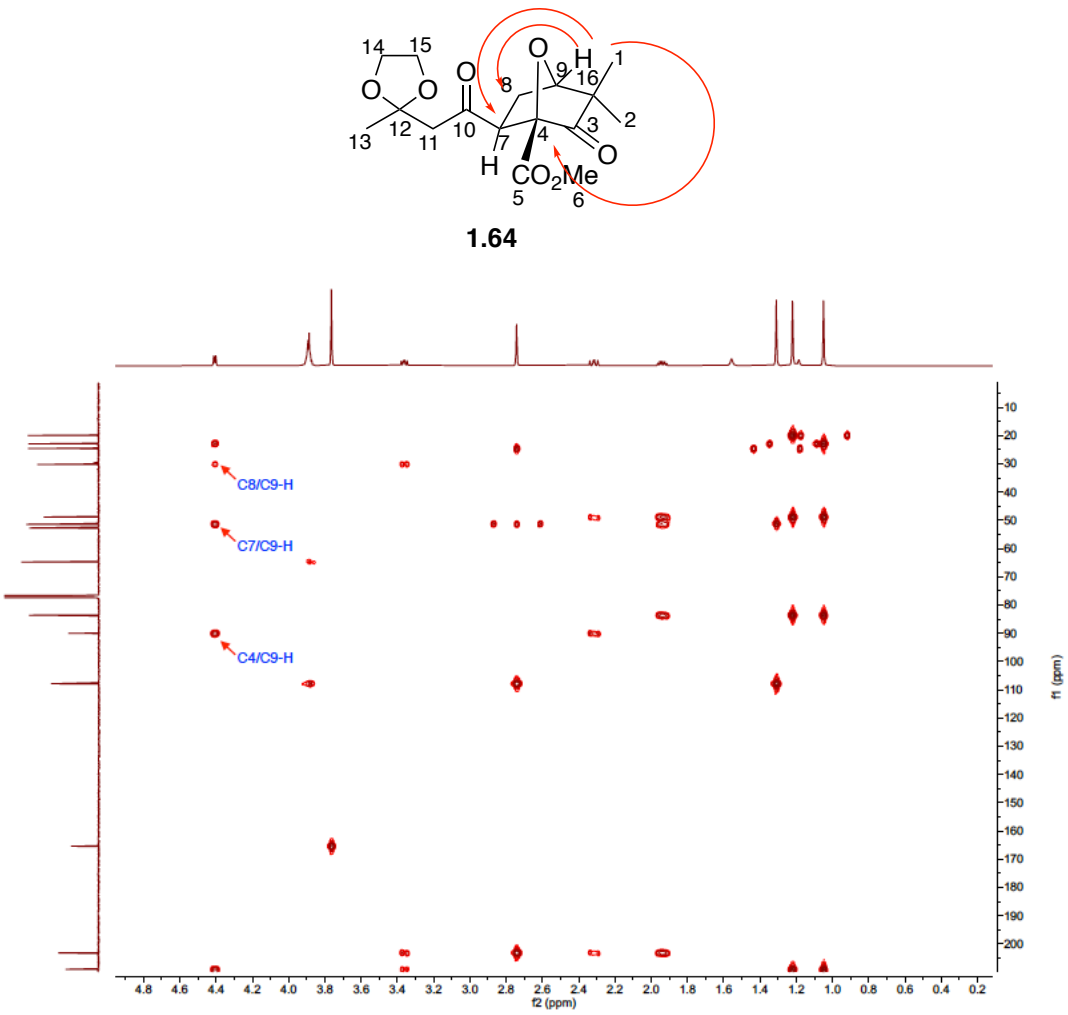

1.64

Figure 4.2. Key HMBC correlations of **1.64**.

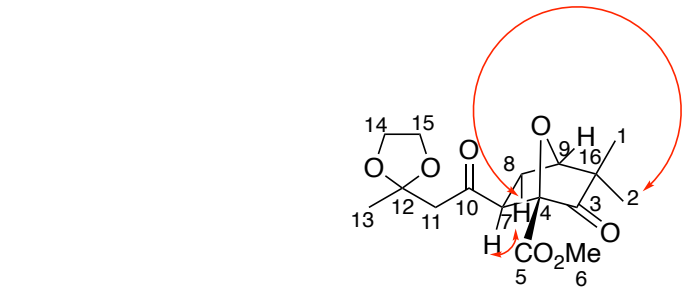

1.64

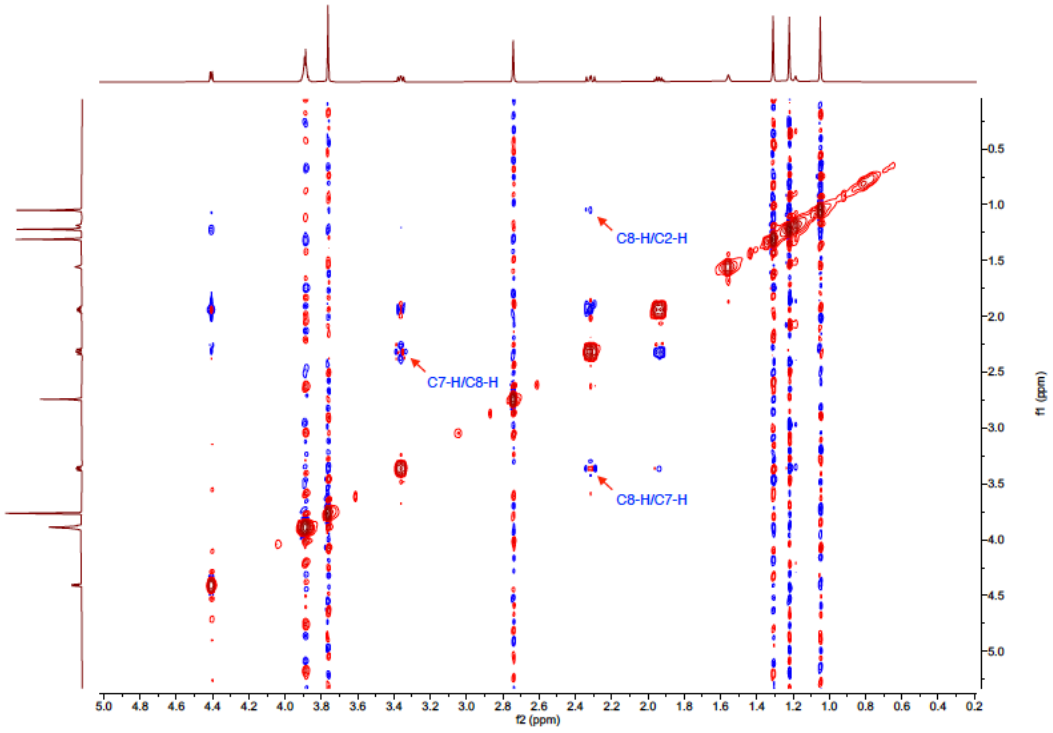

Figure 4.3. Key NOESY correlations of **1.64**.

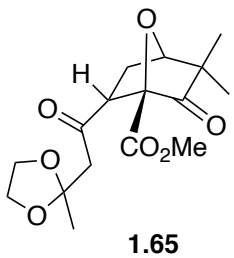

1.65

Methyl (1S,4R,6R)-3,3-dimethyl-6-(2-(2-methyl-1,3-dioxolan-2-yl)acetyl)-2-oxo-7-oxabicyclo[2.2.1]heptane-1-carboxylate (1.65). az-3-245-2-1. ^{1}H NMR (500 MHz, $CDCl_3$-d) δ 4.33 (d, 1 H, *J* = 4.9 Hz), 3.92-3.86 (m, 4 H), 3.78 (s, 3 H), 3.64 (dd, 1 H, *J* = 10.4, 5.7 Hz), 3.13 (d, 1 H, *J* = 14.0 Hz), 2.79 (d, 1 H, *J* = 14.0 Hz), 2.20-2.13 (m, 2 H), 1.32 (s, 3 H), 1.24 (s, 3 H), 1.19 (s, 3 H). ^{13}C NMR (500 MHz, $CDCl_3$-*d*) δ 207.8, 205.8, 166.5, 108.0, 90.7, 84.9, 64.8, 64.4, 54.4, 53.05, 53.01, 50.0, 30.4, 24.4, 24.1, 18.3.

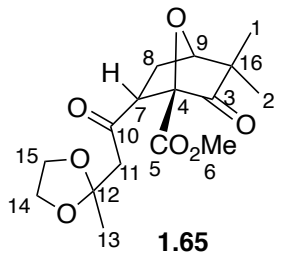

1.65

NMR Assignment. ^{1}H NMR (500 MHz, $CDCl_3$-d) δ 4.33 (d, 1 H, *J* = 4.9 Hz, C9-H), 3.92-3.86 (m, 4 H, C14-H and C15-H), 3.78 (s, 3 H, C6-H), 3.64 (dd, 1 H, *J* = 10.4, 5.7 Hz, C7-H), 3.13 (d, 1 H, *J* = 14.0 Hz, C11-H), 2.79 (d, 1 H, *J* = 14.0 Hz, C11-H), 2.20-2.13 (m, 2 H, C8-H), 1.32 (s, 3 H, C13-H), 1.24 (s, 3 H, C1-H or C2-H), 1.19 (s, 3 H, C1-H or C2-H). ^{13}C NMR (500 MHz, $CDCl_3$-*d*) δ 207.8 (C3), 205.8 (C10), 166.5 (C5), 108.0 (C12), 90.7 (C4), 84.9 (C9), 64.8 (C14), 64.4 (C15), 54.4 (C7), 53.05 (C11), 53.01 (C6), 50.0 (C16), 30.4 (C8), 24.4 (C13), 24.1 (C1 or C2), 18.3 (C1 or C2).

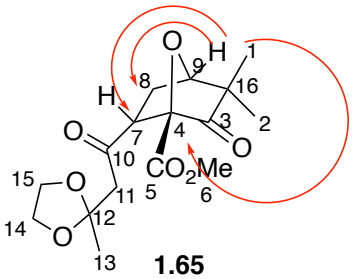

1.65

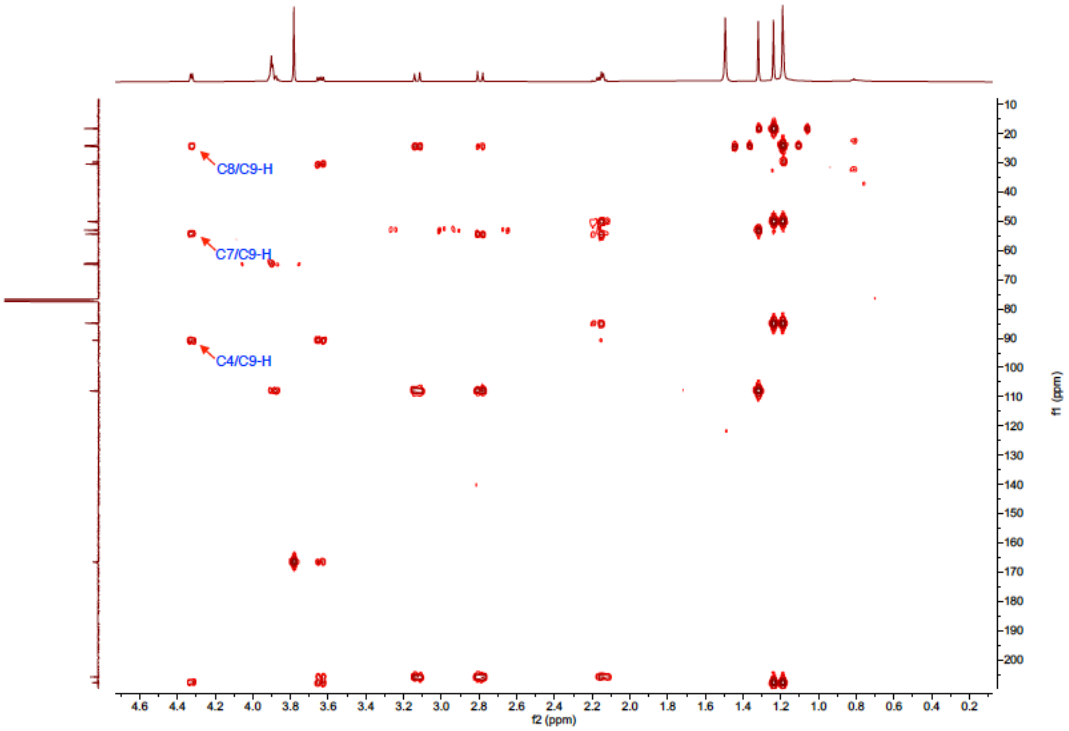

Figure 4.4. Key HMBC correlations of **1.65**.

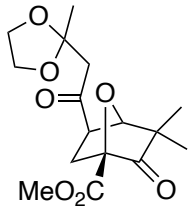

1.66

Methyl(5*R*)-3,3-dimethyl-5-(2-(2-methyl-1,3-dioxolan-2-yl)acetyl)-2-oxo-7-oxabicyclo[2.2.1]heptane-1-carboxylate (1.66). az-3-245-2-2. ^{1}H NMR (500 MHz, $CDCl_3$-d) δ 4.61 (s, 1 H), 3.92-3.88 (m, 4 H), 3.78 (s, 3 H), 3.24 (dd, 1 H, *J* = 9.0, 4.6 Hz), 2.86 (d, 1 H, *J* = 13.9 Hz), 2.79 (d, 1 H, *J* = 13.9 Hz), 2.62 (ddd, 1 H, *J* = 13.9, 4.6, 1.2 Hz), 1.99 (dd, 1 H, *J* = 13.6, 9.0 Hz), 1.34 (s, 3 H), 1.26 (s, 3 H), 1.10 (s, 3 H). ^{13}C NMR

(500 MHz, $CDCl_3$-*d*) δ 209.4, 203.3, 165.8, 108.0, 88.3, 85.7, 64.7, 64.6, 52.9, 50.6, 49.9, 48.8, 30.3, 24.4, 23.0, 19.9.

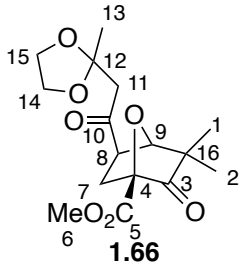

1.66

NMR Assignment. ^{1}H NMR (500 MHz, $CDCl_3$-d) δ 4.61 (s, 1 H, C9-H), 3.92-3.88 (m, 4 H, C14-H and C15-H), 3.78 (s, 3 H, C6-H), 3.24 (dd, 1 H, *J* = 9.0, 4.6 Hz, C8-H), 2.86 (d, 1 H, *J* = 13.9 Hz, C11-H), 2.79 (d, 1 H, *J* = 13.9 Hz, C11-H), 2.62 (ddd, 1 H, *J* = 13.9, 4.6, 1.2 Hz, C7-H), 1.99 (dd, 1 H, *J* = 13.6, 9.0 Hz, C7-H), 1.34 (s, 3 H, C13-H), 1.26 (s, 3 H, C1-H or C2-H), 1.10 (s, 3 H, C1-H or C2-H). ^{13}C NMR (500 MHz, $CDCl_3$-*d*) δ 209.4 (C3), 203.3 (C10), 165.8 (C5), 108.0 (C12), 88.3 (C4), 85.7 (C9), 64.7 (C14), 64.6 (C15), 52.9 (C6), 50.8 (C8), 49.9 (C11), 48.8 (C16), 30.3 (C7), 24.4 (C13), 23.0 (C1 or C2), 19.9 (C1 or C2).

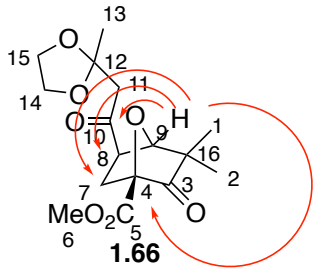

1.66

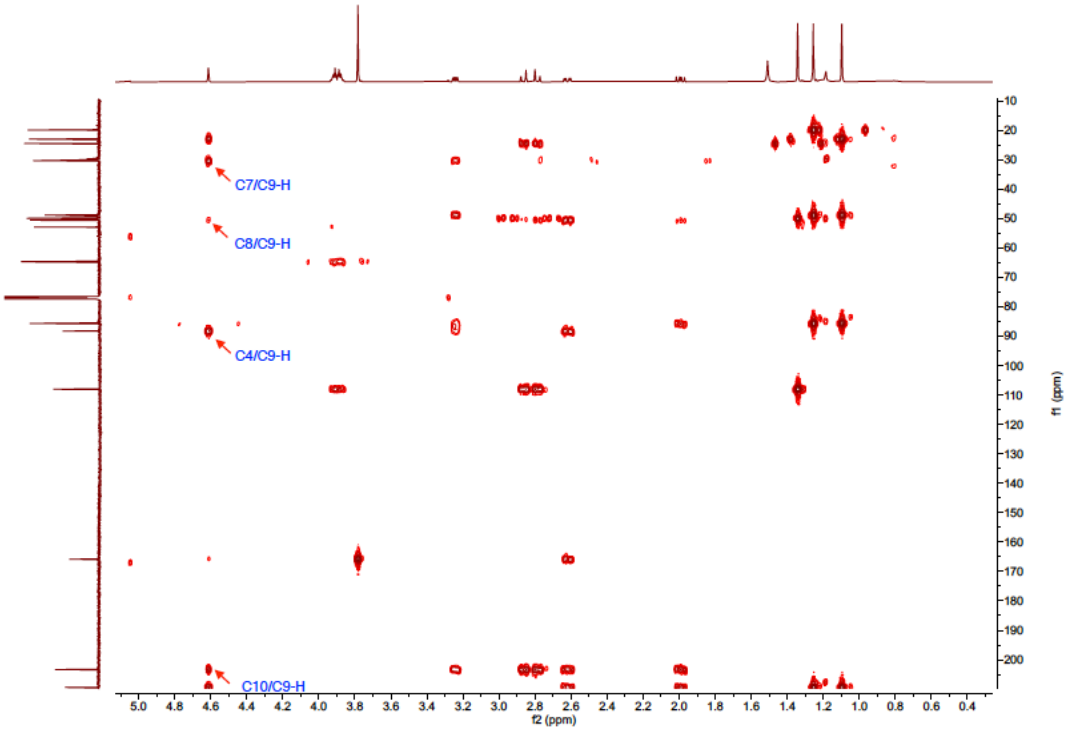

Figure 4.5. Key HMBC correlations of **1.66**.

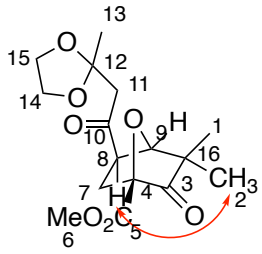

1.66

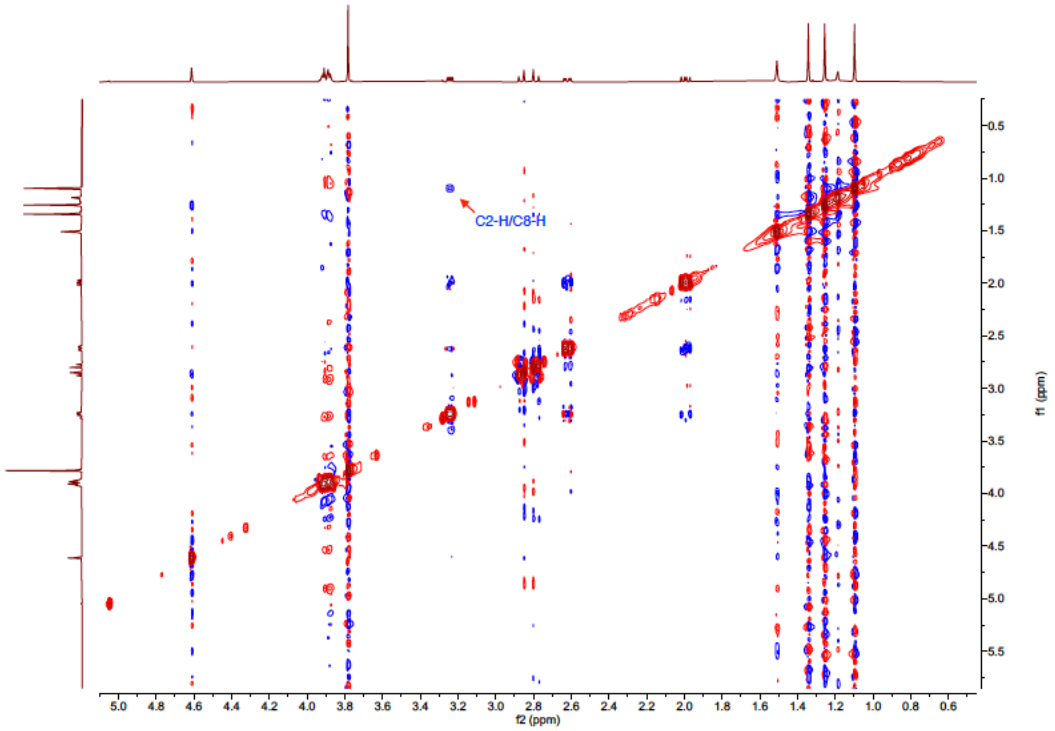

Figure 4.6. Key NOESY correlations of **1.66**.

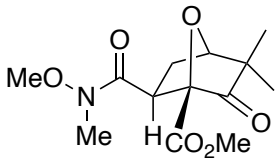

1.73

Methyl (1*S*,4*R*,6*S*)-6-(methoxy(methyl)carbamoyl)-3,3-dimethyl-2-oxo-7-oxabicyclo[2.2.1]heptane-1-carboxylate (1.73). az-3-291. A solution of **1.20** (30 mg, 0.15 mmol), **1.72** (21 mg, 0.18 mmol) and Rh_2OAc_4 (1.3 mg, 0.0030 mmol) in CH_2Cl_2 (1 mL) was stirred under reflux under N_2 for overnight. The solution was cooled to rt, washed with H_2O (3 X 1 mL) and brine (1 mL), dried (Na_2SO_4), filtered and concentrated in *vacuo* to give crude **1.73** as colorless oil. The crude material was purified via flush column chromatography eluting hexanes : EtOAc (5:1) to give 20 mg (47%) **1.73** as white solid.

^{1}H NMR (500 MHz, $CDCl_3$) δ 4.47 (d, J = 5.3 Hz, 1 H), 3.84 (s, 3 H), 3.71 (s, 3 H), 3.39 (t, J = 7.7 Hz, 1 H), 3.17 (s, 3 H), 2.45 (dd, J = 12.9, 9.2 Hz, 1 H), 2.02 (dt, J = 12.3, 5.8 Hz, 1 H), 1.30 (s, 3 H), 1.12 (s, 3 H). ^{13}C NMR (126 MHz, $CDCl_3$) δ 209.5, 171.5, 165.6, 90.2, 83.5, 61.4, 52.7, 48.9, 42.4, 32.3, 31.7, 23.2, 20.1. HRMS (ESI) *m*/*z* calcd for $C_{13}H_{19}NO_6Na^+$ $(M+Na)^+$, 308.1105; found 308.1114.

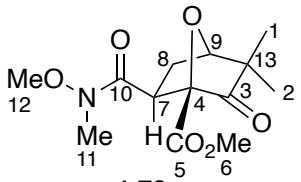

1.73

NMR Assignment. ^{1}H NMR (500 MHz, $CDCl_3$) δ 4.47 (d, J = 5.3 Hz, 1 H, C9-H), 3.84 (s, 3 H, C12-H), 3.71 (s, 3 H, C6-H), 3.39 (t, J = 7.7 Hz, 1 H, C7-H), 3.17 (s, 3 H, C11-H), 2.45 (dd, J = 12.9, 9.2 Hz, 1 H, C8-H), 2.02 (dt, J = 12.3, 5.8 Hz, 1 H, C8-H), 1.30 (s, 3 H, C1-H or C2-H), 1.12 (s, 3 H, C1-H or C2-H). ^{13}C NMR (126 MHz, $CDCl_3$) δ 209.5 (C3), 171.5 (C10), 165.6 (C5), 90.2 (C4), 83.5 (C9), 61.4 (C12), 52.7 (C6), 48.9 (C13), 42.4 (C7), 32.3 (C11), 31.7 (C8), 23.1 (C1 or C2), 20.1 (C1 or C2).

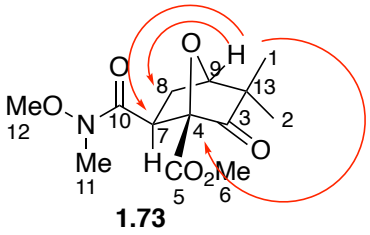

1.73

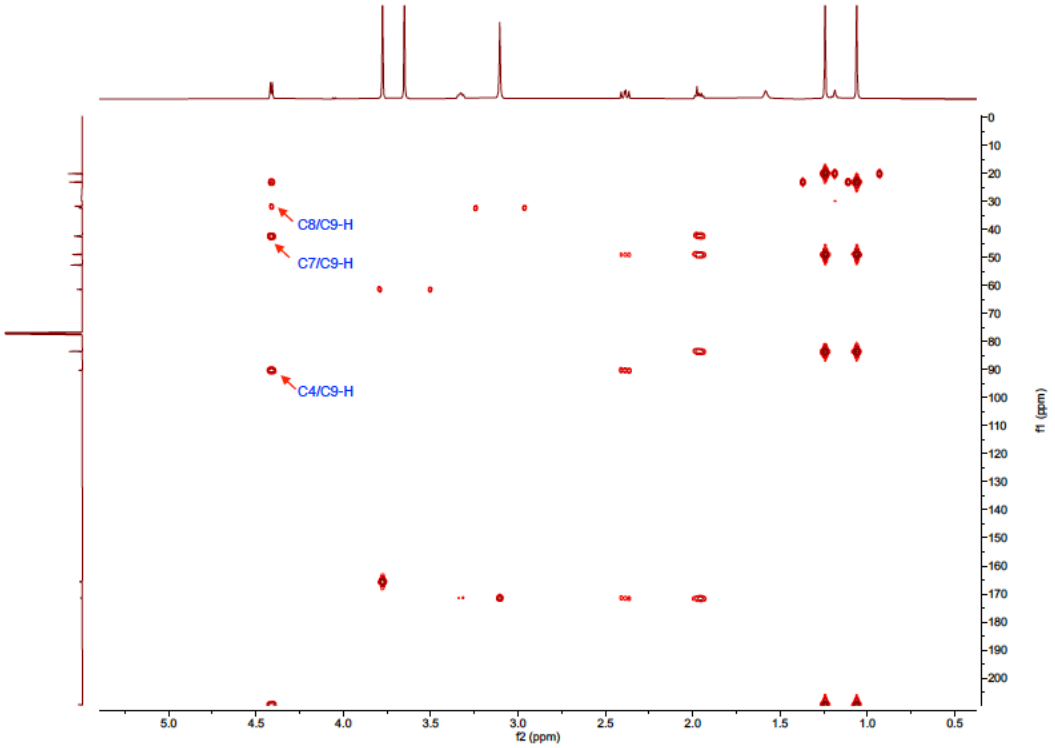

Figure 4.7. Key HMBC correlations of **1.73**.

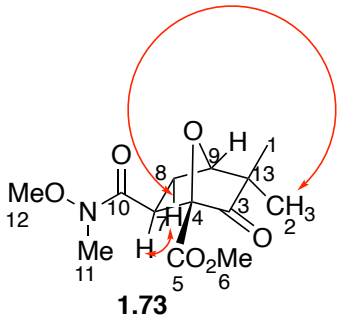

1.73

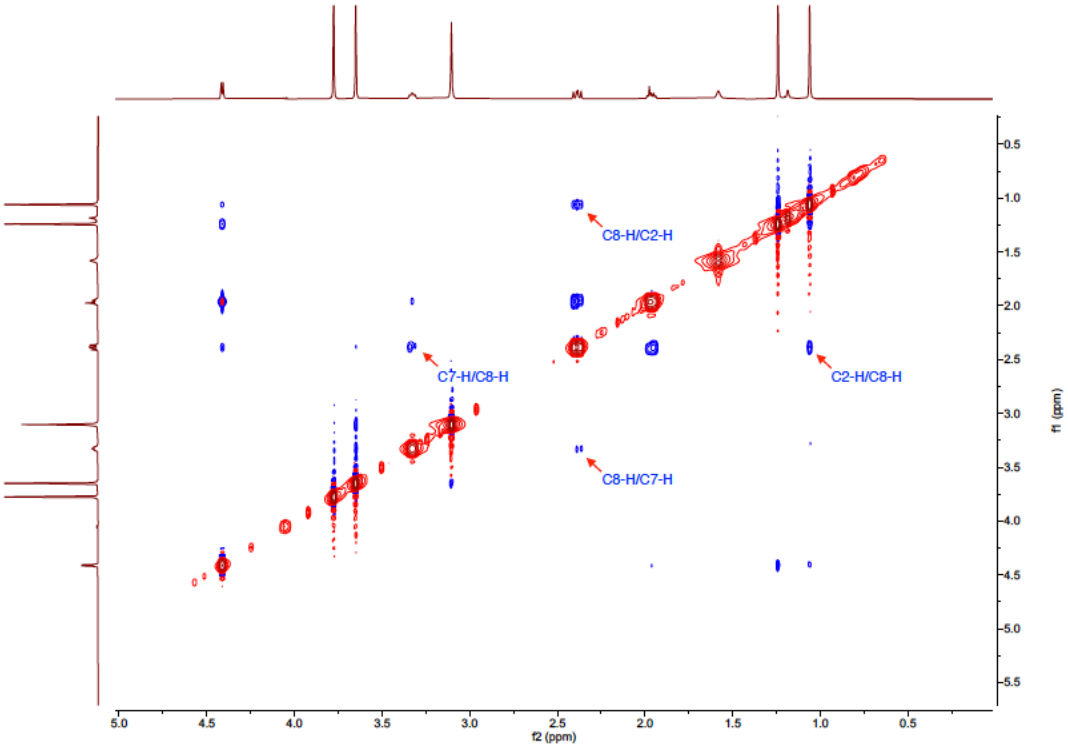

Figure 4.8. Key NOESY correlations of **1.73**.

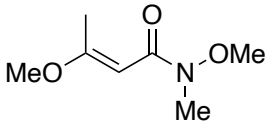

1.80

(*E*)-*N*,3-Dimethoxy-*N*-methylbut-2-enamide (1.80). zw-4-meli5. MeO(Me)NH•HCl (5.170 g, 53.00 mmol) and trimethylaluminum (17.67 mL, 35.34 mmol) were slowly added sequentially to a solution of **1.79** (2.300 g, 17.67 mmol) in CH_2Cl_2 (50 mL) at 0 ºC. The solution was transferred to an oil bath preheated to 40 ºC and stirred for 4 h. The reaction was then cooled to 0 °C, and H_2O (10 mL) and saturated aqueous Rochelle salt (30 mL) were added. The ice-bath was removed, and the resulting mixture was stirred at room temperature for 30 min. The mixture was extracted with CH_2Cl_2 (3 x 30 mL), and

the combined organic fractions were dried (Na_2SO_4), filtered and concentrated under reduced pressure to give crude **1.80** as colorless oil. The crude material was purified via flash column chromatography eluting hexanes : EtOAc (5:1 to 3:1) to give 1.969 g (70%) of **1.80** as colorless oil. ^{1}H NMR (500 MHz, $CDCl_3$) δ 5.52 (s, 1 H), 3.64 (s, 3 H), 3.60 (s, 3 H), 3.15 (s, 3 H), 2.26 (s, 3 H); ^{13}C NMR (126 MHz, $CDCl_3$) δ 171.9, 169.0, 88.6, 61.2, 55.1, 32.4, 18.9; IR (neat) ν_{max} 1738, 1650, 1366, 1233, 1217, 906, 839, 725 cm^{-1}; HRMS (ESI) *m*/*z* calcd for $C_7H_{14}NO_3^+$ $(M+H)^+$, 160.0968; found 160.0970.

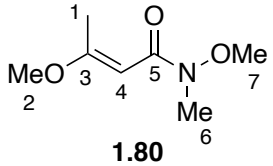

1.80

NMR Assignment. ^{1}H NMR (500 MHz, $CDCl_3$) δ 5.52 (s, 1 H, C4-H), 3.64 (s, 3 H, C2-H or C7-H), 3.60 (s, 3 H, C2-H or C7-H), 3.15 (s, 3 H, C6-H), 2.26 (s, 3 H, C1-H).

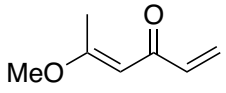

1.18

(*E*)-5-Methoxyhexa-1,4-dien-3-one (1.18). zw-4-meli6. Vinyl magnesium bromide (42.31 mL, 29.62 mmol) was added dropwise to a solution of **1.80** (1.570 g, 9.862 mmol) in THF (50 mL) at 0 ºC, and the resulting solution was stirred overnight at room temperature. The reaction mixture was poured into saturated aqueous NH_4Cl (30 mL) at 0 ºC. The resulting mixture was extracted with CH_2Cl_2 (3 x 20 mL). The combined organic extracts were dried (Na_2SO_4), filtered and concentrated under reduced pressure to give crude **1.18** as yellow oil. The crude material was purified via flash column chromatography eluting hexanes : EtOAc (8:1) to give 1.020 g (82%) of **1.18** as yellow oil. ^{1}H NMR (500

MHz, $CDCl_3$) δ 6.35 (dd, *J* = 17.4, 10.5 Hz, 1 H), 6.12 (d, *J* = 17.4 Hz, 1 H), 5.59 – 5.54 (comp, 2 H), 3.63 (s, 3 H), 2.28 (s, 3 H); ^{13}C NMR (126 MHz, $CDCl_3$) δ 188.6, 174.7, 138.7, 125.5, 97.9, 55.5, 20.0; IR (neat) ν_{max} 1617, 1570, 1403, 1266, 1172, 1117, 1062, 909, 823, 731 cm^{-1}; HRMS (ESI) *m/z* calcd for $C_7H_{11}O_2^+$ $(M+H)^+$, 127.0754; found 127.0755.

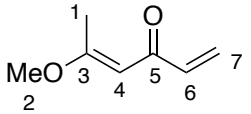

1.18

NMR Assignment. ^1H NMR (500 MHz, $CDCl_3$) δ 6.35 (dd, *J* = 17.4, 10.5 Hz, 1 H, C6-H), 6.12 (d, *J* = 17.4 Hz, 1 H, C7-H *trans*), 5.59 – 5.54 (comp, 2 H, C4-H and C7-H *cis*), 3.63 (s, 3 H, C2-H), 2.28 (s, 3 H, C1-H).

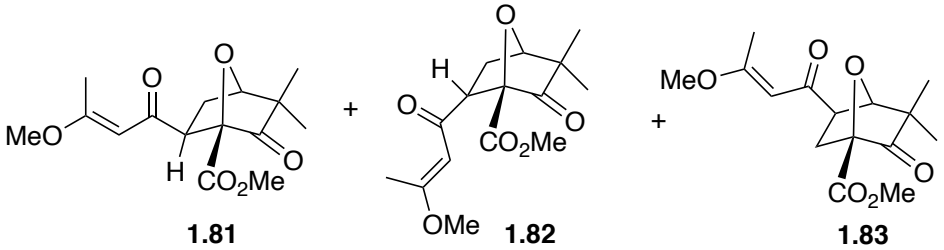

1.81 **1.82** **1.83**

Preparation of 1.81, 1.82, 1.83. A solution of **9** (400 mg, 3.17 mmol), **11** (571 mg, 2.89 mmol) and $Rh_2(HNAc)_4$ (25.3 mg, 0.0578 mmol) in toluene (10 mL) was stirred at 100 ºC for 1 h. The reaction was cooled to room temperature, and the solvent was removed under reduced pressure. The residue was dissolved in CH_2Cl_2 (5 mL), which was washed with H_2O (3 x 5 mL) and brine (5 mL). The solution was dried (Na_2SO_4), filtered and concentrated under reduced pressure to give crude mixture of **1.81**, **1.82** and **1.83** as yellow oil. The crude material was purified via flash column chromatography eluting hexanes :

EtOAc (8:1) to give 522 mg (61%) of **1.81** as white solid: mp 117–121 ºC, 32.2 mg (4%) of **1.82** as colorless oil and 34.0 mg (4%) of **1.83** as colorless oil.

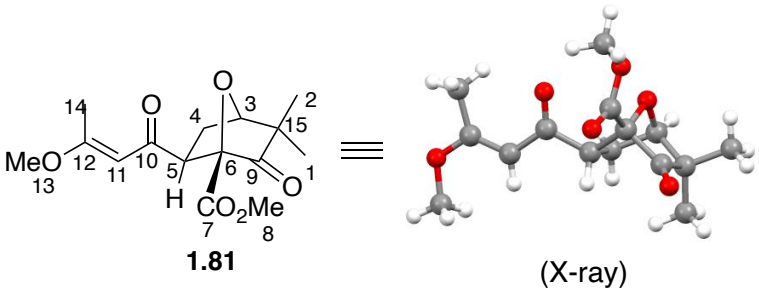

1.81

(X-ray)

Methyl (1S,4R,6S)-6-((E)-3-methoxybut-2-enoyl)-3,3-dimethyl-2-oxo-7-oxabicyclo[2.2.1]heptane-1-carboxylate (1.81). zw-4-meli7. ^{1}H NMR (500 MHz, $CDCl_3$) δ 5.38 (s, 1 H), 4.48 (d, *J* = 5.3 Hz, 1 H), 3.80 (s, 3 H), 3.64 (s, 3 H), 3.09 (dd, *J* = 9.3, 6.3 Hz, 1 H), 2.39 (dd, *J* = 12.9, 9.3 Hz, 1 H), 2.25 (s, 3 H), 2.11 – 2.02 (m, 1 H), 1.28 (s, 3 H), 1.10 (s, 3 H); ^{13}C NMR (126 MHz, $CDCl_3$) δ 209.1, 194.3, 175.6, 165.7, 97.0, 90.5, 83.7, 55.9, 52.7, 52.6, 49.0, 31.1, 23.1, 20.21, 20.17; IR (neat) ν_{max} 2364, 1736, 1580, 1439, 1265, 1113, 1045, 733, 703 cm^{-1}; HRMS (ESI) *m/z* calcd for $C_{15}H_{21}O_6^+$ $(M+H)^+$, 297.1333; found 297.1339.

NMR Assignment. ^{1}H NMR (500 MHz, $CDCl_3$) δ 5.38 (s, 1 H, C11-H), 4.48 (d, *J* = 5.3 Hz, 1 H, C3-H), 3.80 (s, 3 H, C8-H), 3.64 (s, 3 H, C13-H), 3.09 (dd, *J* = 9.3, 6.3 Hz, 1 H, C5-H), 2.39 (dd, *J* = 12.9, 9.3 Hz, 1 H, C4-H *endo*), 2.25 (s, 3 H, C14-H), 2.11 – 2.02 (m, 1 H, C4-H *exo*), 1.28 (s, 3 H, C2-H), 1.10 (s, 3 H, C1-H). ^{13}C NMR (126 MHz, $CDCl_3$) δ 209.1 (C9), 194.3 (C10), 175.6 (12), 165.7 (C7), 97.0 (C11), 90.5 (C6), 83.7 (C3), 55.9 (C13), 52.7 (C5 or C8), 52.6 (C5 or C8), 49.0 (C15), 31.1 (4), 23.1 (C1), 20.21 (C2 or C14), 20.17 (C2 or C14).

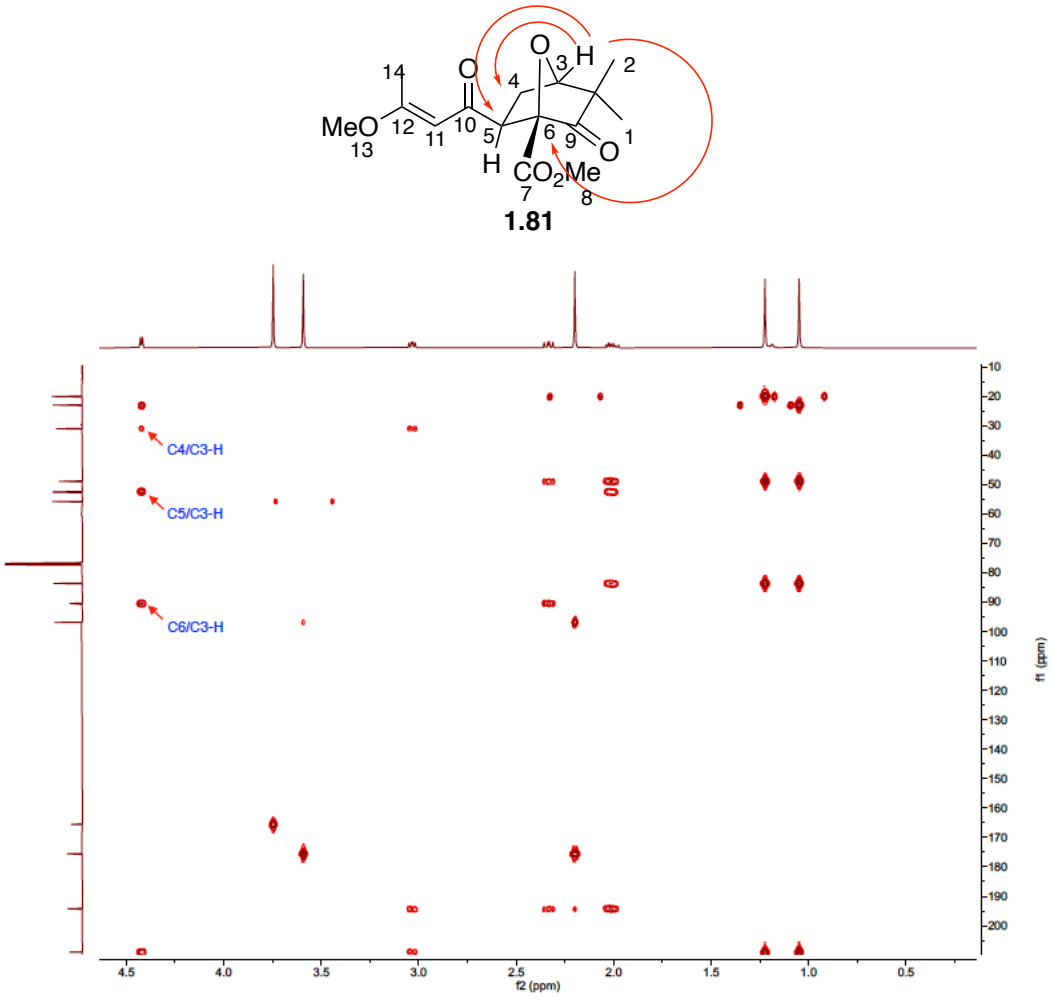

Figure 4.9. Key HMBC correlations of **1.81**.

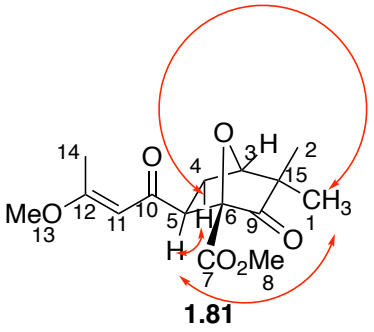

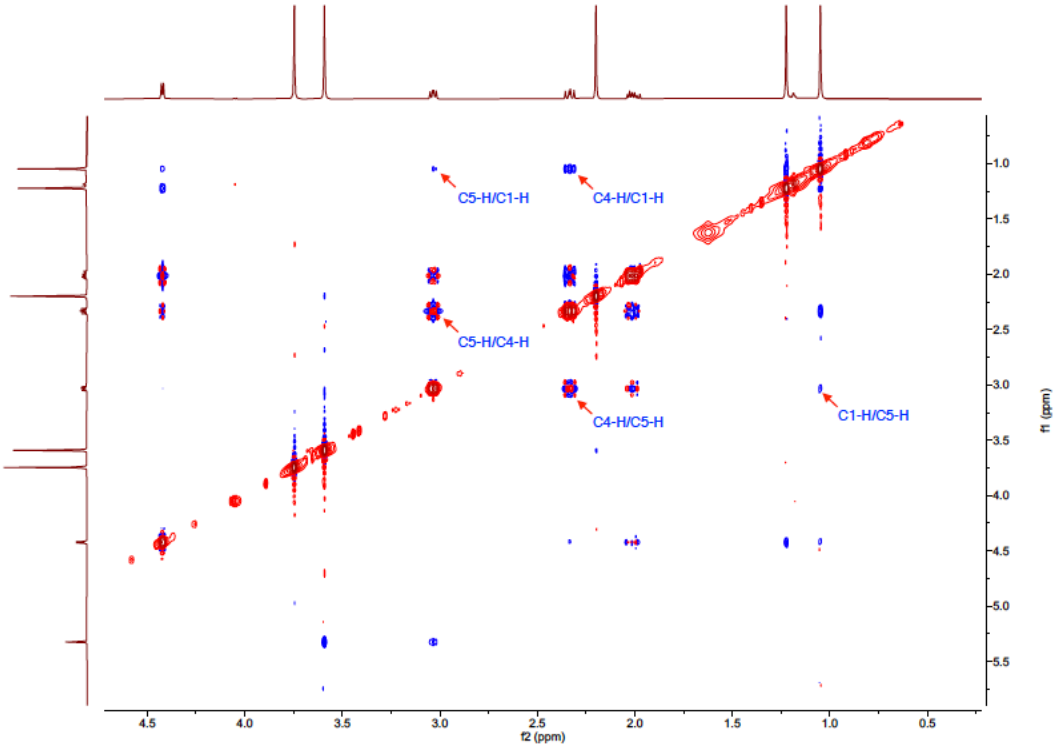

Figure 4.10. Key NOESY correlations of **1.81**.

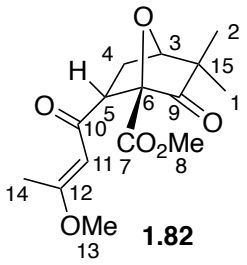

1.82

Methyl (1S,4R,6R)-6-((E)-3-methoxybut-2-enoyl)-3,3-dimethyl-2-oxo-7-oxabicyclo[2.2.1]heptane-1-carboxylate (1.82). zw-4-meli8. ^{1}H NMR (500 MHz, $CDCl_3$) δ 5.72 (s, 1 H), 4.38 (d, J = 5.6 Hz, 1 H), 3.83 (s, 3 H), 3.69 (s, 3 H), 3.48 (dd, J = 11.2, 4.6 Hz, 1 H), 2.36 (dd, J = 12.7, 4.6 Hz, 1 H), 2.27 (s, 3 H), 2.21 (ddd, J = 12.7, 11.2, 5.6 Hz, 1 H), 1.31 (s, 3 H), 1.29 (s, 3 H); ^{13}C NMR (126 MHz, $CDCl_3$) δ 208.5, 194.8, 175.0, 166.9, 100.4, 90.7, 85.1, 55.9, 55.8, 53.0, 50.2, 30.1, 24.3, 20.3, 18.5; IR (neat) ν_{max}

1747, 1583, 1440, 1264, 1114, 1061, 896, 732, 703 cm^{-1}; HRMS (ESI) *m/z* calcd for $C_{15}H_{21}O_6^+$ $(M+H)^+$, 297.1333; found 297.1343.

NMR Assignment. ^1H NMR (500 MHz, $CDCl_3$) δ 5.72 (s, 1 H, C11-H), 4.38 (d, *J* = 5.6 Hz, 1 H, C3-H), 3.83 (s, 3 H, C8-H), 3.69 (s, 3 H, C13-H), 3.48 (dd, *J* = 11.2, 4.6 Hz, 1 H, C5-H), 2.36 (dd, *J* = 12.7, 4.6 Hz, 1 H, C4-H *endo*), 2.27 (s, 3 H, C14-H), 2.21 (ddd, *J* = 12.7, 11.2, 5.6 Hz, 1 H, C4-H *exo*), 1.31 (s, 3 H, C2-H), 1.29 (s, 3 H, C1-H).

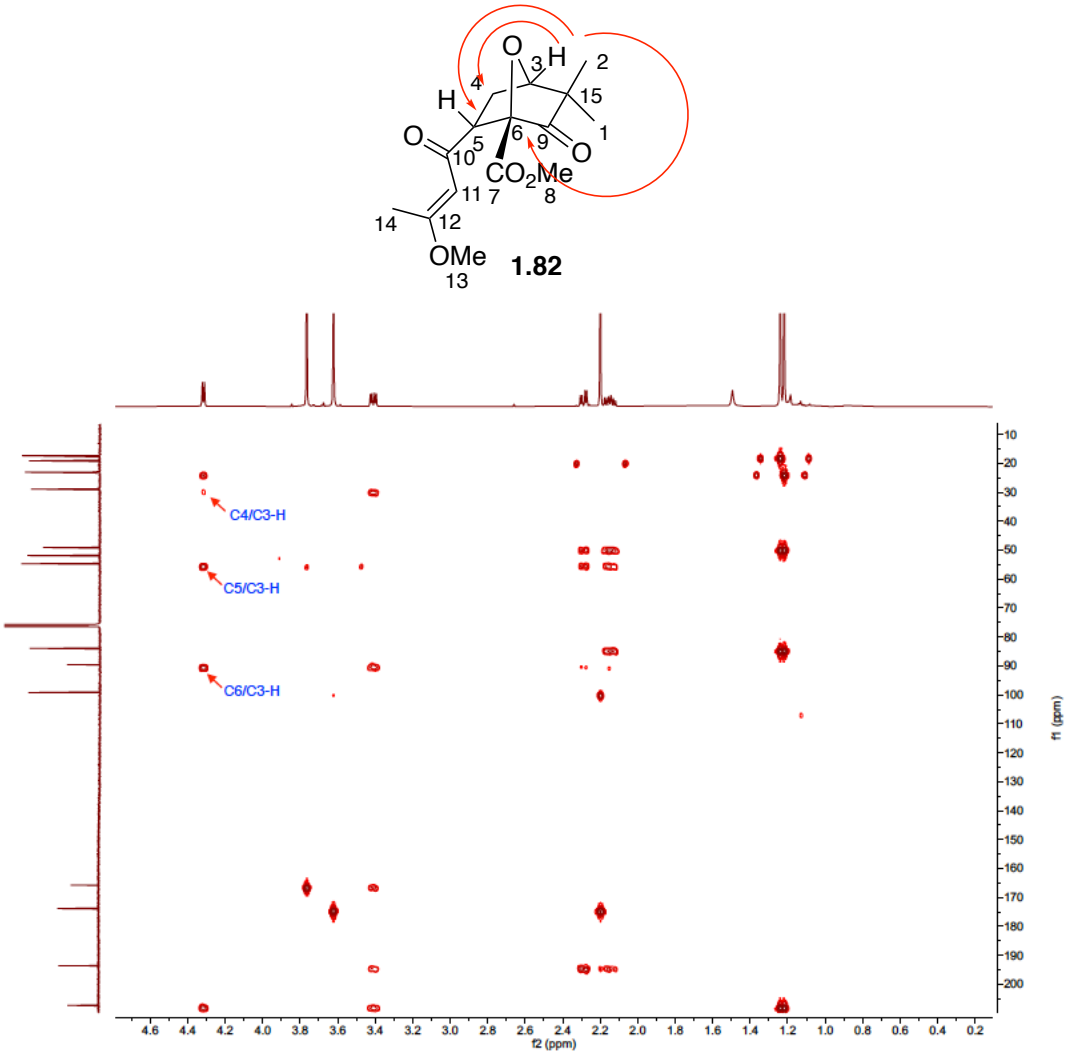

Figure 4.11. Key HMBC correlations of **1.82**.

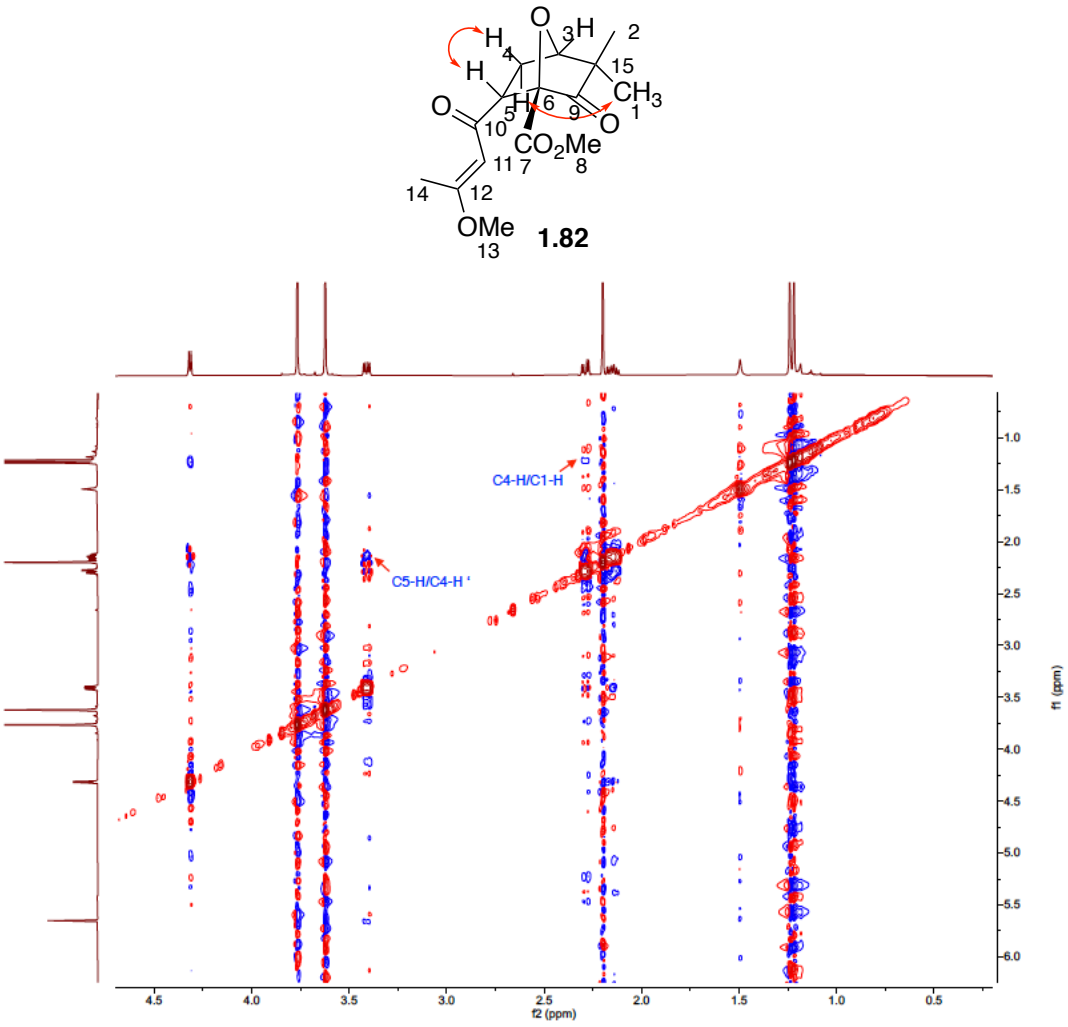

Figure 4.12. Key NOESY correlations of **1.82**.

1.83

Methyl (1S,4R,5R)-5-((E)-3-methoxybut-2-enoyl)-3,3-dimethyl-2-oxo-7-oxabicyclo[2.2.1]heptane-1-carboxylate (1.83). zw-4-meli9. ^{1}H NMR (500 MHz,

$CDCl_3$) δ 5.44 (s, 1 H), 4.65 (s, 1 H), 3.85 (s, 3 H), 3.69 (s, 3 H), 3.10 (dd, *J* = 9.1, 4.5 Hz, 1 H), 2.65 (ddd, *J* = 13.5, 4.5, 1.1 Hz, 1 H), 2.32 (s, 3 H), 2.15 (dd, *J* = 13.5, 9.1 Hz, 1 H), 1.32 (s, 3 H), 1.16 (s, 3 H); ^{13}C NMR (126 MHz, $CDCl_3$) δ 209.8, 195.2, 175.5, 166.1, 96.6, 88.3, 86.6, 55.7, 52.8, 50.2, 48.8, 31.6, 23.0, 20.2, 19.9; IR (neat) ν_{max} 1742, 1578, 1439, 1265, 1146, 1063, 1036, 733, 702 cm^{-1}; HRMS (ESI) *m*/*z* calcd for $C_{15}H_{21}O_6^+$ $(M+H)^+$, 297.1333; found 297.1339.

NMR Assignment. ^{1}H NMR (500 MHz, $CDCl_3$) δ 5.44 (s, 1 H, C11-H), 4.65 (s, 1 H, C3-H), 3.85 (s, 3 H, C8-H), 3.69 (s, 3 H, C13-H), 3.10 (dd, *J* = 9.1, 4.5 Hz, 1 H, C4-H), 2.65 (ddd, *J* = 13.5, 4.5, 1.1 Hz, 1 H, C5-H *exo*), 2.32 (s, 3 H, C14-H), 2.15 (dd, *J* = 13.5, 9.1 Hz, 1 H, C5-H *endo*), 1.32 (s, 3 H, C2-H), 1.16 (s, 3 H, C1-H).

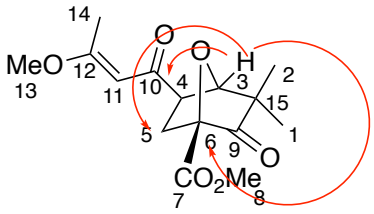

1.83

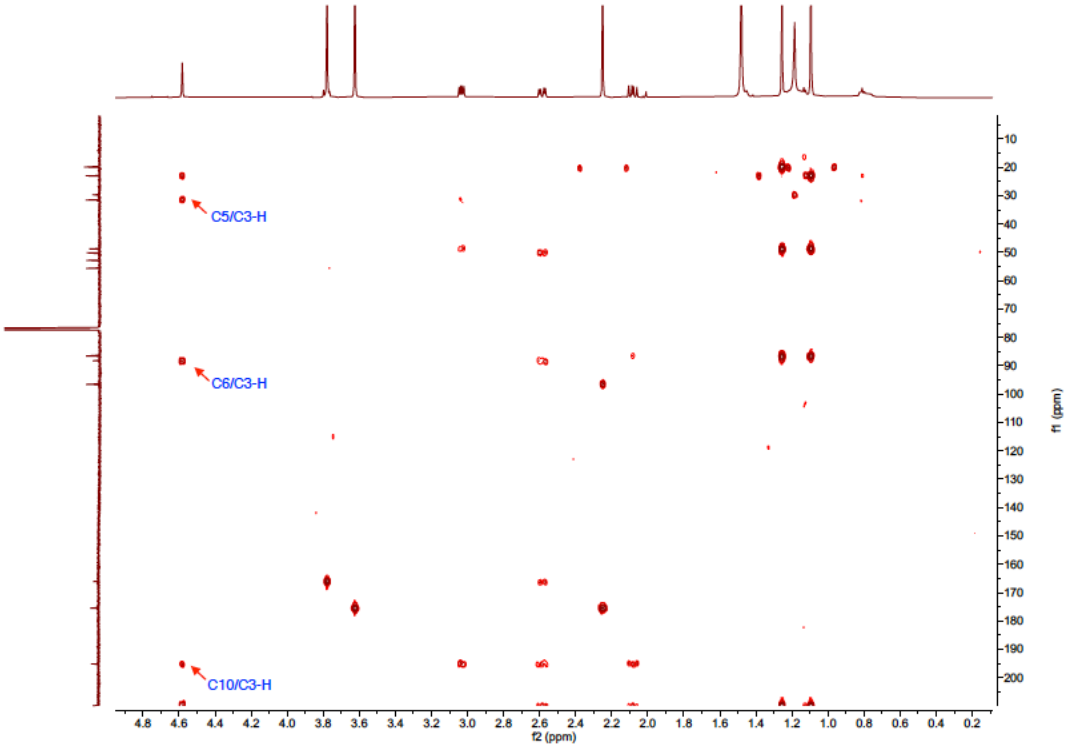

Figure 4.13. Key HMBC correlations of **1.83**.

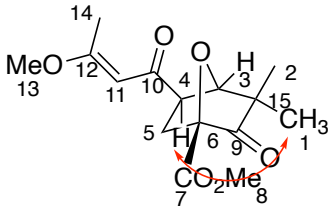

1.83

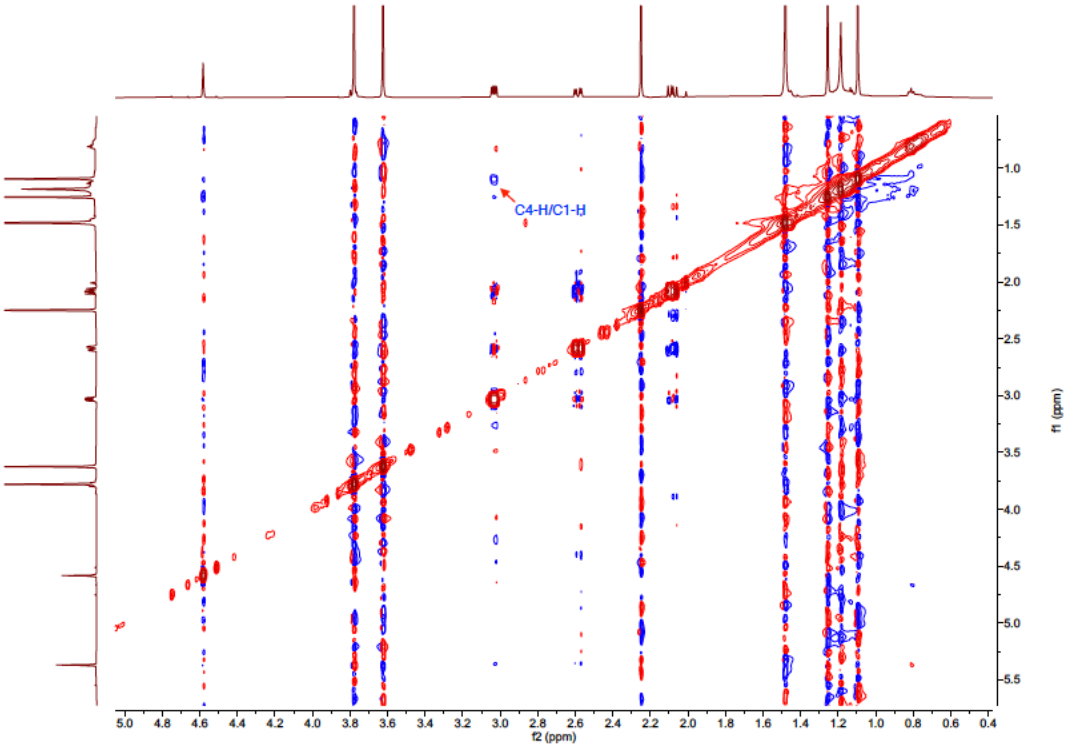

Figure 4.14. Key NOESY correlations of **1.83**.

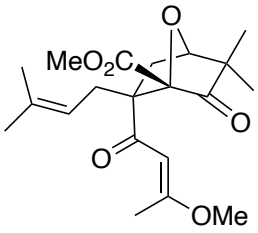

1.78

Methyl (1*S*,2*R*,4*R*)-2-((*E*)-3-methoxybut-2-enoyl)-5,5-dimethyl-2-(3-methylbut-2-en-1-yl)-6-oxo-7-oxabicyclo[2.2.1]heptane-1-carboxylate (1.78). zw-4-meli10. A solution of **1.81** (210 mg, 0.709 mmol) in THF (2 mL) was added dropwise to a solution of NaHMDS (0.541 mL, 1.07 mmol) in THF (4 mL) at –78 ºC, and the solution

was stirred at –78 ºC for 30 min. Freshly prepared prenyl iodide (278 mg, 1.42 mmol) in THF (2 mL) was added dropwise. The resulting solution was stirred at –78 ºC for 30 min. Saturated aqueous NH_4Cl (2 mL) was added, and the mixture was extracted with CH_2Cl_2 (3 x 2 mL). The combined organic layers were washed with H_2O (3 x 2 mL) and brine (2 mL), dried (Na_2SO_4), filtered and concentrated under reduced pressure to give crude **1.78** as yellow oil. The crude material was purified via flash column chromatography eluting hexanes : EtOAc (8:1) to give 168 mg (65%) of **1.78** as yellow oil. ^{1}H NMR (500 MHz, $CDCl_3$) δ 6.37 (s, 1 H), 4.91 – 4.87 (m, 1 H), 4.34 (d, *J* = 5.7 Hz, 1 H), 3.85 (s, 3 H), 3.74 (s, 3 H), 2.90 (d, *J* = 13.1 Hz, 1 H), 2.62 (dd, *J* = 14.4, 5.5 Hz, 1 H), 2.48 (dd, *J* = 14.4, 8.0 Hz, 1 H), 2.22 (s, 3 H), 1.79 (dd, *J* = 13.1, 5.7 Hz, 1 H), 1.67 (s, 3 H), 1.60 (s, 3 H), 1.26 (s, 3 H), 1.12 (s, 3 H); ^{13}C NMR (126 MHz, $CDCl_3$) δ 208.3, 196.1, 175.1, 166.0, 135.9, 117.9, 98.5, 93.0, 83.9, 64.8, 56.0, 52.9, 49.3, 34.2, 34.0, 26.1, 24.3, 20.4, 18.5, 18.3; IR (neat) ν_{max} 1776, 1732, 1578, 1439, 1265, 11136, 1065, 895, 733, 703 cm^{-1}; HRMS (ESI) *m*/*z* calcd for $C_{20}H_{28}O_6Na^+$ $(M+Na)^+$, 387.1778; found 387.1784.

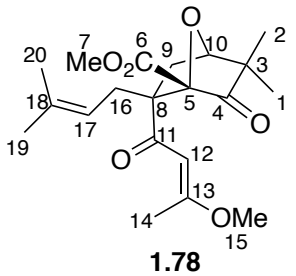

1.78

NMR Assignment. ^{1}H NMR (500 MHz, $CDCl_3$) δ 6.37 (s, 1 H, C12-H), 4.91 – 4.87 (m, 1 H, C17-H), 4.34 (d, *J* = 5.7 Hz, 1 H, C10-H), 3.85 (s, 3 H, C7-H), 3.74 (s, 3 H, C15-H), 2.90 (d, *J* = 13.1 Hz, 1 H, C9-H), 2.62 (dd, *J* = 14.4, 5.5 Hz, 1 H, C16-H), 2.48 (dd, *J* = 14.4, 8.0 Hz, 1 H, C16-H), 2.22 (s, 3 H, C14-H), 1.79 (dd, *J* = 13.1, 5.7 Hz, 1 H, C9-H), 1.67 (s, 3 H, C19-H or C20-H), 1.60 (s, 3 H, C19-H or C20-H), 1.26 (s, 3 H, C1-H

or C2-H), 1.12 (s, 3 H, C1-H or C2-H). ^{13}C NMR (126 MHz, $CDCl_3$) δ 208.3 (C4), 196.1 (C11), 175.1 (C13), 166.0 (C6), 135.9 (C18), 117.9 (C17), 98.5 (C12), 93.0 (C5), 83.9 (C10), 64.8 (C8), 56.0 (C15), 52.9 (C7), 49.3 (C3), 34.2 (C9), 34.0 (C16), 26.1 (C19 or C20), 24.3 (C1 or C2), 20.4 (C14), 18.5 (C1 or C2), 18.3 (C19 or C20).

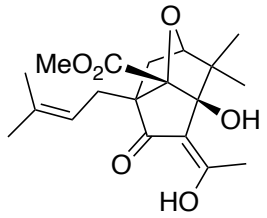

1.16

Methyl (3a*S*,6a*S*,*Z*)-3a-hydroxy-4-(1-hydroxyethylidene)-3,3-dimethyl-6-(3-methylbut-2-en-1-yl)-5-oxohexahydro-6a*H*-2,6-methanocyclopenta[*b*]furan-6a-carboxylate (1.16). zw-4-meli12. Freshly distilled TMS-I (57 mg, 0.29 mmol) was added to a solution of **1.78** (80 mg, 0.22 mmol) in $CHCl_3$ (4 mL), and the solution was stirred at room temperature for 15 min. MeOH (2 mL) was added, and the resulting solution was concentrated under reduced pressure. The residue was dissolved in CH_2Cl_2 (4 mL), and the solution was washed with $NaHSO_3$ (3 x 2 mL), $NaHCO_3$ (3 x 2 mL) and brine (5 mL), dried (Na_2SO_4), filtered and concentrated under reduced pressure. The residue was dissolved in THF (4 mL) at 0 ºC, DBU (67 mg, 0.44 mmol) was added, and the solution was stirred at room temperature for 15 min. Saturated aqueous NH_4Cl (2 mL) was added, and the mixture was extracted with CH_2Cl_2 (3 x 2 mL). The combined organic layers were dried (Na_2SO_4), filtered and concentrated under reduced pressure to give crude **1.16** as colorless oil. The crude material was purified via flash column chromatography eluting hexanes : EtOAc (6:1) to give 58 mg (75%) of **1.16** as white solid: mp 109–112 ºC. ^{1}H NMR (500 MHz, $CDCl_3$) δ 13.84 (s, 1 H), 5.15 (t, J = 7.2 Hz, 1 H), 4.06 (d, J = 5.1 Hz, 1

H), 3.78 (s, 3 H), 2.37 (dd, J = 15.5, 7.2 Hz, 1 H), 2.28 – 2.23 (m, 1 H), 2.14 (s, 3 H), 2.03 (d, J = 13.3 Hz, 1 H), 1.80 (dd, J = 13.3, 5.1 Hz, 1 H), 1.69 (s, 3 H), 1.58 (s, 3 H), 1.26 (s, 3 H), 0.94 (s, 3 H); ^{13}C NMR (126 MHz, $CDCl_3$) δ 205.2, 177.0, 168.7, 134.8, 118.6, 112.9, 100.7, 87.1, 85.9, 58.9, 52.6, 49.5, 37.8, 29.3, 26.1, 22.4, 20.7, 19.5, 18.0; IR (neat) ν_{max} 2359, 2340, 1737, 1653, 1616, 1582, 1456, 1129, 985, 892, 771 cm^{-1}; HRMS (ESI) *m*/*z* calcd for $C_{19}H_{26}O_6Na^+$ $(M+Na)^+$, 373.1622; found 373.1626.

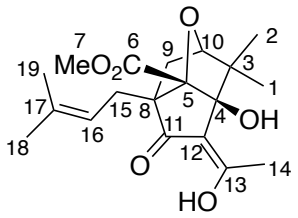

1.16

NMR Assignment. ^{1}H NMR (500 MHz, $CDCl_3$) δ 13.84 (s, 1 H, -OH), 5.15 (t, J = 7.2 Hz, 1 H, C16-H), 4.06 (d, J = 5.1 Hz, 1 H, C10-H), 3.78 (s, 3 H, C7-H), 2.37 (dd, J = 15.5, 7.2 Hz, 1 H, C15-H), 2.28 – 2.23 (m, 1 H, C15-H), 2.14 (s, 3 H, C14-H), 2.03 (d, J = 13.3 Hz, 1 H, C9-H), 1.80 (dd, J = 13.3, 5.1 Hz, 1 H, C9-H), 1.69 (s, 3 H, C18-H or C19-H), 1.58 (s, 3 H, C18-H or C19-H), 1.26 (s, 3 H, C1-H or C2-H), 0.94 (s, 3 H, C1-H or C2-H). ^{13}C NMR (126 MHz, $CDCl_3$) δ 205.2 (C11), 177.0 (C13), 168.7 (C6), 134.8 (C17), 118.6 (C16), 112.9 (C12), 100.7 (C5), 87.1 (C4), 85.9 (C10), 58.9 (C8), 52.6 (C7), 49.5 (C3), 37.8 (C9), 29.3 (C15), 26.1 (C18 or C19), 22.4 (C1 or C2), 20.7 (C1 or C2), 19.5 (C14), 18.0 (C18 or C19).

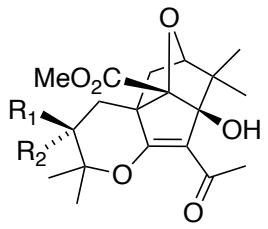

(±)-Melicolone A (**1.1**): R_1 = OH, R_2 = H
(±)-Melicolone B (**1.2**): R_1 = H, R_2 = OH

(±)-Melicolone A (1.1) and (±)-melicolone B (1.2). zw-4-meli13 and zw-4-meli14. A solution of **1.16** (30 mg, 0.086 mmol) in CH_2Cl_2 (1 mL) was added to a solution of *m*-chloroperbenzoic acid (MCPBA) (24 mg, 0.094 mmol) in CH_2Cl_2 (1 mL), and the solution was stirred at room temperature for 30 min. The reaction mixture was then transferred to a cooling bath at -40 ºC, whereupon (+)-camphor-10-sulfonic acid (2.0 mg, 0.0086 mmol) was added. The cooling bath was removed, and the solution was stirred at room temperature for 30 min. The reaction was quenched with Et_3N (0.5 mL), and then washed with Na_2CO_3 (3 x 1 mL), H_2O (3 x 1 mL) and brine (1 mL). The organic fraction was dried (Na_2SO_4), filtered and concentrated under reduced pressure to give crude mixture of **1** and **2** as colorless oil. The crude material was purified via preparative reverse phase HPLC using Eclipse XDB-C18 column (9.4 x 250 mm). HPLC purification gave 14 mg (44%) of (±)-melicolone A (**1.1**) and 13 mg (41%) of (±)-melicolone B (**1.2**), each as colorless oils. (±)-melicolone A (**1.1**) HRMS (ESI) *m*/*z* calcd for $C_{19}H_{27}O_7$ $(M+H)^+$, 367.1751; found 367.1757. (±)-melicolone B (**1.2**) HRMS (ESI) *m*/*z* calcd for $C_{19}H_{27}O_7$ $(M+H)^+$, 367.1751; found 367.1754.

HPLC purification of (±)-melicolone A (1.1) and (±)-melicolone B (1.2):

The crude mixture of (±)-melicolone A (**1.1**) and (±)-melicolone B (**1.2**) was purified via preparative reverse phase HPLC using Eclipse XDB-C18 column (9.4 x 250

mm). Gradient elution was used with MeCN/H_2O (0:100, *v*/*v*) at 0 min to MeCN/H_2O (30:70, *v*/*v*) at 25 min. (±)-melicolone A (**1**) was collected with a retention time of 20.197 min, and (±)-melicolone B (**2**) was collected with a retention time of 18.683 min.

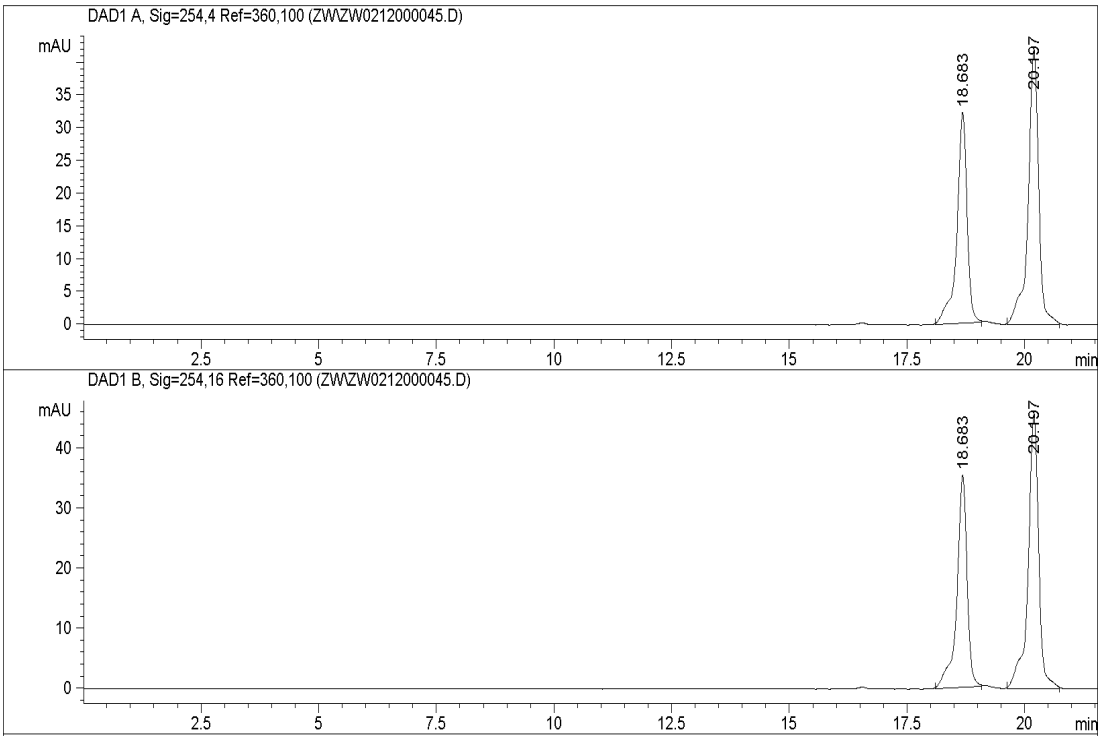

Figure 4.15. HPLC traces for the mixture of (±)-melicolone A (**1.1**) and (±)-melicolone B (**1.2**).

Comparison of natural and synthetic (±)-melicolones A and (±)-melicolones B

Table 4.1. Comparison of ^{1}H spectra for natural and synthetic (±)-melicolone A (**1.1**) in CD_3OD.

^{1}H NMR (δ in ppm, multiplicity, J in Hz)	
Synthetic (500 MHz)	Natural (500 MHz)
0.86 (s, 3 H)	0.86 (s, 3 H)
1.11 (s, 3 H)	1.11 (s, 3 H)
1.38 (s, 3 H)	1.38 (s, 3 H)
1.54 (s, 3 H)	1.54 (s, 3 H)
1.55 (dd, J = 12.2, 4.2 Hz, 1 H)a	1.56 (dd, J = 12.2, 4.5 Hz, 1 H)
1.65 (dd, J = 12.8, 5.3 Hz, 1 H)	1.65 (dd, J = 12.8, 5.2 Hz, 1 H)
1.98 (t, J = 12.2 Hz, 1 H)	1.98 (dd, J = 12.2, 12.2 Hz, 1 H)
2.37 (s, 3 H)	2.37 (s, 3 H)
2.41 (d, J = 12.8 Hz, 1 H)	2.41 (d, J = 12.8 Hz 1 H)
3.65 (dd, J = 12.2, 4.2 Hz, 1 H)	3.65 (dd, J = 12.2, 4.5 Hz, 1 H)
3.80 (s, 3 H)	3.80 (s, 3 H)
4.12 (d, J = 5.3 Hz, 1 H)	4.12 (d, J = 5.2 Hz, 1 H)

[a]The upfield d of the dd was partially obscured by the peak at δ 1.54 (s, 3 H).

Table 4.2. Comparison of ^{13}C spectra for natural and synthetic (±)-melicolone A (**1.1**) in CD_3OD.

^{13}C NMR (δ in ppm)	
Synthetic (126 MHz)	Natural (126 MHz)
19.8	19.7
20.8	20.8
23.2	23.2
27.3	27.3
30.4	30.4
34.6	34.6
42.6	42.6
49.3	49.3
52.4	52.4
53.3	53.3
69.8	69.8
85.9	85.9
88.5	88.5
91.5	91.5
102.1	102.1
117.8	117.7
169.1	169.1
171.3	171.3
199.1	199.2

Table 4.3. Comparison of ^{1}H NMR spectra for natural and synthetic (±)-melicolone A (**1.1**) in DMSO-d_6.

^{1}H NMR (δ in ppm, multiplicity, *J* in Hz)	
Synthetic (600 MHz)[a]	Natural (500 MHz)
0.79 (s, 3 H)	0.79 (s, 3 H)
1.02 (s, 3 H)	1.02 (s, 3 H)
1.30 (s, 3 H)	1.30 (s, 3 H)
1.45 (dd, J = 12.1, 4.2 Hz, 1 H)	1.45 (dd, J = 12.2, 4.5 Hz, 1 H)
1.48 (s, 3 H)	1.48 (s, 3 H)
1.57 (dd, J = 12.7, 5.3 Hz, 1 H)	1.57 (dd, J = 12.8, 5.2 Hz, 1 H)
1.84 (t, J = 12.1, 1 H)	1.84 (dd, J = 12.2, 12.2 Hz, 1 H)
2.30 (d, J = 12.1 Hz, 1 H)b	2.30 (d, J = 12.8 Hz, 1 H)
2.32 (s, 3 H)	2.32 (s, 3 H)
3.55 (ddd, J = 12.1, 4.3 Hz, 1 H)	3.55 (ddd, J = 12.2, 5.0, 4.5 Hz, 1 H)
3.71 (s, 3 H)	3.72 (s, 3 H)
4.09 (d, J = 5.1 Hz, 1 H)	4.10 (d, J = 5.2 Hz, 1 H)
5.02 (br, 0.25 H)	5.06 (br, 1 H)
	5.38 (d, J = 5.0 Hz, 1 H)

[a]The spectrum was obtained at 50 ºC. [b]The downfield peak of the d was partially obscured by the peak at δ 2.32 (s, 3 H).

Table 4.4. Comparison of ^{1}H spectra for natural and synthetic (±)-melicolone B (**1.2**) in CD_3OD.

^{1}H NMR (δ in ppm, multiplicity, *J* in Hz)	
Synthetic (500 MHz)	Natural (500 MHz)
0.89 (s, 3 H)	0.89 (s, 3 H)
1.10 (s, 3 H)	1.10 (s, 3 H)
1.43 (s, 3 H)	1.43 (s, 3 H)
1.50 (s, 3 H)	1.50 (s, 3 H)
1.64 (dd, J = 13.9, 6.9 Hz, 1 H)	1.63 (dd, J = 13.9, 6.9 Hz, 1 H)
1.83 (dd, J = 13.4, 5.3 Hz, 1 H)	1.83 (dd, J = 13.0, 5.2 Hz, 1 H)
2.23 (dd, J = 13.9, 3.4 Hz, 1 H)	2.23 (dd, J = 13.9, 3.4 Hz, 1 H)
2.38 (s, 3 H)	2.38 (s, 3 H)
2.52 (d, J = 13.4 Hz, 1 H)	2.52 (d, J = 13.0 Hz, 1 H)
3.77 (dd, J = 4.9, 3.4 Hz, 1 H)	3.77 (dd, J = 4.9, 3.4 Hz, 1 H)
3.79 (s, 3 H)	3.79 (s, 3 H)
4.07 (d, J = 5.2 Hz, 1 H)	4.07 (d, J = 5.2 Hz, 1 H)

Table 4.5. Comparison of ^{13}C spectra for natural and synthetic (±)-melicolone B (**1.2**) in CD_3OD.

^{13}C NMR (δ in ppm)	
Synthetic (126 MHz)	Natural (126 MHz)
19.8	19.8
23.2	23.2
24.4	24.3
26.9	26.9
30.5	30.5
33.9	34.0
45.0	45.0
49.3	49.2
49.5	49.3
52.4	52.3
69.8	69.8
85.6	85.6
88.8	88.7
91.1	91.2
103.5	103.5
117.5	117.4
169.3	169.3
173.4	173.3
199.2	199.2

Representative procedure for the enantioselective 1,3-dipolar cycloadditions:

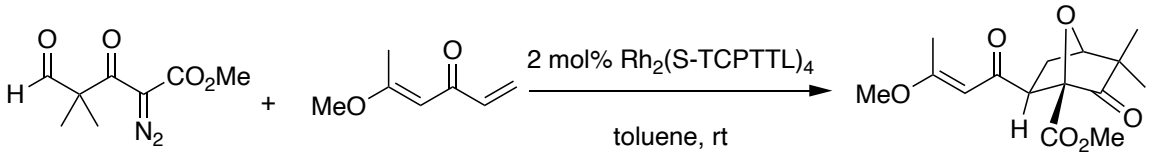

1.20 (1 eq) + **1.18** (1.2 eq) → **1.81** 38%, 15% ee

A solution of **1.20** (20 mg, 0.10 mmol), **1.18** (15mg, 0.12 mmol) and Rh_2(S-TCPTTL)$_4$ (3.6 mg, 0.0020 mmol) in toluene (1 mL) was stirred at room temperature overnight. The solvent was removed under reduced pressure. The residue was dissolved in CH_2Cl_2 (1 mL), which was washed with H_2O (3 x 1 mL) and brine (1 mL). The solution was dried (Na_2SO_4), filtered and concentrated under reduced pressure to give crude mixture of **1.81** as yellow oil. The crude material was purified via flash column chromatography eluting hexanes : EtOAc (8:1) to give 11 mg (38%) of **1.81** as white solid.

HPLC traces for enantioenriched 1.81

Chiralcel OD-H: *i*-PrOH/hexane (20:80, v/v) 1.0 mL/min, obs:254 nm

Racemic (±)-**1.81**:

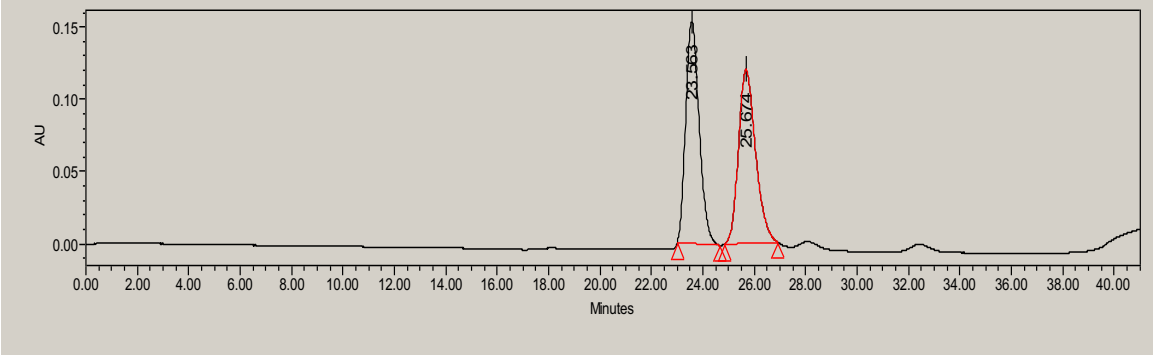

	Retention time (min)	Area (μV*sec)	% area	Height (μV)	Int Type
1	23.563	5574770	50.11	153355	bb
2	25.674	5549787	49.89	120405	bb

Enantioenriched **1.81**:

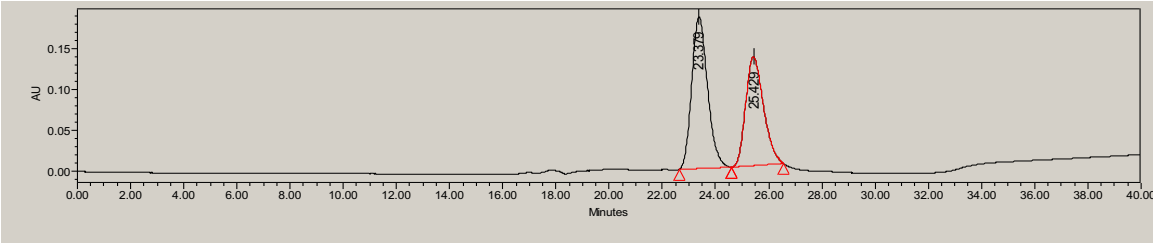

	Retention time (min)	Area (μV*sec)	% area	Height (μV)	Int Type
1	23.379	7696480	57.66	185663	bb
2	25.429	565237	42.34	128292	bb

4.3 EXPERIMENTAL PROCEDURES FOR CHAPTER 3

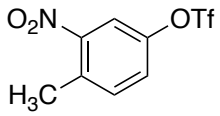

3.8

3-Methyl-4-nitrophenyl trifluoromethanesulfonate (3.8). az-1-002. A solution of **3.7** (2.00 g, 13.1 mmol) in pyridine (1.58 mL, 19.6 mmol) and CH_2Cl_2 (60 mL) was cooled to 0 ºC. Triflic anhydride (3.68 g, 15.7 mmol) was added dropwise over 10 min. The ice water bath was then removed, and the solution was stirred at room temperature for 3 h. Saturated $NaHCO_3$ (30 mL) was added, and the mixture was extracted with CH_2Cl_2 (3 x 30 mL). The combined organic fraction was successively washed with water (3 x 30 mL) and brine (3 x 30 mL). The organic fraction was dried (Na_2SO_4), filtered, and concentrated *in vacuo* to give 3.70 g (~100%) crude **3.8** as a viscous oil (95% pure). The crude material was directly used to carry out the next step without further purification. ^{1}H NMR (400 MHz, $CDCl_3$) δ 8.11 – 7.84 (d, J = 2.16 Hz, 1 H), 7.56 – 7.35 (comp, 2 H), 2.65 (s, 3 H). ^{13}C NMR (126 MHz, $CDCl_3$) δ 149.2, 147.1, 134.6, 134.4, 126.0, 119.9, 118.1, 117.4, 20.2. IR (CH_2Cl_2) ν_{max} 1533, 1426, 1350, 1208, 1136, 937, 850, 732 cm^{-1}. HRMS (CI), *m/z* calculated for $C_8H_7NO_5F_3S^+$ $(M+H)^+$, 285.9997; found 285.9995.

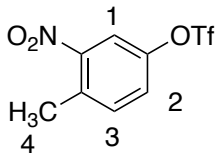

3.8

NMR Assignment. ^{1}H NMR (400 MHz, $CDCl_3$) δ 8.11 – 7.84 (d, J = 2.16 Hz, 1 H, C1-H), 7.56 – 7.35 (comp, 2 H, C2-H, C3-H), 2.65 (s, 3 H, C4-H).

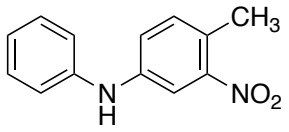

3.9

3-Methyl-4-nitro-N-phenylaniline (3.9). az-3-1213-3. Aniline (0.372 mL, 4.09 mmol) was added to the solution of **3.8** (1.06 g, 3.72 mmol), $Pd(OAc)_2$ (41.6 mg, 0.186 mmol), Cs_2CO_3 (1.44 g, 4.46 mmol), and X-Phos (88.5 mg, 0.186 mmol) in toluene (30 mL) under N_2. The solution was stirred at 100 °C for 2 h. The solution was cooled to room temperature and diluted with CH_2Cl_2 (30 mL). The solution was successively washed with water (3 x 30 mL) and brine (3 x 30 mL). The organic fractions were dried (Na_2SO_4), filtered, and concentrated *in vacuo* to give crude **3.9** as a dark brown syrup. The crude material was purified via flash column chromatography eluting with hexanes : EtOAc (8:1) to give 797 mg (94%) **3.9** as an orange solid. ^{1}H NMR (400 MHz, $CDCl_3$) δ 7.65 (d, J = 2.2 Hz, 1 H), 7.35 – 7.29 (comp, 2 H), 7.19 (dt, J = 8.3, 0.6 Hz, 1 H), 7.15 (dd, J = 8.3, 2.2 Hz, 1 H), 7.10 – 7.07 (comp, 2 H, C1-H), 7.05 – 6.99 (m, 1 H), 2.51 (s, 3 H). ^{13}C NMR (126 MHz, $CDCl_3$) δ 149.7, 142.5, 141.6, 133.5, 129.7, 124.5, 122.5, 121.5, 118.9, 112.2, 19.8. IR (CH_2Cl_2) ν_{max} 3393, 1522, 1495, 1316, 745 cm^{-1}. HRMS (CI) *m/z* calculated for $C_{13}H_{12}N_2O_2^{\bullet+}$ M$^{\bullet+}$, 228.0899; found 228.0900.

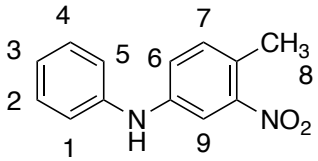

3.9

NMR Assignment. ^{1}H NMR (400 MHz, $CDCl_3$) δ 7.65 (d, J = 2.2 Hz, 1 H, C9-H), 7.35 – 7.29 (comp, 2 H, C2-H, C4-H), 7.19 (dt, J = 8.3, 0.6 Hz, 1 H, C7-H), 7.15 (dd, J = 8.3, 2.2 Hz, 1 H, C6-H), 7.10 – 7.07 (comp, 2 H, C1-H, C5-H), 7.05 – 6.99 (m, 1 H, C3-H), 2.51 (s, 3 H, C8-H).

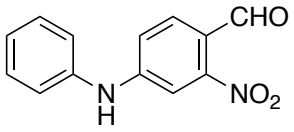

3.17

2-Nitro-4-(phenylamino)benzaldehyde (3.17). az-2-218. DMF-DMA (947 mg, 7.97 mmol) and pyrrolidine (566 g, 7.97 mmol) were added to a solution of **3.9** (900 mg, 3.98 mmol) in DMF (20 mL) under N_2. The solution was heated at 135 ºC for 3 h. The mixture was added to a solution of $NaIO_4$ (1.69 g, 7.97 mmol) in water (20 mL) and DMF (20 mL) at 0 ºC. The solution was stirred at room temperature for 3 h, and diluted with CH_2Cl_2 (50 mL). The mixture was filtered and washed with water (3 x 50 mL) and brine (3 x 50 mL). The organic fraction was dried (Na_2SO_4), filtered, and concentrated *in vacuo* to give crude **3.17** as a dark brown syrup. The crude material was purified via flash column chromatography eluting with hexanes : EtOAc (6:1) to give 828 mg (86%) **3.17** as a red solid. ^{1}H NMR (500 MHz, $CDCl_3$) δ 10.12 (s, 1 H), 7.84 (d, J = 8.6 Hz, 1 H), 7.38 – 7.33 (comp, 3 H), 7.17 – 7.12 (comp, 3 H), 7.08 (dd, J = 8.6, 2.3 Hz, 1 H), 6.37 (s, 1 H). ^{13}C NMR (126 MHz, $CDCl_3$) δ 186.4, 152.5, 149.8, 138.7, 131.6, 130.0, 125.5, 122.3, 120.9, 117.7, 108.7. HRMS (ESI) *m/z* calculated for $C_{13}H_{11}N_2O_3^+$ $(M+H)^+$, 243.0764; found 243.0766.

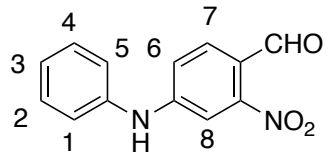

3.17

NMR Assignment. ^{1}H NMR (500 MHz, $CDCl_3$) δ 10.12 (s, 1 H, CHO-H), 7.84 (d, *J* = 8.6 Hz, 1 H, C8-H), 7.38 – 7.33 (comp, 3 H, C2, C4, C7-H), 7.17 – 7.12 (comp, 3 H, C1, C3, C5-H,), 7.08 (dd, *J* = 8.6, 2.3 Hz, 1 H, C6-H), 6.37 (s, 1 H, N-H).

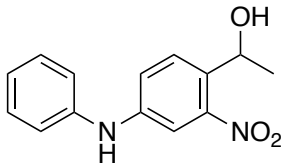

3.18

1-(2-Nitro-4-(phenylamino)phenyl)ethan-1-ol (3.18). az-3-1212-4. $Al(CH_3)_3$ (3.60 mL, 5.86 mmol) was added slowly to a solution of **3.17** (710 mg, 2.93 mmol) in CH_2Cl_2 (30 mL) under N_2 at 0 ºC. The solution was stirred at 0 ºC for 1 h. 1 M aq. NaOH (15 mL) was slowly added, and the mixture was stirred for another 30 min. The solution was extracted with CH_2Cl_2 (3 x 30 mL). The organic fraction was washed with H_2O (3 x 30 mL) and brine (30 mL), then dried (Na_2SO_4) and concentrated *in vacuo* to give crude **3.18** as a brown syrup. The crude material was purified via flash column chromatography eluting with hexanes : EtOAc (5:1) to give 672mg (89%) **3.18** as a viscous brown oil. ^{1}H NMR (400 MHz, $CDCl_3$) δ 7.62 (d, *J* = 8.6 Hz, 1 H), 7.49 (d, *J* = 2.4 Hz, 1 H), 7.36 – 7.28 (comp, 2 H), 7.22 (dd, *J* = 8.6, 2.4 Hz, 1 H), 7.12 – 7.09 (comp, 2 H), 7.05 (td, *J* = 7.3, 1.1 Hz, 1 H), 5.91 (s, 1 H), 5.28 (q, *J* = 6.4 Hz, 1 H), 1.54 (d, *J* = 6.4 Hz, 3 H). ^{13}C NMR (126 MHz, $CDCl_3$) δ 149.0, 144.0, 141.1, 131.7, 129.8, 128.7, 123.3, 121.2, 119.8, 110.9, 65.4, 24.0. HRMS (ESI) *m/z* calculated for $C_{14}H_{14}N_2O_3Na^+$ $(M+Na)^+$, 281.0897; found 281.0903.

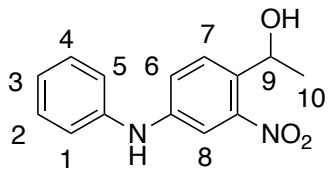

3.18

NMR Assignment. ^{1}H NMR (400 MHz, $CDCl_3$) δ 7.62 (d, *J* = 8.6 Hz, 1 H, C7-H), 7.49 (d, *J* = 2.4 Hz, 1 H, C8-H), 7.36 – 7.28 (comp, 2 H, C1, C5-H), 7.22 (dd, *J* = 8.6, 2.5 Hz, 1 H, C6-H), 7.12 – 7.09 (comp, 2 H, C3, C4-H), 7.05 (td, *J* = 7.3, 1.1 Hz, 1 H, C2-H), 5.91 (s, 1 H, N-H), 5.28 (q, *J* = 6.4 Hz, 1 H, C9-H), 1.54 (d, *J* = 6.4 Hz, 3 H, C10-H).

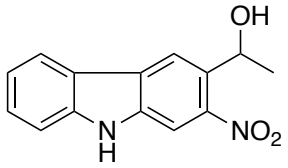

3.5

1-(2-Nitro-9H-carbazol-3-yl)ethan-1-ol (3.5). az-4-cage1. The solution of **3.18** (700 mg, 2.71 mmol), $Pd(OAc)_2$ (30.1 mg, 0.136 mmol), $Cu(OAc)_2$ (981 mg, 5.42 mmol) in PivOH (15 mL) was heated at 110 ºC under O_2 for 24 h. The solution was cooled to room temperature and diluted with CH_2Cl_2 (15 mL). The solution was filtered by vacuum filtration, and saturated $NaHCO_3$ (100 mL) was slowly added to neutralize the solution. The mixture was washed with brine (3 x 50 mL). The organic fraction was dried (Na_2SO_4), filtered, and concentrated *in vacuo* to give crude **3.5** as a dark brown syrup. The crude material was purified via flash column chromatography eluting with hexanes : EtOAc (4:1) to give 270 mg (40%) **3.5** as a brown oil. ^{1}H NMR (400 MHz, $CDCl_3$) δ 8.47 (br, 1 H), δ 8.44 (s, 1 H), 8.12 (ddd, *J* = 7.9, 1.4, 0.8 Hz, 1 H), 8.04 (s, 1 H), 7.58 – 7.45 (comp, 2 H), 7.31 (ddd, *J* = 7.9, 6.8, 1.1 Hz, 1 H), 5.56 (q, *J* = 6.3 Hz, 1 H), 1.69 (d, *J* = 6.3 Hz, 3 H). ^{13}C NMR (126 MHz, $CDCl_3$) δ 146.0, 141.9, 137.4, 132.6, 130.0, 128.3, 127.8, 122.2,

121.7, 121.6, 120.8, 118.9, 111.4, 107.6, 66.2, 29.8, 24.6. HRMS (ESI) *m/z* calculated for $C_{14}H_{12}N_2O_3Na^+$ $(M+Na)^+$, 279.0740; found 279.0742.

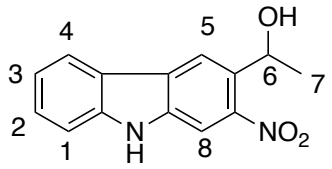

3.5

NMR Assignment. ^{1}H NMR (400 MHz, $CDCl_3$) δ 8.47 (br, 1H, N-H), δ 8.44 (s, 1H, C8-H), 8.12 (ddd, *J* = 7.9, 1.4, 0.8 Hz, 1H, C1-H), 8.04 (s, 1H, C5-H), 7.58 – 7.45 (comp, 2H, C3-H, C4-H), 7.31 (ddd, *J* = 7.9, 6.8, 1.1 Hz, 1H, C2-H), 5.56 (q, *J* = 6.3 Hz, 1H, C6-H), 1.69 (d, *J* = 6.3 Hz, 3H, C7-H).

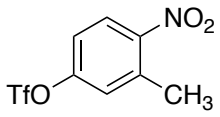

3.21

3-Methyl-4-nitrophenyl trifluoromethanesulfonate (3.21). az-0201-3. A solution of **3.20** (2.00 g, 13.1 mmol) in pyridine (2.64 mL, 19.7 mmol) and CH_2Cl_2 (60 mL) was cooled to 0 ºC. Triflic anhydride (3.68 g, 15.7 mmol) was added dropwise over 10 min. The ice water bath was then removed, and the solution was stirred at room temperature for 3 h. Saturated $NaHCO_3$ (30 mL) was added, and the mixture was extracted with CH_2Cl_2 (3 x 30 mL). The combined organic fraction was successively washed with water (3 x 30 mL) and brine (3 x 30 mL). The organic fraction was dried (Na_2SO_4), filtered, and concentrated *in vacuo* to give 3.70 g (~100%) crude **3.21** as a viscous oil (95% pure).

The crude material was directly used to carry out the next step without further purification. ^{1}H NMR (400 MHz, $CDCl_3$) δ 8.17 – 7.96 (d, *J* = 9.7 Hz, 1 H), 7.30-7.26 (comp, 2 H), 2.66 (s, 3 H). ^{13}C NMR (126 MHz, $CDCl_3$) δ 151.3, 148.3, 137.0, 127.1, 125.4, 119.9, 117.4, 20.6. IR (DCM) 1530, 1427, 1210, 1133, 946, 814. HRMS (CI) m/z calculated for $C_8H_7NO_5F_3S^+$ $(M+H)^+$, 285.9997; found 285.9998.

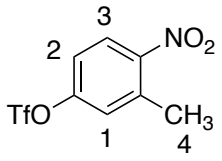

3.21

NMR Assignment ^{1}H NMR (400 MHz, $CDCl_3$) δ 8.17 – 7.96 (d, *J* = 9.7 Hz, 1 H, C3-H), 7.30-7.26 (comp, 2 H, C1-H, C2-H), 2.66 (s, 3 H, C4-H).

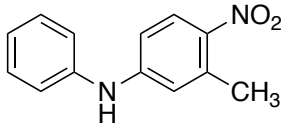

3.22

3-Methyl-4-nitro-N-phenylaniline (3.22). az-0201-1. Aniline (717 mg, 7.71 mmol) was added to the solution of **3.21** (2.00 g, 7.01 mmol), $Pd(OAc)_2$ (157 mg, 0.701 mmol), Cs_2CO_3 (2.74 g, 8.41 mmol), and X-Phos (500 mg, 1.05 mmol) in toluene (70 mL) under N_2. The solution was stirred at 100 ºC for 2 h. The solution was cooled to room temperature and diluted with CH_2Cl_2 (30 mL). The solution was successively washed with water (3 x 30 mL) and brine (3 x 30 mL). The organic fractions were dried (Na_2SO_4), filtered, and concentrated *in vacuo* to give crude **3.22** as a dark brown syrup. The crude material was purified via flash column chromatography eluting with hexanes : EtOAc (8:1) to give 1.55 g (97%) **3.22** as a yellow solid. ^{1}H NMR (400 MHz, $CDCl_3$) δ 8.07 (d, *J* = 9.0

Hz, 1 H, C7-H), 7.38 (dd, *J* = 8.5, 7.4 Hz, 2 H), 7.19 (dt, *J* = 7.4, 1.1 Hz, 2 H), 7.17 – 7.11 (m, 1 H), 6.82 (dd, *J* = 9.0, 2.6 Hz, 1 H), 6.78 – 6.76 (d, *J* = 2.6 Hz, 1 H), 6.16 (s, 1 H), 2.61 (s, 3 H). ^{13}C NMR (126 MHz, $CDCl_3$) δ 148.8, 140.3, 139.4, 137.7, 129.7, 128.1, 124.3, 121.7, 117.2, 112.1, 22.3. IR (CH_2Cl_2) ν_{max} 3330, 1576, 1273, 1254, 1076, 747 cm^{-1}. HRMS (CI) *m/z* calculated for $C_{13}H_{13}N_2O_2^+$ $(M+H)^+$, 229.0977; found 229.0971.

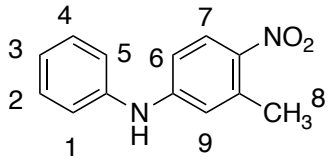

3.22

NMR Assignment. ^{1}H NMR (400 MHz, $CDCl_3$) δ 8.07 (d, *J* = 9.0 Hz, 1 H, C7-H), 7.38 (dd, *J* = 8.5, 7.4 Hz, 2 H, C2-H, C4-H), 7.19 (dt, *J* = 7.4, 1.1 Hz, 2 H, C1-H, C5-H), 7.17 – 7.11 (m, 1 H, C3-H), 6.82 (dd, *J* = 9.0, 2.6 Hz, 1 H, C6-H), 6.78 – 6.76 (d, *J* = 2.6 Hz, 1 H, C9-H), 6.16 (s, 1 H, N-H), 2.61 (s, 3 H, C8-H).

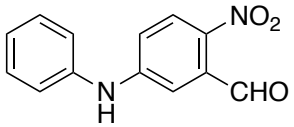

3.23

2-Nitro-5-(phenylamino)benzaldehyde (3.23). az-2-209. DMF-DMA (3.30 g, 27.4 mmol) and pyrrolidine (1.91 g, 27.4 mmol) were added to a solution of **3.22** (3.10 g, 13.7 mmol) in DMF (70 mL) under N_2. The solution was heated at 135 ºC for 3 h. The mixture was added to a solution of $NaIO_4$ (5.84 g, 27.4 mmol) in water (30 mL) and DMF (30 mL) at 0 ºC. The solution was stirred at room temperature for 3 h, and diluted with CH_2Cl_2 (100 mL). The mixture was filtered and washed with water (3 x 100 mL) and brine

(3 x 100 mL). The organic fraction was dried (Na_2SO_4), filtered, and concentrated *in vacuo* to give crude **3.23** as a dark brown syrup. The crude material was purified via flash column chromatography eluting with hexanes : EtOAc (6:1) to give 2.66 g (80%) **3.23** as a yellow solid. ^{1}H NMR (500 MHz, $CDCl_3$) δ 10.43 (s, 1 H), 8.03 (d, J = 9.0 Hz, 1 H), 7.35 (t, J = 7.8 Hz, 2 H), 7.17 – 7.11 (m, 4 H), 7.02 (dd, J = 9.0, 2.7 Hz, 1 H), 6.38 (s, 1 H). ^{13}C NMR (126 MHz, $CDCl_3$) δ 189.4, 150.1, 139.7, 138.7, 135.3, 130.0, 127.8, 125.5, 122.4, 116.1, 113.7. HRMS (ESI) *m/z* calculated for $C_{13}H_{11}N_2O_3^+$ $(M+H)^+$, 243.0764; found 243.0767.

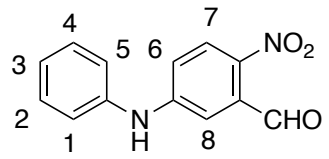

3.23

NMR Assignment. ^{1}H NMR (500 MHz, $CDCl_3$) δ 10.43 (s, 1 H, CHO-H), 8.03 (d, J = 9.0 Hz, 1 H, C7-H), 7.35 (t, J = 7.8 Hz, 2 H, C2, C4-H), 7.17 – 7.11 (m, 4 H, C1, C3, C5, C8-H), 7.02 (dd, J = 9.0, 2.7 Hz, 1 H, C6-H), 6.38 (s, 1 H, N-H).

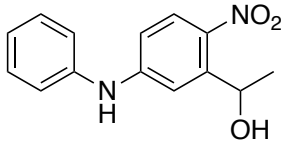

3.24

1-(2-Nitro-5-(phenylamino)phenyl)ethan-1-ol (3.24). az-4-0506. $Al(CH_3)_3$ (12.4 mL, 24.8 mmol) was added slowly to a solution of **3.23** (3.00 mg, 12.4 mmol) in CH_2Cl_2 (60 mL) under N_2 at 0 °C. The solution was stirred at 0 ºC for 1 h. 1M aq. NaOH (30 mL) was slowly added, and the mixture was stirred for another 30 min. The solution was extracted with CH_2Cl_2 (3 x 30 mL). The organic fraction was washed with H_2O (3 x 30

mL) and brine (30 mL), then dried (Na_2SO_4) and concentrated *in vacuo* to give crude **3.24** as a brown syrup. The crude material was purified via flash column chromatography eluting with hexanes : EtOAc (4:1) to give 2.88 g (90%) **3.24** as a viscous brown oil. ^{1}H NMR (500 MHz, $CDCl_3$) δ 7.96 (d, J = 9.1 Hz, 1 H), 7.32 (t, J = 7.7 Hz, 2 H), 7.22 (d, J = 2.6 Hz, 1H), 7.16 – 7.12 (comp, 2 H), 7.09 (t, J = 7.4 Hz, 1 H), 6.82 (dd, J = 9.1, 2.6 Hz, 1 H), 6.26 (s, 1 H), 5.51 (q, J = 6.3 Hz, 1 H), 1.48 (d, J = 6.3 Hz, 3 H). ^{13}C NMR (126 MHz, $CDCl_3$) δ 149.8, 145.2, 139.7, 138.8, 129.9, 128.5, 124.7, 121.9, 112.5, 66.4, 24.1. HRMS (ESI) *m/z* calculated for $C_{14}H_{14}N_2O_3Na^+$ $(M+Na)^+$, 281.0897; found 281.0898.

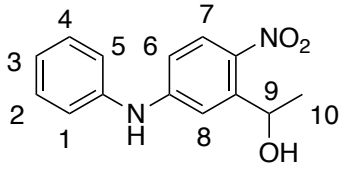

3.24

NMR Assignment. ^{1}H NMR (500 MHz, $CDCl_3$) δ 7.96 (d, J = 9.1 Hz, 1 H, C7-H), 7.32 (t, J = 7.7 Hz, 2 H, C2, C4-H), 7.22 (d, J = 2.6 Hz, 1 H, C8-H), 7.16 – 7.12 (comp, 2 H, C1, C5-H), 7.09 (t, J = 7.4 Hz, 1 H, C3-H), 6.82 (dd, J = 9.1, 2.6 Hz, 1 H, C6-H), 6.26 (s, 1 H, N-H), 5.51 (q, J = 6.3 Hz, 1 H, C9-H), 1.48 (d, J = 6.3 Hz, 3 H, C10-H).

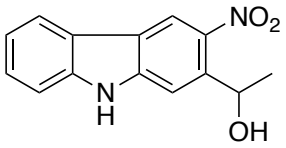

3.6

1-(3-Nitro-9H-carbazol-2-yl)ethan-1-ol (3.6). az-3-0102-cage2. The solution of **3.24** (800 mg, 3.10 mmol), $Pd(OAc)_2$ (35.1 mg, 0.157 mmol), $Cu(OAc)_2$ (1.12 g, 6.20 mmol) in PivOH (15 mL) was heated at 110 ºC under O_2 for 24 h. The solution was cooled to room temperature and diluted with CH_2Cl_2 (15 mL). The solution was filtered by vacuum

filtration, and saturated $NaHCO_3$ (100 mL) was slowly added to neutralize the solution. The mixture was washed with brine (3 x 50 mL). The organic fraction was dried (Na_2SO_4), filtered, and concentrated *in vacuo* to give crude **3.6** as a dark brown syrup. The crude material was purified via flash column chromatography eluting with hexanes : EtOAc (4:1) to give 333 mg (42%) **3.6** as a brown oil. ^{1}H NMR (400 MHz, $CDCl_3$) δ 8.74 (s, 1 H), 8.04 (dt, *J* = 7.9, 1.1 Hz, 1 H), 7.79 (s, 1 H), 7.49 (ddd, *J* = 7.9, 6.7, 1.1 Hz, 1 H), 7.45 (ddd, *J* = 7.9, 1.5, 0.9 Hz, 1 H), 7.31 (ddd, *J* = 7.9, 6.7, 1.5 Hz, 1 H), 5.68 (q, *J* = 6.3 Hz, 1 H), 1.62 (d, *J* = 6.3 Hz, 3 H). ^{13}C NMR (101 MHz, $CDCl_3$) δ 140.8, 127.7, 121.2, 121.1, 118.9, 111.5, 108.5, 66.6, 24.6. HRMS (ESI) *m/z* calculated for $C_{14}H_{12}N_2O_3Na^+$ $(M+Na)^+$, 279.0740; found 279.0744.

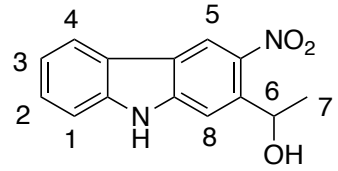

3.6

NMR Assignment .^{1}H NMR (400 MHz, $CDCl_3$) δ 8.74 (s, 1 H, C5-H), 8.04 (dt, *J* = 7.9, 1.1 Hz, 1 H, C4-H), 7.79 (s, 1 H, C8-H), 7.49 (ddd, *J* = 7.9, 6.7, 1.1 Hz, 1 H, C2-H), 7.45 (ddd, *J* = 7.9, 1.5, 0.9 Hz, 1 H, C1-H), 7.31 (ddd, *J* = 7.9, 6.7, 1.5 Hz, 1 H, C3-H), 5.68 (q, *J* = 6.3 Hz, 1 H, C6-H), 1.62 (d, *J* = 6.3 Hz, 3 H, C7-H).

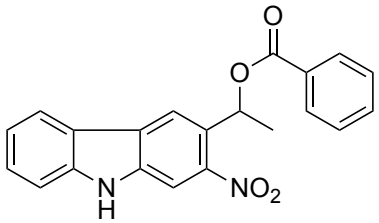

3.29

1-(2-Nitro-9H-carbazol-3-yl)ethyl benzoate (3.29). az-4-cage1ba. A solution of **3.5** (20 mg, 0.077 mmol), benzoic acid (9.4 mg, 0.077 mmol), 4-dimethylaminopyridine (0.94 mg, 0.0077 mmol) and N,N'-dicyclohexylcarbodiimide (17 mg, 0.092 mmol) in CH_2Cl_2 (1 mL) was stirred at room temperature in dark for 2 h where upon water was added, and the solution was diluted with EtOAc (1 mL), and washed with citric acid (3 x 1 mL), H_2O (3 x 1 mL) and brine (3 x 1 mL). The organic fraction was dried (Na_2SO_4) and concentrated *in vacuo* to give crude **3.29** as orange solid. The crude material was purified via flash column chromatography eluting with hexanes : EtOAc (8:1) to give 17 mg (62%) **3.29** as an orange solid. ^{1}H NMR (400 MHz, $CDCl_3$) δ 8.98 (s, 1 H), 8.33 (s, 1 H), 8.15 (s, 1 H), 8.12 – 8.08 (m, 3 H), 7.60 – 7.55 (m, 1 H), 7.51 – 7.49 (m, 2 H), 7.49 – 7.43 (m, 2 H), 7.30 – 7.26 (m, 1 H), 6.73 (q, *J* = 6.4 Hz, 1 H), 1.90 (d, *J* = 6.4 Hz). ^{13}C NMR (126 MHz, $CDCl_3$) δ 133.2, 130.4, 129.8, 128.6, 128.4, 122.1, 121.6, 120.8, 118.6, 111.4, 107.6, 69.6, 29.9, 22.9. HRMS (ESI) *m/z* calculated for $C_{21}H_{16}N_2O_4Na^+$ $(M+Na)^+$, 383.1002; found 383.1005.

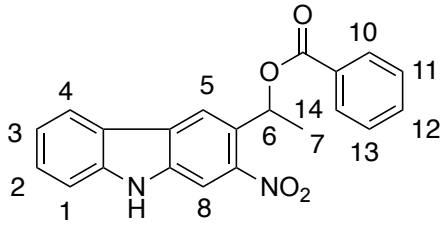

3.29

NMR Assignment. ^{1}H NMR (400 MHz, $CDCl_3$) δ 8.98 (s, 1 H, N-H), 8.33 (s, 1 H, C8-H), 8.15 (s, 1 H, C5-H), 8.12 – 8.08 (m, 3 H, C1-H, C2-H, C4-H), 7.60 – 7.55 (m, 1 H, C12-H), 7.51 – 7.49 (m, 2 H, C10-H, C14-H), 7.49 – 7.43 (m, 2 H, C11-H, C13-H), 7.30 – 7.26 (m, 1 H, C3-H), 6.73 (q, *J* = 6.4 Hz, 1 H, C6-H), 1.90 (d, *J* = 6.4 Hz, 3 H, C7-H).

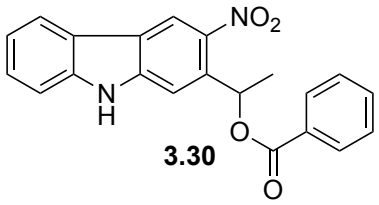

1-(3-Nitro-9H-carbazol-2-yl)ethyl benzoate (3.30). az-3-1219-2. A solution of **3.6** (20 mg, 0.077 mmol), benzoic acid (9.4 mg, 0.077 mmol), 4-dimethylaminopyridine (0.94 mg, 0.0077 mmol) and N,N'-dicyclohexylcarbodiimide (17 mg, 0.092 mmol) in CH_2Cl_2 (1 mL) was stirred at room temperature in dark for 2 h where upon water (1 mL) was added, and the solution was diluted with EtOAc (1 mL), and washed with citric acid (3 x 1 mL), H_2O (3 x 1 mL) and brine (3 x 1 mL). The organic fraction was dried (Na_2SO_4) and concentrated *in vacuo* to give crude **3.30** as a yellow solid. The crude material was purified via flash column chromatography eluting with hexanes : EtOAc (8:1) to give 18 mg (65%) **3.30** as a yellow solid. ^{1}H NMR (400 MHz, $CDCl_3$) δ 8.62 (s, 1 H), 8.41 (s, 1 H), 8.12 - 8.08 (comp, 2 H), 7.91 (ddt, *J* = 7.9, 1.3, 0.7 Hz, 1 H), 7.66 – 7.60 (m, 1 H), 7.53 – 7.46 (comp, 3 H), 7.40 (s, 1 H) 7.36 (dt, *J*= 8.1, 0.8 Hz, 1 H), 7.29 (ddd, *J* = 8.1, 7.2, 1.0 Hz, 1 H), 6.80 (q, *J* = 6.4 Hz, 1 H), 1.79 (d, *J* = 6.4 Hz, 3 H). ^{13}C NMR (126 MHz, $CDCl_3$) δ 165.4, 142.1, 140.6, 137.4, 133.2, 130.2, 129.7, 128.5, 127.6, 122.8, 122.4, 121.1, 121.0, 118.8, 111.2, 107.7, 69.9, 29.7, 22.7. HRMS (ESI) *m/z* calculated for $C_{21}H_{16}N_2O_4Na^+$ $(M+Na)^+$, 383.1002; found 383.1005.

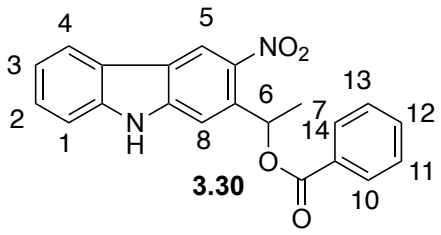

NMR Assignment. ^{1}H NMR (400 MHz, $CDCl_3$-d) δ 8.62 (s, 1 H, C5-H), 8.41 (s, 1 H, N-H), 8.12 - 8.08 (comp, 2 H, C10-H, C14-H), 7.91 (ddt, *J* = 7.9, 1.3, 0.7 Hz, 1 H, C4-H), 7.66 – 7.60 (m, 1 H, C12-H), 7.53 – 7.46 (comp, 3 H, C1-H, C11-H, C13-H), 7.40 (s, 1 H, C8-H) 7.36 (dt, *J*= 8.1, 0.8 Hz, 1 H, C2-H), 7.29 (ddd, *J* = 8.1, 7.2, 1.0 Hz, 1 H, C3-H), 6.80 (q, *J* = 6.4 Hz, 1 H, C6-H), 1.79 (d, *J* = 6.4 Hz, 3 H, C7-H).

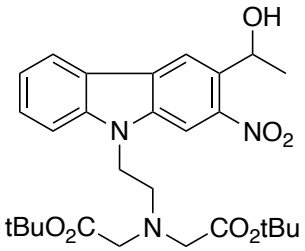

3.39

Di-tert-butyl 2,2'-((2-(3-(1-hydroxyethyl)-2-nitro-9H-carbazol-9-yl)ethyl)azanediyl)diacetate (3.39). az-3-cage1nr. NaH (35.2 mg, 0.881 mmol) was added to a solution of **3.5** (150 mg, 0.587 mmol) in DMF (5 mL) at 0ºC. The solution was stirred at room temperature for 30 min, whereupon **3.38** (206 mg, 0.587 mmol) was slowly added to the solution at 0ºC. The solution was stirred for overnight. The mixture was concentrated in *vacuo* and then it was diluted with CH_2Cl_2 (10 mL), washed with water (15 mL X 3) and brine (15 mL), dried (Na_2SO_4), filtered, and concentrated *in vacuo* to give crude **3.39** as a viscous dark oil. The crude material was purified via flash column chromatography eluting with hexanes : ethyl acetate (8:1) to give 222 mg (73 %) of **3.39** as a yellow oil. ^{1}H NMR (400 MHz, $CDCl_3$) δ 8.46 (s, 1 H), 8.18 (s, 1 H), 8.17 – 8.13 (m, 1 H), 7.56 (d, *J* = 3.8 Hz, 2 H), 7.31 (dt, *J* = 8.0, 4.0 Hz, 1 H), 5.56 (q, *J* = 6.2 Hz, 1 H), 4.58 (t, *J* = 7.3 Hz, 2 H), 3.46 (s, 4 H), 3.14 (t, *J* = 7.3 Hz, 2 H), 1.70 (d, *J* = 6.3 Hz, 3 H), 1.45 (s, 18 H). ^{13}C NMR (500 MHz, $CDCl_3$) δ 170.5, 146.0, 142.7, 138.5, 131.6, 128.0, 126.9, 121.7, 121.5, 120.2, 118.7, 109.5, 105.9, 81.5, 66.0, 57.2, 52.6, 43.2, 28.1, 24.4.

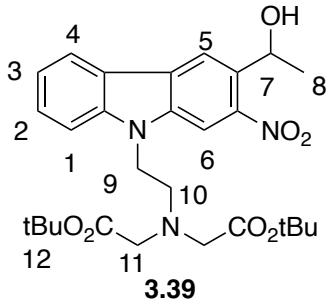

3.39

NMR Assignment. ^{1}H NMR (400 MHz, $CDCl_3$) δ 8.46 (s, 1 H, C6-H), 8.18 (s, 1 H, C5-H), 8.17 – 8.13 (m, 1 H, C1-H), 7.56 (d, *J* = 3.8 Hz, 2 H, C3-H, C4-H), 7.31 (dt, *J* = 8.0, 4.0 Hz, 1 H, C2-H), 5.56 (q, *J* = 6.2 Hz, 1 H, C7-H), 4.58 (t, *J* = 7.3 Hz, 2 H, C9-H), 3.46 (s, 4 H, C11-H), 3.14 (t, *J* = 7.3 Hz, 2 H, C10-H), 1.70 (d, *J* = 6.3 Hz, 3 H, C8-H), 1.45 (s, 18 H, C12-H).

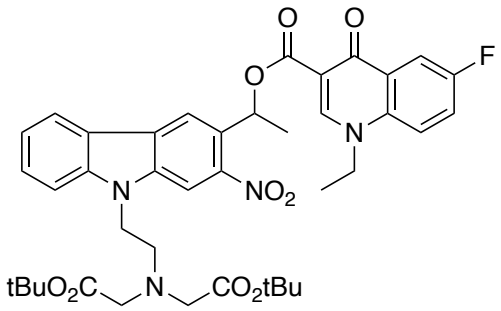

3.48

Di-*tert*-butyl 2,2'-((2-(3-(1-((1-ethyl-6-fluoro-4-oxo-1,4-dihydroquinoline-3-carbonyl)oxy)ethyl)-2-nitro-9*H*-carbazol-9-yl)ethyl)azanediyl)diacetate (**3.48**). **az-3-32**. A solution of **3.39** (20 mg, 0.038 mmol), **3.44** (17 mg, 0.077 mmol), EDCI•HCl (15 mg, 0.077 mmol) and DMAP (20 mg, 0.15 mmol) in DMF (3 mL) was stirred at 80 ºC for 24 h. The solution was diluted with EtOAc (2 mL), and washed with H_2O (3 x 2 mL) and brine (2 mL). The organic fraction was dried (Na_2SO_4) and evaporated in vacuo to give crude **3.48** as yellow oil. The crude material was purified via flash column chromatography

eluting with hexanes : EtOAc (2:1) to give 16 mg (55%) **3.48** as a yellow solid. ^{1}H NMR (500 MHz, $CDCl_3$-*d*) δ 8.73 (s, 1H), 8.39 (s, 1H), 8.22 (dd, *J* = 8.9, 2.8 Hz, 1H), 8.16 (d, *J* = 7.9 Hz, 1H), 8.13 (s, 1H), 7.48 – 7.43 (m, 2H), 7.41 – 7.34 (m, 2H), 7.23 – 7.21 (m, 1H), 6.71 (q, *J* = 6.4 Hz, 1H), 4.48 (t, *J* = 7.6 Hz, 2H), 4.15 (q, *J* = 7.2 Hz, 2H), 3.04 (t, *J* = 7.6 Hz, 2H), 1.84 (d, *J* = 6.4 Hz, 3H), 1.44 (t, *J* = 7.2 Hz, 3H), 1.39 (s, 18H). ^{13}C NMR (126 MHz, $CDCl_3$) δ 170.5, 165.6, 159.0, 148.9, 145.7, 142.6, 138.4, 129.3, 128.0, 127.2, 121.9, 121.8, 120.2, 119.8, 113.4, 113.2, 110.5, 109.3, 105.5, 70.0, 57.2, 56.0, 52.7, 49.2, 43.1, 29.7, 28.2, 22.9, 14.5.

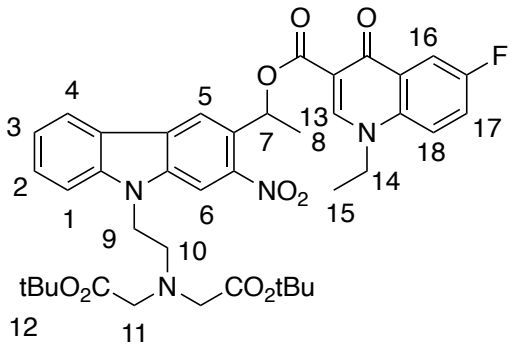

3.48

NMR Assignment. ^{1}H NMR (500 MHz, $CDCl_3$) δ 8.73 (s, 1H, C13-H), 8.39 (s, 1H, C6-H), 8.22 (dd, *J* = 8.9, 2.8 Hz, 1H, C18-H), 8.16 (d, *J* = 7.9 Hz, 1H, C16-H), 8.13 (s, 1H, C5-H), 7.48 – 7.43 (m, 2H, C1, C3-H), 7.41 – 7.34 (m, 2H, C2, C4-H), 7.23 – 7.21 (m, 1H, C2-H), 6.71 (q, *J* = 6.4 Hz, 1H, C7-H), 4.48 (t, *J* = 7.6 Hz, 2H, C9-H), 4.15 (q, *J* = 7.2 Hz, 2H, C14-H), 3.04 (t, *J* = 7.6 Hz, 2H, C10-H), 1.84 (d, *J* = 6.4 Hz, 3H, C8-H), 1.44 (t, *J* = 7.2 Hz, 3H, C15-H), 1.39 (s, 18H, C12-H).

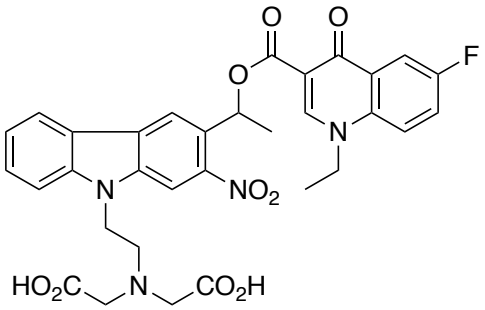

3.55

2,2'-((2-(3-(1-((1-Ethyl-6-fluoro-4-oxo-1,4-dihydroquinoline-3-carbonyl)oxy)ethyl)-2-nitro-9*H*-carbazol-9-yl)ethyl)azanediyl)diacetic acid (**3.55**). **az-4-286**. 4M HCl in dioxane (1 mL) was added to **3.48** (15 mg, 0.020 mmol) at 0 ºC. The solution was stirred at room temperature for 8 h. The solution was concentrated *in vacuo* to give 12 mg (97%) **3.55** as yellow solid. ^{1}H NMR (500 MHz, MeOD) δ 8.89 (s, 1H), 8.86 (s, 1H), 8.55 (s, 1H), 8.25 – 8.17 (comp, 2H), 7.96 (dd, J = 9.7, 4.6 Hz, 1H), 7.67 (dq, J = 10.0, 5.6, 4.3 Hz, 2H), 7.59 (t, J = 7.7 Hz, 1H), 7.36 (t, J = 7.5 Hz, 1H), 6.89 (q, J = 6.3 Hz, 1H), 5.00 (tt, J = 11.4, 5.6 Hz, 2H), 4.51 (q, J = 7.2 Hz, 2H), 4.43 (s, 4H), 3.92 – 3.81 (m, 2H), 3.74 (t, J = 5.8 Hz, 1H), 3.58 (dd, J = 5.5, 4.2 Hz, 1H), 1.84 (d, J = 6.4 Hz, 3H), 1.53 (t, J = 7.2 Hz, 3H). ^{13}C NMR (126 MHz, MeOD) δ 167.1, 149.5, 127.6, 121.2, 121.0, 118.0, 107.5, 70.0, 66.7, 54.6, 52.7, 47.1, 37.8, 21.6, 13.5.

Appendix A:

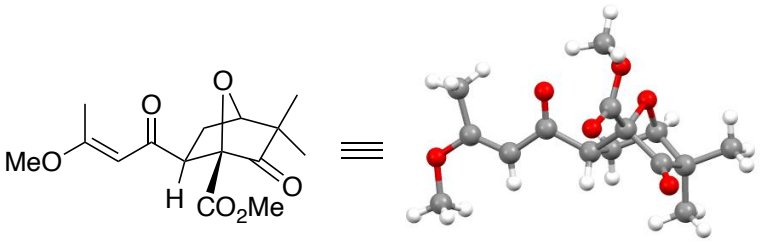

1.81

1.81
(X-ray)

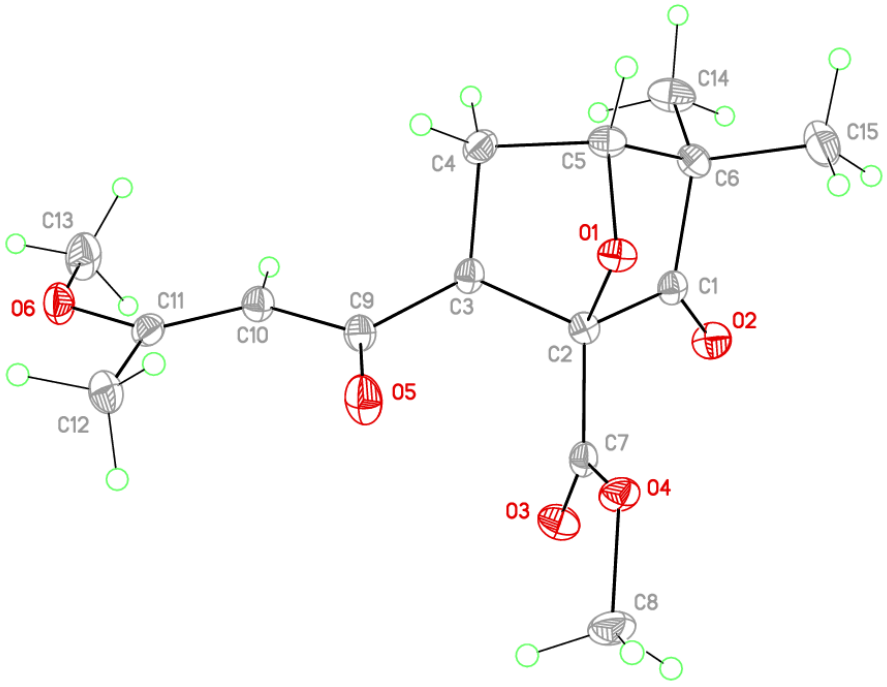

Figure A.1. View of **1.81** showing the atom labeling scheme. Displacement ellipsoids are scaled to the 50% probability level.

X-ray experimental for $C_{15}H_{20}O_6$: Crystals grew as clear, colorless needles by slow evaporation from THF and water. The data crystal was cut from a larger crystal and had approximate dimensions; 0.47 x 0.19 x 0.15 mm. The data were collected at -173 °C on a Nonius Kappa CCD diffractometer using a Bruker AXS Apex II detector and a graphite monochromator with MoKα radiation (λ = 0.71073Å). Reduced temperatures were maintained by use of an Oxford Cryosystems 700 low-temperature device. A total of 1043 frames of data were collected using ω-scans with a scan range of 0.7° and a counting time of 34 seconds per frame. Details of crystal data, data collection and structure refinement are listed in Table A.1. Data reduction were performed using SAINT V8.27B.[252] The structure was solved by direct methods using SHELXT[253] and refined by full-matrix least-squares on F^2 with anisotropic displacement parameters for the non-H atoms using SHELXL-2016/6.[254] Structure analysis was aided by use of the programs PLATON[255], OLEX2[256] and WinGX.[257] The hydrogen atoms bound to carbon atoms were calculated in idealized positions.

The function, $\Sigma w(|Fo|^2 - |Fc|^2)^2$, was minimized, where $w = 1/[(\sigma(Fo))^2 + (0.0519*P)^2 + (0.3482*P)]$ and $P = (|Fo|^2 + 2|Fc|^2)/3$. $Rw(F^2)$ refined to 0.103, with R(F) equal to 0.0392 and a goodness of fit, S, = 1.05. Definitions used for calculating R(F),$Rw(F^2)$ and the goodness of fit, S, are given below.[258] The data were checked for secondary extinction but no correction was necessary. Neutral atom scattering factors and values used to calculate the linear absorption coefficient are from the International Tables for X-ray Crystallography (1992). [259] All figures were generated using SHELXTL/PC.[260] Tables of positional and thermal parameters, bond lengths and angles, torsion angles and figures are found elsewhere.

Table A.1. Crystal data and structure refinement for **1.81.**

Identification code	az-4-74	
Empirical formula	$C_{15}H_{20}O_6$	
Formula weight	296.31	
Temperature	100 K	
Wavelength	0.71073 Å	
Crystal system	monoclinic	
Space group	P 1 21/c 1	
Unit cell dimensions	a = 10.1929(12) Å	a= 90º
	b = 15.9357(17) Å	b= 93.468(6)º
	c = 8.9926(10) Å	g = 90º.
Volume	1458.0(3) $Å^3$	
Z	4	
Density (calculated)	1.350 Mg/m^3	
Absorption coefficient	0.104 mm^{-1}	
F(000)	632	
Crystal size	0.47 x 0.19 x 0.15 mm^3	
Theta range for data collection	2.375 to 28.818º.	
Index ranges	-13<=h<=13, -21<=k<=21, -12<=l<=12	
Reflections collected	22631	
Independent reflections	3798 [R(int) = 0.0480]	
Completeness to theta = 25.242º	100.0 %	
Absorption correction	Semi-empirical from equivalents	
Max. and min. transmission	0.7458 and 0.6576	
Refinement method	Full-matrix least-squares on F^2	
Data / restraints / parameters	3798 / 0 / 195	
Goodness-of-fit on F^2	1.053	
Final R indices [I>2sigma(I)]	R1 = 0.0392, wR2 = 0.0980	
R indices (all data)	R1 = 0.0527, wR2 = 0.1034	
Extinction coefficient	n/a	
Largest diff. peak and hole	0.440 and -0.198 e. $Å^{-3}$	

Reference

(1) Harbaugh, D.T.; Wagner, W.L.; Allan, G.J.; Zimmer, E.A. The Hawaiian Archipelago is a stepping stone for dispersal in the Pacific: an example from the plant genus *Melicope* (Rutaceae). *J. Biogeogr.* **2009**, *36*, 230–241.

(2) Zhang, D.X.; Hartley, T.G. Flora of China (Zhongguo Zhiwu Zhi). Science Press: Beijing, China, 2008, pp. 70–73.

(3) Johnson, A. J.; Kumar, R. A.; Rasheed, S. A.; Chandrika, S. P.; Chandrasekhar, A.; Baby, S.; Subramoniam, A. Antipyretic, analgesic, anti-inflammatory and antioxidant activities of two major chromenes from Melicope lunu-ankenda. *J. Ethnopharmacol.* **2010**, *130*, 267–271.

(4) Sultana, N.; Hartley, T. G.; Waterman, P. G. Two novel prenylated flavones from the aerial parts of Melicope micrococca. *Phytochemistry* **1999**, *50*, 1249–1253.

(5) Chen, I. S.; Chen, H. F.; Cheng, M. J.; Chang, Y. L.; Teng, C. M.; Tsutomu, I.; Chen, J. J.; Tsai, I. L. Quinoline Alkaloids and Other Constituents of *Melicope semecarpifolia* with Antiplatelet Aggregation Activity. *J. Nat. Prod*. **2001**, *64*, 1143–1147.

(6) Chen, J. J.; Cho, J. Y.; Hwang, T. L.; Chen, I. S. Benzoic Acid Derivatives, Acetophenones, and Anti-inflammatory Constituents from *Melicope semecarpifolia. J. Nat. Prod*. **2008**, *71*, 71–75.

(7) Li, G. L.; Zhu, D. Y. Two New Dichromenes from *Evodia lepta*. *J. Nat. Prod.* **1998**, *61*, 390–391.

(8) Adsersen, A.; Smitt, U. W.; Simonsen, H. T.; Christensen, S. B.; Jaroszewski, J. W. Prenylated acetophenone from *Melicope obscura* and *Melicope obtusifolia* ssp. *obtusifolia* var. *arborea* and their distribution in Rutaceae. *Biochem. Syst. Ecol*. **2007**, *35*, 447–453.

(9) Simonsen, H. T. Four novel geminally dialkylated, non-aromatic acetophenone derivatives from *Melicope coodeana*. *Phytochem. Lett.* **2012**, *5*, 371–375.

(10) Xu, J. F.; Zhao. H. J.; Wang, X. B.; Li, Z. R.; Luo, J.; Yang. M. H.; Yang, L.; Yu, W. Y.; Yao, H. Q.; Luo, J. G.; Kong, L. Y. (±)-Melicolone A and B, Rearranged Prenylated Acetophenone Stereoisomers with an Unusual 9-Oxatricyclo[3.2.1.1^{3,8}]nonae Core from the Leaves of *Melicope ptelefolia*. *Org. Lett*. **2015**, *17*, 146–149.

(11) Abas, F.; Lajis, N. H.; Israf, D. A.; Khozirah, S.; Kalsom, Y. U. Antioxidant and nitric oxide inhibition activities of selected Malay traditional vegetables. *Food Chem*. **2006**, *95*, 566–573.

(12) Xu, J. F.; Han, C.; Xue, G. M.; Wang, X. B.; Luo, J.; Yang, M. H.; Luo, J. G.; Kong, L. Y. Novel rearranged acetophenone derivatives possessing diverse architectures from the leaves of *Melicope ptelefolia*. *Tetrahedron* **2019**, *75*, 130784–130791.

(13) Hauser, N. Total Synthesis of (+)-Shearinine D and Towards the Total Synthesis of Melicolones A and B and Investigation of the Structure-Odor Relationship of 2,2 Bis(prenyl)-3-oxobutyronitrile and Congeners. Swiss Federal Institute of Technology in Zürich, 2019.

(14) Zhu, C. Studies Toward the Total Synthesis of Alsmaphorazine D and Melicolone B. Zhejiang University, 2017.

(15) Shimada, N.; Hanari, T.; Kurosaki, Y.; Takeda, K.; Anada, M.; Nambu, H.; Shiro, M.; Hashimoto, S. Catalytic Asymmetric Synthesis of the *endo*-6-Aryl-8-oxabicyclo[3.2.1]oct-3-en-2-one Natrual Product from *Ligusticum chuanxing* via 1,3-Dipolar Cycloaddition of a Formyl-Derived Carbonyl Ylide Using Rh_2(*S*-TCPTTL)$_4$. *J. Org. Chem.* **2010**, *75*, 6039−6042.

(16) Shimada, N.; Hanari, T.; Kurosaki, Y. Anada, M.; Nambu, H.; Hashimoto, S. Catalytic asymmereic synthesis of descurainin via 1,3-dipolar cycloaddition of a carbonyl ylide using Rh_2(*S*-TCPTTL)$_4$. *Tetrahedron Lett.* **2010**, *51*, 6572–6575.

(17) Padwa, A.; Weingarten, M. D. Cascade Processes of Metallo Carbenoids. *Chem. Rev*. **1996**, *96*, 223-269.

(18) Mehta, G.; Muthusamy, S. Tandem cyclization-cycloaddition reactions of rhodium generated carbenoids from α-diazo carbonyl compounds. *Tetrahedron*, **2002**, *58*, 9477–9504.

(19) Padwa, A. Domino reactions of rhodium(II) carbenoids for alkaloid synthesis. *Chem. Soc. Rev*. **2009**, *38*, 3072–3081.

(20) Hodgson, D. M.; Labande, A. H.; Muthusamy, S. Organic reactions. John Wiley & Sons: Hoboken, NJ, 2013, pp 133–496.

(21) Ford, A.; Miel, H.; Ring, A.; Slattery, C. N.; Maguire, A. R.; McKervey, M. A. Modern Organic Synthesis with α-Diazocarbonyl Compounds. *Chem. Rev.* **2015**, *115*, 9981–10080.

(22) Kinder, F. R.; Bair, K. W. Total Synthesis of (±)-Illudin M. *J. Org. Chem*. **1994**, *59*, 6965–6967.

(23) Pirrung, M. C.; Kaliappan, K. P. Dipolar Cycloaddition of Rhodium-Generated Carbonyl Ylides with *p*-Quinones. *Org. Lett.* **2000**, *2*, 353–355.

(24) Padwa. A.; Hornbuckle, S. F. Ylide formation from the reaction of carbenes and carbenoids with heteroatom lone pairs. *Chem. Rev*. **1991**, *91*, 263–309.

(25) Doyle, M. P.; McKervey, M. A.; Ye, T. Modern Catalytic Methods for Organic Synthesis with Diazo Compounds: From Cyclopropanes to Ylides. John Wiley & Sons, New York, 1998, pp. 163–220.

(26) Hodgson, D. M.; Bruckl, T.; Glen, R.; Labande, A. H.; Selden, D. A.; Dossetter, A. G.; Redgrave, A. J. Catalytic enantioselective intermolecular cycloadditions of 2-diazo-3,6-diketoester-derived carbonyl ylides with alkene dipolarophiles. *Proc. Natl. Acad. Sci. U.S.A.* **2004**,*101*, 5450–5454.

(27) Hashimoto, T.; Maruoka, K. Recent Advances of Catalytic Asymmeric 1,3-Dipolar Cycloadditions. *Chem. Rev*. **2015**, *115*, 5366–5412.

(28) Shimada, N.; Oohara, T.; Krishnamurthi. J.; Nambu, H.; Hashimoto, S. Catalytic Enantioselective Intermolecular Cycloaddition of Diazoketoester-Derived Carbonyl Ylids with Indoles Using Chiral Dirhodium(II) Carboxylates. *Org. Lett.* **2011**, *13*, 6284–6287.

(29) Heng, R.; Koch, G.; Schlapbach, A.; Seiler, M. P. PCT Int. Appl. 2008034600.

(30) Curphey, T. J. Preparation of *p*-Toluenesulfonyl Azide. A Cautionary Note. *Org. Prep. Proced. Int*. **1981**, *13*, 112–115.

(31) Bauer. J.; Brandenburg. K.; Zahringer. U, Rademann. J. Chemical Synthesis of a Glycolipid Library by a Solid-Phase Strategy Allows Elucidation of the Structural Specificity of Immunostimulation by Rhamnolipids. *Chem. Eur. J.* **2006**, *12*, 7116–7124.

(32) Regitz, M. New Methods of Preparative Organic Chemistry. Transfer of Diazo Groups. *Angew. Chem. Int. Ed*. **1967**, *6*, 733–749.

(33) Lowe, G.; Ransay, M. V. Synthetic studies related to nuclear analogues of the penicilins and cephalosporins. *J. Chem. Soc., Perkin Trans. 1*, **1973**, 479–484.

(34) Cavender, C. J.; Shiner, V. J. Jr. Trifluoromethanesulfonyl azide. Its reaction with alkyl amines to form alkyl azides. *J. Org. Chem*. **1972**, *37*, 3567–3569.

(35) Balli, H.; Low, R.; Muller, V.; Rempfler, H.; Sezen-Gezgin, G. 7. Azidiniumsalze. 19. Mitteilung [1]. Einführung der Diazogruppe in reaktive Methylenverbindungen mit Azidiniumsalzen. *Helv. Chim. Acta* **1978**, *61*, 97–103.

(36) Curphey, T. J. Preparation of *p*-Toluenesulfonyl Azide. A Cautionary Note. *Org. Prep. Proced. Int*. **1981**, *13*, 112–115.

(37) Taber, D.F.; Ruckle, R. E.; Hennessy, M. J. Mesyl azide: a superior reagent for diazo transfer. *J. Org. Chem*. **1986**, *51*, 4077–4078.

(38) Goddard-Borge, E. D.; Stick, R. V. An Efficient, Inexpensive, and Shelf-Stable Diazotransfer Reagent: Imidazole-1-sulfonyl Azide Hydrochloride. *Org. Lett.* **2007**, *9*, 3797–3800.

(39) Rodriguez, A.; Nomen, M.; Spur, B. W.; Godfroid, J. J. Selective oxidation of primary silyl ethers and its application to the synthesis of natural products. *Tetrahedron Lett.* **1999**, *40*, 5161–5164.

(40) Aggarwal, V. K.; Abdel-Rahman, H.; Jones, R. V. H.; Lee, H. Y.; Reid, B. D. Novel Catalytic Cycle for the Synthesis of Epoxides from Aldehydes and Sulfur Ylides Mediated by Catalytic Quantities of Sulfides and $Rh_2(OAc)_4$. *J. Am. Chem. Soc.* **1994**, *116*, 5973–5974.

(41) Muzart. J. Silyl Ethers as Protective Groups for Alcohols: Oxidative Deprotection and Stability under Alcohol Oxidation Conditions. *Synthesis*, **1993**, *1*, 11–27.

(42) Wu, Y.; Huang, J.; Shen, X.; Hu, Q.; Tang, C.; Li, L. Facile Cleavage of Triethylsilyl (TES) Ethers Using *o*-Iodoxybenzoic Acid (IBX) without Affecting *tert*-Butyldimethylsilyl (TBS) Ethers. *Org. Lett*. **2002**, *4*, 2141−2144.

(43) Padwa, A. Intramolecular cycloaddition of carbonyl ylides as a strategy for natural product synthesis. *Tetrahedron*, **2011**, *67*, 8057–8072.

(44) Kim, C. H.; Jang, K. P.; Choi, S. Y.; Chung, Y. K.; Lee, E. A Carbonyl Ylide Cycloaddition Approach to Platensimycin. *Angew. Chem. Int. Ed*. **2008**, *47*, 4009–4011.

(45) Graening, T.; Bette, V.; Neudoerfl, J.; Lex, J.; Schmalz, H. G. Total Synthesis of (-)-Colchicine via a Rh-Triggered Cycloaddition Cascade. *Org. Lett.* **2005**, *7*, 4317–4320.

(46) Padwa, A.; Brodney, M. A.; Marino, J. P.; Sheehan, S. M. Utilization of the Intramolecular Cycloaddition-Cationic π-Cycloaddition of an Isomunchnone Derivative for the Synthesis of (±)-Lycopodine. *J. Org. Chem*. **1997**, *62*, 78–87.

(47) Buchner, E.; Curtis, T. Synthese von Ketonsäureäthern aus Aldehyden und Diazoessigäther. Ber. Dtsch. Chem. Ges. 1885, 18, 2371–2377.

(48) Padwa, A. Huisgen R. In 1,3-Dipolar Cycloaddition Chemistry. Wiley: New York, 1984, pp. 1–176.

(49) De March, P.; Huisgen, R. Carbonyl ylides from aldehydes and carbenes. *J. Am. Chem. Soc*. **1982**, *104*, 4952–4953.

(50) Russell, A. E.; Brekan, J.; Gronenberg, L.; Doyle, M. P. Divergence of Carbonyl Ylide Reactions as a Function of Diazocarbonyl Compound and Aldehyde Substituent: Dioxolanes, Dioxolenes, and Epoxides. *J. Org. Chem*. **2004**, *69*, 5269–5274.

(51) Doyle, M. P.; Hu, W.; Timmons, D. J. Epoxides and Aziridines from Diazoacetates via Ylide Intermediates. *Org. Lett*. **2001**, *3*, 933–935.

(52) Ibata, T.; Toyoda, J.; Sawada, M.; Tanaka, T. Formation and reaction of carbonyl ylides. Structure of 2:1-cycloadducts of 1-methoxy-2-benzopyrylium-4-olate with isocyanates. *J. Chem. Soc., Chem. Commun.* **1986**, 1266.

(53) Ibata, T.; Toyoda, J. Formation and Reaction of Carbonyl Ylides. Production of 2 : 1-Cycloadducts of 2-Benzopyrylium-4-olates with Carbonyl Compounds. *Bull. Chem. Soc. Jpn.* **1986**, *59*, 2489–2493.

(54) Gillon, A.; Ovadia, D.; Kapon, M.; Bien, S. Intramolecular cycloaddition of carbonyl ylides generated from α-diazo ketones. *Tetrahedron* **1982**, *38*, 1477–1484.

(55) Huisgen, R. Electrocyclic Ring Opening Reactions of Ethylene Oxides. *Angew. Chem. Int. Ed.* **1977**, *16*, 572–585.

(56) Ruf, S. G.; Bergstrasser, U.; Regitz, M. Synthesis and Reactivity of a Polycyclic, Oxa-Bridged Phosphaalkene. *Eur. J. Org. Chem.* **2000**, *12*, 2219–2225.

(57) Bekhazi, M.; Smith, P. J.; Warkentin, J. Substituent effects on rates of formation of methoxy-substituted carbonyl ylides from 2-aryl-2-methoxy- and 5-aryl020methoxy-Δ^3-1,3,4-oxadiazolines. *Can. J. Chem*. **1984**, *62*, 1646–1652.

(58) Sharma, P. K.; Warkentin, J. Generation and trapping of a silyloxy carbonyl ylide. *Tetrahedron Lett*. **1995**, *36*, 7591–7594.

(59) Padwa, A. Generation and utilization of carbonyl ylide via the tandem cyclization-cycloaddition method. *Acc. Chem. Res*. **1991**, *24*, 22–28.

(60) Paulissen, R.; Reimlinger, H.; Hayez, A.; Hubert, A. J.; Teyssie, P. H. Transition metal catalyzed reactions of diazocompounds – II insertion in the hydroxylic bond. *Tetrahedron Lett.* **1973**, *24*, 2233–2236.

(61) Padwa, A.; Carter, S. P.; Nimmesgern, H. Tandem cyclization-cycloaddition reactions of α-diazoacetophenone derivatives. *J. Org. Chem*. **1986**, *51*, 1157–1158.

(62) Padwa, A.; Carter, S. P.; Nimmesgern, H.; Stull, P.D. Rhodium(II) acetate induced intramolecular dipolar cycloadditions of o-carboalkoxy-α-diazoacetophenone derivatives. *J. Am. Chem. Soc*. **1988**, *110*, 2894–2900.

(63) Padwa, A.; Fryxell, G. E.; Zhi, L. Photodemethylation of methoxy-substituted 9,10-anthraquinones in methanol. *J. Org. Chem*. **1988**, *53*, 2877–2878.

(64) Padwa, A.; Fryxell, G. E.; Zhi, L. Tandem cyclization-cycloaddition reaction of rhodium carbenoids. Scope and mechanistic details of the process. *J. Am. Chem. Soc*. **1990**, *112*, 3100–3109.

(65) Padwa, A.; Chinn, R. L.; Zhi. L. Synthesis of *exo* and *endo*-brevicomin via the rhodium acetate catalyzed cycloaddition reaction of 1-diazo-2,5-hexanedione. *Tetrahedron Lett*. **1989**, *12*, 1491–1494.

(66) Padwa, A.; Chinn, R. L.; Hornbuckle, S. F.; Zhi, L. Cyclic carbonyl ylide formation from the rhodium(II) acetate catalyzed reaction of 1-diazoalkanediones. *Tetrahedron Lett*. **1989**, *3*, 301–304.

(67) Padwa, A.; Krumpe, K.; Zhi, L. Cycloalkenone formation by the intramolecular addition of a α-diazoketone to an acetylenic π-bond. *Tetrahedron Lett*. **1989**, *20*, 2633–2636.

(68) Padwa, A.; Dean, D. C.; Zhi, L. 1,3-Dipole cascade. A new method for azomethine ylide formation. *J. Am. Chem. Soc*. **1989**, *111*, 6451–6452.

(69) Houk, K.; Yamaguchi, K. In 1,3-Dipolar Cycloaddition Chemisty, Padwa, A., Ed.; Wiley: New York, 1984, pp. 407–450.

(70) Houk, K. N.; Sims, J.; Duke, R. E.; Strozier, R. W.; George, J. K. Frontier molecular orbitals of 1,3 dipoles and dipolarophiles. *J. Am. Chem. Soc*. **1973**, *95*, 7287–7301.

(71) Sustmann, R. A Simple Model For Substituent Effects in Cycloaddition Reactions. I. 1,3-Dipolar Cycloadditions. *Tetrahedron Lett*. **1971**, *29*, 2717–2720.

(72) Padwa, A.; Chinn, R. L.; Hornbuckle, S. F.; Zhi, L. Cyclic Carbonyl Ylide Formation from the Rhodium(II) Acetate Catalyzed Reaction of 1-Diazoalkanediones. *Tetrahedron Lett*. **1989**, *30*, 301–304.

(73) Padwa, A.; Sandanayaka, V. P.; Curtis, E. A. Synthetic studies toward Illudins and Ptaquilosin. A highly convergent approach via the dipolar cycloaddition of carbonyl ylides. *J. Am. Chem. Soc*. **1994**, *116*, 2667–2668.

(74) McMorris, T. C.; Cong, Q.; Kelner, M. J. Structure-Activity Relationship Studies of Illudins: Analogues Possessing a Spiro-cyclobutane Ring. *J. Org. Chem*. **2003**, *68*, 9648–9653.

(75) Deslongchamps, P.; Bélanger, A.; Berney, D. J. F.; Borschberg, H. J.; Brousseau, R.; Doutheau, A.; Durand, R.; Katayama, H.; Lapalme, R.; Leturc, D. M.; Liao, C. C.; MacLachlan, F. N. The total synthesis of (+)-ryanodol. Part II. Model studies for rings B and C of (+)-anhyroryanodol. Preparation of a key pentacyclic intermediate. *Can. J. Chem*. **1990**, *68*, 127–152.

(76) Valot, G.; Maihol, D.; Regens, C. S.; O'Malley, D. P.; Godineau, E.; Takikawa, H.; Philipps, P.; Furstner, A. Concise Total Synthesis of Amphidinolides C and F. *Chem. Eur. J.* **2015**, *21*, 2398–2408.

(77) Padwa, A.; Curtis, E. A.; Sandanayaka, V. P. Generation and Cycloaddition Behavior of Spirocyclic Carbonyl Ylide. Application to the Synthesis of the Pterosin Family of Sesquiterpenes. *J. Org. Chem*. **1996**, *61*, 73–81.

(78) Curtis, E. A.; Sandanayaka, V. P.; Padwa, A. An efficient dipolar-cycloaddition route to the pterosin family of sesquiterpenes. *Tetrahedron Lett*. **1995**, *36*, 1989–1992.

(79) Essig, S.; Bretzke, S.; Muller, R.; Menche, D. Full Stereochemical Determination of Ajudazols A and B by Bioinformatics Gene Cluster Analysis and Total Synthesis of Ajudazol B by an Asymmetric Ortholithiation Strategy. *J. Am. Chem. Soc*. **2012**, *134*, 19362–19365.

(80) Essig, S.; Bretzke, S.; Müller, R.; Menche, D. Full Stereochemical Determination of Ajudazols A and B by Bioinformatics Gene Cluster Analysis and Total Synthesis of Ajudazol B by an Asymmetric Ortholithiation Strategy. *J. Am. Chem. Soc*. **2012**, *134*, 19362–19365.

(81) Padwa, A. The domino cycloaddition/N-acyliminium ion cyclization cascade. *Chem. Commun*. **1998**, 1417–1424.

(82) Padwa, A.; Austin, D. J.; Hornbuckle, S. F.; Semones, M. A.; Doyle, M. P.; Protopopova, M. N. Control of chemoselectivity in catalytic carbenoid reactions. Dirhodium(II) ligand effects on relative reactivities. *J. Am. Chem. Soc*. **1992**, *114*, 1874–1876.

(83) Shimada, N.; Anada, M.; Nakamura, S.; Nambu, H.; Tsutsui, H.; Hashimoto, S. Catalytic Enantioselective Intermolecular Cycloaddition of 2-Diazo-3,6-diketoester-Derived Carbonyl Ylides with Alkynes and Styrenes Using Chiral Dirhodium(II) Carboxylates. *Org. Lett*. **2008**, *10*, 3603–3606.

(84) Suga, H.; Inoue, K.; Inoue, S.; Kakehi, A.; Shiro, M. Chiral 2,6-Bis(oxazolinyl)pyridine-Rare Earth Metal Complexes as Catalysts for Highly Enantioselective 1,3-Dipolar Cycloaddition Reactions of 2-Benzopyrylium-4-olates. *J. Org. Chem*. **2005**, *70*, 47–56.

(85) Diaz-Muñoz, G.; Miranda, I. L.; Sartori, S. K.; Cristina de Rezende, D.; Diaz, M. A. N. Use of chiral auxiliaries in the asymmetric synthesis of biologically active compounds: A review. *Chirality*. **2019**, *31*, 776–812.

(86) Kasahara, K.; Iida, H.; Kibayashi, C. Asymmetric Total Synthesis of (+)-Negamycin and (–)-3-Epnegamycin via Enantioselective 1,3-Dipolar Cycloaddition. *J. Org. Chem*. **1989**, *54*, 2225–2233.

(87) Waldmann, H.; Bläser, E.; Jansen, M.; Letschert, H. P. Asymmetric Control of 1,3-Dipolar Cycloaddition Reactions with Azomethine Ylides by Means of Proline Esters as Chiral Auxiliary Groups. *Chem. Eur. J*. **1995**, *1*, 150–154.

(88) Mish, M. R.; Guerra, F. M.; Carreira, E. M. Asymmetric Dipolar Cycloadditions of Me_3SiCHN_2. Synthesis of a Novel Class of Amino Acids: Azaprolines. *J. Am. Chem. Soc.* **1997**, *119*, 8379–8380.

(89) Doyle, M. P.; Forbes, D. C.; Protopopova, M. N.; Stanley, S. A.; Vasbinder, M. M.; Xavier, K. R. Stereocontrol in Intermolecular Dirhodium(II)-Catalyzed Carbonyl Ylide Formation and Reactions. Dioxolanes and Dihydrofurans. *J. Org. Chem*. **1997**, *62*, 7210–7215.

(90) Hodgson, D. M.; Stupple, P. A.; Johnstone, C. Catalytic Enantioselective Tandem Carbonyl Ylide Formation-Cycloaddition. *Tetrahedron Lett*. **1997**, *38*, 6471–6472.

(91) Hodgson, D. M.; Labande, A. H.; Pierard, F. Y. T. M.; Exposito Castro, M. A. The Scope of Catalytic Enantioselective Tandem Carbonyl Ylide Formation-Intramolecular [3+2] Cycloadditions. *J. Org. Chem*. **2003**, *68*, 6153–6159.

(92) Hodgson, D. M.; Glen, R.; Redgrave, A. J. [3+2] Cycloaddition Reactions of Arylacetylenes with Carbonyl Ylides Derived from 1-Aryl-1-diazohexane-2,5-diones. *Tetrahedron Lett*. **2002**, *43*, 3927–3930.

(93) Hodgson, D. M.; Labande, A. H.; Glen, R.; Redgrave, A. J. Catalytic Enantioselective Intermolecular Cycloadditions of a 2-Diazo-3,6-diketonester-Derived Carbonyl Ylide with Alkyne and Strained Alkene Dipolarophiles. *Tetrahedron Asymmetry* **2003**, *14*, 921–924.

(94) Hodgson, D. M.; Bruckl, T.; Glen, R.; Labande, A. H.; Selden, D. A.; Dossetter, A. G.; Redgrave, A. J. Catalytic Enantioselective Intermolecular Cycloaddition of 2-Diazo-3,6-diketoester-Derived Carbonyl Ylides with Alkene Dipolarophiles. *Proc. Natl. Acad. Sci. U.S.A.* **2004**, *101*, 5450–5454.

(95) Kitagaki, S.; Anada, M.; Kataoka, O.; Matsuno, K.; Umeda, C.; Watanabe, N.; Hashimoto, S. Enantiocontrol in Tandem Carbonyl Ylide Formation and Intermolecular 1,3-Dipolar Cycloaddition of α-Diazo Ketones Mediated by Chiral Rhodium(II) Carboxylate Catalyst. *J. Am. Chem. Soc*. **1999**, *121*, 1417–1418.

(96) Hashimoto, S. I.; Watanabe, N.; Sato, T.; Shiro, M.; Ikegami, S. Enhancement of Enantioselectivity in Intramolecular C-H Insertion Reactions of α-Diazo β-Keto Esters Catalyzed by Chiral Dirhodium(II) Carboxylate. *Tetrahedron Lett*. **1993**, *34*, 5109–5112.

(97) Nambu, H.; Hikime, M.; Krishnamurthi, J.; Kamiya, M.; Shimada, N.; Hashimoto, S. Asymmetric Approach to the Pentacyclic Skeleton of Aspidosperma Alkaloids via Enantioselective Intramelucular 1,3-Dipolar Cycloaddition of Carbonyl Ylides Catalyzed by Chiral Dirhodium(II) Carboxylates. *Tetrahedron Lett*. **2009**, *50*, 3675–3678.

(98) Tsutsui, H.; Shimada, N.; Abe, T.; Anada, M.; Nakajima, M.; Nakamura, S.; Nambu, H.; Hashimoto, S. Catalytic Enantioselective Tandem Carbonyl Ylide Formation/1,3-Dipolar Cycloaddition Reactions of α-Diazo Ketones with Aromatic Aldehydes using Dirhodium(II) Tetrakis[N-benzene-fused-phthaloyl-(S)-valinate]. *Adv. Synth. Catal*. **2007**, *349*, 521–526.

(99) Kurosaki, Y.; Shimada, N.; Anada, M.; Nambu, H.; Hashimoto, S. Catalytic Asymmetric Construction of the Exo-7-Aryl-6,8-dioxabicycl[3.2.1]octane Framework of Psoracorylifols B and C Using a Carbonyl Ylide Cycloaddition Strategy. *Bull. Korean Chem. Soc*. **2010**, *31*, 694–696.

(100) Kitagaki, S.; Anada, M.; Kataoka, O.; Matsuno, K.; Umeda, C.; Watanabe, N.; Hashimoto, S. Enantiocontrol in Tandem Carbonyl Ylide Formation and Intermolecular 1,3-Dipolar Cycloaddition of α-Diazo Ketones Mediated by Chiral Dirhodium(II) Carboxylate Catalyst. *J. Am. Chem. Soc.* **1999**, *121*, 1417–1418.

(101) Davies, H. M. L.; Bruzinski, P. R.; Lake, D. H.; Kong, N.; Fall, M. J. Asymmetric Cyclopropanations by Rhodium(II) N-(Arylsulfonyl)prolinate Catalyzed Decomposition of Vinyldiazomethanes in the Presence of Alkenes. Practical Enantioselective Synthesis of the Four Stereoisomers of 2-Phenylcyclopropan-1-amino Acid. *J. Am. Chem. Soc*. **1996**, *118*, 6897–6907.

(102) Jung, M. E.; Lyster, M. A. Quantitative dealkylation of alkyl ethers via treatment with trimethylsilyl iodide. A new method for ether hydrolysis. *J. Org. Chem*. **1977**, *42*, 3761–3764.

(103) Tu, Y.; Wang, Z. X.; Shi, Y. An Efficient Asymmetric Epoxidation Method for *trans*-Olefins Mediated by a Fructose-Derived Ketone. *J. Am. Chem. Soc*. **1996**, *118*, 9806–9807.

(104) Adam, W.; Curci, R.; Edwards, J. O. Dioxiranes: a new class of powerful oxidants. *Acc. Chem. Res.* **1989**, *22*, 205–211.

(105) Wang, Z. X.; Tu, Y.; Frohn, M.; Zhang, J. R.; Shi, Y. An Efficient Catalytic Asymmetric Epoxidation Method. *J. Am. Chem. Soc*. **1997**, *119*, 11224–11235.

(106) Brandes, B. D.; Jacobsen, E. N. Highly Enantioselective, Catalytic Epoxidation of Trisubstituted Olefins. *J. Org. Chem*. **1994**, *59*, 4378–4380.

(107) Wang, W. J.; Xue, J. J.; Tian, T.; Jiao, Y. D.; Li, Y. The first asymmetric total synthesis of (+)-coriandrone A and B. *Org. Biomol. Chem.* **2013**, *11*, 6686–6690.

(108) Inoue, S.; Nakagawa, C.; Hayakawa, H.; Iwasaki, F.; Hoshino, Y; Honda, K. Regioselective Synthesis of Furan-Fused 3-Hydroxy-2,2-dimethylchroman, NG121 Model Compound. *Synlett* **2006**, *9*, 1363–1366.

(109) Nicolaou, K. C.; Prasad, C. V. C.; Somers, P. K.; Hwang, C. K. Activation of 6-endo over 5-exo hydroxy epoxide openings. Stereoselective and ring selective synthesis of tetrahydrofuran and tetrahydropyran systems. *J. Am. Chem. Soc*. **1989**, *111*, 5330–5334.

(110) Morimoto, Y.; Nishikawa, Y.; Ueba, C.; Tanaka, T. Reagent-Controlled Switching of 5-*exo* to 6-*endo* Cyclizations in Epoxide Openings. *Angew. Chem. Int. Ed*. **2006**, *45*, 810–812.

(111) Mayer, G.; Heckel, A. Biologically Active Molecules with a "Light Switch". *Angew. Chem. Int. Ed*. **2006**, *45*, 4900–4921.

(112) Nicolaou, K. C.; Hummel, C. W.; Nakada, M.; Shibayama. K.; Pitsinos, E. N.; Saimoto, H.; Mizuno, Y.; Baldenius, K. U.; Smith, A. L. Total synthesis of calicheamicin γ1. The final stages. *J. Am. Chem. Soc*. **1993**, *115*, 7625–7635.

(113) Gareau, Y.; Zamboni, R.; Wong, A. W. Total synthesis of N-methyl TLC_4: a novel methodology for the monomethylation of amines. *J. Org. Chem*. **1993**, *58*, 1582–1585.

(114) Klan, P.; Solomek, T.; Bochet, C. G.; Blanc, A.; Givens, R.; Rubina, M.; Popik, V.; Kostikov, A.; Wirz, J. Photoremovable Protecting Groups in Chemistry and Biology: Reaction Mechanism and Efficacy. *Chem. Rev*. **2013**, *113*, 119–191.

(115) Young, D.; Deiters, A. Photochemical Activation of Protein Expression in Bacterial Cells. *Angew. Chem. Int. Ed*. **2007**, *46*, 4290–4292.

(116) Shao. Q.; Xing, B. Photoactive molecules for applications in molecular imaging and cell biology. *Chem. Soc. Rev*. **2010**, *39*, 2835–2846.

(117) Shestopalov, I. A.; Chen, J. K. Chemical technologies for probing embryonic development. *Chem. Soc. Rev*. **2008**, *37*, 1294–1307.

(118) Rossi, F. M.; Margulis, M.; Tang, C. M.; Kao, J. P. Y. N-Nmoc-L-Glutamate, a New caged Glutamate with High Chemical Stability and Low Pre-photolysis Activity. *J. Biol. Chem.* **1997**, *272*, 32933–32939.

(119) Barltrop, J. A.; Schofield, P. Photosensitive Protecting Groups. *Tetrahedron Lett.* **1962**, *16*, 697–699.

(120) Barton, D. H. R.; Chow, Y. L.; Cox, A.; Kirby, G. W. Photosensitive Protection of Functional Groups. *Tetrahedron Lett*. **1962**, *3*, 1055–1057.

(121) Sheehan, J. C.; Wilson, R. M. Photolysis of Desyl Compounds. A New Photolytic Cyclization. *J. Am. Chem. Soc*. **1964**, *86*, 5277–5281.

(122) Patchornik, A.; Amit, B.; Woodward, R. B. Photosensitive Protecting Groups. *J. Am. Chem. Soc.* **1970**, *92*, 6333–6335.

(123) Kaplan, J. H.; Forbush, B.; Hoffman, J. F. Rapid Photolytic Release of Adenosine 5'-Triphosphate from a Protected Analogue: Utilization by the Na: K Pump of Human Red Blood Cell Ghosts. *J. Am. Chem. Soc*. **1978**, *17*, 1929–1935.

(124) Engles, J.; Schlaeger, E, -J. Synthesis, structure, and reactivity of adenosine cyclic 3',5'-phosphate-benzyltriesters. *J. Med. Chem*. **1977**, *20*, 907–911.

(125) Šolomek, T.; Mercier, S.; Bally, T.; Bochet, C. G. Photolysis of Ortho-Nitrobenzylic Derivatives: The Importance of the Leaving Group. *Photochem. Photobiol. Sci.* **2012**, *11*, 548.

(126) Šolomek, T.; Bochet, C. G.; Bally, T. The Primary Steps in Excited-State Hydrogen Transfer: The Phototautomerization of *o*-Nitrobenzyl Derivatives. *Chem. Eur. J.* **2014**, *20*, 8062–8067.

(127) Il'ichev, Y. V.; Schwörer, M. A.; Wirz, J. Photochemical Reaction Mechanisms of 2-Nitrobenzyl Compounds: Methyl Ethers and Caged ATP. *J. Am. Chem. Soc.* **2004**, *126*, 4581–4595.

(128) Kohl-Landgraf, J.; Buhr, F.; Lefrancois, D.; Mewes, J. M.; Schwalbe, H.; Dreuw, A.; Wachtveitl, J. Mechanism of the Photoinduced Uncaging Reaction of Puromycin Protected by a 6-Nitroveratryloxycarbonyl Group. *J. Am. Chem. Soc.* **2014**, *136*, 3430–3438.

(129) Schaper, K.; Etinski, M.; Fleig, T. Theoretical Investigation of the Excited States of 2-Nitrobenzyl and 4,5-Methylendioxy-2-nitrobenzyl Caging Groups. *Photochem. Photobiol*. **2009**, *85*, 1075–1081.

(130) Zou, K; Miller, T. W.; Givens, R. S.; Bayley, H. Caged Thiophophotyrosine Peptides. *Angew. Chem. Int. Ed*. **2001**, *40*, 3049–3051.

(131) Zou, K.; Cheley, S.; Givens, R. S.; Bayley, H. Catalytic Subunit of Protein Kinase A Caged at the Activating Phophothreonine. *J. Am. Chem. Soc*. **2002**, *124*, 8220–8229.

(132) Arbely, E.; Kolbus, J. T.; Deither, A.; Chin, J. W. Photocontrol of Tyrosine Phosphorylation in Mammalian Cells via Genetic Encoding of Photocaged Tyrosine. *J. Am. Chem. Soc*. **2012**, *134*, 11912–11915.

(133) Deiters, A.; Groff, D.; Ryu, Y.; Xie, J.; Schultz, P. G. A Genetically Encoded Photocaged Tyrosine. *Angew. Chem. Int. Ed*. **2006**, *45*, 2728–2731.

(134) Reichmanis, E.; Smith, B. C.; Gooden, R. *o*-Nitorbenzyl photochemistry: Solution vs solid-state behavior. *J. Polym. Sci.* **1985**, *23*, 1–8.

(135) Reichmanis, E.; Gooden, R.; Wilkins, C. W. Jr.; Schonhorn, H. A study of the photochemical response of o-nitrobenzyl cholate derivatives in P(MMA-MMA) matrices. *J. Polym. Sci*. **1983**, *21*, 1075–1083.

(136) Allan, A. C.; Ward, J. L.; Beale, M. H.; Trewavas, A. J. Caged plant growth regulators. *Methods Enzymol*. **1998**, *291*, 474–483.

(137) Ajayaghosh, A.; Pilai, V. N. R. Polymer-supported synthesis of protected peptide segments on a photosensitive o-nitro(α-methyl)bromobenzyl resin. *Tetrahedron* **1988**, *44*, 6661–6666.

(138) Specht, A.; Goeldner, M. 1-(o-Nitrophenyl)-2,2,2-trifluoroethyl Ether Derivatives as Stable and Efficient Photoremovable Alcohol-Protecting Groups. *Angew. Chem. Int. Ed*. **2004**, *43*, 2008–2012.

(139) Cameron, J. F.; Frechet, J. M. Photogeneration of Organic Bases from o-Nitrobenzyl-Derived Carbamates. *J. Am. Chem. Soc*. **1991**, *113*, 4303–4313.

(140) Neenan, T. X.; Houlihan, F. M.; Reichmanis, E.; Kometani, J. M.; Bachman, B. J.; Thompson, L. F. Photo- and Thermochemistry of Select 2,6-Dinotrobenzyl Esters in Polymer Matrices: Studies Pertaining to Chemical Amplication and Imaging. *Macromolecules* **1990**, *23*, 145–150.

(141) Wang, P.; Photolabile Protecting Groups: Structure and Reactivity. *Asian J. Org. Chem*. **2013**, *2*, 452–464.

(142) Momotake, A.; Lindegger, N.; Niggli, E.; Barsotti, R. J.; Ellis-Davies, G. C. R. The nitrodibenzofuran chromophore: a new caging group for ultra-efficient photolysis in living cells. *Nat. Methods* **2006**, *3*, 35–40.

(143) Bader, T. K.; Xu, F.; Hodny, M. H.; Blank, D. A.; Distefano, M. D. Methoxy-Substituted Nitrodibenzofuran-Based Protecting Group with an Improved Two-Photon Action Cross-Section for Thiol Protection in Solid Phase Peptide Synthesis. *J. Org. Chem*. **2020**, *85*, 1614–1625.

(144) Hammers, M. D.; Hodny, M. H.; Bader, T. K.; Mahmoodi, M. M.; Fang, S.; Fenton, A. D.; Nurie, K.; Trial, H. O.; Xu, F.; Healy, A. T.; Ball, Z. T.; Blank, D. A.; Distefano, M. D. Two-photon uncaging of bioactive thiols in live cells at wavelengths above 800 nm. *Org. Biomol. Chem*. **2021**, *19*, 2213–2223.

(145) Mahmoodi, M. M.; Abate-Pella, D.; Pundsack, T. J.; Palsuledesai, C. C.; Goff, P. C.; Blank, D. A.; Distefano, M. D. Nitrodibenzofuran: A One- and Two-Photon Sensitive Protecting Group That Is Superior to Brominated Hydroxycoumarin for Thiol Caging in Peptides. *J. Am. Chem. Soc*. **2016**, *138*, 5848–5859.

(146) Becker, Y.; Unger, E.; Fichte, M. A. H.; Gacek, D. A.; Dreuw, A.; Wachtveitl, J.; Walla, P. J.; Heckel, A. A red-shifted two-photon-only group for three dimensional photorelease. *Chem. Sci*. **2018**, *9*, 2797–2802.

(147) Friedrich, F.; Klehs, K.; Fichte, M. A. H.; Junek, S.; Heilemann, M.; Heckel, A. A two-photon activated amino acid linker for the induction of fluorescence. *Chem. Commun*. **2015**, *51*, 15382–15385.

(148) Momotake, A.; Lindegger, N.; Niggli, E.; Barsotti, R. J.; Ellis-Davies, G. C. R. The nitrodibenzofuran chromophore: a new caging group for ultra-efficient photolysis in living cells. *Nat. Methods* **2006**, *3*, 35–40.

(149) Sõrmus, T.; Lavogina, D.; Enkvist, E.; Uri, A.; Viht, K. Efficient photocaging of a tight-binding bisubstrate inhibitor of cAMP-dependent protein kinase. *Chem. Commun*. **2019**, *55*, 11147.

(150) Gatterdam, V.; Ramadass, R.; Stoess, T.; Fichte, M. A. H.; Wachtveitl, J.; Heckel, A.; Tampé, R. Three-Dimensional Protein Networks Assembled by Two-Photon Activation. *Angew. Chem. Int. Ed*. **2014**, *53*, 5680–5684.

(151) Bader, T. K.; Xu, F.; Hodny, M. H.; Blank, D. A.; Distefano, M. D. Methoxy-Substituted Nitrodibenzofuran-Based Protecting Group with an Improved Two-Photon Action Cross-Section for Thiol Protection in Solid Phase Peptide Synthesis. *J. Org. Chem*. **2020**, *85*, 1614–1625.

(152) Becker, Y.; Unger, E.; Fichte, M. A. H.; Gacek, D. A.; Dreuw, A.; Wachtveitl, J.; Walla, P. J.; Heckel, A. A red-shifted two-photon-only group for three dimensional photorelease. *Chem. Sci*. **2018**, *9*, 2797–2802.

(153) Friedrich, F.; Klehs, K.; Fichte, M. A. H.; Junek, S.; Heilemann, M.; Heckel, A. A two-photon activated amino acid linker for the induction of fluorescence. *Chem. Commun*. **2015**, *51*, 15382–15385.

(154) Komori, N.; Jakkampudi, S.; Motoishi, R.; Abe, M.; Kamada, K.; Furukawa, K.; Katan, C.; Sawada, W.; Takahashi, N.; Kasai, H.; Xue, B.; Kobayashi, T. Design and synthesis of a new chromophore, 2-(4-nitrophenyl)benzofuran, for two-photon uncaging using near-IR light. *Chem. Commun*. **2016**, *52*, 331–334.

(155) Dreuw, A.; Polkehn, M. A.; Binder, R.; Heckel, A.; Knippenberg, S. Computational Design of Improved Two-Photon Active Caging Compounds Based on Nitrodibenzofuran. *J. Compt. Chem*. **2012**, *33*, 1797–1805.

(156) Komori, N.; Jakkampudi, S.; Motoishi, R.; Abe, M.; Kamada, K.; Furukawa, K.; Katan, C.; Sawada, W.; Takahashi, N.; Kasai, H.; Xue, B.; Kobayashi, T. Design and synthesis of a new chromophore, 2-(4-nitrophenyl)benzofuran, for two-photon uncaging using near-IR light. *Chem. Commun*. **2016**, *52*, 331–334.

(157) Hasan, A.; Foote, R. S.; Cornwell, P.; Ishame, K. R.; Gigerich, H.; Stengele, K. -P.; Pfleiderer, W.; Sachleben, R. A. Photolabile Protecting Groups for Nucleosides: Synthesis and Photodeprotection Rates. *Tetrahedron*, **1997**, *53*, 4247–4264.

(158) Beier, M.; Hohersel, J. D.; Production by Quantitative Photolithographic Synthesis of Individually Quality Checked DNA Microarrays. *Nucleic Acid Res*. **2000**, *28*, e11.

(159) Berroy, P.; Viriot, M. L.; Carre, M. C. Photolabile group for 5'-OH protection of nucleoside: synthesis and photodeprotection reate. *Sens. Actuators, B* **2001**, *74*, 186–189.

(160) Bhushan, K. R. Light-directed maskless synthesis of peptide arrays using photolabile amino acid monomers. *Org. Biomol. Chem*. **2006**, *4*, 1857–1859.

(161) Specht, A.; Thomann, J. -S.; Alarcon, K.; Wittayanan, W.; Ogden, D.; Furuta, T.; Kurakawa, Y.; Goeldner, M. New Photoremovable Protecting Groups for Carboxylic Acids with High Photolytic Efficiencies at Near-UV Irradiation. Application to the Photocontrolled Release of L-Glutamate. *ChemBioChem* **2006**, *7*, 1690–1695.

(162) Gug. S.; Charon, S.; Specht, A.; Alarcon, K.; Odgen, D.; Zietz, B.; Léonard, J.; Haacke, S.; Bolze, F.; Nicoud, J. -F.; Goeldner, M. Photolabile Glutamate Protecting Group with High One- and Two-Photon Uncaging Efficiencies. *ChemBioChem* **2008**, *9*, 1303–1307.

(163) Donato, L.; Mourot, A.; Davenport, C. M.; Herbivo, C.; Warther, D.; Léonard, J.; Bolze, F.; Nicoud, J. F.; Kramer, R. H.; Goeldner, M.; Specht, A. Water-Soluble, Donor-Acceptor Biphenyl Derivatives in the 2-(*o*-Nitrophenyl)propyl Series: Highly Efficient Two-Photon Uncaging of the Neurotransmitter γ-Aminobutyric Acid at λ = 800 nm. *Angew. Chem. Int. Ed*. **2012**, *51*, 1840–1843.

(164) Röthlingshöfer, M.; Gorska, K.; Winssinger, N. Nucleic Acid-Templated Energy Transfer Leading to a Photorelease Reaction and its Application to a System Displaying a Nonlinear Response. *J. Am. Chem. Soc*. **2011**, *133*, 18110–18113.

(165) Amit, B.; Ben-Efraim, D. A.; Parchornik, A. Light-sensitive amides. The photolysis of substituted 1-acyl-7-nitroindolines. *J. Am. Chem. Soc*. **1976**, *98*, 843–844.

(166) Amit, B.; Patchornik, A. The photorearrangement of N-substituted ortho-nitroanilides and nitroveratramides. A potential photosensitive protecting group. *Tetrahedron Lett*. **1973**, *14*, 2205–2208.

(167) Amit, B.; Ben-Efraim, D. A.; Patchornik, A. Light-sensitive amides. Photocleavage of N-acyl-1,2,3,4-tetrahydro-8-nitroquinolines to give free carboxylic acids. *J. Chem. Soc., Perkin Trans. 1* **1976**, *1*, 57–63.

(168) Morrison, J.; Wan, P.; Corrie, J. E. T.; Papageorgiou, G. Mechanism of photorelease of carboxylic acids from 1-acyl-7-nitroindolines in solutions of varying water content. *Photochem. Photobiol. Sci*. **2002**, *1*, 960–969.

(169) Cohen, A. D.; Helgen, C.; Bochet, C. G.; Toscano, J. P. The Mechanism of Photoinduced Acylation of Amines by N-Acyl-5,7-dinitroindoline as Determined by Time-Resolved Infrared Spectroscopy. *Org. Lett*. **2005**, *7*, 2845–2848.

(170) Corrie, J. E. T.; Barth, A.; Papageorgiou, G. Synthesis and characterization of ^{13}C and ^{15}N isotopomers of a 1-acyl-7-nitroindoline. *J. Labelled Compd. Radiopharm*. **2001**, *44*, 619–626.

(171) Papageorgiou, G.; Corrie, J. E. T. Synthesis of an anionically substituted nitroindoline-caged GABA reagent that has reduced affinity for GABA receptors. *Tetrahedron* **2007**, *63*, 9668–9676.

(172) Maier, W.; Corrie, J. E. T.; Papageorgiou, G.; Laube, B.; Grewer, C. Comparative analysis of inhibitory effects of caged ligands for the NMDA receptor. *J. Neurosci. Methods* **2005**, *142*, 1–9.

(173) Tanaka, J. I.; Horiike, Y.; Matsuzaki, M.; Miyazaki, T.; Ellis-Davies, G. C. R.; Kasai, H. Protein Synthesis and Neurotrophin-Dependent Structural Plasticity of Single Dentritic Spines. *Science* **2008**, *319*, 1683–1687.

(174) Kantevari, S.; Matsuzaki, M.; Kanemoto, Y.; Kasai, H.; Ellis-Davies, G. C. R. Two-color, two-photon uncaging of glutamate and GABA. *Nat. Methods* **2010**, *7*, 123–125.

(175) Débieux, J. -L.; Bochet, C. G. The all-photochemical synthesis of an OGP(10-14) precursor. *Chem. Sci*. **2012**, *3*, 405–406.

(176) Sheehan, J. C.; Umezawa, K. Phenacyl photosensitive blocking groups. *J. Org. Chem.* **1973**, *38*, 3771–3774.

(177) Givens, R. S.; Athey, P. S.; Kueper III, L. W.; Matuszewski, B.; Xue, J. Y. Photochemistry of α-keto phosphate esters: photorelease of a caged cAMP. *J. Am. Chem. Soc*. **1992**, *114*, 8708–8710.

(178) Givens, R. S.; Athey, P. S.; Matuszewski, B.; Kueper III, L. W.; Xue, J. Y.; Fister, T. Photochemistry of phosphate esters: α-keto phosphate as a photoprotecting group for caged phosphate. *J. Am. Chem. Soc*. **1993**, *115*, 6001–6012.

(179) An, H. Y.; Kwok, W. M.; Ma, C.; Guan, X.; Kan, J. T. W.; Toy, P. H.; Phillips, D. L. Photophysics and Photodeprotection Reactions of *p*-Methoxyphenacyl Phototriggers: An Ultrafast and Nanosecond Time-Resolved Spectroscopic and Density Functional Theory Study. *J. Org. Chem*. **2010**, *75*, 5837–5851.

(180) Banerjee, A.; Falvey, D. E. Direct Photolysis of Phenacyl Protecting Groups Studied by Laser Flash Photolysis: An Excited State Hydrogen Atom Abstraction Pathway Leads to Formation of Carboxylic Acids and Acetophenone. *J. Am. Chem. Soc*. **1998**, *120*, 2965–2966.

(181) Givens, R. S.; Rubina, M.; Wirz, J. Applications of *p*-hydroxyphenacyl (*p*HP) and coumarin-4-ylmethyl photoremovable protecting groups. *Photochem. Photobiol. Sci.* **2012**, *11*, 472–488.

(182) Park, C. H.; Givens, R. S. New photoactivated Protecting group. 6. *p*-Hydroxyphenacyl: A Phototrigger for Chemical and Biochemical Probes. *J. Am. Chem. Soc.* **1997**, *119*, 2453–2464.

(183) Givens, R. S.; Park, C. H. *p*-Hydroxyphenacyl ATP: A new phototrigger. *Tetrahedron Lett*. **1996**, *35*, 6259–6262.

(184) Zabadal, M.; Pelliccioli, A. P.; Klán, P.; Wirz, J. 2,5-Dimethylphenacyl Esters: A Photoremovable Protecting Group for Carboxylic Acids. *J. Phys. Chem. A* **2001**, *105*, 10329–10333.

(185) Klán, P.; Zabadal, M.; Heger, D. 2,5-Dimethylphenacyl as a New Photoreleasable Protecting Group for Carboxylic Acids. *Org. Lett*. **2000**, *2*, 1569–1571.

(186) Klán, P.; Pelliccioli, A. P.; Pospíšil, T.; Wirz, J. 2,5-Dimethylphenacyl esters: A photoremovable protecting group for phosphates and sulfonic acids. *Photochem. Photobiol. Sci*. **2002**, *1*, 920–923.

(187) Literák, J.; Wirz, J.; Klán, P. 2,5-Dimethylphenacyl carbonates: A photoremovable protecting group for alcohols and phenols. *Photochem. Photobiol. Sci*. **2005**, *4*, 43–46.

(188) Kammari, L.; Plíštil. L; Wirz, J.; Klán, P. 2,5-Dimethylphenacyl carbamates: a photoremovable protecting group for amines and amino acids. *Photochem. Photobiol. Sci*. **2007**, *6*, 50–56.

(189) Tseng, S. S.; Ullman, E. F. Elimination Reactions Induced by Photoenolization of O-Alkylbenzophenones. *J. Am. Chem. Soc.* **1976**, *98*, 541–544.

(190) Pirrung, M. C.; Roy, B. G.; Gadamsetty, S. Structure-reactivity realationships in (2-hydroxyethyl)benzophenone photoremovable protecting groups. *Tetrahedron* **2010**, *66*, 3147–3151.

(191) Pika, J.; Konosonoks, A.; Robinson, R. M.; Singh, P. N. D.; Gudmundsdottir, A. D. Photoenolization as a Means To Release Alcohols. *J. Org. Chem.* **2003**, *68*, 1964–1972.

(192) Jia, J.; Sarker, M.; Steinmetz, M. G.; Shukla, R.; Rathore, R. Photochemical Elimination of Leaving Groups from Zwitterionic Intermediates Generated via Electrocyclic Ring Closure of α,β-Unsaturated Anilides. *J. Org. Chem.* **2008**, *73*, 8867–8879.

(193) Jia, J.; Steinmetz, M. G.; Shukla, R.; Rathore, R. Photochemical electrocyclization of α,β-unsaturated anilides to give zwitterionic intermediates which eliminate carboxylate and phenolate leaving groups. *Tetrahedron Lett*. **2008**, *49*, 4621–4623.

(194) Misetic, A.; Boyd, M. K. The Pixyl (Px) Group: A Novel Photocleavable Protecting Group for Primary Alcohols. *Tetrahedron Lett*. **1998**, *39*, 1653–1656.

(195) Coleman, M. P.; Boyd, M. K. The S-Pixyl Group: An Efficient Photocleavable Protecting Group for the 5'-Hydroxy Function of Deoxyribonucleosides. *Tetrahedron Lett*. **1999**, *40*, 7911–7915.

(196) Ren, M.-G.; Bi, N.-M.; Mao, M.; Song, Q.-H. 2-(1′-Hydroxyethyl)-anthraquinone as a Photolabile Protecting Group for Carboxylic Acids. *J. Photochem. Photobiol. A Chem.* **2009**, *204*, 13–18.

(197) Furuta, T.; Torigai, H.; Sugimoto, M.; Iwamura, M. Photochemical Properties of New Photolabile cAMP Derivatives in a Physiological Saline Solution. *J. Org. Chem.* **1995**, *60*, 3953–3956.

(198) Zhou, L.; Yang, H.; Wang, P. Development of Trityl-Based Photolabile Hydroxyl Protecting Groups. *J. Org. Chem.* **2011**, *76*, 5873–5881.

(199) Yang, H.; Zhang, X.; Zhou, L.; Wang, P. Development of a Photolabile Carbonyl-Protecting Group Toolbox. *J. Org. Chem.* **2011**, *76*, 2040–2048.

(200) Wang, P.; Huayou, H.; Wang, Y. Novel Photolabile Protecting Group for Carbonyl Compounds. *Org. Lett*. **2007**, *9*, 1533–1535.

(201) Hagen, V.; Bendig, J.; Frings, S.; Eckardt, T.; Helm, S.; Reuter, D.; Kaupp, U. B. Highly Efficient and Ultrafast Phototriggers for cAMP and cGMP by Using Long-Wavelength UV/Vis-Action. *Angew. Chem. Int. Ed. Engl*. **2001**, *40*, 1045– 1048.

(202) Cameron, J. F.; Frechet, J. M. J. Base Catalysis in Imagine Materials. 1. Design and Synthesis of Novel Light-Sensitive Urethanes as Photoprecursors of Amines. *J. Org. Chem.* **1990**, *55*, 5919–5922.

(203) Schmidt, R.; Geissler, D.; Hagen, V.; Bendig, J. Kinetics Study of the Photocleavage of (Coumarin-4-yl)methyl Esters. *J. Phys. Chem. A* **2005**, *109*, 5000–5004.

(204) Schmidt, R.; Geissler, D.; Hagen, V.; Bendig, J. Mechanism of Photocleavage of (Coumarin-4-yl)methyl Esters. *J. Phys. Chem. A* **2007**,*111*, 5768–5774.

(205) Yu, H.; Li, J.; Wu, D.; Qiu, Z.; Zhang, Y. Chemistry and biological applications of photo-labile organic molecules. *Chem. Soc. Rev*. **2010**, *39*, 464–473.

(206) Fournier, L.; Gauron, C.; Xu, L.; Aujard, I.; Saux, T. Le; Gagey-eilstein, N.; Maurin, S.; Dubruille, S.; Baudin, J.; Bensimon, D.; et al. A Blue-Absorbing Photolabile Protecting Group for in Vivo Chromatically Orthogonal Photoactivation. *ACS Chem. Biol.* **2013**, *8*, 1528–1536.

(207) Velema, W. A.; van der Berg. J. P.; Szymanski, W.; Driessen, A. J. M.; Feringa, B. L. Bacterial patterning controlled by light exposure. *Org. Biomol. Chem*. **2015**, *13*, 1639–1642.

(208) Goswami, P. P.; Syed, A.; Beck, C. L.; Albright, T. R.; Mahoney, K. M.; Unash, R.; Smith, E. A.; Winter, A. H. BODIPY-Derived Photoremovable Protecting Groups Unmasked with Green Light. *J. Am. Chem. Soc*. **2015**, *137*, 3783–3786.

(209) Rubinstein, N.; Liu, P.; Miller, E. W.; Weinstain, R. *meso*-Methylhydroxy BODIPY: a scaffold for photo-labile protecting groups. *Chem. Commun*. **2015**, *51*, 6369–6372.

(210) Peterson, J. A.; Fischer, L. J.; Gehrmann, E. J.; Shrestha, P.; Yuan. D.; Wijesooriya, C. S.; Smith, E. A.; Winter, A. H. Direct Photorelease of Alcohols from Boron-Alkylated BODIPY Photocages. *J. Org. Chem*. **2020**, *85*, 5712–5717.

(211) Kand, D.; Pizarro, L.; Angel, I.; Avni, A.; Friedmann-Morvinski, D.; Weinstain, R. Organelle-Targeted BODIPY Photocages: Visible-Light-Mediated Subcellular Photorelease. *Angew. Chem. Int. Ed*. **2019**, *58*, 4659–4663.

(212) Palao, E.; Slanina, T.; Muchova, L.; Šolomek, T.; Vítek, L.; Klán, P. Transition-Metal-Free CO-Releasing BODIPY Derivatives Activated by Visible to NIR Light as Promising Bioactive Molecules. *J. Am. Chem. Soc*. **2016**, *138*, 126–133.

(213) Shretha, P.; Dissanayake, K. C.; Gehrmann, E. J.; Wijesooriya, C. S.; Mukhopadhyay, A.; Smith, E. A.; Winter, A. H. Efficient Far-Red/Near-IR

Absorbing BODIPY Photocages by Blocking Unproductive Conical Intersections. *J. Am. Chem. Soc*. **2020**, *142*, 15505–15512.

(214) Slanina, T.; Shretha, P.; Palao, E.; Kand, D.; Perterson, J. A.; Dutton, A. S.; Rubinstein, N.; Weinstain, R.; Winter, A. H.; Klán, P. In search of the Perfect Photocage: Structure-Reactivity Relationships in *meso*-Methyl BODIPY Photoremovable Protecting Groups. *J. Am. Chem. Soc*. **2017**, *139*, 15168–15175.

(215) Umeda, N.; Takahashi, H.; Kamiya, M.; Ueno, T.; Komatsu, T.; Terai, T.; Hanaoka, K.; Nagano, T.; Urano, Y. Boron Dipyrromethene As a Fluorescent Caging Group for Single-Photon Uncaging with Long-Wavelength Visible Light. *ACS Chem. Biol*. **2014**, *9*, 2242–2246.

(216) Takeda, A.; Komatsu, T.; Nomura, H.; Naka, M.; Matsuki, N.; Ikegaya, Y.; Terai, T.; Ueno, T.; Hanaoka, K.; Nagano, T.; Urano, Y. Unexpected Photo-instability of 2,6-Sulfonamide-Substituted BODIPYs and Its Application to Caged GABA. *Chembiochem* **2016**, *17*, 1233–1240.

(217) Sambath, K.; Zhao, T.; Wan, T.; Zhang, Y. Photo-uncaing of BODIPY oxime ester for histone deacetylases induced apoptosis in tumor cells. *Chem. Commun*. **2019**, *55*, 14162–14165.

(218) Hwu, J. R.; Tsay, S. C.; Hong, S. C.; Leu, Y. J.; Liu, C. F.; Chou, S. S. P. Oxime esters of anthraquinone as photo-induced DNA-cleaving agents for single- and double- strand scissions. *Tetrahedron Lett*. **2003**, *44*, 2957–2960.

(219) Hwu, J. R.; Yang, J. R.; Tsay, S. C.; Hsu, M. H.; Chen, Y. C.; Chou, S. S. P. Photo-induced DNA cleavage by (heterocyclo)carbonyl oxime esters of anthraquinone. *Tetrahedron Lett*. **2008**, *49*, 3312–3315.

(220) Šebej, P.; Winter, J.; Müller, P.; Slanina, T.; Al Anshori, J.; Antony, L. A. P.; Klán, P.; Wirz, J. Fluorescein Analogues as Photoremovable Protecting Groups Absorbing at ~520 nm. *J. Org. Chem*. **2013**, *78*, 1833–1843.

(221) Antony, L. A. P.; Slanina, T.; Šebej, P.; Šolomek, T.; Klán, P.; Fluorescein Analogue Xanthene-9-Carboxylic Acid: A Transition-Metal-Free CO Releasing Molecule Activated by Green Light. *Org. Lett*. **2013**, *15*, 4552–4555.

(222) Wang, X.; Kalow, J. A. Rapid Aqueous Photouncaging by Red Light. *Org. Lett*. **2018**, *20*, 1716–1719.

(223) Chen, Y.; Steinmetz, M. G. Photochemical Cyclization with Release of Carboxylic Acids and Phenol from Pyrrolidino-Substituted 1,4-Benzoquinones Using Visible Light. *Org. Lett*. **2005**, *7*, 3729–3732.

(224) Chen, Y.; Steinmetz, M. G. Photoactivation of Amino-Substituted 1,4-Benzoquinones for Release of Carboxylate and Phenolate Leaving Groups Using Visible Light. *J. Org. Chem*. **2006**, *71*, 6053–6060.

(225) Norris, S.; Warner, C. C.; Thooft, A. M.; Demirci, S. K.; Lampkin, B. J.; Miner, K.; Ellern, A.; Van Veller, B. Blue-Light Photocleavable Protecting Groups Based on Benzothiazole Scaffolds. *Org. Lett*. **2020**, *22*, 270–273.

(226) Zimmerman, H. E. Meta-Ortho Effect in Organic Photochemistry: Mechanistic and Exploratory Organic Photochemistry. *J. Phys. Chem. A* **1998**, *102*, 5616–5621.

(227) Narumi, T.; Miyata, K.; Nii, A.; Sato, K.; Mase, N.; Furuta, T. 7-Hydroxy-*N*-Methylquinolinium Chromophore: A Photolabile Protecting Group for Blue-Light Uncaging. *Org. Lett*. **2018**, *20*, 4178–4182.

(228) Senda, N.; Miwa, Y.; Tanaka, J.; Momotake, A.; Arai, T. Tsukuba-green: A Fluorescent Dye that Emits Fluorescence Useful for Live-cell Imaging. *Chem. Lett*. **2010**, *39*, 308–310.

(229) Parish, J. A.; Kurt, F. J.; Rox, R. A. Erythema and melanogenesis action spectra of normal human skin. *Photochem. phototobiol*. **1982**, *36*, 187-191.

(230) Xiong, X. D.; Deng, C. L.; Peng, X. S.; Miao, Q.; Wong, H. N. C. Heteroatom-Bridged Tetraphenylenes: Synthesis, Structures, and Properties. *Org. Lett*. **2014**, *16*, 3252–3255.

(231) Loic, D.; Alexandre, M.; Christopher, M. D.; Cyril, H.; David, W.; Maurice, G.; Alexandre, S. Water-Soluble, Donor–Acceptor Biphenyl Derivatives in the 2-(o-Nitrophenyl)propyl Series: Highly Efficient Two-Photon Uncaging of the Neurotransmitter γ-Aminobutyric Acid at λ=800 nm. *Angew. Chem. Int. Ed*. **2012**, *51*, 1840–1843.

(232) Lusic, H.; Uprety, R.; Deiters, A. Improved Synthesis of the Two-Photon Caging Group 3-Nitro-2-Ethyldibenzofuran and Its Application to a Caged Thymidine Phosphoramidite. *Org. Lett*. **2010**, *12,* 916–919.

(233) Komori, N.; Jakkampudi, S.; Motoishi, R.; Abe, M.; Kamada, K.; Furukawa, K.; Katan, C.; Sawada, W.; Takahashi, N.; Kasai, H.; Xue, B.; Kobayashi, T. Design and synthesis of a new chromophore, 2-(4-nitrophenyl)benzofuran, for two-photon uncaging using near-IR light. *Chem. Commun*. **2016**, *52*, 331–334.

(234) Neises, B.; Steglich, W. Simple Method for the Esterification of Carboxylic Acids. *Angew. Chem. Int. Ed*. **1978**, *17*, 522–524.

(235) Lee, J.; Seliger, H. H. Quantum Yield of the Ferrioxalate Actinometer. *J. Chem. Phys.* **1964**, *40*, 519-523.

(236) Arbely, E.; Kolbus, J. T.; Deither, A.; Chin, J. W. Photocontrol of Tyrosine Phosphorylation in Mammalian Cells via Genetic Encoding of Photocaged Tyrosine. *J. Am. Chem. Soc*. **2012**, *134*, 11912–11915.

(237) Deiters, A.; Groff, D.; Ryu, Y.; Xie, J.; Schultz, P. G. A Genetically Encoded Photocaged Tyrosine. *Angew. Chem. Int. Ed*. **2006**, *45*, 2728–2731.

(238) Stewart, H. L.; Hanby, A. R.; King, T. A.; Bond, A. D.; Moss, T. A.; Sore, H. F.; Spring, D. R. An efficient, stereocontrolled and versatile synthetic route to bicyclic partially saturated privileged scaffolds. *Chem. Commun*. **2020**, *56*, 6818–6821.

(239) Azuma, Y.; Imanishi, M.; Yoshimura, T.; Kawabata, T.; Futaki, S. Cobalt(II)-Responsive DNA Binding of a GCN4-bZIP Protein Containing Cystein Residues Functionalized with Iminodiacetic Acid. *Angew. Chem. Int. Ed*. **2009**, *48*, 6853–6856.

(240) Ding, R.; He, Y.; Wang, X.; Xu, J.; Chen, Y.; Feng, M.; Qi, C. Treatment of Alcohols with Tosyl Chloride Does Not always Lead to the Formation of Tosylates. *Molecules* **2011**, *16*, 5665–5673.

(241) Field, L.; Settlage, P. H. Alkanesulfonic Acid Anhydrides. *J. Am. Chem. Soc*. **1954**, *76*, 1222–1225.

(242) Andersson, M. I.; MacGowan, A. P. Development of the quinolones. *J. Antimicrob. Chemother*. **2003**, *51*, Suppl S1, 1–11.

(243) Appelbaum, P. C.; Hunter, P. A. The fluoroquinolone antibacterials: past, present and future perspectives. *Int. J. Antimicrob. Agents* **2000**, *16*, 5–15.

(244) Lesher, G. Y.; Froelich, E. J.; Gruett, M. D.; Bailey, J. H.; Brundage, R. P. 1,8-Naphthyridine Derivatives. A New Class of Chemotherapheutic Agents. *J. Med. Pharm. Chem.* **1962**, *91*, 1063–1065.

(245) Cozzarelli, N. R. DNA gyrase and the supercoiling of DNA. *Science* **1980**, *207*, 953–960.

(246) Tillotson, G. S. Quinolones: structure-activity relationships and future predictions. *J. Med. Microbiol*. **1996**, *44*, 320–324.

(247) Velema, W. A.; van der Berg. J. P.; Szymanski, W.; Driessen, A. J. M.; Feringa, B. L. Bacterial patterning controlled by light exposure. *Org. Biomol. Chem*. **2015**, *13*, 1639–1642.

(248) Velema, W. A.; van der Berg. J. P.; Szymanski, W.; Driessen, A. J. M.; Feringa, B. *ACS Chem. Biol*. **2014**, *9*, 1969–1974.

(249) Still, W. C.; Kahn, M.; Mitra, A., Rapid Chromatographic Technique for Preparative Separations with Moderate Resolution. *J. Org. Chem*. **1978**, *43*, 2923-2925.

(250) Essig, S.; Bretzke, S.; Müller, R.; Menche, D. Full Stereochemical Determination of Ajudazols A and B by Bioinformatics Gene Cluster Analysis and Total Synthesis of Ajudazol B by an Asymmetric Ortholithiation Strategy. *J. Am. Chem. Soc*. **2012**, *134*, 19362−19365.

(251) Kumar, P.; Jiang, T.; Li, S.; Zainul, O.; Laughlin, S. T. Caged Cyclopropenes for Controlling Bioorthogonal Reactivtiy. *Org. Biomol. Chem*. **2018**, *16*, 2081–2085.

(252) SAINT V8.34A Bruker AXS Inc, (2013), Madison, WI.

(253) Sheldrick, G. M. (2015). SHELXT. Acta Cryst. A71, 3-8.

(254) Sheldrick, G. M. (2015). SHELXL-2016/6. Program for the Refinement of Crystal Structures. Acta Cryst., C91, 9-18.

(255) Spek, A. L. (2009). PLATON, A Multipurpose Crystallographic Tool. Utrecht University, The Netherlands. Acta Cryst. D65, 148-155.

(256) WinGX 1.64. (1999). An Integrated System of Windows Programs for the Solution, Refinement and Analysis of Single Crystal X-ray Diffraction Data. Farrugia, L. J. *J. Appl. Cryst*. 32. 837-838.

(257) OLEX2. Dolomanov, O. V., Bourhis, L. J., Gildea, R. J., Howard, J. A. K. and Puschmann, H. A Complete Structure Solution, Refinement and Analysis Program. *J. Appl. Cryst.* 42, 339-341.

(258) $Rw(F^2) = \{\Sigma w(|Fo|^2 - |Fc|^2)^2/\Sigma w(|Fo|)^4\}^{1/2}$ where w is the weight given each reflection.

$R(F) = \Sigma (|Fo| - |Fc|)/\Sigma|Fo|\}$ for reflections with $Fo > 4(\sigma (Fo))$.

$S = [\Sigma w(|Fo|^2 - |Fc|^2)^2/(n - p)]^{1/2}$, where n is the number of reflections and p is the number of refined parameters.

(259) International Tables for X-ray Crystallography (1992). Vol. C, Tables 4.2.6.8 and 6.1.1.4, A. J. C. Wilson, editor, Boston: Kluwer Academic Press.

(260) Sheldrick, G. M. (1994). SHELXTL/PC (Version 5.03). Siemens Analytical X-ray Instruments, Inc., Madison, Wisconsin, USA.